PHYSIOLOGY DIRECTED DRUG DISCOVERY IN MULTIDRUG RESISTANT *PLASMODIUM FALCIPARUM*

A Dissertation
submitted to the Faculty of the
Graduate School of Arts and Sciences
of Georgetown University
in partial fulfillment of the requirements for the
degree of
Doctor of Philosophy
in Chemistry

By

Amila Chathuranga Siriwardana, B. S.

Washington, DC
April 20, 2017

PHYSIOLOGY DIRECTED DRUG DISCOVERY IN MULTIDRUG RESISTANT *PLASMODIUM FALCIPARUM*

Amila Chathuranga Siriwardana, B. S.

Thesis Advisor: Paul D. Roepe, Ph. D.

ABSTRACT

Resistance to front-line antimalarial therapies is a widespread issue, from early chloroquine failure to the more recent concerns of Artemisinin Combination Therapy (ACT) failure. Traditional methods of quantifying drug resistance focused on growth inhibitory, or IC_{50}, concentrations of drug. In the clinical setting, however, parasites are exposed to much higher concentrations of drug that kill parasites within hours. Defined as cytocidal activity, these concentrations have only recently begun to be explored. Recent reports suggest that, drug targets and molecular mechanisms of drug resistance differ at cytostatic versus cytocidal levels. To investigate these possible targets and mechanisms of resistance at cytocidal levels of drug, immunofluorescence assays were conducted to visualize PfAtg8 localization in chloroquine sensitive versus resistant parasites treated at cytocidal drug concentrations.

In addition to understanding chloroquine resistance, the recent emergence of a delayed clearance phenotype (DCP) and piperaquine resistance further warrant novel methods of probing molecular mechanisms of drug resistance. Mutations in the propeller domains of a Kelch domain-containing protein on chromosome 13 (K13) have been linked to DCP and traditional methods of quantifying cytostatic or cytocidal activities of drugs fail to distinguish K13-mutant parasites from wild-type parasites. In 2013, Witkowski *et al.* developed the ring-stage susceptibility assay (RSA) using dihydroartemisinin to correlate DCP with an *in vitro* measurement: increased parasite

survival. This method was modified to investigate other endoperoxide drugs and of the seven compounds tested, OZ439 was only compound that circumvented the endoperoxide cross-resistance pattern.

A high-throughput screen identified several potent antimalarials, including phosphatidylinositol 3-kinase (PI3K) inhibitors. These PI3K inhibitors are not only extremely potent antimalarials, but they were also found to inhibit the formation of Atg8 puncta in parasites and were highly synergistic with ART derivatives. Based on recent studies suggesting the involvement of elements in the autophagy cascade in artemisinin resistance, immunofluorescence assays were done with K-13 mutant and wild type parasites and results suggest a dysregulation of an autophagy-like process in the K13-mutant parasites. These results guided me towards conducting single-point Chou-Talalay combination analyses to investigate the efficacy of traditional ACTs in comparison with novel combinations involving an endoperoxide compound plus various PI3K inhibitors. Synergy was observed in OZ439-PI3K combinations in both DCP and wild-type strains.

I dedicate this work to my family and friends who have been there to help and support me every day and without whom I would not have been able to achieve this.

Many thanks,
Amila Chathuranga Siriwardana

TABLE OF CONTENTS

LIST OF FIGURES AND SCHEMES

LIST OF TABLES

LIST OF ABBREVIATIONS

3MA	3-methyl adenine
ACT	Artemisinin combination therapy
AMS	Artemisone
AQ	Amodiaquine
ART	Artemisinin
Atg	Autophagy-related
ATM	Artemether
ATQ	Atovaquone
ATS	Artesunate
BLAST	Basic local alignment search tool
CCD	Charge-coupled device
cDNA	Complementary deoxyribonucleic acid
CM	Complete media
CQ	Chloroquine
CQR	Chloroquine resistant
CQR^{CC}	Cytocidal chloroquine resistance
CQR^{CS}	Cytostatic chloroquine resistance
CQS	Chloroquine sensitive
C-T	Chou-Talalay
DAPI	4´,6-Diamidino-2-Phenylindole
DCP	Delayed clearance phenotype
DHA	Dihydroartemisinin

DIC	Differential interference contrast
DMSO	Dimethyl sulfoxide
DNA	Deoxyribonucleic acid
DV	Digestive vacuole
EGTA	Ethylene glycol-bis(β-aminoethyl ether) –*N,N,N´,N´*-tetraacetic acid
ELISA	Enzyme-linked immunosorbent assay
ER	Endoplasmic reticulum
EtOH	Ethanol
FACS	Fluorescence activated cell sorting
FDA	U.S. Food and Drug Administration
FIC	Fractional inhibitory concentration
FLD	Fractional lethal dose
GSK	GSK-2126458
HBSS	Hank's balanced salts solution
Hr(s)	Hour(s)
Hsp90	Heat shock protein 90
IC_{50}	Half maximal inhibitory concentration
IFA	Immunofluorescence assay
IM	Incomplete media
iRBC	Infected red blood cell
K13	Kelch domain containing protein on chromosome 13
LD_{50}	Half maximal lethal dose
LOD	Logarithm of odds

LSCM	Laser scanning confocal microscopy
LUM	Lumefantrine
MDR	Multi-drug resistance
MDR1	Human multi-drug resistance transporter
mETC	Mitochondrial electron transport chain
MOA	Mode of action
MQ	Mefloquine
MTDR	MitoTracker® Deep Red (FM)
mTOR	Mammalian target of rapamycin
NCATS	National Center for Advancing Translational Science
NIH	National Institutes of Health
NVP	NVP-BGT226
OZ277	Arterolane
OZ439	Artefenomel
PBS	Phosphate buffered saline
PCD	Programmed cell death
PE	Phosphatidylethanolamine
PfAtg8	*Plasmodium falciparum* autophagy-related protein 8
PfCRT	*Plasmodium falciparum* chloroquine resistance transporter
Pfcrt	*Plasmodium falciparum* chloroquine resistance transporter gene
PfEMP1	*Plasmodium falciparum* erythrocyte membrane protein 1
PfExp1	*Plasmodium falciparum* exported protein 1
PfHsp60	*Plasmodium falciparum* heat-shock protein 60

PfK13	*Plasmodium falciparum* kelch domain containing gene on chromosome 13
PfK13	*Plasmodium falciparum* kelch domain containing protein on chromosome 13
PfMDR1	*Plasmodium falciparum* multi-drug resistance transporter
PfMDR1	*Plasmodium falciparum* multi-drug resistance transporter
PfREX1	*Plasmodium falciparum* ring-exported protein 1
PfVps34	*Plasmodium falciparum* vacuolar protein sorting 34
PHIL	Public Health Image Library
PI	Phosphatidyl inositol
PI(3)P	Phosphatidyl inositol 3´ phosphate
PI3K	Phosphatidyl inositol 3´ kinase
PPQ	Piperaquine
PVM	Parasitophorous vacuolar membrane
QD	Quinidine
qHTS	Quantitative high-throughput screen
QN	Quinine
QNR	Quinine resistant
QTL	Quantitative trait loci
RBC	Red blood cell
ROI	Region of interest
ROS	Reactive oxygen species
RSA	Ring-stage susceptibility assay
$RSLD_{50}$	Half maximal lethal dose in ring-stage susceptibility assay
S.D.	Standard deviation

S.E.M.	Standard error of the mean
SCP	Single cell photometry
SDCM	Spinning disk confocal microscopy
SDS	Sodium dodecyl sulfate
SEM	Scanning electron microscopy
SG	SYBR® Green I
SNP	Single nucleotide polymorphism
SP	Sulfadoxine-pyrimethamine
TgAtg8	*Toxoplasma gondii* autophagy-related protein 8
TOR	Target of rapamycin
UPR	Unfolded protein response
UV	Ultraviolet
VPL	Verapamil
Vps34	Vacuolar protein sorting 34
WHO	World Health Organization
ZFN	Zinc-finger nuclease

CHAPTER I

INTRODUCTION

1.1 General Background

Malaria is a deadly disease affecting 300-500 million people worldwide and causes approximately 600,000 deaths annually[1]. It is an infectious disease that mainly affects tropical and subtropical regions of the globe (Figure 1.1), with almost half of the world's population living in areas that are at risk for malaria transmission[1-2].

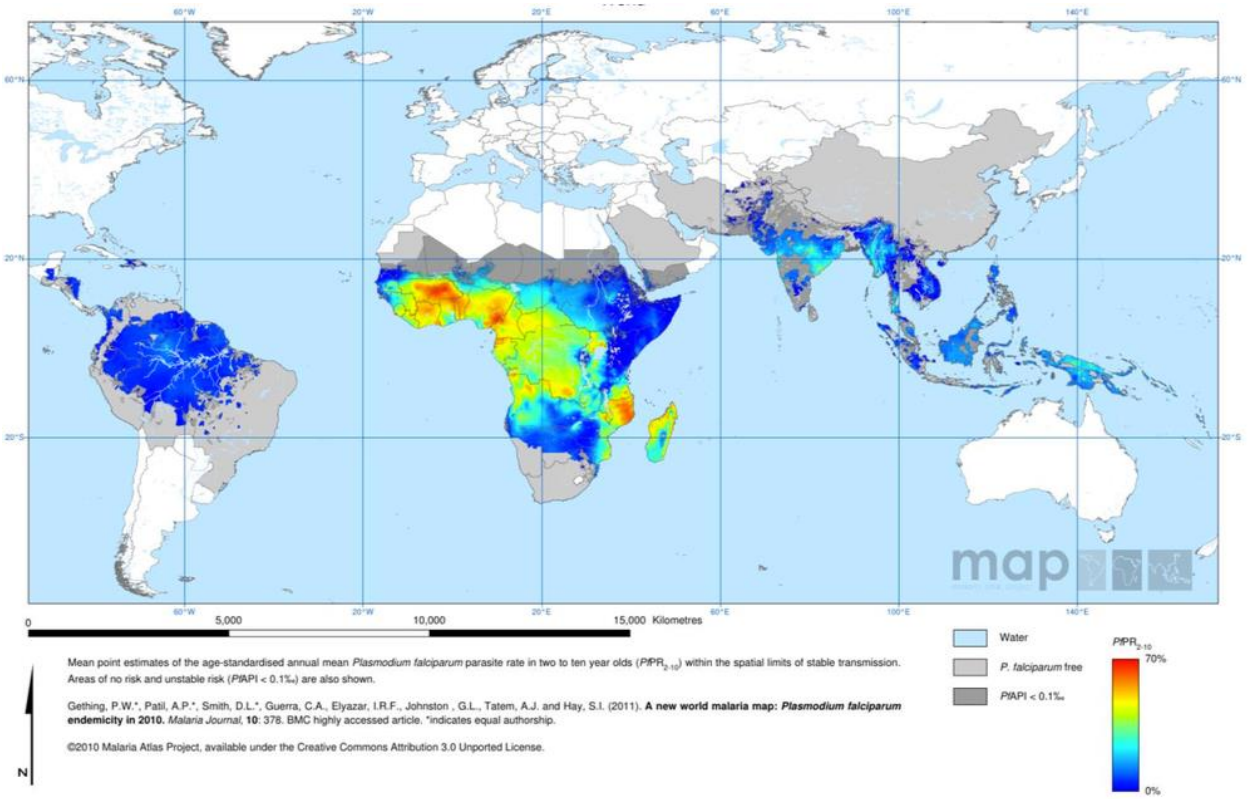

Figure 1. 1 Spatial distribution of *Plasmodium falciparum* malaria endemicity in 2010[2]. Mean point estimates of the age-standardized annual mean of *P. falciparum* parasite rate in two to ten year-old ($PfPR_{2-10}$) within spatial limits of stable transmission. Areas of no risk and unstable risk (PfAPI < 0.1%) are also shown. © 2010 Malaria Atlas Project, available under the Creative Commons Attribution 3.0.

Malaria is a vector-borne disease caused by the unicellular Apicomplexan parasites of the genus *Plasmodia.* There are more than a 100 species, of which 5 are known to infect humans: *P. vivax, P. ovale, P. malariae, P. knowlesi* (zoonotic), and *P. falciparum*[3]. There have also been recent reports of a sixth zoonotic species infecting humans with *P. cynomolgi*[4]. *P. vivax* infections are the most widespread, however, *P. falciparum* is the most lethal species.

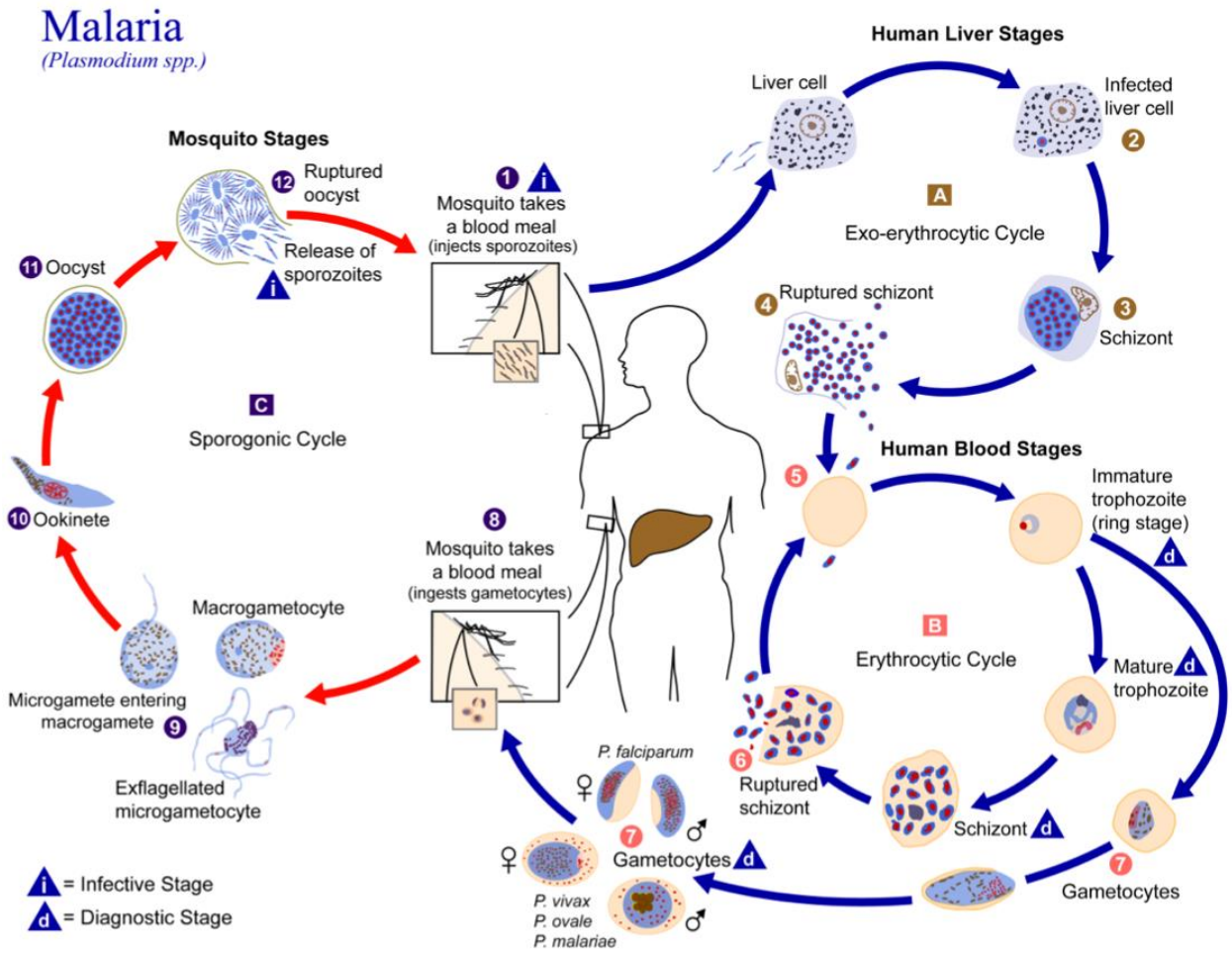

Figure 1. 2 Malaria parasite life-cycle. Credit CDC, Alexander J. da Silva, PhD, and Melanie Moser, 2002[5]. Public domain content available from the Public Health Image Library (PHIL), ID# 3405.

The *Plasmodium* parasite has two hosts: human (asexual reproduction phase) and the female *Anopheles* mosquito vector (sexual reproduction phase). Transmission occurs through a

bite from an infected female A*nopheles* mosquito. Injected sporozoites first invade and infect the liver hepatocytes and then mature into schizonts during the exo-erythrocytic cycle (Figure 1.2), which rupture to release merozoites into the human blood stream. Once in the blood stream, parasites infect red blood cells (RBC), which is the stage responsible for the symptomatic phase of the disease. Inside the RBC, parasites pass through a series of distinct developmental stages over a 48-hour period (Figure 1.3): ring (0-15 h), early trophozoite (15-19 h), mid-trophozoite (19-25 h), late trophozoite (25-30 h), schizont (30-44 h), RBC rupture producing merozoites (44-48 h), re-infection (0 h). Malaria parasites in the intraerythrocytic stage can also differentiate into the sexual stage called gametocytes, of which male (microgametocyte) and female (macrogametocyte) forms exist. These forms can be ingested by an *Anopheles* mosquito during a blood meal, where they then undergo sexual reproduction in the mosquito midgut to form oocysts, which then rupture to release sporozoites. These migrate to the mosquito's salivary glands and can be inoculated into a new human host to continue the parasite life-cycle.

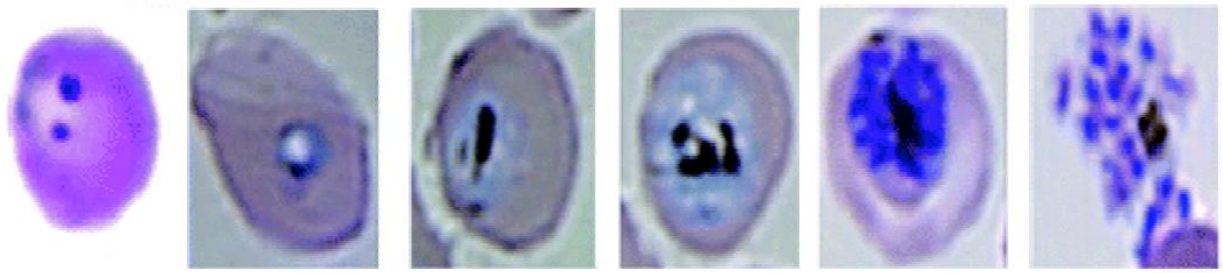

Figure 1. 3 Representative giemsa-stained parasites showing erythrocytic stage morphologies. From left to right: ring (0-15 h), early trophozoite (15-19 h), mid-trophozoite (19-25 h), late trophozoite (25-30 h), schizont (30-44 h), schizont burst releasing merozoites (44-48 h). Black regions denote hemozoin (malaria pigment). Reproduced with permission from Gligorijevic *et al.*[6]

During the trophozoite stage, the parasite is enclosed by the outer parasitophorous vacuolar membrane and the inner plasma membrane, which are separated by the parasitophorous space (Figure 1.4). This double-membrane structure encloses the parasite cytosol which contains a highly

specialized lysosomal organelle called the digestive vacuole (DV). It is within this DV that host RBC hemoglobin is actively degraded to obtain amino acids and make space for parasite development within the RBC. It is important to note that *P. falciparum* parasites have the ability to obtain all amino acids necessary for survival through degradation of host hemoglobin with the exception of isoleucine, which is not present in adult human hemoglobin[7]. Thus, it has been shown that parasites can be starved by removal of isoleucine from the culture medium[8].

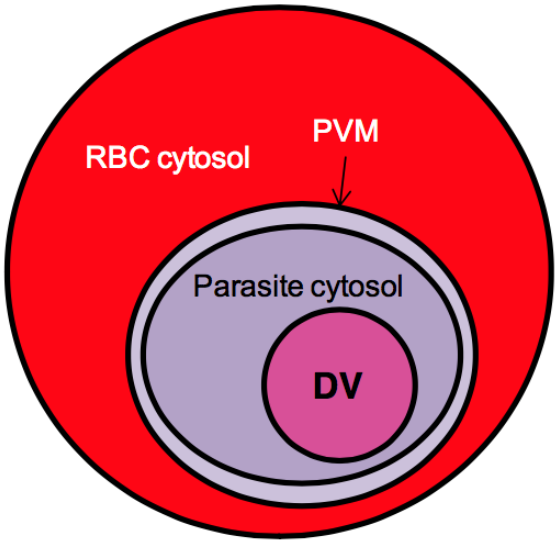

Figure 1. 4 Representation of a trophozoite infected RBC. **S**hows the RBC cytosol, parasitophorous vacuolar membrane (PVM), parasite cytosol and parasite digestive vacuole (DV).

1.2 Autophagy in Apicomplexan Parasites

1.2.1 Cytocidal Drug Resistance

The quantification of antimalarial drug potency is typically conducted via long-term continuous growth inhibition assays which allow for the calculation of an IC_{50} – or the concentration required to inhibit cell growth by fifty percent – for each drug tested[9]. These data were extremely important in elucidating the distinction between chloroquine sensitive (CQS) versus chloroquine resistant (CQR) malaria. It was then discovered, by Fidock *et al.* that the

molecular mechanism of resistance to CQ is primarily driven by mutations in the *Plasmodium falciparum* Chloroquine Resistance Transporter (*Pf*CRT)[10]. A QTL analysis was later conducted, which supported the conclusion that mutated *Pf*CRT is associated with elevated CQ IC_{50}[11]. Mutated *Pf*CRT leads to decreased accumulation of CQ in the parasite digestive vacuole (DV), which in turn, prevents CQ from acting on its target and confers resistance to CQ[3]. There has been extensive work done to characterize the various isoforms of *Pf*CRT and these studies show that there are differing levels of CQ and quinoline resistance conferred by the various isoforms of *Pf*CRT[12-13].

All of the aforementioned studies, however, focus on growth inhibitory effects of quinoline drugs and fail to recognize that, in a clinical setting, parasites are eliminated within hours, which suggests that successful antimalarial therapy not only slows parasite growth but also kills parasites[14]. Typically, plasma concentrations of CQ are in the 1-10 μM range, whereas IC_{50} levels of CQ are in the 10-200 nM range. Resistance to quinolines at clinically relevant concentrations found in human plasma had not been studied until recently. Cabrera *et al.* investigated CQ accumulation at clinically relevant, or cytocidal, concentrations and found that a much higher than expected concentration of CQ or fluorescent NBD - CQ can be found within parasites exhibiting cytocidal CQ resistance[15]. To study drug resistance at clinically relevant concentrations, Paguio *et al.* developed an efficient assay to calculate LD_{50}, or the drug concentration required to kill fifty percent of parasites in a population[14]. Results obtained through this assay showed that fold-differences at IC_{50} shown by CQS versus CQR parasites do not parallel fold-differences shown at LD_{50} – for example, whereas HB3 (CQS) versus Dd2 (CQR) IC_{50}s are ten-fold different, the corresponding LD_{50}s are over one-hundred-fold different[14]. This analysis was conducted on several other quinoline drugs and results showed a similar trend. Taken together, these data led to

the conclusion that molecular mechanisms of quinoline resistance must differ at cytostatic versus cytocidal concentrations[14]. In order to better understand these differences, it is necessary to investigate drug-induced death mechanisms in malaria.

1.2.2 Malaria Cell Death Mechanisms

Since *Plasmodium* parasites lack caspase genes and other genes necessary to encode key apoptosis regulators, it is unlikely that the apoptosis pathway is the cause of drug-induced death in malaria[16]. Importantly, no molecular alterations in the apoptosis pathway have been found for CQR malaria. A QTL analysis on the progeny of a cross between *P. falciparum* strains HB3 (CQS) and Dd2 (CQR) revealed three major loci associated with LD_{50} CQ resistance[17]. First, similar to a QTL analysis done with relation to CQ IC_{50}[11], *Pf*CRT also segregates with elevated LD_{50}; however, the LOD score was ~21 compared to ~40 when IC_{50} is the measured phenotype. This suggests that, although mutations in *Pf*CRT may contribute to observed LD_{50} differences, they are not sufficient to describe the entire cytocidal phenotype. Second, two new chromosomal loci that were not previously associated with cytostatic CQR were found to be associated with elevated LD_{50}. These included a contribution from chr6 and defined a pairwise interaction between chr6 x chr8 loci. Inspection of the chr6 and chr8 loci reveals multiple genes involved in processes linked to vesicle traffic, proteasome function/proteolysis and lipid metabolism. For example, at least 6 genes within the chr8 locus encode proteins putatively involved in the proteasome pathway. Candidate genes were also ranked based on the sequence similarity of strain HB3 (CQS) and strain Dd2 (CQR), and the correlation of expression levels with the LD_{50} phenotype. Four previously vetted methods[18] were used to identify genes or pathways that are most likely relevant to LD_{50}. Interesting genes within the chr6 and chr8 loci that have high CDS scores include putative orthologues of autophagy genes ATG11 and ATG14, several key metabolic regulators, multiple

kinases, and a putative E3 ubiquitin ligase. Also of note are several genes in the chr6 locus linked to response to oxidative stress. Since autophagy is an orchestrated, vesicle mediated, proteolysis/degradative pathway that is distinct from apoptosis and since "vesicle traffic", "proteasome/proteolysis", "lipid metabolism", "oxidative stress" and autophagy pathways often overlap mechanistically, these findings suggested that an autophagy-like pathway may be responsible for drug-induced death at cytocidal drug concentrations in *P. falciparum.*

Autophagy is a mechanism of intracellular degradation that is mediated by double-membrane organelles called autophagosomes[19-20]. Autophagosome formation is dependent on several autophagy-related (Atg) proteins, which were first identified in *S. cerevisiae* yeast[20-21]. These proteins form distinct complexes necessary during initiation and elongation of the autophagosomal membrane[22]. First, the initiation step requires the Atg1-Atg13-Atg17-Atg31-Atg29 complex and Atg9-containing vesicles. Next, the phosphatidylinositol 3-kinase (PI3K) complex (Vps30/Atg6-Atg14-Vps15-Vps34) produces phosphatidylinositol 3-phosphate (PI3P) which recruits the Atg2-Atg18 complex. And finally, the Atg12-Atg5-Atg16 complex and Atg8-phosphatylethanolamine (PE) conjugate are required for elongation of the phagophore membrane and completion of the closure of the autophagosome (Figure 1.5). These proteins are highly conserved in eukaryotes[23].

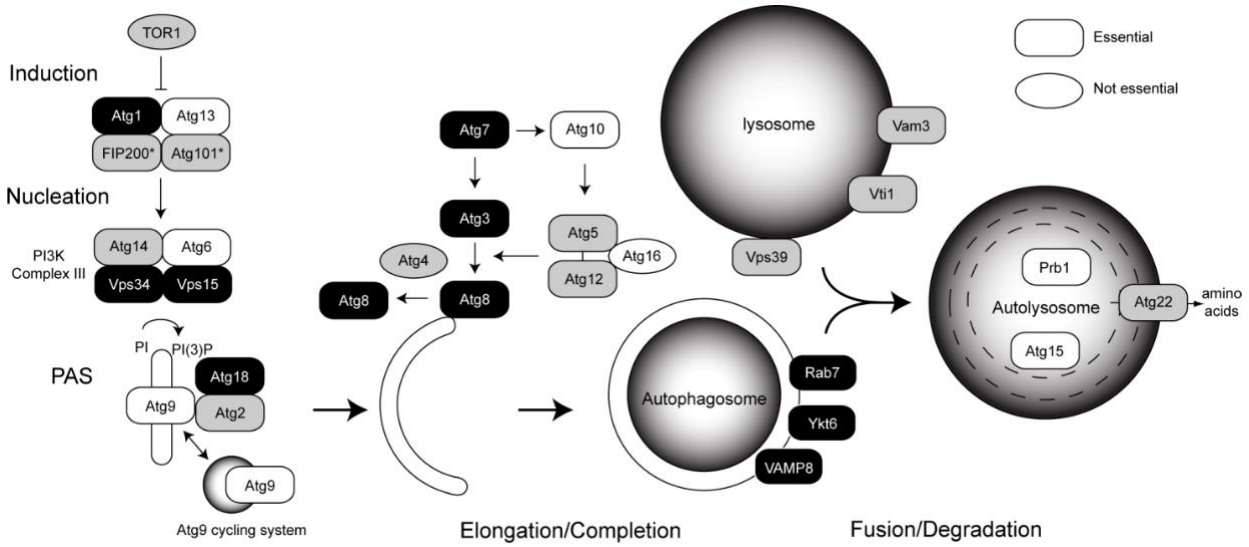

Figure 1.5 Conservation of autophagy proteins in *Plasmodium*. Proteins essential for autophagy are depicted as rectangles. Ovals represent proteins whose essentiality is not known. Black indicates strong evidence for homology (e-value < 1^{-10} in initial BLAST within PlasmoDB). Gray indicates homology less clear (initial e-value cutoff of 0.012). White indicates no orthologue was identified. *Human proteins FIP200 and Atg101 thought to be functional homologues of yeast Atg31/Atg17/Atg29. Reproduced from Hain *et al*[24], available under the creative commons attribution.

However, in apicomplexan parasites such as *P. falciparum* or the related *T. gondii*, only a partial list of Atg proteins are conserved[25] (see also Figure 1.5). Importantly, in both *P. falciparum* and *T. gondii*, the Atg8 conjugation system, including Atg3, Atg4, Atg7, and Atg8, are conserved[26]. Thus, most autophagy related studies in *P. falciparum* and *T. gondii* have focused on Atg8 as a marker protein for the autophagosome[26]. Furthermore, although no orthologue of mTOR has been found in *Plasmodium*, homologues have been discovered of 15 of the 30 autophagy proteins that have been identified in yeast[24]. These include Atg1, Atg2, Atg5, Atg6, Atg12, Atg14, Atg17, Atg18 and Vps34, which may be conserved in *P. falciparum*[25, 27-28] and Atg1, Atg5, Atg6, Atg9, Atg15, Atg18 and Vps34 in *T. gondii*[29]. Interestingly, to date, Vps34 is the only phosphatidylinositol 3'-kinase (PI3K) that has been identified in the *Plasmodium* genome and suggests a possible regulation step in the absence of an mTOR homologue.

Plasmodium parasites lack caspase genes required for apoptosis mediated cell death and no evidence has been found of alterations in the apoptosis pathway in relation to quinoline drug resistance. Because many homologues of autophagy related proteins have been identified in *Plasmodium* and recent discoveries implicate the autophagy pathway in cytocidal chloroquine resistance, it is imperative that the functionality and role as a cell death mechanism of this pathway be further investigated in malaria parasites. It is also useful to investigate the autophagy pathway in related apicomplexan parasites, such as *T. gondii*.

Autophagy is a pathway that utilizes the lysosome as the final organelle in which cellular component are deposited for degradation[24]. In higher eukaryotes, Rab7 is a key regulator in trafficking of endosomal material to the lysosome[30]. Rab7 is necessary to the autophagy pathway in mammalian cells due to its influence on the maturation of autophagosomes[31] and during amino acid starvation, Atg8 and Rab7 colocalize on the autophagosomal membrane[32]. Apicomplexans contain a basic set of Rabs, including Rab7[33]. Specifically, *P. falciparum* parasites possess a family of 11 Rab proteins including a single Rab7 GTPase[34], suggesting that components of the pathway involved with autophagosome maturation exist in malaria parasites. Through electron micrographs, Tomlins *et al.* show that *Pf*Atg8 localizes to double-membrane structures containing *Pf*Rab7 that were near or inside of the parasite DV, which implicates the parasite DV as the final lysosomic compartment during the malaria parasite autophagy cascade[35] and further supports the hypothesis that malaria response to cell death includes an autophagy-like pathway rather than an apoptosis pathway.

1.2.3 Autophagy is a Stress Response Mechanism

Several reports have investigated the role of the autophagy pathway in apicomplexan parasites as a response to external stress, which leads to cell death. This pathway has been

implicated as a cell death mechanism in response to starvation, a commonly known method of inducing autophagy, in both *P. falciparum* and *T. gondii*[17, 29, 31, 35-39]. Atg8 is commonly used as a marker of autophagy as it is associated with the pre-autophagosome membrane at an early stage and remains associated with the autophagosome during fusion with the lysosome, making it an excellent indicator of autophagosome localization in the parasite[35]. In yeast and mammals, Atg8 has a diffuse, cytoplasmic distribution under nutrient rich conditions that becomes punctate upon induction of autophagy[40].

In 2013, Gaviria *et al.*, primarily through immunofluorescence assays using antibodies to the autophagy indicator protein, Atg8, showed that a phenomenon similar to that described in yeast was observed in *P. falciparum*[17]. Under control or nutrient rich conditions, the observed Atg8 staining pattern was diffuse and localized to the parasite cytoplasm. However, upon exposure to nutrient depleted or starvation conditions, the Atg8 distribution changed to a punctate appearance (Figure 1.6)[17]. This suggests that, similar to yeast and other eukaryotes, the autophagy-like pathway in *P. falciparum* can be induced through starvation conditions.

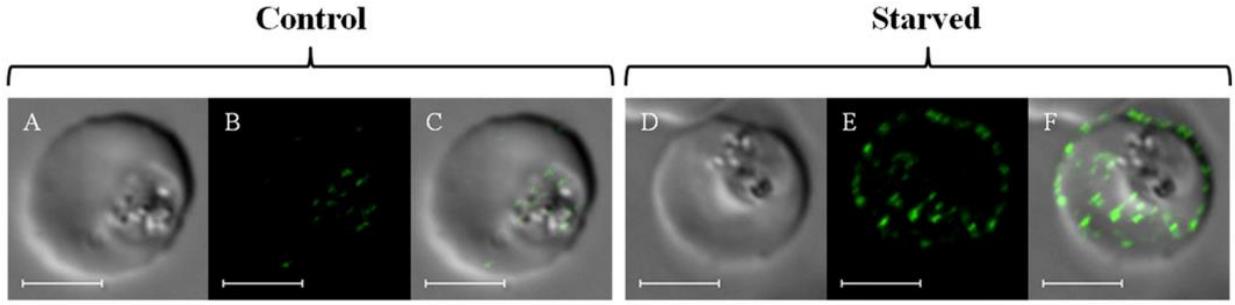

Figure 1. 6 *P. falciparum* parasite immunofluorescence staining visualized using spinning disk confocal microscopy. Atg8 was labelled using TgAtg8 antisera. Panels A and D are transmittance; B and E are Atg8 fluorescence; and C and F are overlays respectively. Left side are control intraerythrocytic HB3 P. falciparum; right side are HB3 starved for 6 hours as described in methods. Bar = 5 µm.

Investigating the role of autophagy as a response to stress in the related apicomplexan parasite, *T. gondii* can also provide useful information about this process. Unlike most

apicomplexans, *T. gondii* parasites are readily amenable to genetic manipulations in the laboratory. Additionally, cell biology studies are more readily performed in *T. gondii* due to the high efficiency of transient and stable transfection, the availability of many cell markers, and the relative ease with which the parasite can be studied using advanced microscopic techniques[41]. Thus, for many experimental questions, *T. gondii* is a useful model system to study the biology of other, related apicomplexan parasites.

In 2012, Ghosh *et al.* described experiments to probe the autophagy pathway in *T. gondii*[38]. It was first observed that under starvation conditions, the single mitochondrion in *T. gondii* cells becomes fragmented, leading to parasite death. To determine the process by which the mitochondrion becomes fragmented, the established PI3K inhibitor, 3-methyl adenine (3-MA) was used. 3-MA is also known to inhibit autophagy by blocking the recruitment of lipid to the autophagosome. Upon addition of 3-MA to the starvation treatment, mitochondrial fragmentation was effectively blocked, suggesting that an autophagy-like process is responsible for *T. gondii* cell-death under starvation conditions. Although these results implicate mitophagy as the process for stress-induced cell death in *T. gondii*, similar mitochondrial fragmentation has not been observed in *P. falciparum*.

Further work by Besteiro *et al.* investigates the localization of TgAtg8 containing vesicles in *T. gondii*[29]. As previously mentioned, Atg8 localization is a commonly used method to probe the activity of the autophagy pathway and under starvation conditions, Atg8 containing vesicles can be seen in a punctate pattern. Besteiro *et al.* conducted immunofluorescence microscopy to visualize the localization of TgAtg8 under nutrient-rich conditions and it was observed that Atg8 is cytosolically localized, as expected. Under amino acid starvation, Atg8 staining was observed

to be punctate, with the number of puncta per parasite also increasing as the incubation time in starvation media was increased to eight hours.

In eukaryotic cells, Atg8 contains a C-terminal arginine residue, which is catalytically cleaved by Atg4 to expose a C-terminal glycine residue on Atg8[42]. However, in apicomplexan parasites, such as *P. falciparum* and *T. gondii,* Atg8 does not possess this C-terminal arginine residue. Instead, the C-terminal glycine residue is constitutively exposed[29, 43-44]. Thus, it is thought that the Atg4 homolog is responsible for recycling improperly conjugated Atg8[42]. When Besteiro *et al.* mutated TgAtg8 to code for a terminal alanine rather than the native glycine, it was observed that fewer or no autophagosomes were labelled with Atg8. Additionally, using known PI3K inhibitors such as 3-MA or wortmannin to investigate the inhibition of autophagy in combination with nutrient depletion showed a reduction in the number of Atg8 labelled puncta. These results provide a strong correlation between Atg8 puncta and induction of the autophagy pathway through starvation. It was also shown that upon Atg3 depletion, few to no autophagosomes were labelled with Atg8, which implies that Atg3 is also necessary for association of Atg8 to the autophagosome membrane.

1.2.4 Autophagy as a Drug Target

Since there is evidence that an autophagy-like process may be responsible for starvation-induced cell-death in *P. falciparum* and *T. gondii*, it is logical, then, to investigate the role of autophagy in drug-induced parasite death as well. Thus, Gaviria *et al.* investigated the effect of CQ on Atg8 labelled puncta in *P. falciparum*[17]. CQ is a lysosomatropic agent that is known to prevent autophagosome-lysosome fusion in higher eukaryotes[45], which is the final step in the autophagy cascade[46-47]. Similar to previous results under starvation conditions, a redistribution of Atg8 puncta was observed under cytocidal concentrations of CQ but not with cytostatic

concentrations of CQ. In addition to the observations from the previously mentioned QTL analysis, in which a novel interaction between chr6 x chr8 was discovered implicating the autophagy pathway, these observations support the hypothesis that cytocidal drug targets and mechanisms of drug resistance are different from that of cytostatic drug targets and mechanisms of resistance. Gaviria *et al.* also discovered that this autophagy-like cascade is dysregulated in CQR parasites[17]. When CQS and CQR parasites are subjected to the same absolute dose of 2XCQS LD_{50} CQ (250 nM CQ), CQS parasites show an induction of Atg8 containing puncta but CQR parasites do not. Upon treatment with similarly effective pharmacologic doses of 2XLD_{50} CQ (250 nM for CQS and 32 µM for CQR), CQR parasites do show an induction of Atg8 containing puncta, however, similar to previous observations under IC_{50} treatment, there are significantly fewer punta per cell vs. CQS parasites (Figure 1.7).

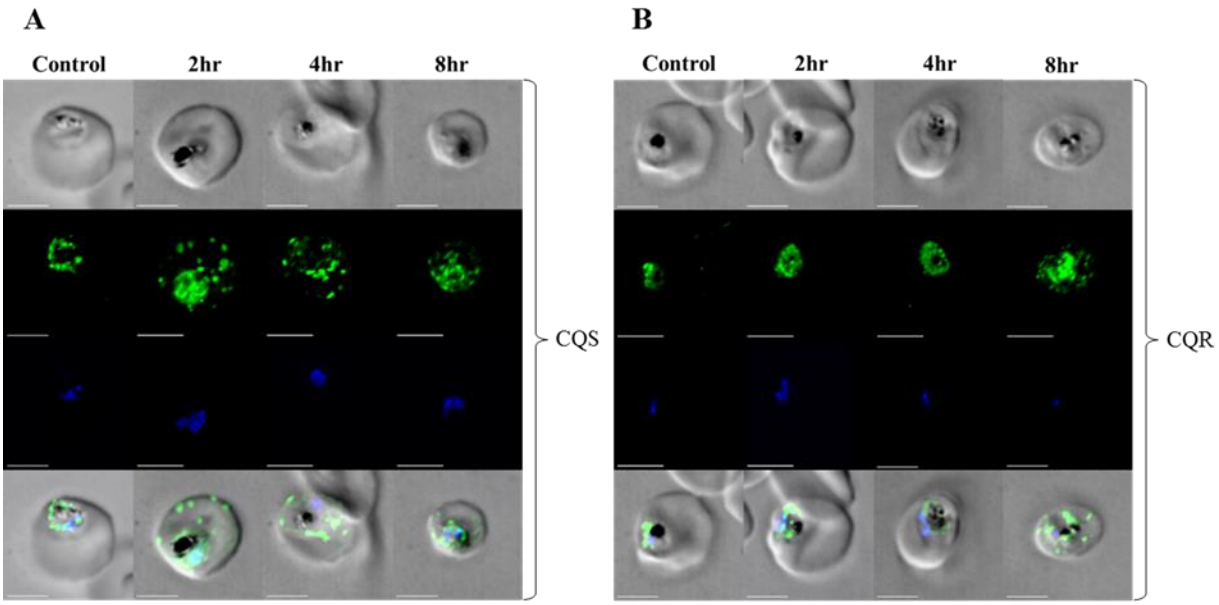

Figure 1. 7 PfAtg8 redistribution, CQ vs. time. Parasites were treated with 2 x LD_{50} dose (250 nM for (A) HB3 [CQS], and 32 µM for (B) Dd2 [CQR]. In each case the transmittance-fluorescence overlay is shown beneath the Atg8 fluorescence alone. Bar = 5 µm. Reproduced with permission from Gaviria *et al.*[17], available under the creative commons attribution.

The importance of the autophagy pathway in drug-induced parasite cell death is further supported by work done in the related apicomplexan parasite *T. gondii*[37-39]. As described above, *T. gondii* parasites provide an easily accessible model organism for studying common pathways in other apicomplexan parasites. Lavine *et al.* investigated *T. gondii* cell death in response to monensin treatment. Similar to *Plasmodium* parasites, no evidence was found to implicate an apoptosis pathway in *T. gondii*[39]. However, treatment of *T. gondii* parasites to a 6 or 24 hour pulse of monensin yielded morphological changes that could be attributed to an autophagy-like pathway[39]. Under treatment with monensin, *T. gondii* parasites experienced a fragmentation of the mitochondria. This result is consistent with previous observations of mitophagy by Ghosh *et al.*[38]. It has also been found that monensin treatment causes an upregulation of Atg1 in *T. gondii*[48]. This is important since Atg1 must be activated in order to initiate the autophagy process[24]. Lavine *et al.* also observed a redistribution of Atg8 labelled puncta upon treatment of monensin, similar to previously described observations[29]: within 3 hours 80% of parasites showed increased Atg8 puncta and decreased cytosolic localization. These results corroborate the findings by Ghosh *et al.* which, together, suggest that a mitophagy process is involved in starvation-mediated and drug-induced *T. gondii* cell death.

Due to the overwhelming evidence that an autophagy-like pathway exists in *P. falciparum* and related apicomplexan parasites, further studies have been conducted to investigate the effects of other antimalarial compounds on the autophagy pathway in *P. falciparum.* In 2015, Mott *et al.* showed that cytocidal concentrations of artemether (ATM) and lumefantrine, components of one of the main-line therapies currently used in artemisinin combination therapies (ACTs), also induce the punctate appearance of Atg8[49]. Artemisinins have been reported to be activated by hemoglobin degradation products, presumably heme or ferrous iron, thus inducing oxidative stress within the

DV[50-51]. These results suggest that oxidative stress is another factor capable of inducing autophagy in *Plasmodium* parasites. Additionally, it was shown that Atg8 puncta are induced by cytocidal concentrations of amodiaquine as well[49].

In addition to studying the ability of stress, such as nutrient starvation or drug-induced cell death, to induce an autophagy-like response in parasites, the inhibition of this pathway has also been studied. The WHO strongly recommends the use of combination antimalarial therapies as opposed to drug monotherapies as a method of reducing the risk of parasite development of drug resistance[1]. By investigating drugs that induce the autophagy pathway and those that independently inhibit this pathway, it should be possible to engineer novel drug combinations that act on the same pathway in different manners, thus reducing the ability of *P. falciparum* parasites to adapt and develop resistance to either drug used in the combination. This thesis begins to explore this principle.

PI3K regulation is essential to the autophagy pathway in all eukaryotes[24-25]. Since Vps34 is the only known PI3K present in *P. falciparum*, the effects of known inhibitors of mammalian PI3Ks – such as GSK-2126458 (GSK) or NVP-BGT226 (NVP) – could provide crucial information on a novel drug target in *Plasmodium* parasites, as well as provide a method of inhibiting the autophagy pathway that may be induced by current front-line antimalarial therapies. Mott *et al.*, via immunofluorescence imaging, showed that when parasites under starvation conditions were treated simultaneously with GSK or NVP, there was a significant decrease in the amount of Atg8 positive-puncta compared to starvation conditions[49] alone – similar to previous observations in *T. gondii* where the known autophagy inhibitor, 3-MA, reduced the number of Atg8 containing puncta[29]. Autophagy is mainly a pro-survival response; however, overstimulation of the autophagy response can lead to cell death[52]. When parasites are starved, their fitness is

compromised, thus autophagy is induced as a survival mechanism. However, administration of an inhibitor simultaneously could also lead to parasite death through blockade of this survival response[49]. If GSK or NVP actually do inhibit *Pf*Vps34 function, it suggests a role for this key regulator protein in the parasite autophagy response. It also suggests that this could be a crucial drug target and that targeting this survival mechanism is deleterious to parasites.

The autophagy process in *Plasmodium* has also been tentatively linked to the recent emergence of the artemisinin (ART) resistance phenotype[53-54]. ART is widely thought to cause oxidative damage in malaria parasites through breakage of the endoperoxide bond. In 2015, Wang *et al.* used a fluorescent ART analog to probe targets of ART in parasites in a proteomics study[53]. Interestingly, it was found that Atg18, which is a phosphatidylinositol 3-phosphate (PI3P) binding protein that is essential to the autophagy pathway, covalently binds to the fluorescent ART probe[55]. This suggests that Atg18 may be one of the molecular targets of ART therapies and further supports the role of autophagy as a response to drug-induced cell death in *P. falciparum*. Additionally, a recent genome-wide association study identified that a locus on chr10 containing Atg18 was associated with decreased sensitivity to DHA and ATM[53]. This analysis was done employing common antimalarials and several genetic loci associated with them were found in 94 *P. falciparum* isolates from the China-Myanmar border area, a region with the longest history of ART therapy. Specifically, it was discovered that a T38N mutation in Atg18 was associated with decreased DHA and ATM susceptibility. This suggests that, not only is Atg18 a potential molecular target of ART therapies, but also Atg18 could be linked to the observed ART delayed clearance phenotype observed in Southeast Asia.

ART resistance is primarily characterized by mutations in the kelch domain of a protein on chromosome 13 (K13) in *P. falciparum* parasites[56-57]. A study by Mbengue *et al.* investigating the

role of Vps34 in ART resistance[54] discovered that K13 mutant parasites show increased levels of Vps34 and, in turn, increased levels of the Vps34 product, PI3P. This study implies that increased expression of Vps34 may be linked to decreased sensitivity to ART compounds in mutant K13 parasite strains[54]. This further highlights the necessity of investigating novel methods to target the autophagy pathway in *P. falciparum* in order to circumvent developing drug resistance – the use of PI3K inhibitors is just one method of attacking this problem.

Taken together, the aforementioned studies provide evidence that first, cytocidal – or cell-kill effects of antimalarial drug must be investigated to better understand the molecular targets of these drugs. Also, it is important to note that multiple studies have shown that apicomplexan parasites such as *P. falciparum* and *T. gondii* possess machinery necessary for the autophagy pathway and that this pathway may be a response to stress, either by starvation or drug treatment. Most significantly, the autophagy pathway has been implicated as a mechanism of *P. falciparum* resistance to quinolines as well as artemisinins. Additionally, there is evidence that this pathway can be independently targeted by PI3K inhibitors, as a means to suppress the parasite survival mechanism under external stress. In turn, investigating these approaches can lead to novel candidate antimalarial combination therapies that are more effective at killing parasites and preventing the rise of antimalarial drug resistance.

1.3 Resistance to Artemisinin Combination Therapies

1.3.1 Artemisinin Combination Therapies

Artemisinin (ART) Combination Therapies (ACT) are currently the front-line therapy for treating *Plasmodium falciparum* malaria. The World Health Organization strongly urges regulatory authorities in malaria endemic countries to halt the production and use of antimalarial monotherapies in favor of using combination therapies[1]. It is widely accepted that drug combination therapies are more effective at killing parasites than monotherapies and are vital in reducing the possibility of parasites developing resistance to either compound. These recommended drug combinations typically include a fast-acting compound (such as artemisinin, which exerts its effects within 1-2 hours to quickly kill parasites and is eliminated from the body within hours) and a slow-acting partner drug (such as quinolines, which have a longer half-life on the order of days and exist in the human blood-stream for extended periods of time after treatment to prevent recurrence of the parasite infection). Commercial ACTs include combinations of: artemether-lumefantrine (Coartem) and dihydroartemisinin-piperaquine (Duo-cotecxin), two of the few ACTs still effective against multidrug-resistant *P. falciparum* in Southeast Asia. Recent reports of an artemisinin Delayed Clearance Phenotype (DCP) in *P. falciparum* may portend the evolution of resistance to artemisinin related endoperoxide compounds and commonly used ACTs[58-60]. The development of artemisinin resistance is of significant concern especially in Cambodia and Thailand, where the first reports of DCP originated[61-63], especially since the Thai-Cambodia border is considered the world's hot-spot for the development of *P. falciparum* multidrug resistance[64]. Artemisinin resistance was first suspected in 2002 to 2005 and the first cases of DCP were reported in 2008 and 2009.

1.3.2 Delayed Clearance Phenotype

Clinically, the artemisinin resistance phenotype is defined as either: 1) a patient having a parasite clearance half-time of greater than 5 hours or 2) a patient having detectable parasitemia on the third day of drug treatment[58]. Recently, resistance to the partner drug in Duo-Cotecxin – piperaquine (PPQ) – has also been reported[53, 65-67]. Previous reports showed a delayed parasite clearance, however, patients were still cured of malaria. Delayed clearance meant that ACT treatment may have been required for 4 days instead of the normal 3 day treatment[68]. However, recent reports have been published of complete ACT treatment failure, which implies parasites have become resistant to both the fast-acting and slow-acting drugs in the combination[53, 65-67]. Additionally, the possibility of spread or emergence of artemisinin resistance within Africa, where the majority of malaria related deaths occur[69], is of enormous concern as well as the complete failure of other ACTs. Thus, it is crucial to investigate the mechanisms of ART resistance and examine compounds that may be able to circumvent these resistance mechanisms before ART resistance becomes a more widespread issue.

Traditionally, the quantification of drug resistance has been done by comparing IC_{50} values. These assays quantify the concentration of drug required to inhibit parasite growth by 50%. In other words, IC_{50} calculates the cytostatic potency of a drug. However, reports have shown that the IC_{50} assay cannot distinguish the ART resistance phenotype[61-63]. In 2010, Witkowski *et al.* reported on a parasite strain that was subjected, under laboratory conditions, to three years of artemisinin drug pressure. This strain, F32-ART, was able to tolerate up to 9 µM ART and was established as a laboratory derived artemisinin resistant strain[70]. Interestingly, the F32-ART strain was not distinguishable from the F32-control (non-drug pressured) strain via IC_{50} (~9.9 nM ART IC_{50}). Thus, Witkowski *et al.* reported the first assay to successfully correlate in-vitro findings with

ART sensitivity. An assay was developed in which parasites were treated with high micromolar doses of ART for 48 or 96 hours, after which the parasites were returned to drug-free media and allowed to grow. The time it took for cultures to reach 5% parasitemia was recorded by giemsa staining as well as by Rhodamine 123 fluorescent staining. Not only did this assay correlate a quicker recovery time with the F32-ART resistant strain, but also it elucidated a quiescence mechanism displayed by synchronized, ring-stage parasites as a method of ART tolerance.

1.3.3 Ring-Stage Susceptibility Assay

In 2013, Witkowski *et al.* developed an assay to better quantify the ART resistance phenotype and characterized several laboratory adapted isolates using the ring-stage susceptibility assay (RSA)[57, 71]. In the RSA, early ring-stage parasites are bolus-dosed with 700 nM dihydroartemisinin (DHA) for six hours (a physiologically relevant dose and incubation time)[72-73]. The parasites are then washed, cultured in drug-free media, and relative survival then determined at 66 hours after removal of the drug. In the Witkowski method, parasite survival is measured microscopically from giemsa smears, by two microscopists from whom each other's data were masked[57]. Each microscopist counted at least 10,000 erythrocytes from giemsa smears of each sample. If the disagreement between the two microscopists was greater than 20%, a third microscopist would assess the slides. Quantitatively, the RSA allows for the calculation of percentage of parasite survival after a bolus dose of 700 nM DHA and survival rates were directly correlated with observations of clinical clearance time. Typically, sensitive parasite strains have an RSA survival of ~0-1% and resistant strains have an RSA survival of >10%.

Amaratunga *et al.* subsequently introduced the use of two-color flow-cytometry to accelerate analysis of RSA data[74]. This method utilizes the DNA intercalating properties of SYBR Green I and the membrane potential response of MitoTracker Deep Red to identify infected

erythrocytes and subsequently categorize them as viable or non-viable. While MitoTracker Deep Red has been shown to selectively accumulate within intact mitochondrial membranes in mammalian cells as an indicator of a large membrane potential[75], there has been little evidence to discern the mitochondrial membrane potential in *P. falciparum* parasites. *P. falciparum* parasites have acristate mitochondria[76] and, although they do not conduct oxidative phosphorylation, there is evidence that these parasites still require mitochondrial energy in the form of the electron transport chain[77]. MitoTracker dyes accumulate within membranes with high potential energy and it is still unknown whether *P. falciparum* parasite mitochondria possess a membrane potential great enough to cause MitoTracker accumulation. However, results from the Amaratunga *et al.* RSA[74] do agree with results from the Witkowski *et al.* RSA[57] and thus, the Amaratunga *et al.* method is used as a more effective method of quantifying ART sensitivity (Figure 1.8).

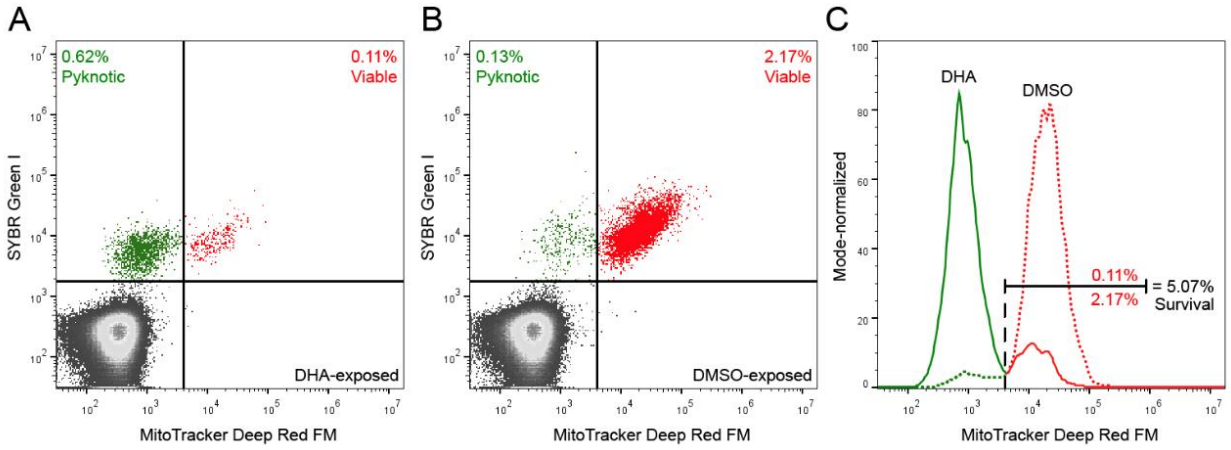

D

	KH1 (wildtype)		KH2 (C580Y)		KH3 (R539T)		KH4 (Y493H)	
	Microscopy	Flow cytometry	Microscopy	Flow cytometry	Microscopy	Flow cytometry	Microscopy	Flow cytometry
% survival	0.00	1.13	8.58	12.86	27.38	28.31	3.12	4.70
% survival	0.27	1.06	10.51	10.51	27.00	30.44	4.13	4.29
% survival	0.33	0.64	9.23	12.55	29.86	30.90	4.63	5.02
Mean % survival	0.20	0.94	9.44	11.97	28.08	29.88	3.96	4.67
Std. Deviation	0.18	0.26	0.98	1.28	1.55	1.38	0.77	0.36
p-value	0.10		0.20		0.20		0.20	

Figure 1. 8 Flow cytometry scatterplots. Scatterplots of DHA- **(A)** and DMSO-exposed **(B)** *Plasmodium falciparum* parasites stained with SYBR® Green I (SG) and MitoTracker® Deep Red FM (MTDR). In each plot, the percentage of viable parasites in 250,000 events is shown in the upper-right quadrant. In a mode-normalized histogram overlay **(C)** of these upper quadrants, populations of viable and pyknotic parasites are clearly separated in both samples. Percent survival values for four Cambodian parasite isolates that differ in KH subpopulation (KH1, KH2, KH3, and KH4) and K13-propeller allele (WT, C580Y, R539T, and Y493H) are shown in **(D)**. For each isolate, percent survival values calculated from microscopy or flow cytometry data were not significantly different. Data from three independent experiments per isolate are shown. Reprinted with permission from Amaratunga *et al.*[74].

1.3.4 Molecular Marker of Artemisinin Resistance

There are many reports published that seek to determine the molecular mechanisms of ART resistance[50, 54, 56, 68, 78-82]. Approaches such as long-term growth assays, genome-wide association analyses, genetic engineering of *P. falciparum* parasites, and targeted drug screens have been done in an attempt to discover the molecular target of artemisinins as well as the mechanism by which parasites evade artemisinin treatment.

Multiple reports agree that a prolonged ring-stage and a quiescence mechanism during the ring-stage contribute to ART resistance[70, 83-86]. It is believed that ARTs require hemoglobin metabolism in order to exert oxidative damage to parasites, leading to parasite death[51]. Thus, a quiescent mechanism – or a method of prolonging the ring-stage – in essence, shields ART resistant parasites from the toxic effects of the drug. Witkowski *et al.* used a laboratory derived ART resistant strain (F32-ART- can withstand up to 9 µM ART) to microscopically visualize the effects of ART treatment compared to parasites grown under control conditions over the same course of 4 days[70]. Witkowski *et al.* effectively showed that the F32-ART resistant parasites were able to enter a quiescent state, evidenced by the continual appearance of ring-stages only during a 48-hour drug incubation (Figure 1.9). After removal of the drug, the parasites recovered and proceeded through the normal parasite life-cycle stages.

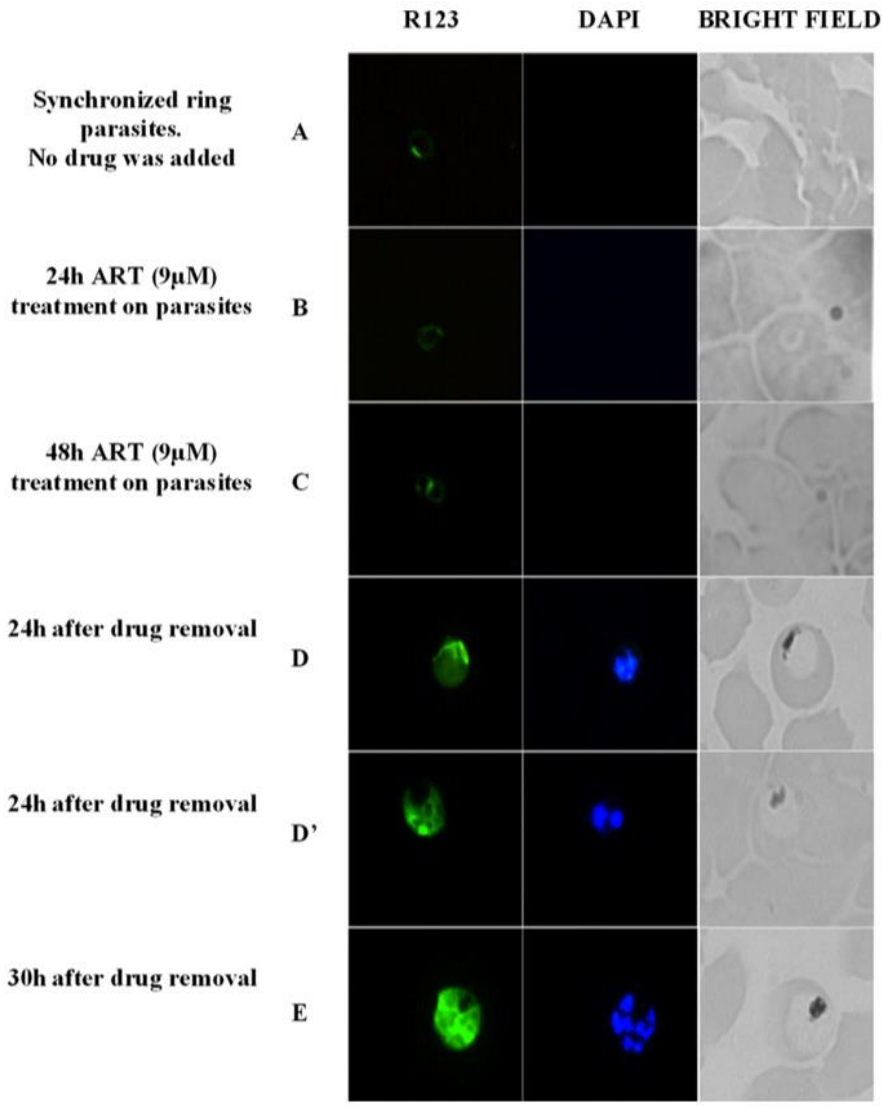

Figure 1. 9 Epifluorescence observations of parasites with or without drug pressure. **(A)** Before drug pressure, ring forms are present (Rhodamine123 [R123] positive; not detectable with DAPI; no visible hemozoin). **(B)** After 24 h of drug pressure, quiescent ring forms are the only viable stage present. **(C)** After 48 h of drug pressure, quiescent ring forms are the only viable stage present. **(D and D')** Restoration of the parasite cycle with the presence of mature trophozoites and young schizonts, respectively, 24 h after drug removal. **(E)** The presence of mature schizonts 30 h after drug removal. Reprinted with permission from Witkowski *et al*.[70].

Another consensus has been reached in the field is that single-nucleotide polymorphisms (SNPs) in the propeller domains of a kelch domain-containing protein on chromosome 13 (K13)

confer ART resistance[56, 87]. In 2014, Straimer *et al.* genetically engineered *P. falciparum* laboratory adapted isolates from Cambodia, as well as non-Cambodian parasite strains, to more quantitatively assess the contribution of these K13 mutations to the RSA phenotype of each strain[87]. The RSA has been shown to correlate well with clinical observations of ART resistance displayed by delayed clearance and is used to predict clinical outcomes through in-vitro methods[57, 74]. Straimer *et al.* effectively show that, by introducing a novel K13 mutation to non-Cambodian laboratory strains (that were previously K13-wild type), it is possible to induce ART resistance evidenced by a higher percentage survival in the RSA[87]. Importantly, these findings also suggest that, while K13 mutations are necessary to explain the RSA and clinical phenotype of ART resistance, these mutations are not sufficient to account for the full observed phenotype (Figure 1.10). In other words, Cambodian isolates with differing genetic backgrounds and identical K13 mutations show varying RSA phenotypes. This implies that there are other factors in the parasite genetic background, separate from the K13 locus, which also determine ART sensitivity.

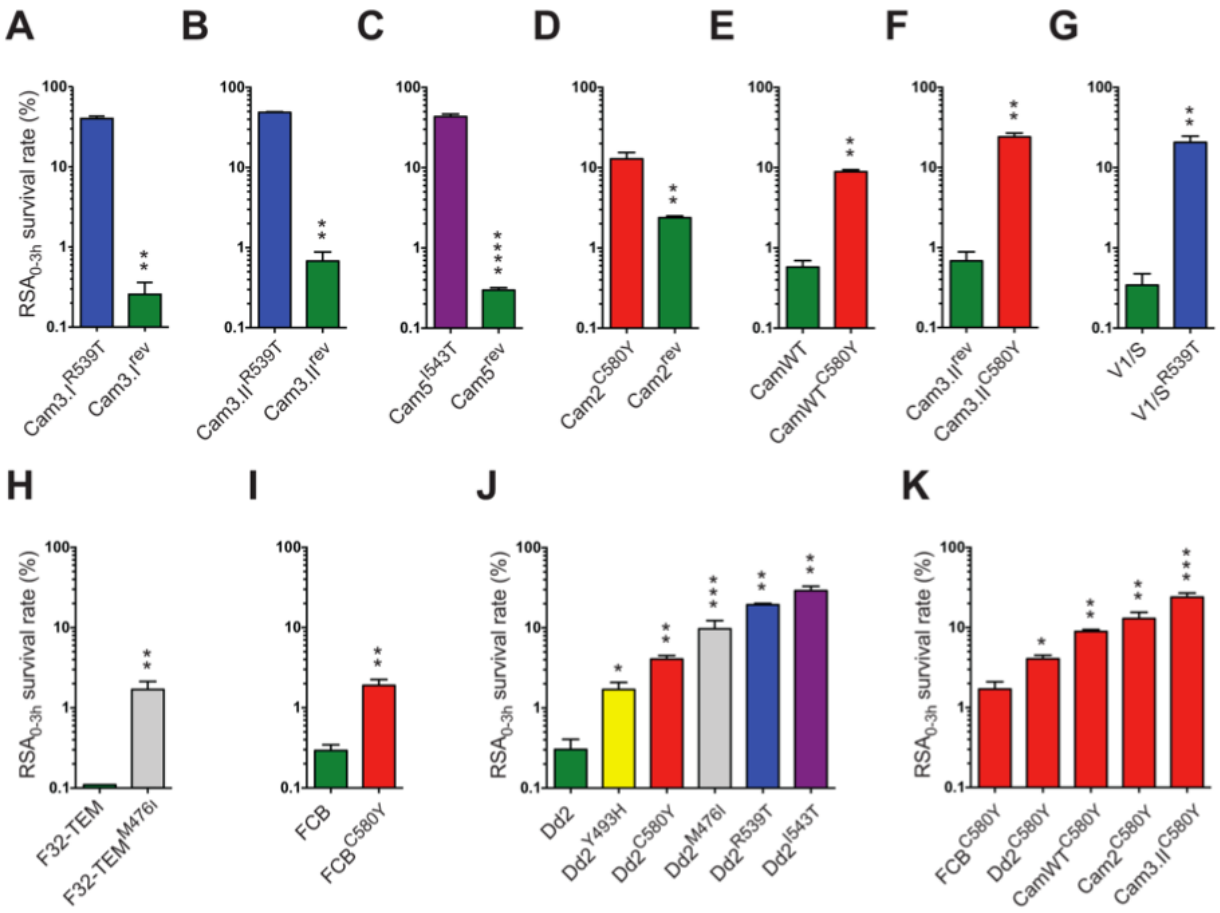

Figure 1. 10 K13-propeller mutations confer artemisinin resistance in clinical isolates and reference lines in vitro, as defined in the Ring-stage Survival Assay (RSA0-3h). (A–D) RSA0-3h survival for Cambodian isolates harboring native K13 mutations (shown in superscript) and ZFN-edited isogenic clones carrying wild-type K13 alleles (superscript "rev"). (E–I) RSA0-3h survival for Cambodian isolates and reference lines harboring wild-type K13 alleles and ZFN-edited isogenic clones carrying individual K13 mutations (shown in superscripts). (J) Impact of different K13 mutations on RSA0-3h survival in the Dd2 reference line, showing that I543T and R539T confer the highest levels of resistance. (K) Introduction of C580Y into multiple Cambodian clinical isolates and reference lines, showing that this mutation confers varying degrees of in vitro resistance depending on the parasite genetic background. Reprinted with permission from Straimer et al.[87]

While it is widely accepted that K13 mutations are a marker of ART resistance, Straimer *et al.*, indicate that there are other molecular mechanisms that are also responsible for the observed phenotype. Also, it is not clear what the function of the K13 protein might be, since the protein

has no known orthologues in other eukaryotes. It might be possible then that the unknown function of PfK13 involves some role in autophagy or autophagy signaling.

Components in the autophagy process in *Plasmodium* have also been tentatively linked to the recent emergence of the artemisinin (ART) resistance phenotype. A recent genome-wide association study identified that a locus on chr10 containing Atg18 was associated with decreased sensitivity to DHA and ATM[53]. A study by Mbengue *et al.* investigating the role of Vps34 in ART resistance discovered that K13 mutant parasites show increased levels of Vps34 and suggested that this may be linked to decreased sensitivity to ART compounds in mutant K13 parasite strains[54]. Studies have been done to investigate possible additional factors leading to ART resistance, including genome-wide analyses of ART resistant and sensitive isolates from Cambodia. These studies have found multiple targets of endoperoxide compounds in *P. falciparum* parasites. Some such targets include fd (ferredoxin), arps10 (apicoplast ribosomal protein 10), mdr2 (multidrug resistance protein 2), and crt (chloroquine resistance transporter)[81]. In addition to the widely-studied SNPs found in K13 associated with ART resistance, other SNPs have been implicated as possibly contributing to ART resistance as well. These include SNPs on chromosomes 10, 13 (apart from the K13 locus) and 14[80].

In 2015, Mok *et al.* found 487 genes that were up-regulated and 511 genes that were down-regulated in association with longer clearance half-life and thus also in association with ART resistance[82]. In particular, genes that were up-regulated included those involved in protein metabolism, such as endoplasmic reticulum retention sequences, un-folded protein binding, protein folding, protein export, posttranslational translocation, signal recognition particle (SRP), proteasome, and phagosome. Most of the up-regulated pathways are known to participate in the

overall unfolded protein response (UPR) in other eukaryotic species. Mok *et al.* suggest that an up-regulated UPR may contribute to ART resistance in *P. falciparum*.

The aforementioned studies show that while there is a general understanding of markers of ART resistance, much is still unknown about the molecular mechanisms of *P. falciparum* ART resistance.

1.4 Drug Combination Analysis

As previously mentioned, artemisinin combination therapies are currently the frontline treatment for *P. falciparum* malaria worldwide and the WHO strongly recommends against the use of antimalarial monotherapies[1]. The use of *Artemisia annua* (Qing Hao) as a traditional Chinese pharmacopeia included the treatment of fevers and chills[88-89]. In the 1970s, the active principle in this extract was isolated and identified as artemisinin, a sesquiterpene lactone. The effectiveness of artemisinin is structurally due to the trioxane pharmacophore and compound activation occurs via the cleavage of the endoperoxide bridge[90]. Optimization for solubility and other desirable pharmacokinetic properties led to the development of related endoperoxide compounds: artemether (ATM), dihydroartemisinin (DHA), artesunate (ATS), and artemisone (AMS). Recently, the synthetic ozonide compounds OZ277 and OZ439, have also been developed to add to the repertoire of compounds thought to cause oxidative damage in *P. falciparum* parasites[91-92].

Typically, ACTs consist of a fast-acting compound (such as artemisinin, which exerts its effects within 1-2 hours to quickly kill parasites and is eliminated from the body within hours) and a slow-acting partner drug (such as quinolines, which have a longer half-life on the order of days and exist in the human blood-stream for extended periods of time after treatment preventing the recurrence of the parasite infection). Commercial ACTs include combinations of: artemether-lumefantrine (Coartem) and dihydroartemisinin-piperaquine (Duo-cotecxin).

The available reports of ART-lumefantrine (LUM) synergy trace back to a study by Alin *et al*. in 1999 that utilized a commonly-used technique known as checkerboard analysis to quantify the interaction via a probit method of data analysis[93]. Examining two strains, T-996 and LS-21, the authors noted synergy at the IC_{50}, IC_{90}, and IC_{99} levels, by converting growth data into quantile units. The determination of synergy is based on predicted growth of the parasites, assuming the two compounds act independently[93]. Additionally, a study in 2007 by Thriemer *et al.* identified IC_{50} synergy between LUM and DHA utilizing the isobologram method[94], and Wong *et al*. identified slight synergy between DHA and the LUM metabolite desbutyl-lumefantrine utilizing the same technique[95].

As previously described, the Thai-Cambodia border region is a hot-spot for emerging drug resistance in *P. falciparum* and most recently, resistance to ART and PPQ have been reported as well. It is imperative that novel drug combinations be explored before complete failure of front-line antimalarial therapies. Techniques to identify synergistic partner drugs, as mentioned above, include altering the concentrations and relative ratios of drugs through a checkerboard pattern on the assay plate, as well as fixed-ratio serial dilutions. Either technique can be used to generate the plot used to identify the interaction, known as an isobologram. Isobologram analysis requires the analysis of many ratios of concentrations of the drugs in question, which leads to an extremely time consuming experiment, requiring many assays to complete.

In 1984, Chou and Talalay developed a simpler method to identify the type of drug interaction which only examines one drug concentration ratio at a time[96]. The fractional inhibitory concentration (FIC) for each drug are calculated (Equation 1-3), which compare the activity of each drug in combination with their activities when used as monotherapies. However, instead of

plotting them on a graph as with isobolograms, these values are summed to generate a combination index, or fractional inhibitory concentration index (FIC_{Index}).

$$FIC_A = \frac{IC_{50}\ of\ Drug\ A\ in\ Combination}{IC_{50}\ of\ Drug\ A\ alone} \qquad \text{(Equation 1)}$$

$$FIC_B = \frac{IC_{50}\ of\ Drug\ B\ in\ Combination}{IC_{50}\ of\ Drug\ B\ alone} \qquad \text{(Equation 2)}$$

$$FIC_{Index} = FIC_A + FIC_B \qquad \text{(Equation 3)}$$

The Chou-Talalay analysis also provides a clear definition of synergy versus additivity versus antagonism[96]. For instance, if the presence of an inactive compound simply augments the activity of a drug, this is not synergy; it is potentiation. Synergy requires the presence of two active compounds. Additionally, the combined activity of drugs A and B being greater than the monotherapies does not mean the combination is necessarily synergistic; such a result could be caused by additive or slight antagonistic interactions[97]. Based on their calculations, Chou and Talalay define additivity when the FIC_{Index} equals 1. When the FIC_{Index} is less than 1, the interaction is synergistic; when it is greater than 1, the interaction is antagonistic[96]. Synergy could potentially arise from inhibition of pathways that undergo downstream cross-talk, or through interacting with the same pathway in two different locations, or perhaps by inhibiting two different pathways completely. The isobologram or Chou-Talalay analysis only determines the nature of the interaction, not how it comes to be.

Although those cut-offs hold mathematically, experimental variance leads to alteration. The cut-offs used in experimental analysis can vary from synergy less than 0.5 and antagonism greater than 4[98], to just expanding the additive range to run from 1 to 2[99]. The choice of cut-offs can be somewhat arbitrary. The Chou-Talalay method has been widely used to investigate the interactions of antimalarial compounds such as artemisinin in combination with other natural

products isolated from ART tea[100], the analysis of possible drug partners emetine/DHA[99], tapsigargin/ART, tapsigargin/OZ227[101], and the interaction of chalcone derivatives and ART[102].

Importantly, until recently all examination of drug combinations *in vitro* focused on cytostatic conditions. Recent examination of combinations at both the cytostatic and cytocidal levels demonstrates the possibility of altered interaction, not only between CQS and CQR strains, but also within the same strain at different levels[103]. For instance, the combination of CQ and amodiaquine (AQ) in Dd2 parasites is additive at the cytostatic level, but highly antagonistic under cytocidal conditions. Such differences reinforce the need to examine possible novel combination therapies at both cytostatic and cytocidal levels to generate a complete description of the interaction.

1.5 Objectives

To completely understand resistance to a drug, it is important to understand the targets of the drug not only at the cytostatic level but also the cytocidal level. Mechanism of resistance at the cytostatic level may give vital insight in to developing therapies to overcome resistance, however, the more critical mechanisms of resistance that aids in developing therapies appear when investigating drug resistance at a cytocidal level. This is the level of drug the parasites endure clinically and thus are killed by. The importance of investigating parasite resistance to drug-induced death gets amplified when looking at the obstacle of drug resistance from a clinical perspective. The first part of this study will aim to achieve exactly this: studying the resistance to CQ at cytocidal levels of the drug. Traditionally drug resistance has always been studied with respect to the difference in IC_{50} or growth inhibitory concentrations. However, as mentioned above, parasites are killed when a drug is administered to a patient, not merely growth inhibited. This was made accessible by the development of an efficient assay to assess cytocidal activity of

drugs by Paguio *et al.* Using this assay in combination with quantitative trait loci (QTL) analysis, genetic loci associated with cytocidal CQ resistance will be studied. Results from this initial analysis will be further investigated giving new insight into death mechanisms in *Plasmodium* parasites as well as the mechanisms of resistance to drug-induced cell kill.

It is important, not only to investigate cidality in *Plasmodium* parasites, but also to identify novel therapies to overcome resistance to cydality. This can be done by identifying drugs that are active against resistant as well as sensitive parasites. The current recommendation by the WHO is to administer drugs as combinations in order to prevent the rise of resistance to new therapies: ACTs are examples. Although effective, most ACTs were found empirically without investigation of drug-drug interactions or mode of action (MOA). This has resulted in ACTs that have partner drugs that act on similar pathways: Coartem is an example. Thus, mutations that alter the sensitivity to one drug may also alter the effectiveness the partner drug. Ideal partner drugs would have compatible pharmacokinetics and pharmacodynamics, modes of action (MOA) that do not promote concurrent resistance, efficacy against existing drug-resistant parasites, and no toxicity. To identify such combinations, our laboratory pursued a high-throughput drug combination screen in collaboration with the National Center for Advancing Translational Science (NCATS), using compounds having diverse MOAs. Leads from these assays were further analyzed to understand drug targets and *in vivo* activity.

A more recent and critical burden faced in efforts to eliminate malaria from the world is the emergence of resistance to ACTs. What first appeared as a delayed clearance phenotype (DCP) has now developed in to treatment failure and recrudescence. Thus, the most significant challenge the malaria community faces now is identifying mechanisms of resistance to ACTs and developing combination therapies to overcome resistance. As mentioned above, previous efforts to develop

ACTs did not consider drug MOAs when choosing partner drugs. Thus, ACTs such as ATM-LUM (Coartem) consist of two drugs that act on similar pathways. Going forward, it is crucial to investigate combination therapies that take into account the drug MOAs and pair two compounds that are not only potent antimalarials but also target different molecular pathways in malaria parasites or target the same pathway at different locations. Mutations in the kelch domain of a protein on chromosome 13 (K13) have been shown to correlate with the clinical DCP. Due to the rise of resistance to current treatments containing ART, ATM or DHA, additional endoperoxide containing compounds and novel synthetic ozonides will be investigated against both wild-type and mutant K13 parasite strains to investigate cross-resistance. More recent studies have also implicated components of the autophagy pathway in the mechanism of resistance to artemisinins. Thus, the autophagy pathway in parasites exhibiting a mutated as well as wild-type K13 will be investigated. Finally, drugs such as PI3K - which possess a potentially different mechanism of action versus endoperoxides - inhibitors will be evaluated as potential partner drugs along with traditional artemisinins as well as more recently discovered ozonide endoperoxide compounds, particularly OZ439, which have shown promise in clinical trials as monotherapy.

CHAPTER II

MATERIALS & METHODS

2.1 Materials

Routine chemicals, media, and solvents were reagent grade or better, purchased from Sigma-Aldrich (St. Louis, MO) or Fisher Scientific (Newark, DE), and used without further purification, unless otherwise noted. Sterile Tissue culture and all other laboratory plastics were purchased from Fisher Scientific (Newark, DE).

AQ dihydrochloride dihydrate, CQ diphosphate, and QD hydrochloride monohydrate were purchased from Sigma-Aldrich (St. Louis, MO). Compounds for high-throughput screening were obtained from suppliers such as Tocris Bioscience, Selleck Chemicals, Santa Cruz Biotechnology and Sigma Aldrich. GSK212, NVP BGT226, Torin2, and PIK 93 were provided by the Thomas Laboratory at the National Center for Advancing Translational Science (NCATS) at the National Institutes of Health (NIH)

Plasmodium falciparum clone HB3 (Honduras, CQS), Dd2 (Indochina, CQR), 7G8 (Brazil, CQR), and FCB (Thailand/S. Africa, CQR), and progeny of the HB3 × Dd2 genetic cross GCO3 (CQS) were obtained from the Malaria Research and Reference Reagent Resource Center (Manassass, VA). CamWT, CamWT^{C580Y}, Cam3.II^{Rev}, Cam3.II^{C580Y} and Cam3.II^{R539T} were obtained from Dr. David Fidock at the Department of Microbiology and Immunology at Columbia University.

Fura-2 AM and dextran-conjugated Fura-2 were purchased from Invitrogen Corporation (Carlsbad, CA). Ionomycin, poly-L-lysine, RPMI 1640, hypoxanthine, and Giemsa stain were from Sigma-Aldrich (St. Louis, MO). No. 1.5 coverslips and HBSS buffer (without free calcium, magnesium, and phenol) were ordered from Fisher Scientific (Pittsburgh, PA). EGTA was

obtained from VWR (Batavia, IL). All other chemicals were reagent grade or better and purchased from commercial sources.

Rabbit anti-TgAtg8 antisera and affinity-purified Rabbit anti-TgAtg8 IgG were obtained from Dr. Anthony Sinai at University of Kentucky. Mouse anti-TgAtg8 monoclonal antibodies are described in section 2.2.5. Rabbit anti-PfREX1 antiserum was obtained from Dr. Don Gardiner at The Queensland Institute of Medical Research. Rat anti-PfACP antibodies were obtained from Dr. Sean Prigge at Johns Hopkins University. Goat serum, goat anti-rabbit and, goat anti-mouse fluorescently-labeled secondary antibodies (conjugated to DyLight 488, 594, and 649 fluorophores) were obtained from Jackson Immunoresearch Laboratories, Inc (West Grove, PA). Goat anti-rat AlexaFluor594 secondary antibodies were obtained from Invitrogen. 10X PBS, 10X PBS-Tween 20, and 100% Triton X-100 were obtained through Fisher Scientific (Pittsburgh, PA). Paraformaldehyde, 10% glutaraldehyde, and Fluoregel mounting media with TES buffer were obtained from Electron Microscopy Sciences (Hatfield, PA).

2.2 Methods

2.2.1 *Plasmodium falciparum* Culturing

Off-the-clot, heat-inactivated pooled type O^+ human serum and type O^+ human whole blood were purchased from Valley Biomedical Products and Services, Inc. (Winchester, VA). Custom 5% O_2/5% CO_2/90% N_2 gas blend was purchased from Roberts Oxygen (Rockville, MD).

All *P. falciparum* strains were maintained using the method of Trager and Jensen[104] with minor modifications[15]. Briefly, cultures were maintained under an atmosphere containing 5% CO_2, 5% O_2, and 90% N_2 gaseous mix at 2% hematocrit and 1-2% parasitemia in RPMI 1640 supplemented with 10% type O^+ human serum, 25 mM HEPES (pH 7.4), 23 mM $NaHCO_3$, 11 mM glucose, 0.75

mM hypoxanthine, and 20 μg/L gentamicin, with regular media changes every 48 h. Parasites were synchronized to the ring stage by treatment with 5% (w/v) sorbitol for 10 min, as needed. Parasitemia was cut down regularly by getting an aliquot of the iRBC culture and diluting with freshly washed RBCs. Fresh RBCs were initially washed 4 times with incomplete media (IM) (RPMI 1640, 24mM $NaHCO_3$, 11mM glucose, 0.75mM hypoxanthine, pH 7.4), kept as a 50% suspension in IM, and stored at 4 °C. For experiments, hematocrit was cut to 1% and parasitemia set to > 5%.

All cultures were routinely synchronized by 5% D-sorbitol treatments to obtain rings as described in detail[6]. The first two treatments are in cell cycle 1, 4 and 14 h after the first visually observed RBC invasion event (most of the culture consists of schizonts). In this way, 0−4-hour-old rings are primarily left after the first synchronization, and lingering other stages are further eliminated at 14 h. The third treatment is 4 h after the first observed invasion in the following cell cycle. In general, parasite cultures were centrifuged at 1500 rpm for 5 minutes and the supernatant discarded. 5% D-sorbitol was added at 5 times the volume of the pellet and incubated for 10 min. 5 mL of complete media (CM) were added and the sample centrifuged as before. The washed pellet was resuspended in CM. The parasites were then returned to culture conditions until the next synchronization. When quantification of PfATG8 puncta was desired, CQ pulse was done for 6 hours using highly synchronized parasites at the mid trophozoite stage, followed by washing to remove drug as described[14].

2.2.2 Sample Preparation for Single Cell Photometry

Coverslips were prepared by pipetting 500 μL of 0.1% (w/v) poly-L-lysine on to them and leaving for 10 min. They were then dried and stored at 4 ºC until used. Trophozoite-infected RBCs

were resuspended at 0.5% hematocrit in IM supplemented with 25 mM HEPES pH 7.4 and 200 uL were placed on a poly-L-lysine coated coverslip; the cells were incubated for 3 min under standard cell culture atmosphere. Non-adherent cells were washed off and the coverslip was mounted on a custom-designed perfusion chamber for microscopy work. For perfusion experiments, the parasites were always maintained under constant perfusion at 3 mL/min of a physiologic buffer (HBSS with 5% O_2, 5%CO_2, and 90% N_2 at 37º C). Fura-2 AM (in DMSO stocks) was added to the samples at a final concentration of 5 μM. 0.1% v/v Pluronic F-127 was added to improve dye loading into iRBCs. Samples were kept at 37 °C for 45 minutes.

2.2.3 *In situ* Calcium Calibration of Fura-2

For calibrations, perfusates were prepared from 2 stocks: 1) HBSS + 25 mM HEPES + 10 mM EGTA (pH 7.4); 2) HBSS + 10 mM EGTA +25 mM HEPES + 10 mM CaCl2 (pH 7.4). Solutions of designated concentrations of free calcium were prepared by mixing both stocks at different ratios. The free calcium concentration was calculated using the "winmaxc32" engine (provided by Professor Chris Patton from Stanford University http://www.stanford.edu/~cpatton/webmax/webmaxcS.htm); parameters were set at pH 7.4, 37ºC, EGTA, ionic strength 150 mM. Before experiments, 10 uM ionomycin was added in order to clamp the internal free calcium concentration to the concentration in the perfusate. Intact trophozoite-stage parasites were first perfused with with calcium-free buffer (without ionomycin) at a rate of 1 mL/min. Ratiometric measurements were performed in 5 cells corresponding to resting free calcium. This process was repeated for each perfusate containing ionomycin and a designated level of calcium (54, 127, 217, 488, 1,000, and 23,700 nM); ratiometric data were collected for ~15 cells at each calcium concentration and within both compartments.

Data were processed and analyzed with Microsoft Excel, SigmaPlot 12.0, and Origin 5.0. Calibration curves were fitted to sigmoidal curves and calcium concentrations were extrapolated from the best fit.

2.2.4 Single Cell Photometry

Single cell experiments were done as previously described[105] . The single cell photometry (SCP) apparatus consisted of a custom-built Nikon Diaphot epifluorescence microscope equipped with a 100X oil immersion objective capable of UV transmission (Fluoro, N.A. 1.25, 160/017); a 16-bit Sensys CCD camera (Tucson, AR) was attached to the side port of the microscope. Excitation light was provided by a computer controlled xenon arc lamp (LAMBDA LS, Novato, CA). 2 band-pass filters at 340 nm and 380 nm filtered UV light for ratiometric illumination of Fura-2 (Asahi Spectra Co., Ltd., San Jose, CA). The filters were housed in a Lambda-10 filter wheel controlled through the acquisition software (Imaging Workbench). The excitation light was transported by a liquid light guide (Novato, CA), collimated, and passed through the microscope optics. A filter cube housing a 400 nm dichroic mirror combined with a 410 nm long-pass filter was used to separate excitation from emission light. The power before objective was measured with a near UV power meter (Metrologic Model No. 45-545). In my experiments, the exposure time was set at 500 ms followed by a 10 sec recovery in total darkness. For ratiometric measurements, data from 2 excitations (340 and 380 nm) were collected from a region of interest (ROI) within the parasite. A second region of interest was drawn in the vicinity of the parasite for background subtraction.

2.2.5 Preparation of Affinity Purified ATG8 IgG and ATG8 Monoclonal Antibody 2K19

A RACE validated cDNA encoding *Toxoplasma gondii* TgATG8 (ToxoDB accession number TGGT1_003400) was used as template to amplify the full length coding region using the primers (CACCATGCCATCGATTCGCGACGAAGTGTCC and TTACCCCAGAGTGTTCTCTGAA--GAGTATTCCACGTACA) in the laboratory of our colleague Dr. Anthony Sinai (University of Kentucky). The amplicon was subcloned into pET100 establishing an in frame N-terminal His tag. Following expression in *E. coli*, the recombinant His-TgATG8 was purified on nickel magnetic beads (Invitrogen) and used as the immunogen to immunize a single rabbit (Cocalico, Reamstown,PA). The resulting antiserum was affinity purified using the bead immobilized crosslinked antigen and eluted using low pH.

Generation of a monoclonal antibody was contracted to AbMART.com (Shanghai, China) and accomplished using a synthetic polyprotein containing 6 tandemly arrayed epitopes. Epitopes were selected based on the highest homology between TgATG8 and PfATG8. Supernatants from clones yielding > 3 fold signal in an ELISA at 1:128K dilution were screened by IFA on both Toxoplasma and Plasmodium. Multiple clones recognizing the epitope HRIRAKYPNR in Toxoplasma (HKIRSKYPNR in Plasmodium) gave excellent reactivity in both organisms. The clone 2K19 was selected for detailed work as it was found to be an IgG1 isotype (data not shown) and gave the best-defined signal in both organisms.

2.2.6 Immunohistochemistry

For starvation, cells at the mid trophozoite stage were pelleted and resuspended in HBSS supplemented with 0.1 mg/mL hypoxanthine, 25 mM HEPES, and 20mM sodium bicarbonate. Cells were gassed and incubated at 37ºC for a desired interval (typically 6 hours) before fixation.

For drug treatments, highly synchronized mid stage trophozoites were treated as described[14] using drug concentrations noted in the text. Resultant cell pellets were resuspended in complete media and treated as below. Cells were washed 3 times with 25 mM HEPES, fixed with 4% formaldehyde/0.0075% glutaraldehyde in PBS for 30 min, permeabilized with 0.1% Triton X-100 for 10 min, reduced with 0.3 mg/mL sodium triacetoxyborohydride for 10 min, blocked with 5% goat serum for 1 hour, and sequentially treated with antibodies diluted in 5% goat serum/PBS Tween-20 with PBS washes in between; antibody treatments lasted 1 hour at 37ºC in the dark. The primary antibody was raised in either rabbit (TgAtg8) or mouse (monoclonal 2K19); the secondary antibody was raised in goat against rabbit or goat against mouse IgG and conjugated to secondary antibodies described previously. Cells were attached to #1.5 coverslips and mounted using "Fluorogel" mounting media. Samples were imaged using a customized Nikon Eclipse TE 2000-U spinning disk confocal microscope with 405, 491, 561, and 642 nm laser lines at 200 ms exposure and 35% laser power. For experiments involving mouse antibodies, the primary antibody solutions were prepared at 1:250 and the secondary (typically goat anti mouse DyLight488) at 1:500. For experiments involving primary antibodies raised in rat or rabbit, primary solutions were prepared at 1:250 and secondary solutions (goat anti rat AlexaFluor594 and goat anti rabbit DyLight488 or DyLight649) at 1:500.

2.2.7 Spinning Disk Confocal Microscopy

2.2.7.1 SDCM Setup

Spinning disk confocal microscopy (SDCM) was performed as previously described[6, 106]. A 2003 model Perkin-Elmer UltraView SDCM device was used, containing a Yokogawa CSU21 spinning disc confocal scan head with a fixed 50 μm pinhole, and a Nikon TE 2000 inverted

microscope (Figure 2.1). Image acquisition was done using SlideBook 6 software. The microscope was fitted with 1.40 NA oil condenser and with a 1.49 NA, 100 x TIRF oil objective with a correction collar. Important additions to the commercially available instrument include a Uniblitz high-speed shutter, a Hamamatsu ORCA ER cooled CCD camera, a Coherent Innova 300 Ar/Kr laser capable of 800 mW output power, and a NEOS acousto-optic tunable filter (AOTF) (for fast illumination control). This system was fitted with customized Nikon differential interference contrast (DIC) optics consisting of a linear polarizer, an analyzer, a condenser, and objective Nomarski prisms. In addition, the customized apparatus is mounted on a Newport Corp. pneumatic vibration isolation table to further minimize image blurring and other artifacts. For acquisition of transmittance images, DIC optics were used. Interference by polarized light is divided by the first and recombined by the second Nomarski prism.

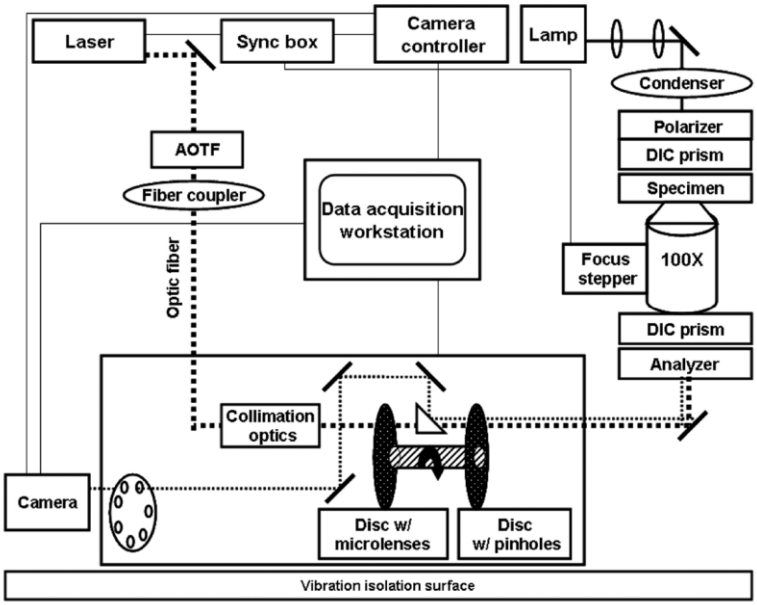

Figure 2. 1 Schematic of the customized SDCM device used in this work. For DIC experiments illumination of the sample follows the halogen lamp light path through the condenser, polarizer, and Wollaston prism to the specimen and then through the second prism, analyzer, spinning disc with pinholes, dichroic mirror, and emission filter to the camera. For fluorescence measurements, light is from the laser through the AOTF, fiber coupler, and then via an optic fiber through the collimation optics and both spinning discs, to the specimen. On the way to the camera, fluorescent light passes back through the disc pinholes, a dichroic mirror, and then again, an emission filter in reaching the camera.

2.2.7.2 Image Acquisition

Prior to data acquisition in DIC mode, the Köhler equal field illumination was achieved. This was done in the following manner: the sample was mounted, lamp turned on, the lamp iris and the condenser iris would be completely closed. Only a diffuse circle inside the field of view was illuminated. The objective was focused on the sample and the condenser was aligned to show a sharp bright octagon in the field of view. The octagon was centered with the condenser centering screws, condenser iris opened enough to illuminate the whole field of view and the lamp iris opened fully. DIC data were collected with type A immersion oil (η= 1.515), a halogen lamp for transmittance illumination, and an LP520 filter for transmittance filtering. Spacing in z- was set to 0.2 μm according to Nyquist criterion[107], appropriate for deconvolution. Transmittance was focused until hemozoin (Hz) within the parasite DV was clearly visible and presented the largest diameter possible. This put the initially defined z-axis focal plane well within the confines of the DV. Once found, this z-axis position was defined as "0 μm". A series of DIC images were acquired in successive 0.2 μm z-axis displacements, scanned through the parasite from the -3 μm to +3 μm positions.

For acquisition of fluorescent images, λ= 405, 491, 561, and 642 nm laser lines was used. Fluorescence collection experiments were done similarly to DIC experiments described previously. Transmittance was focused until Hz presented the largest diameter possible, which defined the z-axis position as "0". The microscope settings were then switched to fluorescence imaging and a series of images was acquired in successive 0.2 μm z-axis displacements (Figure 2.2).

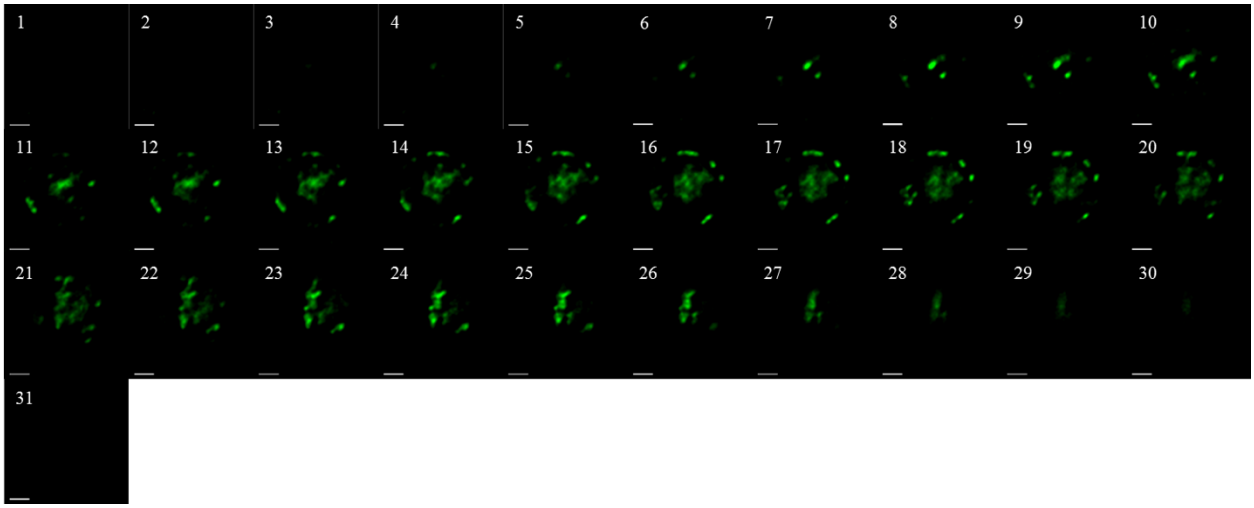

Figure 2. 2 Representative 31 z -slices acquired to generate the 3-dimentional image using Imaris.

2.2.7.3 Cell Fluorescence Data Analysis

Deconvolution of the fluorescent data was performed with the iterative maximum likelihood estimation (MLE) algorithm adapted by AutoQuant X2[108], which allows either a theoretically calculated[109] or experimentally obtained point spread function (PSF). An experimental PSF can be obtained by mixing subresolution (d= 0.17 μm) fluorescent beads in cell culture and then imaging them under the same conditions that were used for data collection for parasites. The PSF was used to initialize the deconvolution routine, and data sets (z-stacks) were deconvolved using 15 iterations[110-111]. The deconvolved z-stacks were assembled to generate a 3-dimentional image using Imaris 7.5.2 (Figure 2.3). Using the "spots" routine in Imaris 7.5.2, puncta were defined and distances were measured from each spot to a single point within the DV as defined by the center of hemozoin optical density [6]. These distances were exported to Microsoft Excel and the resulting data were plotted as number of puncta vs. distance from hemozoin.

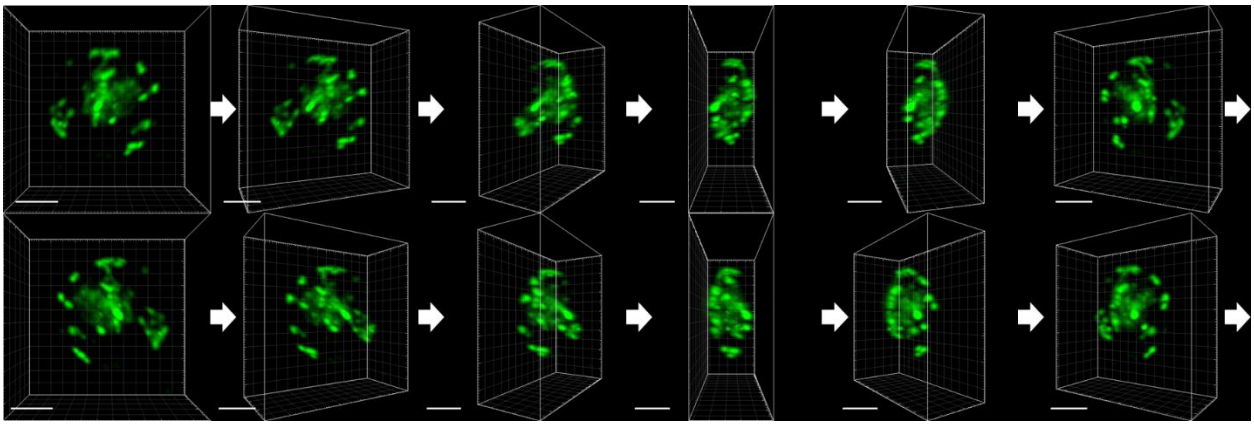

Figure 2. 3 Multiple angles of a representative 3-dimentional image generated using the z-slices in Figure 2.2. Imaris 7.5.2 was used for this process.

2.2.8 Antiplasmodial Assays

Antiplasmodial cytostatic (growth inhibitory, or IC_{50}) and cytocidal (cell killing, or LD_{50}) activity was determined for the strains discussed above as previously described [9, 14], with minor modifications. The cytocidal assay utilizes a 6-hour bolus dose with high concentrations of drug followed by washing drug away and growth in the absence of drug for 48 h, while the cytostatic assay utilizes continuous growth for 72 hours in the constant presence of low concentrations of drug. For both assays, test compounds were dissolved in deionized water, 50% EtOH, or DMSO.

In the IC_{50} assay, serial drug dilutions were made using complete media and 100 µL aliquots were transferred to 96-well clear-bottom black plates. Culture for plate examination is prepared by generating a Giemsa smear to count parasitemia. This culture is prepared at 4% hematocrit and 1% parasitemia. Following addition of 100 µL of culture to the plated drugs, the cultures in the plate are now at 1% parasitemia, 2% hematocrit. Plates were transferred to an airtight chamber gassed with 5% CO2/5% O2/90% N_2 and incubated at 37 °C for 72 hours.

For the LD_{50} assay, asynchronous or synchronous *P. falciparum* cultures at 2% hematocrit and 2% parasitemia were treated with drugs for 6 hours and then the drug was completely washed away. This was done by first spinning the culture containing plate at 700*g* for 3 mins using the

Eppendorf 5804 centrifuge. The supernatant is removed and the pellet is re-suspended in 200 μL of fresh complete media. This washing step is done 2 more times. After a final re-suspension, washed plates were incubated at 37 °C for 48 h.

After 72 hours for IC_{50} plates or 48 hours for LD_{50} plates, 50 μL of 10X SYBR Green I dye (diluted using complete media from a 10,000X DMSO stock) was added and plates were incubated for an additional 1 hour at 37 °C to allow DNA intercalation. Fluorescence was measured at 538 nm emission (485 nm excitation) using a Spectra GeminiEM plate reader (Molecular Devices; Sunnyvale, CA). Linear standard curves of measured fluorescence vs. known parasitemia were prepared immediately prior to plate analysis. Background controls included fluorescence from un-infected red blood cells. Data was analyzed using MS Excel and IC_{50} and LD_{50} values were obtained from sigmoidal curve fits to % growth/survival vs. drug concentration data using SigmaPlot 12.0. Reported values are the average of three independent assays, with each assay conducted in triplicate (nine determinations total) and reported ± standard error of the mean (S.E.M.), unless otherwise noted.

2.2.9 Drug Combination Assays Using the Chou-Talalay Method

The effect of combining two drugs together was assayed through use of the Chou-Talalay method of fixed-ratio analysis[96, 112]. Briefly, the two compounds were initially screened for their individual cytostatic and cytocidal activities, as described in Section 2.2.8. Combination analyses were initially run at fixed ratios of these determined values (1:1 unless noted). This results in a set of concentrations all at a multiple or fraction of the compounds' individual IC_{50}s or LD_{50}s. A combination stock, set at four times the IC_{50} or LD_{50}, is serially diluted seven times to yield a range

of concentrations that can generate a combination growth or survival curve, see Table 2.1 for a diagram of the plate layout.

Table 2.1 Sample diagram of plate for Chou-Talalay method assay

	HB3 (CQS)						Dd2 (CQR)					
	1	**2**	**3**	**4**	**5**	**6**	**7**	**8**	**9**	**10**	**11**	**12**
A	100 nM ATM/ 80 nM NVP			No drug HB3			100 nM ATM/ 80 nM NVP			No drug Dd2		
B	50 nM ATM/ 40 nM NVP						50 nM ATM/ 40 nM NVP					
C	25 nM ATM/ 20 nM NVP						25 nM ATM/ 20 nM NVP					
D	12.5 nM ATM/ 10 nM NVP						12.5 nM ATM/ 10 nM NVP					
E	6.25 nM ATM/ 5 nM NVP						6.25 nM ATM/ 5 nM NVP					
F	3.13 nM ATM/ 2.5 nM NVP						3.13 nM ATM/ 2.5 nM NVP					
G	1.56 nM ATM/ 1.25 nM NVP						1.56 nM ATM/ 1.25 nM NVP					
H	0.78 nM ATM/ 0.63 nM NVP						0.78 nM ATM/ 0.63 nM NVP					

These samples are processed as described above, using conditions of either the cytostatic or cytocidal assay. These data are then plotted versus each drug's individual concentrations. For each drug in each assay, there is a 50% point, termed the "pseudo"-IC_{50} or "pseudo"-LD_{50}, that represents the activity of one drug in the combination. This value is then used to generate a fractional inhibitory concentration (FIC) or fractional lethal dose (FLD) using the following equations for compounds A and B [96, 112]

$$(1) \qquad FIC_A = \frac{Pseudo - IC_{50A}}{IC_{50A}} \qquad FIC_B = \frac{Pseudo - IC_{50B}}{IC_{50B}}$$

By summing these two values, a combination index (or FIC_{Index}, FLD_{Index}) can be generated[96, 112].

$$(2) \qquad FIC_{Index} = FIC_A + FIC_B$$

The FIC index of a combination is then used to assign synergy, additivity, or antagonism. The cut-off values for these designations vary [113], but those selected for this work were [114]:

Synergy- $FIC_{Index} \leq 1.0$

Additivity- $1.0 < FIC_{Index} \leq 2.0$

Antagonism- $FIC_{Index} > 2.0$

FIC_{Index} and FLD_{Index} values were averaged from at least 2 independent trials, each trial done in triplicate and are shown +/- standard error of the mean (SEM).

2.2.10 High-Throughput Screening of Drug Combinations

Initial IC50-based screening for drug synergies were made possible through a fortuitous collaboration with the Thomas Laboratory, National Center for Advancing Translational Sciences (NCATS), National Institutes of Health (NIH) [49].

2.2.10.1 Parasites, Parasite Culture, Quantitative High Throughput Drug Assay and Matrix Combination Screening

Methods for the SYBR qHTS and calculation of IC_{50} and definition of curve classes have been described [115-117]. Plating of compounds in matrix formation using acoustic droplet ejection and numerical characterization of synergy, additivity and/or antagonism have also been described [118]. This format is capable of testing compounds in pairwise matrix blocks for the rapid and systematic classification of drug pairs. Briefly, 5 μL of cells are plated using a Multidrop Combi dispenser (Thermo Fisher Scientific) and a small cassette into a 1,536-well tissue culture treated plate. Cells were directly added to the plates immediately after the compounds were acoustically dispensed using an ATS-100 (EDC Biosystems). The plates were covered with stainless steel cell culture lids and incubated at 37 °C with 5% CO_2, under 95% humidity. This high-throughput screening study was only possible due to the development and optimization of the acoustic compound dispense method at the National Center for Advancing Translational Sciences (NCATS). It is a valuable recourse and my lab was fortunate to form a collaboration with NCATS which gave me access to this remarkable facility and its work.

2.2.10.2 Compound Screening Collection

The compound screening collection consisted of most known antimalarials and an annotated set of all FDA approved drugs for all disease indications as well as commercially available molecules in advanced clinical stages of development. The latter were obtained by NCATS, from suppliers such as Tocris Bioscience, Selleck Chemicals, Santa Cruz Biotechnology and Sigma Aldrich (among others). Priority was given to compounds based on known or generally accepted mechanisms of action, clinical status, FDA approval, or novelty in MOA.

2.2.10.3 Quality Control Criteria

The quality control score is a numerical characterization of the quality of a combination that attempts to take into account single agent performance and the presence of noise in the dose combination region of the matrix [118].

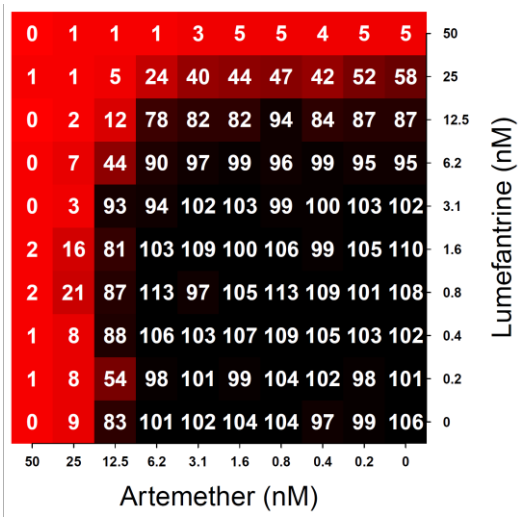

Figure 2.4 Example of heat map generated by high-throughput screening at NCATS.

It is composed of a number of heuristics, developed by examination of a series of matrix screening runs[118]. The calculation, done at NCATS, is performed on the bounded (0-100) response matrix and considers the following conditions:

DMSO negative control response lies between 80 and 100. Both single agents should display a valid dose response curve and provide a valid IC50 value. If single agents have a valid curve fit, the range of growth responses should have a relative standard deviation greater than 20 [117]. For a combination matrix, the relative standard deviation of the dose combination sub-matrix should be greater than 25. The responses in the dose combination should also not exhibit random distribution across the matrix. This is measured by Morans I [119]. It is considered that a combination will exhibit spatial autocorrelation if the p-value is less than 0.05.

Each combination is tested against the five conditions and the result is expressed as a vector, defined as

$$C = \{C_i\}, i = 1 \ldots 5$$

where C_i=1 if the i'th condition is true, 0 otherwise.

The final score is obtained by computing the dot product of the binary vector and a weight vector, W of the same length as C. The latter allows us to assign an importance to each of the five conditions noted above. The final score is given by

$$QCScore = \sum_{i=1}^{5} C_i W_i$$

Currently, the weight vector is defined as W = { 2, 5, 3, 5, 3 } allowing for a minimum score of 0 (the combination passes all QC criterion) and maximum score of 18 (combination fails all QC criterion). A combination with a score of 0 is deemed as good quality and suitable for further consideration. Increasing values of the QCScore indicate poorer quality combination responses. It should be noted that the score can identify false positive – combinations that are scored well, but on visual inspection turn out to be poor quality. The score is meant to provide an initial ranking and should not preclude manual inspection.

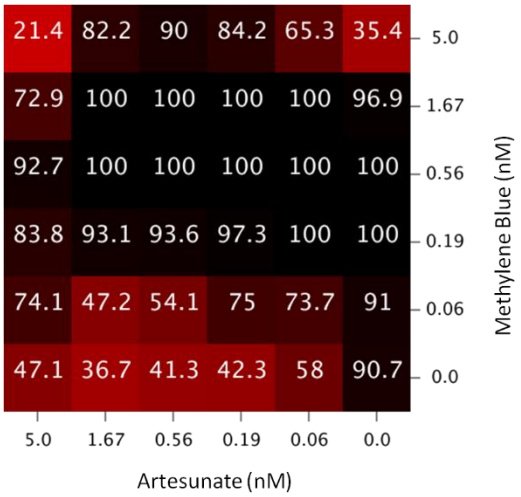

Figure 2.5 Example of an unacceptable heat map generated by high-throughput screen at NCATS.

In addition to the previously described metrics[118], analysis of combinations at NCATS was expanded to include two other quantifiers of synergy - DBsumPos and DBsumNeg. These are defined as the sum of positive deviations from the Bliss model and the sum of the negative deviations from the Bliss model, which defines synergy and antagonism in terms of predicted additive activity as the sum of the monotherapy activities minus their product. Positive deviations in the observed activity denote antagonism, while negative deviations denote synergy [120]. In contrast to simply summing all the deviations from the Bliss model, these two variables characterize the extent of synergy and antagonism within a set of dose combinations.

2.2.11 QTL Analysis

Using mean LD_{50} for each of the progeny of the HB3 x Dd2 cross, genome-wide scans were run using Pseudomarker 2.04 to detect quantitative trait loci (QTL) associated with the drug response. Genome-wide significance thresholds which correct for multiple testing errors were determined by permutation testing (n=1000 permutations). The strength of the association between a given locus and the trait (LD_{50}) is expressed as a logarithm of odds (LOD) score. Loci that exceeded the 99^{th} percentile ($p<0.01$), the 95^{th} percentile ($p<0.05$), and the 37^{th} percentile ($p<0.63$) were identified respectively as highly significant, significant, and suggestive QTL. Two-dimensional linear regression genome scans were run to test for potential loci interactions and joint LOD scores were calculated to identify significant interactions.

Candidate genes within QTL loci were selected as described previously [121]. In brief, candidate genes were selected based on four selection criteria: (1) genomic position, (2) structural polymorphisms, (3) correlation between LD_{50} and expression phenotypes for each parasite, and (4) gene annotations and enrichment analysis. PlasmoDB verion 8.2 was used for SNP density

scoring (CDS), and gene annotations. Gene enrichment analysis for biological processes and molecular functions was performed using MADIBA 8.2(2011.10). Expression phenotypes for genes within our loci taken from Gonzales *et al.*[122]. Permutation testing (n=1000) confirmed significance of GO enriched terms within the loci of interest.

2.2.12 Ring-Stage Susceptibility Assay (RSA)

The RSA was developed based on the observation that wild-type versus parasites that contain mutations in the propeller domains of a kelch domain-containing protein on chromosome 13 (K13) respond differently to drug treatments at the early ring stage of development [57]. In this assay, highly synchronized early ring stage parasites were exposed to 700 nM dihydroartemisinin for 6 h, washed with IM supplemented with 25 mM HEPES (pH 7.4) to remove drug, resuspended in complete medium (RPMI 1640 supplemented with 0.5% Albumax II, 25 mM HEPES (pH 7.4), 23 mM $NaHCO_3$, 11 mM glucose, 0.75 mM hypoxanthine, and 20 μg/L gentamicin), and cultured at 37°C under an atmosphere containing 5% CO_2, 5% O_2, and 90% N_2 gaseous mix. In this original method thin blood smears were prepared and stained with Giemsa and survival rates were assessed microscopically by counting the proportion of viable parasites with normal morphology at 66 h after drug removal. This method was subsequently improved by the introduction of the use of two-color flow-cytometry to accelerate analysis of RSA data [74]. In this method, SYBR green I was used to stain DNA in both viable and pyknotic parasites and MitoTracker deep red FM was used to selectively stain mitochondria in only viable parasites. I modified the RSA to obtain dose-response curves in order to quantify potency of the different endoperoxide drugs [123].

2.2.13 Flow Cytometry

Flow cytometry experiments were conducted as previously described[74]. Briefly, a Becton Dickinson (BD) FACSaria IIu flow cytometer was used. Data was collected in the FSC (forward scatter), SSC (side scatter), FITC (488 nm excitation, 520 nm emission / 30 nm band pass filter) and APC (633 nm excitation, 660 nm emission / 20 nm band pass filter) channels. On the FSC x SSC plot, data were gated to exclude cellular debris. On the FITC x APC plot, data were gated to exclude uninfected RBCs (Y axis) and to distinguish low (less viable) vs high (viable) MitoTracker Deep Red staining (X axis) using contour plots. Once gating limits were established for control (no drug treatment), the same gating was used for each sample exposed to variable drug concentrations. FCS Express 4 and Microsoft Excel software were used to calculate % survival. Sigmoidal curve fits of the raw data using SigmaPlot 12.0 were used to calculate $RSLD_{50}$.

CHAPTER III

A PROCESS SIMILAR TO AUTOPHAGY IS ASSOCIATED WITH CYTOCIDAL CHLOROQUINE RESISTANCE IN *PLASMODIUM FALCIPARUM*

Chapter III previously published in part as; Gaviria, D.; Paguio, M. F.; Turnbull, L. B.; Tan, A.; **Siriwardana, A.**; Ghosh, D.; Ferdig, M. T.; Sinai, A. P.; Roepe, P. D. A Process Similar to Autophagy Is Associated with Cytocidal Chloroquine Resistance in *Plasmodium falciparum*. *PLoS One*. **2013**, *8*, e79059, doi:10.1371/journal.pone.0079059

Contributions of authors:

A.S. performed cell culture, immunological experiments and developed the method and carried out puncta quantification via Imaris, and contributed to writing the manuscript.

3.1 Abstract

Antimalarial drug resistance is a constant threat and it is imperative that molecular mechanisms of this resistance be elucidated so that novel therapies can be targeted to these pathways. Previous work has shown that cytostatic versus cytocidal concentrations of chloroquine (CQ) could have different cellular targets. Since clinically relevant treatment of malaria involves parasite death induced by high plasma concentrations of drug, further studies are required to better understand the possible mechanisms of cell-death in *Plasmodium* parasites and how these relate to

drug-induced death as well as drug resistance. As part of a large, interdisciplinary project in our laboratory to elucidate cytocidal antimalarial drug resistance, immunofluorescence studies were conducted to visualize PfAtg8, a commonly used marker of autophagy. Results show that an autophagy-like pathway is induced at cytocidal concentrations of chloroquine and that this response is dysregulated in chloroquine resistant parasites.

3.2 Background

Many antimicrobial drugs are both cytostatic and cytocidal, including quinoline antimalarial drugs such as CQ [14, 124-125]. That is, under certain conditions a drug slows the rate of cell growth or impairs cell division such that the rate of proliferation of a mass population of the microbe is reduced, and under other conditions the drug kills the microbial cell. Often, cytocidal (cell kill) activity requires higher dose of drug, longer drug exposure time, or both. Cytostatic potency is usually quantified via IC_{50} values, whereas cytocidal potency is quantified via LD_{50} values.

However, to date, almost all laboratory based quantification of antimalarial drug potency, and hence quantification of all antimalarial drug resistance phenomena, has been done with IC_{50} values alone. Such quantification has proved critical for defining the genetics and biochemistry behind resistance to the cytostatic effects of CQ (CQR^{CS})[10-11, 126-128] and for identifying new drug leads with excellent cytostatic potential vs CQR malaria[129]. It is sometimes assumed that IC_{50} values measure the "cell kill" effect of a drug. Although this can be true in specific cases, in many others this is not the case. Since laboratory CQ IC_{50} are in the 10^{-9}–10^{-8} M range, but peak plasma levels of CQ in patients are ~1000 times higher (10^{-6}–10^{-5} M range)[130-132], clarification of these points is essential for fully understanding CQR.

That is, although the mechanism of CQR^{CS} is becoming clear, much less is known about resistance to the cytocidal effects of CQ (CQR^{CC}). This is a critical piece of missing information, given that parasite survival determines the rate of adaptation to selection by drugs. A recent report suggests that although decreased CQ accumulation within CQR *P. falciparum* is clearly related to elevated CQ IC_{50}, it is not necessarily relevant for elevated CQ LD_{50}[15]. Surprisingly, much higher concentrations of CQ or fluorescent NBD - CQ can be found within parasites exhibiting cytocidal CQ resistance, even though reduced drug uptake is generally accepted to be the principle basis of CQR[15]. It has also been reported that, for both 4 amino quinolines similar to CQ and quinoline methanols similar to quinine (QN), IC_{50} is correlated with the ability of the drugs to inhibit hemozoin crystallization under close to physiologic conditions, but LD_{50} for the same drugs is not[133-134]. Patterns of IC_{50} versus LD_{50} for a variety of quinoline drugs also suggest that the mechanisms for cytostatic versus cytocidal CQ resistance in *P. falciparum* are not entirely the same[14]. Taken together these data suggest that the cellular targets relevant for quinoline antimalarial drug cytocidal activities may differ from targets for cytostatic activities. Drug DV localization and drug/heme binding is the likely basis of CQ cytostatic pharmacology, but perhaps not the entire basis of CQ cytocidal pharmacology[15, 133-134]. Since drug resistance is due to disruption of drug/drug target interactions, then different targets for cytostatic versus cytocidal effects predict distinct mechanisms of cytostatic vs cytocidal resistance, unless resistance is merely due to increased catabolism of the drug (which is not the case for CQR or QNR in *P. falciparum*).

With respect to *P. falciparum* CQR^{CS}, elevated CQ IC_{50} and reduced parasite CQ accumulation are well correlated with mutations in the DV membrane CQ transporter PfCRT[128], suggesting that CQR^{CS} is due to decreased drug accessibility to heme targets within the parasite DV[135]. However, resistance to the cytocidal effects of CQ is predicted to include alterations in

additional targets, access to these additional targets[15], and/or to encompass mutations in key regulators of *P. falciparum* cell death pathways as recently hypothesized[16]. With regard to this last point, being a single celled organism, and due to the lack of caspase genes and other genes that encode key apoptosis regulators within the *P. falciparum* genome, it is questionable whether the canonical apoptosis pathway is the cause of drug - induced cell death for the malarial parasite[16]. Some evidence for an apoptotic - like cell death pathway for *P. falciparum* involving metacaspases has been presented[136-139] but there is disagreement on how relevant these observations are for *P. falciparum* death via different drugs[140]. More importantly, no molecular alterations in apoptosis have been found for CQR malaria.

These points led us to rank the progeny of the HB3 (CQS) × Dd2 (CQR) *P. falciparum* cross for CQ LD_{50} and to perform LD_{50}–directed quantitative trait loci (QTL) analysis. Progeny of this genetic cross have proven invaluable to analysis of CQR phenomena[10-11, 126, 141]. By quantifying CQ IC_{50} values for these progeny, a single locus on chr7 was previously identified as controlling the difference between CQR and CQS strain CQ IC_{50}[10]. Subsequent sequencing, in vitro drug pressure, and transfection results showed that multiple amino acid substitution mutations within a single gene in the chr7 locus, pfcrt, causes the large shift in IC_{50} values that has historically defined CQR and CQS status[10, 142-143]. Allelic exchange experiments that directly replaced the "wild type" CQS associated pfcrt allele with mutant CQR associated pfcrt resulted in elevated CQ IC_{50} without the need to condition or select cells with CQ[144]. The degree to which CQ IC_{50} was elevated for these allelic exchange transfectants was analogous to that seen for highly drug selected CQR strains (70%–90% of the corresponding strain IC_{50} shift)[144], suggesting that the presence of mutant PfCRT protein was in-and-of-itself sufficient (or nearly sufficient) for conversion to a CQR phenotype. However, subsequent QTL analyses suggested that additional genetic components,

such as inheritance of different chr5 loci containing mutations and varying copies of pfmdr1, may combine with PfCRT mutations in various isolates to confer the range of CQ IC_{50} and variable IC_{50} patterns for different drugs now known to exist across the globe[11, 126-127, 141]. In contrast, QTL analysis in this paper shows a complete lack of the key chr5 locus previously identified for CQR^{CS}, and identifies additional and unique genomic loci specific to CQR^{CC}. Examination of genes in these loci suggests candidate pathways that may contribute to CQR^{CC}. Relatedly, LD_{50} analysis of pfcrt allelic exchange progeny further supports my overall conclusion that although some PfCRT mutations in and of themselves confer nearly complete resistance to CQ cytostatic effects as defined by IC_{50} shift[144], they are less important for cytocidal CQ resistance as defined by LD_{50} shift. Using antibodies to the autophagy indicator protein ATG8 and high - resolution fluorescence microscopy, it was observed that a drug-induced autophagy-like cascade is dysregulated in CQR^{CC} *P. falciparum*. Taken together, and considered alongside additional recent work with the related parasite *T. gondii*[38], my data suggest that a dysregulated autophagy-like process, combined with PfCRT mutations, promotes elevated CQ LD_{50} in CQR *P. falciparum*.

3.3 Results

Using a more rapid SYBR Green assay[9] in place of traditional ^{3}H-hypoxanthine incorporation, our quantification of CQ IC_{50} for pfcrt transfectants agrees with that published previously (Table 3.1). Clones $C4^{Dd2}$ and $C6^{7G8}$ [144] show approximately 8–fold and 6–fold shifted CQ IC_{50}, relative to control transfectants ($C2^{GC03}$) or the parental CQS strain GCO3 (Table 1; e.g. 187 nM/24 nM, $C4^{Dd2}$ vs $C2^{GCO3}$). That is, cytostatic CQ resistance for these clones is very close to that seen for laboratory strains Dd2 and 7G8 as noted earlier[144], suggesting that the Dd2 mutant PfCRT isoform and the 7G8 mutant PfCRT isoform are necessary and sufficient (or nearly

sufficient) for the IC_{50} quantified CQR phenotypes in these widely studied drug selected strains. As hypothesized previously[144], it is perhaps possible that somewhat lower expression of PfCRT in the allelic exchange transfectants relative to the laboratory strains might be responsible for the measured IC_{50} shifts of 80% –90% of that observed in strains Dd2 and 7G8[145].

Table 3. 1 Average CQ IC_{50} and CQ LD_{50} (+/− [S.E.M.]). At least 3 separate assays in each case, each assay done in triplicate for ≥9 determinations each) for strains GC03 (CQS), Dd2 (CQR), 7G8 (CQR), $C2^{GCO3}$ (control CQS transfectant), $C4^{Dd2}$ (CQS strain GC03 after allelic exchange with CQR Dd2 pfcrt allele), and $C6^{7G8}$ (CQS strain GC03 after allelic exchange with CQR 7G8 pfcrt allele).

Strain	**CQ IC_{50} (nM +/- [SEM])**	**CQ LD_{50} (µM +/- [SEM])**
GCO3	22.1 [1.7]	0.0531 [0.005]
Dd2	206 [26.3]	15.7 [1.82]
7G8	161 [14.1]	3.99 [0.62]
$C2^{GCO3}$	24.4 [1.9]	0.0960 [0.008]
$C4^{Dd2}$	187 [21.0] (90%)	1.10 [0.082] (7 %)
$C6^{7G8}$	128 [12.8] (79%)	0.910 [0.067] (23%)

Regardless, recently it was shown that when expressed as a ratio of LD_{50}, "cytocidal" CQR was not the same as "cytostatic" CQR defined by IC_{50} ratios[14]. When CQ LD_{50} are quantified for CQR clones $C4^{Dd2}$ and $C6^{7G8}$ as described[14] and the ratio versus control clone $C2^{GCO3}$ calculated, our group find that these clones are 10–fold and 8–fold cytocidal CQR ("CQR^{CC}"), whereas strains Dd2 and 7G8 are 130–fold and 35–fold CQR^{CC}, respectively (Table 3.1 and see also Paguio *et al.*[14]). That is, in contrast to exhibiting 80% – 90% of the CQ IC_{50} shifts, the allelic exchange transfectants exhibit only 7% – 23% of the CQ LD_{50} shifts for laboratory strains harboring the same PfCRT mutant isoform (Table 3.1). This indicates that although mutant PfCRT protein is indeed responsible for most of the CQR^{CS} phenotype (measured by CQ IC_{50}), it makes a smaller contribution to the CQR^{CC} phenotype (measured by CQ LD_{50}) observed in the same strains.

Thus, the QTL mapping approach was leveraged within an available genetic cross to compare genetic profiles of the two phenotypes and to search for additional genetic loci contributing to CQR^{CC}. CQ LD_{50} was quantified for progeny of the HB3 (CQS) × Dd2 (CQR) cross using the recently described high throughput assay[14] (Table S3.1, Appendix A). Three major QTL loci associated with LD_{50} were identified. First, similar to CQ IC_{50}– directed QTL[10] the chr7 locus harboring pfcrt segregates with the elevated LD_{50} phenotype (not shown, see Fidock *et al.*[10]). The LOD score (~21) is lower than the LOD score when IC_{50} is the measured phenotype (~40)[10-11]. It should be emphasized that the magnitude of the LOD score reveals how well a locus segregates with a phenotype across a given population (in this case, progeny from the HB3 × Dd2 cross), but does not define the relative biochemical contribution of proteins encoded by that locus to the phenotype in question. Behavior of pfcrt transfectants that isolate PfCRT mutations in a common genetic background shows that the biochemical contribution of mutant PfCRT to elevated CQ LD_{50} is lower relative to its contribution to elevated CQ IC_{50} (Table 3.1), nonetheless, PfCRT mutations remain a prominent contribution to the mechanism of elevated LD_{50}.

Second, two new chromosomal loci, not previously associated with any CQR phenomena, are associated with elevated CQ LD_{50} in CQR progeny of the HB3 × Dd2 cross (Figure 3.1). One is a novel contribution from chr6 (0 cM –17.3 cM) that can increase CQ LD_{50} for CQR progeny of the cross (Figure 3.1B). Furthermore, this locus interacts with chr8 (77.5 cM) with significant additive effects (Figure 3.1E). In addition to defining a genetic architecture for CQ LD_{50} that is distinct from that previously defined for CQ IC_{50} (Figure 3.1C), the loci contain genes that may contribute to CQR^{CC} but that are not involved in CQR^{CS}. In contrast, QTL scans of IC_{50} for the same CQR progeny identify a segment of chr5 (carrying the pfmdr1 amplicon) as contributing to elevated IC_{50}[11] (Figure 3.1A), and as described previously[11], pairwise interaction between the chr5

segment and the chr7 locus is associated with elevated IC_{50} in the CQR progeny (Figure 3.1D). Results from many studies show that the relevant gene in this segment of chr5 is likely pfmdr1[146-149]. However, importantly, LD_{50} - directed QTL analysis does not identify this chr5 fragment (Figure 3.1C) or the chr5×chr7 pairwise interaction. Instead, it isolates a fragment of chr6 (Figure 3.1B), and defines a chr6 × chr8 pairwise interaction relevant for elevated LD_{50} (Figure 3.1E). In sum, these data force us to conclude that the LD_{50} and IC_{50} phenotypes share a critical feature (mutant PfCRT found on chr7) but are otherwise genetically distinct.

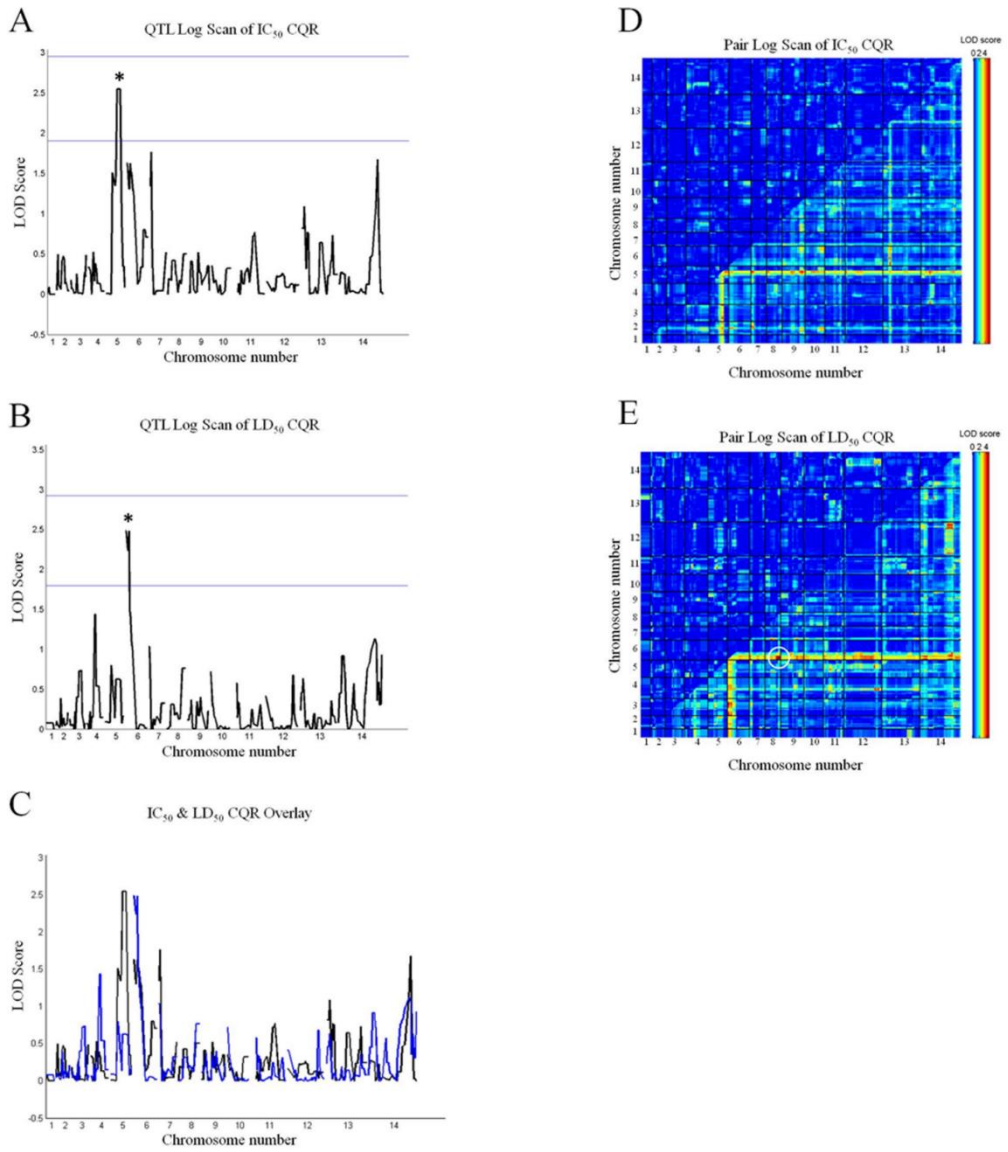

Figure 3. 1 LD_{50} vs IC_{50} directed QTL analyses for CQR HB3 × Dd2 cross progeny. A) IC_{50} QTL scan for CQR progeny shows a peak on chr5 (asterix) that encompasses pfmdr1 as previously described[11]. Notably, the chr6 locus that is pertinent for the LD_{50} scan (Figure 3.1B) does not pass the suggestive threshold on this IC_{50} scan. B) LD_{50} QTL scan for CQR progeny shows a peak on chr6 (asterix; L.O.D.=2.5, passing the suggestive threshold). The locus that includes pfmdr1 does not pass the suggestive threshold for this scan (Figure 3.1C). C) To more clearly highlight the differences in genetic architecture for LD_{50} vs IC_{50} phenotypes, an overlay of the two QTL scans is shown. The CQR progeny LD_{50} QTL scan is shown in blue, while the CQR progeny IC_{50} QTL scan is in black. The overlay shows quite clearly that the pfmdr1 locus does not factor at all into the LD_{50} phenotype, and that the chr6 locus does not factor at all into the IC_{50} phenotype. Thus, the IC_{50} and LD_{50} phenotypes are genetically distinct. D) Similarly, the interaction locus between chr6 & 8 does not appear on a IC_{50} pair-wise scan. However, additive effects between chr5 and chr7 loci are seen, as previously reported[11]. E) Pair-wise scan of the CQR progeny shows that chr6 and chr8 loci (circle) have additive effects on LD_{50} (L.O.D.=4.3).

Our interpretation is that the CQR^{CC} and CQR^{CS} mechanisms overlap (each requires mutant PfCRT), but that the relative contribution of PfCRT to CQR^{CC} is less than, or mechanistically distinct from, its contribution to CQR^{CS} (Table 3.1) and that high level CQR^{CC} requires additional factors (Figure 3.1B, E). The question then becomes how might genes in chr7, chr6, and chr8 loci act together to elevate CQ LD_{50} up to 250-fold (Table S3.1, Appendix A; note CQ LD_{50}=32 μM for 3BA6), when Dd2 mutant PfCRT in and of itself only appears to elevate CQ LD_{50} 10-fold (Table 3.1).

Inspection of the chr6 and chr8 loci reveals multiple genes involved in processes linked to "vesicle traffic", "proteasome function/proteolysis" and "lipid metabolism" (Table S3.2 & S3.3, Appendix A). For example, at least 6 genes within the chr8 locus encode proteins putatively involved in the proteasome pathway (Table S3.3, Appendix A). Candidate genes were also ranked based on the sequence similarity of strain HB3 (CQS) and strain Dd2 (CQR), and the correlation of expression levels with the LD_{50} phenotype (Tables S3.2 & S3.3, Appendix A). Thus, four previously vetted methods[18] were used to identify genes or pathways that are most likely relevant to LD_{50}. Interesting genes within the chr6 and chr8 loci that have high CDS scores include putative orthologues of autophagy genes ATG11 and ATG14, several key metabolic regulators, multiple kinases, and a putative E3 ubiquitin ligase (Table S3.2 & S3.3, Appendix A). Also of note are several genes in the chr6 locus linked to response to oxidative stress. Due to the nature of chromosomal fragment inheritances in the HB3 × Dd2 cross, the chr6 × chr8 additive effect defines a much smaller region of the chr6 segment. This segment harbors only 20 genes, with 7 of those encoding proteins involved in lipid metabolism.

Elevated LD_{50} indicates resistance to cell death. Cell death is often mediated by signal transduction that controls a programmed cell death (PCD) pathway[16]. Importantly then, it was

observed that the chr6 and chr8 loci do not harbor any candidate Pf metacaspases[137] or other molecules that typically regulate apoptotic PCD. In other words, no genetic evidence was found from the HB3 × Dd2 cross for atypical apoptosis related to CQR^{CC}. Autophagy ("self-eating" upon starvation or stress) is an alternate pathway that has been linked to cell death for several cell types[150-152], including the related apicomplexan parasite *T. gondii*[38-39]. It is an orchestrated, vesicle mediated, proteolysis/degradative pathway that is distinct from apoptosis. Since apoptosis genes were not found in chr6 or chr8 loci, and since "vesicle traffic", "proteasome/proteolysis", "lipid metabolism", "oxidative stress" and autophagy pathways often overlap mechanistically, we wondered if altered autophagy might be related to LD_{50}.

However, no experiments to our knowledge have been done to test if autophagy occurs in intraerythrocytic *P. falciparum*. The universal stimulus for autophagy is starvation, which also unambiguously induces cell death. An unambiguous feature of induction of autophagy in eukaryotes is redistribution of ATG8 protein (called LcIII in mammals) from a more localized and diffuse pattern to a more widely disbursed, more punctate pattern that defines the sites of autophagosome formation and/or recruitment of autophagosomal "cargo"[153]. Specific ATG8 antisera raised versus *T. gondii* ATG8 protein (anti TgATG8) show excellent cross reactivity vs *P. falciparum* ATG8 because PfATG8 is ~70% identical to TgATG8[16]. A PfATG8 doublet was identified at predicted masses of 15 & 17 kDa in immunoblots of fractionated parasites (Fig. 3.2D) that is consistent with well-known de-lipidated and lipidated forms of ATG8[153]. IFA analysis using ATG8 antiserum suggests an autophagy-like process is active in intraerythrocytic *P. falciparum* trophozoites (Figure 3.2, 3.3). As expected, control iRBC trophozoite parasites grown in complete media show a cytosolic PfATG8 distribution (Figure 3.2A, green) that appears somewhat punctate, perhaps due to at least partial localization to the apicoplast[27]. However, notably, when highly

synchronized trophozoites are placed in starvation medium for 6 hrs, PfATG8 is redistributed in a much more expanded punctate fashion (Figure 3.2B, green), as recently reported[16]. Closer inspection reveals puncta at the parasite periphery, possibly near the RBC membrane. Co – staining with a marker for Maurer's cleft (anti - PfREX1, red) shows that some PfATG8 appears to be routed to very near Maurer's cleft (MC) (yellow dots, Figure 3.2B middle). The well - characterized inhibitor of autophagy, 3-methyl adenine (3-MA) partially reverses the starvation induced PfATG8 puncta redistribution (Figure 3.2C), similar to what has recently been found for *T. gondii*[38].

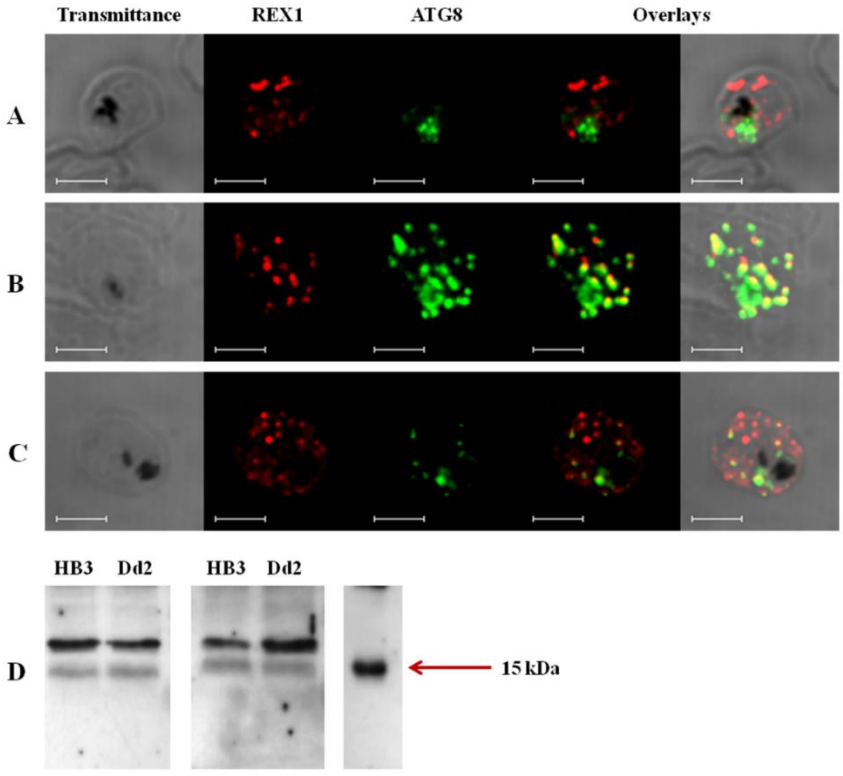

Figure 3. 2 PfATG8– positive puncta. Shown are puncta for (A) control HB3 iRBC grown under normal culture conditions (B) HB3 iRBC grown for 6 hours under starvation conditions and (C) HB3 iRBC grown under starvation conditions plus the autophagy inhibitor 3 methyl adenine (3 MA). Shown are transmittance (left), immunofluorescence vs antiPfREX1 (Maurer's cleft marker; red; second column), immunofluorescence vs antiTgATG8 (cross reacts with PfATG8; green, third column) and overlays (right). Bar=5 µm. Also shown (D) are western blot data for iRBC harboring HB3 (CQS) and Dd2 (CQR) trophozoites grown under control culture conditions. Two separate gels for two independent sets of samples (two iRBC isolations for each culture) are shown. This data show a clear doublet at 15 and 17 kDa, similar to all other studies of eukaryotic ATG8 protein.

Our group is aware of only one exception[27], where ATG8 was resolved to a single band instead of the usual doublet with a polyclonal antisera raised against a recombinant GST-PfATG8 fusion. We suggest three possible reasons for the discrepancy: 1) the use of higher density [15% acrylate] gels relative to Kitamura *et al*. in order to resolve the low mass doublet, 2) not using parasites solubilized with saponin as in Kitamura *et al*. which would release de-lipidated ATG8 into wash supernatant, 3) perhaps abundance of one PfATG8 species (presumably de-lipidated) is higher in trophozoites relative to schizonts examined in Kitamura *et al*.

Affinity purified IgG from the antisera as well as monoclonal antibody 2K19 raised against a highly conserved Apicomplexan ATG8 motif yield results similar to polyclonal TgATG8 antisera (Figure 3.3). Another recent report[27] presents data consistent with some localization of PfATG8 to the parasite apicoplast for control schizonts growing in normal media. My colleague, David Gaviria and I also obtain data consistent with partial (but not exclusive) localization of PfATG8 to the apicoplast for control trophozoites and schizonts, by co – staining for apicoplast – specific PfACP protein (Figure 3.4). We note that the trophozoite (feeding) and schizont (nuclear division/parasite replication) stages of parasite development would be expected to utilize autophagy machinery in different ways[154-155] and that further study of PfATG8 in trophozoites vs schizonts is warranted.

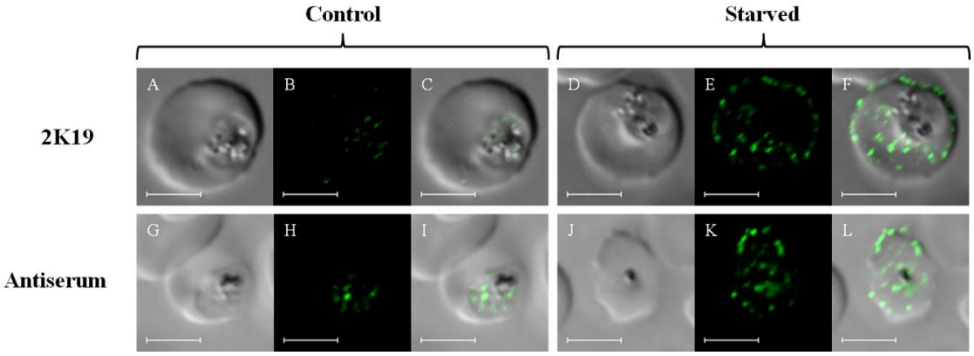

Figure 3. 3 Comparison of antisera vs monoclonal Ab staining. Shown are results for TgATG8 antisera (bottom row) vs staining using a monoclonal antibody raised versus a highly conserved Apicomplexan ATG8 epitope (top row). Panels A, G, D, J are transmittance, B, H, E, K are ATG8 fluorescence, and C, I, F, L are overlays, respectively. Left side is control intraerythrocytic HB3 *P. falciparum*; right side is HB3 starved for 6 hours as described in methods. Bar=5 μm.

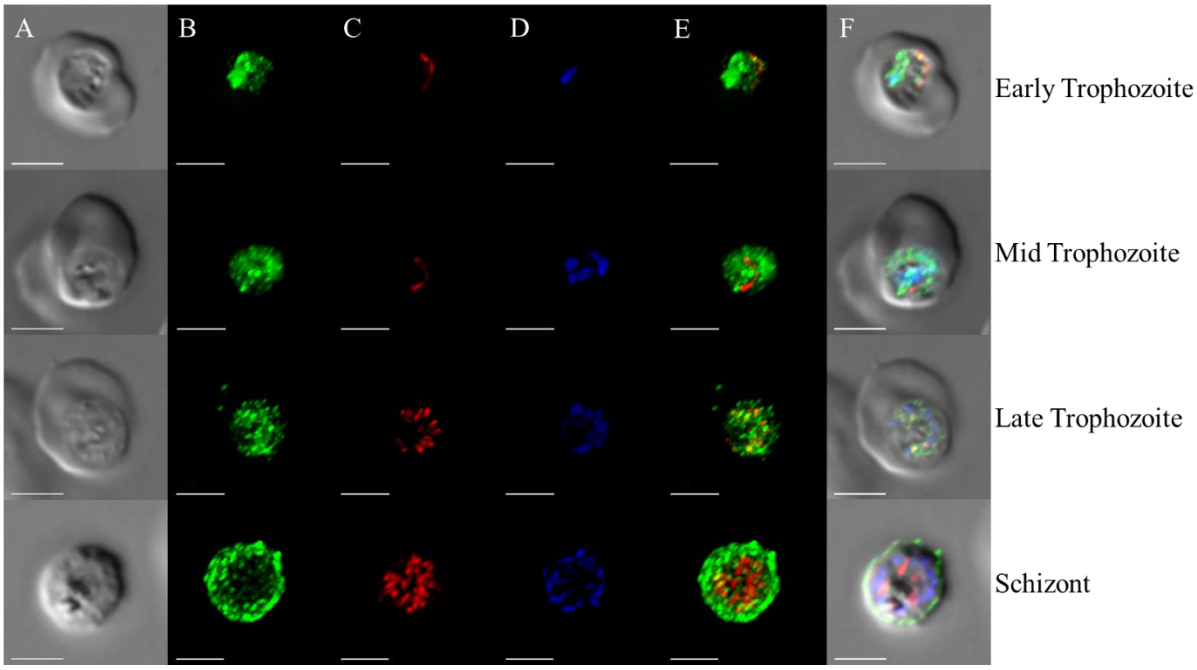

Figure 3.4 Parasites co-stained with anti-ATG8 (green) and anti-apicoplast (red) antibodies. Panel A: transmittance image. Panel B: anti-PfAtg8 antibody imaging. Panel C: anti-ACP antibody (apicoplast) imaging. Panel D: DAPI nuclear staining. Panel E: a merged image of the Atg8 and ACP channels. Panel F: a merged image of all three channels. Some overlap between ATG8 and apicoplast localized ACP (E and F) suggests partial (but not complete) co-localization of PfATG8 and apicoplast as previously suggested[27]. Scale bar = 5µm.

My colleague, David Gaviria and I next tested if cytocidal levels of CQ induced similar PfATG8 redistribution. Indeed, CQS parasites show similar extensively distributed PfATG8 puncta when they are treated at 2×LD50 cytocidal dose of CQ (Figure 3.5A), but not when they are treated with 2×IC50 cytostatic dose (Figure 3.6). Thus, the autophagy – like cascade induced by starvation is also involved in the response to cytocidal levels of CQ, but not response to cytostatic levels. When CQR parasites are treated with the same absolute dose (2×CQS LD_{50} dose; 250 nM), the punctate redistribution of PfATG8 was not observed. However, when CQR parasites are treated with 2×CQR parasite LD_{50} dose (e.g. a similar effective pharmacologic dose, ~32 µM for strain Dd2) some PfATG8 redistribution is observed (Figure 3.5B), but the ATG8 response appears somewhat muted.

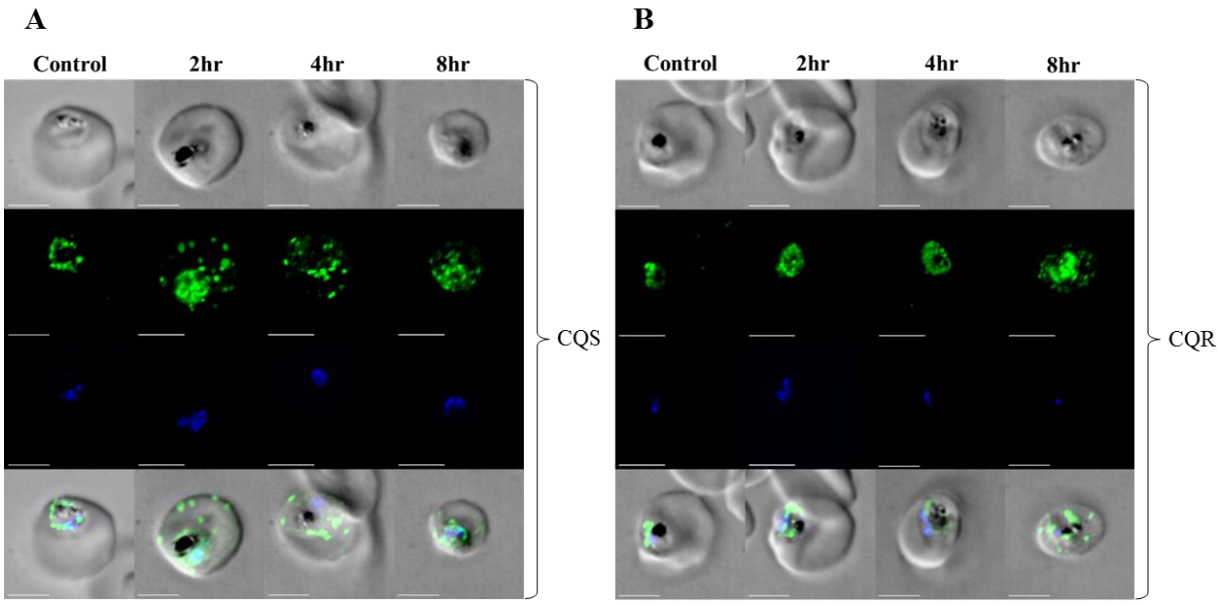

Figure 3. 5 PfATG8 re-distribution, CQ vs time. CQS (strain HB3; A) and CQR (strain Dd2; B) parasites were grown in control media (left column) or in media plus 2×LD_{50} dose of CQ (250 nM for HB3 Figure 3.4A, 32 µM for Dd2, Figure 3.4B) for 2, 4 or 8 hours (column 2, 3, 4 respectively). The top row in panels A and B is transmittance, the second (green) is staining for PfATG8, the third is DAPI to visualize the single trophozoite nucleus, and the bottom row for each panel presents the overlay. Bar=5 µm.

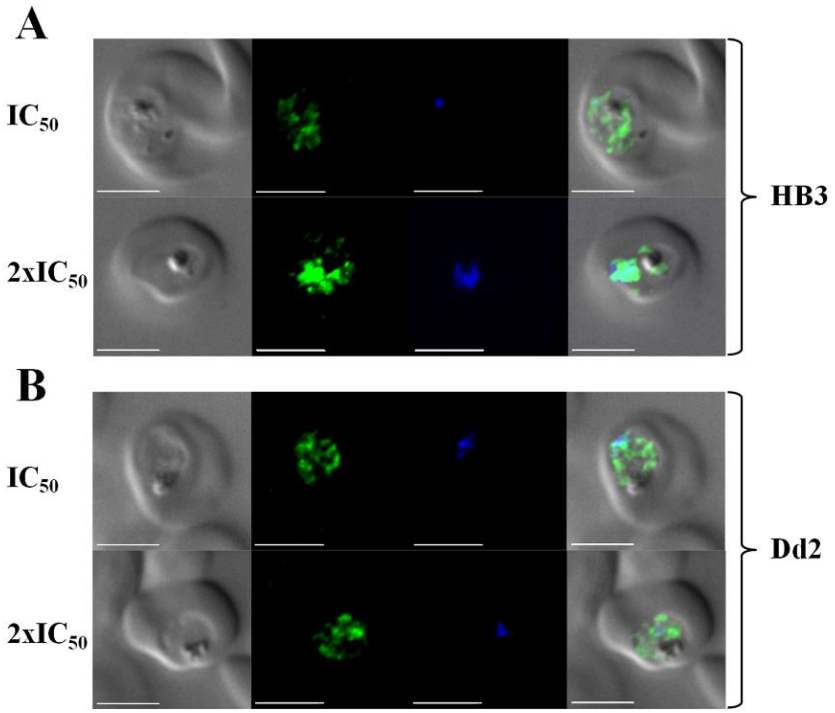

Figure 3. 6 CQS (HB3, A) and CQR (Dd2, B) parasites treated with IC_{50} (top row each panel) and 2 x IC_{50} (bottom row) doses of CQ (25, 50 nM and 125, 250 nM, respectively) for 6 hours.

To quantify this behavior, our group devised a method based on spinning disk confocal microscopy and 3D Imaris rendering of z stacks to plot radial distributions of PfATG8 puncta relative to hemozoin optical density (Figure 3.7). Essentially, very optically dense hemozoin within the DV is used to define a "center" point of reference for the iRBC parasite (Figure 3.7 left) and distinct, clearly defined spots of ATG8 fluorescence (Figure 3.7 middle, Scheme 3.1) are then measured for their relative distance (x,y,z) from the center of hemozoin optical density (white lines, Figure 3.7 right).

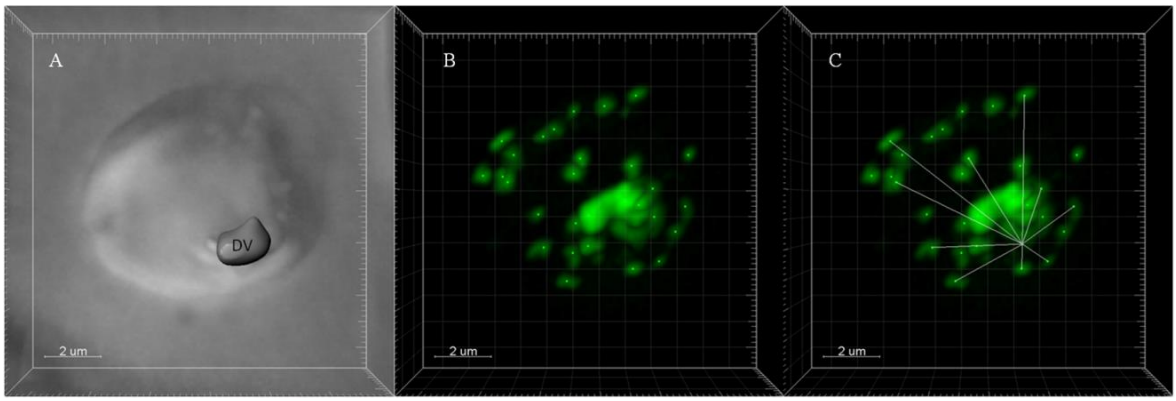

Figure 3. 7 Semi automated computational method for quantifying the distribution of ATG8 puncta relative to hemozoin crystals within the DV. A) Hemozoin within the DV is detected by transmittance, the outline of <10% transmittance is defined (labeled "DV", left panel) and the center of this outline then defined by voxel analysis using Imaris software. (B) The center of distinct ATG8 puncta (bright green dots) are labeled using the option 'Add new measurement points' in Imaris. (C) Distances from the hemozoin center to the ATG8 puncta centers are then computed (white lines) and data collated in Excel.

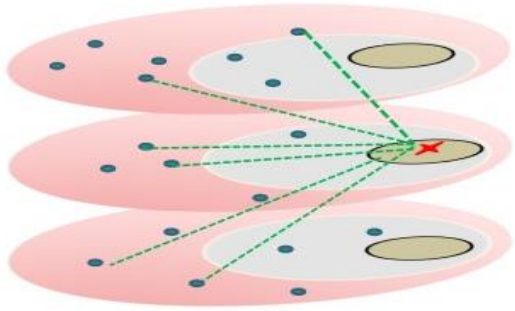

Scheme 3. 1 Cartoon representation of 3D puncta quantification method used in the present work. Hemozoin density (red "x") is used as the origin, and distances to PfATG8 positive puncta are defined for the reconstructed confocal z stack of images, relative to hemozoin, using 3D Cartesian

(x,y,z) coordinates. The cartoon shows an abbreviated depiction of 3 SDCM "slices", but as described in methods the z stack data set for each cell is a fully assembled, iteratively deconvolved 3D image constructed from approximately 15 – 20 z slices (see Gligorijevic et al.[106] for additional detail).

Using these methods, I quantified PfATG8 puncta abundance at >3.5 μm for CQS HB3, CQR Dd2 and $C4^{Dd2}$ parasites +/− starvation and across a range of bolus CQ dosages (Figure 3.8). These puncta distributions show that starvation produces similar number and similar radially distributed patterns of peripheral PfATG8 puncta for CQS and CQR parasites (compare far left and far right bars in each panel Figure 3.8), but that 2×CQS LD_{50} dose of CQ (250 nM) only produces high numbers of distal radially - distributed puncta for CQS strain HB3 (Figure 3.8A top), not for CQR strain Dd2 (Figure 3.8B middle). $C4^{Dd2}$ transfectants, wherein CQR is mediated solely by allelic exchange with CQR associated mutant pfcrt, show PfATG8 behavior that is intermediate relative to CQS HB3 and CQR Dd2 (Figure 3.8C bottom), and again, Dd2 shows a muted ATG8 response (hashed bars indicate 2×LD50 dose for each strain).

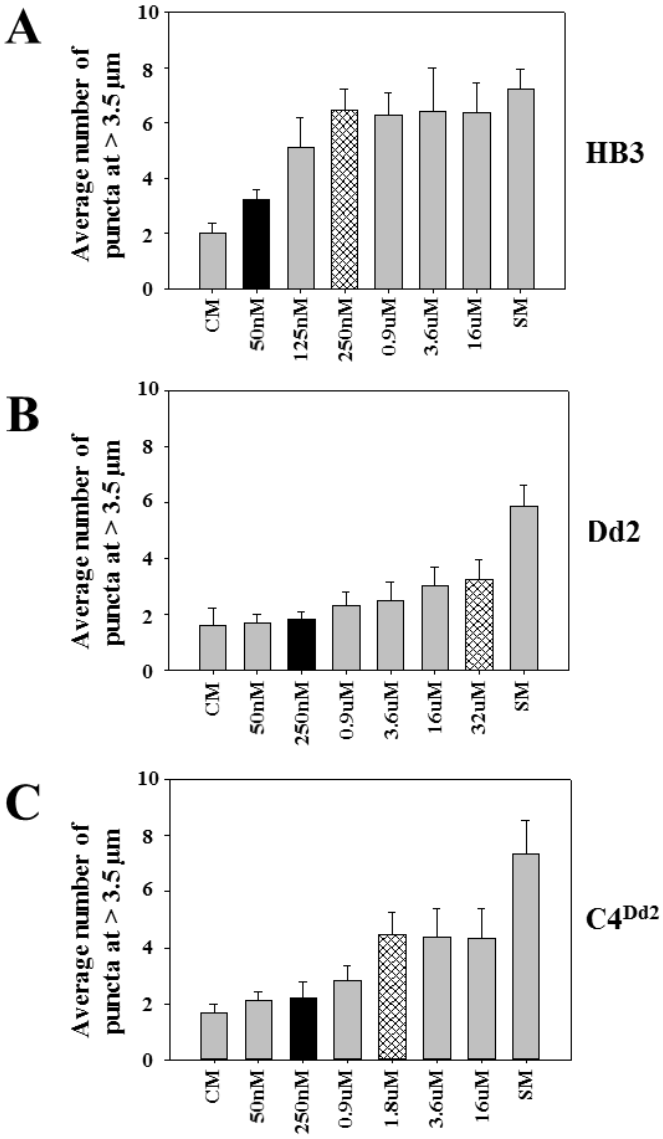

Figure 3. 8 Quantified PfATG8 puncta distribution for synchronized trophozoite parasites. Shown are CQS HB3 (top) CQR Dd2 (middle) and transfectant $C4^{Dd2}$ (bottom) under different conditions. Far left, "CM"=control culture conditions, far right, "SM"=iRBC in starvation media for 6 hr. In between are puncta quantified for iRBC treated for 6 hrs with the indicated [CQ]. Black bars in each panel denote $2\times IC_{50}$ [CQ] for the strain, hashed bars denote $2\times LD_{50}$ [CQ] for the strain. Data are the average of at least 20 iRBC, +/−S.E.M, and puncta that are ≥3.5 µm from DV hemozoin optical density are plotted. The three phenotypes are distinct, as evidenced by statistical comparison of results upon 250 nM and 3.6 µM treatments common to all three strains; for 3.6 µM data, HB3 vs Dd2, HB3 vs $C4^{Dd2}$, and Dd2 vs $C4^{Dd2}$, P value <0.05 in each case. For 250 nM data, HB3 vs Dd2 or HB3 vs $C4^{Dd2}$, P value <0.05, but Dd2 vs $C4^{Dd2}$>0.05. That is, as proposed in the text, $C4^{Dd2}$ is intermediate relative to HB3 and Dd2: both Dd2 and $C4^{Dd2}$ differ from HB3, but $C4^{Dd2}$ shows behavior similar to Dd2 at lower dose CQ, but different behavior vs Dd2 at higher dose.

My colleague, David Gaviria and I further tested the association between peripherally distributed PfATG8–positive puncta and CQR status by examining 4 other well-characterized strains, two CQS (strains 3D7 and Sudan 106) and two CQR (strains FCB and 7G8). Upon starvation for 6 hours, all 4 strains distribute PfATG8–positive puncta in a peripheral fashion similar to starved HB3, Dd2, and $C4^{Dd2}$ (Figure 3.9). However, CQR strains do not show an increase peripheral puncta at 250 nM CQ (2×CQS LD_{50}) whereas both CQS strains do. Also, even though 2×CQR LD_{50} (32 µM) induces formation of peripheral puncta for the CQR strains, similar to CQR strain Dd2 (Figure 3.9), the numbers are reduced relative to 2×CQS LD_{50} treated CQS. In terms of statistical significance of these data, $P<0.01$ when puncta produced for any CQS strain is compared to puncta data for any CQR strain upon 250 nM CQ exposure. However, P values are >0.5 when any two CQR or any two CQS strains treated with the same dose are compared. This suggests that redistribution of PfATG can serve as a marker to quantify sensitivity to cytocidal CQ.

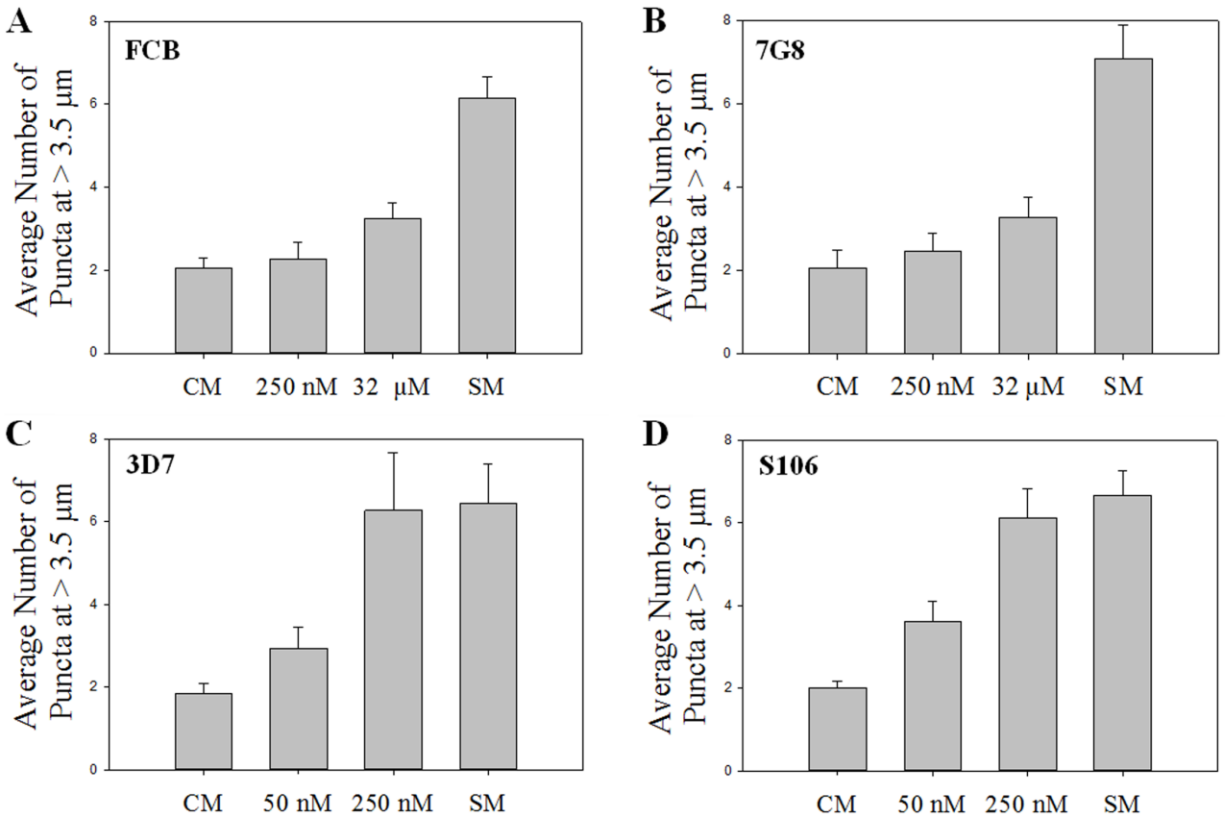

Figure 3. 9 Quantified PfATG8 puncta at ≥3.5 µm from hemozoin for synchronized trophozoites. Two additional CQR and two additional CQS strains are analyzed. Shown are puncta counts for at least 20+/− S.E.M. grown under control conditions ("CM", left side each panel), upon starvation (SM; far right, each panel) and upon dosing for 6 hrs with either $2\times IC_{50}$ or $2\times LD_{50}$ concentrations of CQ (50 nM and 250 nM for CQS strains, and 250 nM and 32 µM for CQR strains, respectively).

My colleague David Gaviria next inventoried sequences of all *P. falciparum* orthologues of autophagy pathway proteins that can be identified at this time (see also Brennand *et al.* 2011[36]) using available genomes, and note that a number of putative orthologues of key autophagy proteins are mutated in Dd2 (CQR) vs HB3 and 3D7 (CQS) parasites. For example, a recently identified *P. falciparum* PI3´-kinase (PF3D7_0515300)[156] appears to us to be a Vps34 orthologue, based on its very high identity to ScVps34 (E-value=1×10^{-73}; homology index score=567). A similar conclusion was also reached by Kitamura *et al.*[27]. During autophagy in other eukaryotic cells, Vps34 produces copious PI3P at the developing autophagosome, where ATG8 protein also

localizes. PfVps34 from CQR strain Dd2 shows point mutations and deletions relative to CQS strains HB3 and 3D7 that could conceivably affect function or regulation. Quite interestingly then, this enzyme has recently been localized to near Maurer's cleft organelles[156], very similar to the PfATG8 relocalization upon starvation that is reported here. It remains to be determined if these additional autophagy gene mutations uniformly segregate with CQR^{CC} phenomena for geographically distinct isolates of CQR *P. falciparum*. Importantly, LD_{50} quantification for these isolates will need to be performed, which will require the ability to culture these isolates over long time periods.

3.4 Discussion

Data in this paper reveal three important concepts:

1. Mutant PfCRT protein, while responsible for the majority of the shift in CQ IC_{50} that has traditionally characterized CQR *P. falciparum* strains Dd2 and 7G8[144], is only responsible for 10–20% of the shift in CQ LD_{50} for the same strains of CQR parasites. PfCRT is thought to confer CQR^{CS} by reducing access of CQ to DV–localized heme target and thereby reduce the ability of the drug to inhibit heme → hemozoin biomineralization[128, 143]. However, recent data[15] shows that DV levels of CQ are not necessarily correlated with CQ LD_{50}. In addition, other recent work[133-134] shows that the ability of CQ or QN analogues to inhibit hemozoin formation correlates with their IC_{50} activity, but not with their LD_{50} activity. Thus, our observations are not as surprising as they might initially appear, and one important implication is that targets in addition to inhibition of hemozoin crystallization are likely relevant for the cytocidal activity of quinoline antimalarial drugs.

2. LD_{50}– directed QTL analysis in the well-characterized HB3 × Dd2 genetic cross shows that the chr5 segment previously identified as modulating PfCRT mediated CQR^{CS} does not contribute to CQR^{CC}. Other distinct differences in genetic architecture include two novel loci, on chr6 and chr8, associated with elevated LD_{50}. These loci are enriched for genes that encode proteins linked to proteosome and autophagy pathways, but do not contain genes encoding metacaspases or other proteins that regulate apoptosis (Tables S3.2–S3.7, Appendix A). Several recent observations suggest interesting cross talk between proteasome and autophagy pathways[157-158], thus enrichment for both processes in the LD_{50} loci is intriguing.
3. Staining for a definitive marker of autophagy (ATG8 protein puncta) shows cell death from LD_{50} CQ treatment is linked to an autophagy – like process and that this process is altered in CQR parasites. Interestingly, the Roepe laboratory finds that starvation and CQ-induced death lead to accumulation of PfATG8– positive puncta to near Maurer's clefts (MC). These poorly understood organelles are known to be involved in export of proteins from the parasite to the red cell plasma membrane but they are also believed to have several other functions, including vesicle fusion[159].

To our knowledge, only three studies have attempted to distinguish CQ cytostatic and cytocidal activities in vitro[14, 124, 160] but only recently has LD_{50} been quantified[14], allowing QTL analyses as presented here. All previous cellular quantification of antimalarial drug resistance phenomena of which we are aware has been solely via IC_{50} ratios. IC_{50} does not quantify cytocidal (parasite kill) potency; formally it defines growth inhibition potency versus mass populations of parasites. It is certainly true that killing some parasites over time with a drug prevents growth seen in control cultures, but it can also be true that a drug in continuous culture does not kill parasites, but merely slows the cell cycle, changes multiplicity of schizogony, or has other effects that yield

IC_{50} of a given value for mass populations of parasites[125]. CQ appears to exhibit both dose dependent ("C_{max}") (Gligorijevic *et al.*[125] and this work) and time dependent ("T_{MIC}")[161] parasite killing. In studies that report IC_{90} data there may be greater "mixing" between CQ cytostatic and cytocidal effects relative to studies that report IC_{50} data. In this paper, we made the first attempt in our knowledge to more fully separate CQ IC_{50} and LD_{50} phenomena for progeny of the HB3×Dd2 cross.

It has been previously reported that some strains are much more CQR^{CC} than CQR^{CS} [14], and that the rank order of LD_{50} and IC_{50} for different drugs varies (meaning the drugs to which a parasite shows the highest IC_{50} are not necessarily the drugs to which it shows the highest LD_{50}[14]). Plotting CQ IC_{50}[10] vs CQ LD_{50} (Table S3.1, Appendix A) for HB3×Dd2 progeny yields poor correlation ($r^2<0.4$; not shown). Also, a recent study shows that CQ transport ability for 13 mutant PfCRT isoforms found in 13 different CQR strains does not correlate with CQ IC_{50} for those strains[162]. Considering these observations along with the current data suggests that parasite resistance to cytocidal effects of CQ is influenced by additional genetic or physiological events, along with PfCRT mutations. The initial analysis suggests these events include alterations in a novel pathway showing some similarities to autophagy.

In all eukaryotic cell types examined, the re-distribution of ATG8 protein to more widely disbursed puncta marks the induction of autophagy by starvation[153]. In all other examples, the membranes to which ATG8 is routed are synthesizing double membraned autophagosomes and copious phosphatidyl inositol 3′ phosphate (PI3P) via Vps34. It is striking then that previous work completely unrelated to the present study places PfVps34 near MC, similar to above observed localization for some re-routed PfATG8[156]. In all eukaryotic cell types examined, autophagosomes containing high levels of ATG8 and PI3P lipid then engulf cytosolic or organellar targets, fuse

with lysosomes, and the contents are then degraded, serving as nutrient pools that temporarily keep the starving cell alive. In the case of *P. falciparum*, the parasite trophozoite undergoes heightened accumulation of PfATG8– associated vesicles at or near the MC upon starvation and cytocidal CQ treatment. The parasite trophozoite does not appear to engulf and degrade its sole mitochondrion to provide additional food upon starvation. Indeed, starvation induced mitochondrial fragmentation by autophagy in *T. gondii* causes cell death[38]. Instead, the unique properties of the RBC, which is devoid of de novo biosynthetic activity as a host cell, necessitates enhanced endocytosis to acquire extracellular food. We suggest that under starvation pressure the parasite up regulates additional endocytosis from the red cell cytosol using (at least in part) the vesicle formation and fusion functions of encoded autophagy machinery. This might be consistent with PfATG8 vesicles eventually interacting with the parasite DV, analogous to ATG8 positive vesicle fusion to lysosomes in other eukaryotes after they recruit nutritional "cargo".

In yeast and higher eukaryotes, membrane association of ATG8 is mediated by lipidation. The terminal G residue of ATG8 that becomes lipidated is blocked, necessitating proteolytic cleavage by ATG4 as a prelude to membrane association[153]. Notably however, *P. falciparum* PfATG8 terminates with G, thus ATG4 proteolysis to reveal G as in other species is absent, suggestive of constitutive membrane association[155]. In reality however, PfATG8 exists in both the unlipidated and lipidated forms (Figure 3.2D) suggesting mechanisms other than ATG4 regulate PfATG8 dynamics. We propose that a low level of constitutively activated autophagy is present in iRBC parasites, and that CQR parasites have developed resistance to CQ induced perturbations in autophagy. Accumulation of PfATG8 puncta upon toxic CQ treatment is consistent with either upregulation of puncta formation or inhibition of autophagosome fusion, so CQR parasites could in theory have perturbations in either (or both) steps of the autophagy pathway.

Interestingly then, CQ is a known potent inhibitor of autophagy in other cell types. Its diprotic weak base character promotes profound accumulation in acidic compartments such as lysosomes, autophagosomes, and vacuoles. At doses that correspond to LD_{50}, CQ is known to block the fusion of autophagosomes with lysosomes/vacuoles and also raises the pH of these compartments, thereby inhibiting processes that require acidic pH (e.g. intra lysosomal proteolysis[150, 152]). A few molecular possibilities specific to *P. falciparum* are that LD_{50} dosages of CQ (i) block the fusion of endocytic vesicles carrying hemoglobin to the DV (in fact, a somewhat overlooked paper[163] shows that CQ LD_{50} doses do indeed lead to a buildup of undigested Hb trapped within arrested parasite vesicles), (ii) inhibit falcipain and plasmepsin activity by raising the pH in endocytic vesicles and/or the DV, (iii) inhibit fusion of autophagosomes and/or other vesicles with their target organelles. Other lysosomotropic agents would be expected to mimic this CQ pharmacology. Interestingly then, certain alkaloids that inhibit autophagy also show antimalarial activity[164-165]. One example is voacamine, a tertiary alkaloid isolated from *Peschiera fuchsiaefolia* stem bark that shows good antimalarial activity (238 ng/mL vs strain D6 and 290 ng/mL vs strain W2), and which has also been reported to chemosensitize MDR cancer cells in an autophagy-dependent manner[166]. Overall, since *P. falciparum* has been subjected to decades of cytocidal CQ selective pressure, it is logical that the parasites would evolve resistance to CQ autophagy inhibition.

With regard to the starvation effects that we observe, work in the Goldberg laboratory has shown that *P. falciparum* meets its amino acid requirements by a combination of hemoglobin degradation and uptake of free amino acids from the medium[8, 167-168]. When some extracellular amino acids are removed, the parasite responds by up-regulating additional hemoglobin transport and degradation; hemoglobin, however, lacks the essential amino acid Ile, so parasite survival is

conditional under these circumstances[168]. Conversely, if the hemoglobin pathway is inhibited, the parasite survives by acquiring additional amino acids from the extracellular medium. If Ile is withdrawn the parasite can enter a hibernatory state[8]. These observations suggest that (i) malaria parasites are able to sense amino acid levels in the medium and (ii) they possess a system that can respond to the lack of some extracellular amino acids by regulating intracellular transport to the vacuole. During starvation induced autophagy, other eukaryotic cells respond to low amino acid levels in the medium by trapping cytosolic material in transport vesicles, which will eventually fuse and release cargo into a lysosome or vacuole to then be digested to amino acids. Although for intraerythrocytic *P. falciparum* the "cargo" is presumably within the host cell cytosol, starvation induced autophagy reported here could be somewhat reminiscent of elevated hemoglobin endocytosis in *P. falciparum*.

We wondered if autophagy genes in the identified chr6/chr8 loci might be hinting at mutations in other Pf autophagy gene (PfATG gene) orthologues for CQR parasites. A partial inventory of PfATG gene orthologues has been published[36] but does not include important co factors such as Vps34, Pex14, Vps15, etc. My colleague David Gaviria re-queried the Pf genome with a more complete set of 42 autophagy related genes. Remarkably, a number of candidate orthologues (16 of 42) lie within QTL loci previously associated with drug resistance phenomena, or within "eQTL" gene sets that are up/down regulated in trans by resistance associated eQTL[169]. Also, after alignment of Dd2 (CQR) vs HB3 and 3D7 (CQS) alleles via Broad Institute data (http://www.broadinstitute.org/) for one particularly intriguing candidate PfVps34 (PF3D7_0515300; E-value 10^{-73} and homology index score 567 relative to ScVps34), our group finds that the alleles encode K at codon 423 for Dd2 in place of Q found for HB3 and 3D7, deletion of a N residue found at position 578 for HB3 and 3D7, and a deletion of 24 codons relative to HB3

and 3D7 (from codon 931 to 955). Interestingly, this deletion is within what could be predicted as a C2 regulatory domain that presumably binds Ca^{2+}; a similar C2 domain prediction for this protein has also been made by two other groups[156, 170]. Since a clear TOR orthologue is missing within the *P. falciparum* genome[36] altered regulation via mutant PfVps34 is one possibility for the altered cascade seen in CQR strain Dd2.

Regardless, we predicts that multiple routes to dysregulated autophagy will be found for various strains and isolates of CQR^{CC} *P. falciparum*, analogous to how multiple routes to dysregulated programmed cell death are found in various multidrug resistant tumor cell lines[171]. At LD_{50} doses, via its well-known lysosomotropic behavior[163, 172] CQ will inhibit vesicle formation and vesicle fusion, two processes that are essential to autophagy. Since these processes are controlled by a number of proteins, many mutations are possible for altering CQ response.

In sum, we find that mutant PfCRT protein confers the majority of CQR^{CS} as defined by CQ IC_{50} shift, but only partial CQR^{CC} as defined by LD_{50} shift. Not surprisingly then, the data also show that distinct genetic architecture is associated with CQR^{CS} vs CQR^{CC}, that a specialized *P. falciparum* autophagy cascade is induced by LD_{50} doses of CQ but not IC_{50} doses of the drug, and that altered regulation of this unique autophagy-like process is present in CQR^{CC} parasites. Consistent with a clear role for autophagy in cell death for other apicomplexa[38-39], altered PfATG8 redistribution indicative of a novel autophagy-like cascade appears to be associated with CQR^{CC} for intraerythrocytic *P. falciparum* trophozoites. Elucidating additional molecular events controlling perturbation of autophagy signaling for CQR *P. falciparum*, potentially involving at least two dozen autophagy gene orthologues[36], should prove to be a fertile area of future research. Among additional data needed to elucidate the pathway further are precise measurements of ATG8

puncta flux, meaning the rate of ATG8 vesicle production versus presumed fusion with either MC and perhaps the DV.

Finally, regardless the exact role of the novel autophagy-like process for iRBC trophozoites that is described here, we propose that CQR^{CC} requires prior acquisition of CQR^{CS}, meaning that parasites must first be able to survive lower IC_{50} dose via PfCRT mutations, before they can survive higher LD_{50} dose via acquiring additional autophagy mutations. Precise measurements of IC_{50} vs LD_{50} phenomena among geographically diverse isolates of CQR *P. falciparum* will further test this hypothesis.

3.5 Appendix A

Table S3. 1 CQ LD_{50} values of the HB3 x Dd2 cross progeny. Averages (+/- S.E.M.) from at least 3 independent experiments, each done in triplicate. Also shown is pfcrt allele expressed in the strains ("R" = Dd2, "S" = HB3 allele). See Methods and Paguio et al.[14] for additional detail.

Strain	***pfcrt allele***	***CQ LD_{50} (nM)***	***S.E.M.***
7C170	S	36.5	2.2
7C188	S	41.0	2.9
7C159	S	41.2	3.7
QC13	S	41.6	2.8
B4R3	S	48.1	3.1
CH3-61	S	48.4	4.0
SC05	S	49.7	4.5
QC01	S	50.7	4.3
GC03	S	53.1	5.2
7C7	S	53.4	4.9
7C3	S	71.4	6.0
TC08	S	78.8	7.3
B1SD	S	85.1	6.8
7C126	S	89.1	5.1
7C46		8047.5	654
7C183	R	11,747.2	40
TC05	R	14,298.1	1621
7C424	R	15,129.5	877
D43	R	18,251.2	1916
QC34	R	18,455.7	1823
1BB5	R	19,798.1	1772
7C421	R	20,475.4	1303
7C12	R	20,478.0	1343
7C408		21,552.4	2169
3BD5	R	21,579.4	2107
7C111	R	23,778.1	1137
SC01	R	23,997.2	2576
GC06	R	27,394.9	1175
3BA6	R	31,837.2	2934

Table S3. 2 All genes included in the LD_{50} chromosome 6 locus. HB3×Dd2 CDS Score from PlasmoDB version 9.3 (2013) depicts the number of SNPs per 1000 basepairs.

Gene ID PlasmoDB 9.3	Description	cM	HB3×Dd2 CDS Score	Expression Correlation
PF3D7_0622100	conserved Plasmodium protein, unknown function	17.3	0.25	-
PF3D7_0622200	radical SAM protein, putative	17.3	0.39	-
PF3D7_0622300	conserved Plasmodium protein, unknown function	17.3	-	0.3
PF3D7_0622400	conserved Apicomplexan protein, unknown function	17.3	-	-
PF3D7_0622500	RNA methyltransferase, putative	17.3	-	-
PF3D7_0622600	conserved Plasmodium protein, unknown function	17.3	-	-0.22
PF3D7_0622700	conserved Plasmodium membrane protein, unknown function	17.3	-	0.2
PF3D7_0622800	leucyl tRNA synthase	17.3	0.69	0.15
PF3D7_0622900	transcription factor with AP2 domain(s), putative (ApiAP2)	17.3	0.17	0.13
PF3D7_0623000	chorismate synthase (CS)	17.3	1.26	-0.33
PF3D7_0623100	coronin binding protein, putative	17.3	-	0.15
PF3D7_0623200	ferredoxin NADP reductase (FNR)	17.3	0.9	-0.14
PF3D7_0623300	EGF-like membrane protein, putative	17.3	-	-
PF3D7_0623400	RNA-binding protein mei2 homologue, putative	17.3	-	0.11
PF3D7_0623500	superoxide dismutase (SOD2)	17.3	-	-
PF3D7_0623600	transcription or splicing factor-like protein, putative	17.3	0	-
PF3D7_0623700	ATP dependent DEAD-box helicase, putative	17.3	0.59	0.43
PF3D7_0623800	protein kinase, putative (TKL4)	17.3	1.11	0.19
PF3D7_0623900	ribonuclease HII, putative	17.3	1.15	-0.43
PF3D7_0624000	hexokinase (HK)	17.3	-	-0.24
PF3D7_0624100	conserved Plasmodium protein, unknown function	14.4	-	-
PF3D7_0624200	conserved Plasmodium protein, unknown function	14.4	-	-0.24
PF3D7_0624300	conserved Plasmodium protein, unknown function	14.4	-	-
PF3D7_0624400	conserved Plasmodium protein, unknown function	14.4	-	-0.43
PF3D7_0624500	anaphase promoting complex subunit, putative	14.4	-	-0.38
PF3D7_0624600	SNF2 helicase, putative (ISWI)	11.5	0.12	0.01
PF3D7_0624700	N-acetylglucosaminylphosphatidylinositol deacetylase, putative	11.5	-	0.09
PF3D7_0624800	conserved Plasmodium protein, unknown function	11.5	0	-
PF3D7_0624900	conserved Plasmodium protein, unknown function	11.5	-	-
PF3D7_06250001	phosphatidic acid phosphatase (PAP)	2.9	-	-0.09
PF3D7_06250002	phosphatidic acid phosphatase	2.9	-	-0.09
PF3D7_0625100	sphingomyelin synthase, putative	2.9	0.83	-0.11
PF3D7_0625200	conserved Plasmodium protein, unknown function	2.9	0.86	0.1
PF3D7_0625300	DNA polymerase 1, putative	2.9	0.46	0.12

Table S3.2 (cont.)

Gene ID PlasmoDB 9.3	Description	cM	HB3×Dd2 CDS Score	Expression Correlation
PF3D7_0625400	conserved Plasmodium protein, unknown function	2.9	1.61	0.39
PF3D7_0625500	conserved Plasmodium membrane protein, unknown function	2.9	-	0.47
PF3D7_0625600	poly(A) polymerase PAP, putative	2.9	0.53	-0.21
PF3D7_0625700	conserved Plasmodium protein, unknown function	2.9	-	-
PF3D7_0625800	conserved Plasmodium protein, unknown function	2.9	-	-
PF3D7_0625900	conserved Plasmodium protein, unknown function	2.9	-	-0.38
PF3D7_0626000	conserved Plasmodium protein, unknown function	2.9	0.38	-0.08
PF3D7_0626100	oxidoreductase, short-chain dehydrogenase family, putative	2.9	0.87	0.24
PF3D7_0626200	conserved Plasmodium protein, unknown function	2.9	-	-0.52
PF3D7_0626300	3-oxoacyl-acyl-carrier protein synthase I/II (FabB/FabF)	2.9	-	0.33
PF3D7_0626400	Sec14 domain containing protein	2.9	2.59	0.12
PF3D7_0626500	conserved Plasmodium protein, unknown function	2.9	1.05	-
PF3D7_0626600	conserved Plasmodium protein, unknown function	2.9	-	0.05
PF3D7_0626700	conserved protein, unknown function	2.9	0.89	-0.16
PF3D7_0626800	pyruvate kinase (PyrK)	2.9	1.3	-0.32
PF3D7_0626900	mitochondrial ribosomal protein L46 precursor, putative	2.9	-	-0.38
PF3D7_0627000	conserved Plasmodium protein, unknown function	2.9	-	-
PF3D7_0627100	ankyrin-repeat protein, putative	2.9	0.19	0.21
PF3D7_0627200	myosin light chain, putative	2.9	0	0.12
PF3D7_0627300	c3h4-type ring finger protein, putative	2.9	-	-0.17
PF3D7_0627400	mitochondrial import inner membrane translocase subunit, putative	2.9	-	-0.34
PF3D7_0627500	4-methyl-5(B-hydroxyethyl)-thiazol monophosphate biosynthesis enzyme	2.9	-	-0.12
PF3D7_0627600	conserved Plasmodium protein, unknown function	2.9	0.84	0.27
PF3D7_0627700	transportin	2.9	1.16	-0.14
PF3D7_0627800	acetyl-CoA synthetase, putative	2.9	2.67	-0.18
PF3D7_0627900	conserved Plasmodium protein, unknown function	2.9	-	0.2
PF3D7_0628000	6-pyruvoyltetrahydropterin synthase (PTPS)	2.9	-	-0.25
PF3D7_0628100	HECT-domain (ubiquitin-transferase), putative	2.9	0.55	0.39
PF3D7_0628200	protein kinase PK4 (PK4)	2.9	0.76	0.01
PF3D7_0628300	choline/ethanolaminephosphotransferase, putative (CEPT)	0	-	0.24
PF3D7_0628400	conserved Plasmodium membrane protein, unknown function	0	-	0.04
PF3D7_0628500	conserved Plasmodium protein, unknown function	0	1.05	-
PF3D7_0628600	conserved Plasmodium protein, unknown function	0	-	0.23

Table S3.2 (cont.)

Gene ID PlasmoDB 9.3	Description	cM	HB3×Dd2 CDS Score	Expression Correlation
PF3D7_0628700	conserved Plasmodium protein, unknown function	0	0.58	-0.4
PF3D7_0628800	glutamyl-tRNA(Gln) amidotransferase subunit B, putative	0	6.8	-0.07
PF3D7_0628900	RAP protein, putative	0	0	-0.41
PF3D7_0629000	conserved protein, unknown function	0	-	-
PF3D7_0629100	nicotinate phosphoribosyltransferase, putative	0	-	-0.32
PF3D7_0629200	DnaJ protein, putative	0	-	0.03
PF3D7_0629300	phosphatidylcholine-sterol acyltransferase precursor, putative (PL)	0	0.77	0.29
PF3D7_0629400	RNA binding protein, putative	0	-	-0.29
PF3D7_0629500	amino acid transporter, putative	0	0.55	-0.08
PF3D7_0629600	conserved Plasmodium protein, unknown function	0	-	-
PF3D7_0629700	SET domain protein, putative (SET1)	0	0.99	-0.13
PF3D7_0629800	cullin-like protein, putative	0	0.29	-
PF3D7_0629900	sec14-like cytosolic factor or phosphatidylinositol/ phosphatidylcholine transfer protein, putative	0	-	0.39
PF3D7_0630000	CPW-WPC family protein	0	0	-
PF3D7_0630100	conserved Plasmodium protein, unknown function	0	-	-0.03
PF3D7_0630200	secreted ookinete protein, putative (PSOP6)	0	-	-
PF3D7_0630300	DNA polymerase epsilon, catalytic subunit a, putative	0	0.69	-0.21
PF3D7_0630400	conserved Plasmodium protein, unknown function	0	-	-
PF3D7_0630500	microtubule-associated protein ytm1 homologue, putative	0	1.34	-
PF3D7_0630600	conserved Plasmodium protein, unknown function	0	3.91	0.07
PF3D7_0630700	conserved Plasmodium protein, unknown function	0	0.51	-0.39
PF3D7_0630800	conserved Plasmodium protein, unknown function	0	3.38	-0.05
PF3D7_0630900	DEAD/DEAH box ATP-dependent RNA helicase (Has1p)	0	2.77	0.31
PF3D7_0631000	Tetratricopeptide repeat protein, putative	0	-	-
PF3D7_0631100	Plasmodium exported protein (PHISTb),unknown function	0	-	-
PF3D7_0631200	erythrocyte membrane protein 1 (PfEMP1), pseudogene (VAR pseudogene)	0	-	-
PF3D7_0631300	RESA-like protein	0	-	-
PF3D7_0631400	Pfmc-2TM Maurer's cleft two transmembrane protein (MC-2TM)	0	-	-0.31
PF3D7_0631500	Plasmodium exported protein (hyp4), unknown function	0	-	0.16
PF3D7_0631600	Plasmodium exported protein (hyp5), unknown function	0	-	0.13
PF3D7_0631700	rifin, pseudogene	0	-	-
PF3D7_0631800	rifin (RIF)	0	9.72	-0.24
PF3D7_0631900	stevor (stevor)	0	-	0.03
PF3D7_0632000	rifin (RIF)	0	-	-0.09

Table S3.2 (cont.)

Gene ID PlasmoDB 9.3	Description	cM	HB3×Dd2 CDS Score	Expression Correlation
PF3D7_0632100	rifin (RIF)	0	-	-
PF3D7_0632200	rifin (RIF)	0	-	-
PF3D7_0632300	rifin (RIF)	0	-	-
PF3D7_0632400	rifin (RIF)	0	-	-
PF3D7_0632500	erythrocyte membrane protein 1, PfEMP1 (VAR)	0	-	0.05
PF3D7_0632600	rifin, pseudogene (RIF pseudogene)	0	-	-
PF3D7_0632700	rifin (RIF)	0	-	-
PF3D7_0632800	erythrocyte membrane protein 1, PfEMP1 (VAR)	0	-	-0.25

Table S3. 3 All genes included in the LD_{50} interaction Chr6 (cM11.5) × Chr8 (cM77.5). HB3×Dd2 CDS Score from PlasmoDB version 9.3 (2013) depicts the number of SNPs per 1000 basepairs.

Gene ID PlasmoDB 9.3	Chr	Description	HB3 × Dd2 CDS Score	Expression Correlation
PF3D7_0808000	8	conserved Plasmodium protein, unknown function	1.22	-0.3
PF3D7_0807900	8	tyrosyl-tRNA synthetase, putative	-	-0.24
PF3D7_0807700	8	serine protease, putative	-	0.4
PF3D7_0807600	8	conserved Plasmodium protein, unknown function	4.24	0.13
PF3D7_0807500	8	proteasome subunit alpha, putative	-	-0.38
PF3D7_0807300	8	Rab GTPase 18 (RAB18)	-	0.08
PF3D7_0807200	8	conserved Plasmodium membrane protein, unknown function	-	-0.07
PF3D7_0807000	8	gas41 homologue, putative	-	0.41
PF3D7_0806600	8	kinesin-like protein, putative	0.35	0.35
PF3D7_0806400	8	glycosyltransferase family 28 protein, putative	-	-0.01
PF3D7_0806300	8	ferlin like protein, putative	0.59	0.38
PF3D7_0806200	8	conserved Plasmodium membrane protein, unknown function	0.33	-0.26
PF3D7_0805900	8	conserved Plasmodium protein, unknown function	0	0.3
PF3D7_0805800	8	conserved Plasmodium protein, unknown function	0	0.3
PF3D7_0805100	8	conserved Plasmodium protein, unknown function	-	0.38
PF3D7_0805000	8	alpha/beta hydrolase, putative	-	-0.28
PF3D7_0804500	8	conserved Plasmodium membrane protein, unknown function	1.58	-0.36
PF3D7_0804400	8	methionine aminopeptidase 1c, putative (MetAP1c)	0.45	0.21
PF3D7_0804300	8	conserved Plasmodium protein, unknown function	2.99	-0.01
PF3D7_0803800	8	20S proteasome beta subunit	-	-0.03

Table S3.3 (cont.)

Gene ID PlasmoDB 9.3	Chr	Description	HB3 × Dd2 CDS Score	Expression Correlation
PF3D7_0805400	8	acetyltransferase, putative	-	-
PF3D7_0805500	8	conserved Plasmodium protein, unknown function	-	-
PF3D7_0805600	8	apicoplast phosphatidic acid phosphatase, putative	-	-
PF3D7_0805700	8	serine/threonine protein kinase, FIKK family (TSTK0)	-	-
PF3D7_0807400	8	conserved Plasmodium protein, unknown function	-	-
PF3D7_0807800	8	proteasome subunit alpha type 5, putative	-	-0.11
PF3D7_0807100	8	RNA helicase, putative	0.25	0.09
PF3D7_0806900	8	conserved Plasmodium protein, unknown function	-	0.01
PF3D7_0806800	8	vacuolar proton translocating ATPase subunit A, putative	-	0.15
PF3D7_0806700	8	conserved Plasmodium membrane protein, unknown function	1.94	0.13
PF3D7_0806500	8	DnaJ protein, putative	0.49	0.18
PF3D7_0806100	8	conserved Plasmodium protein, unknown function	-	0.18
PF3D7_0806000	8	AAA family ATPase, putative	0.82	0.05
PF3D7_0805300	8	conserved Plasmodium protein, unknown function	0.53	0.48
PF3D7_0805200	8	conserved Plasmodium protein, unknown function	-	0.42
PF3D7_0804900	8	GTPase activator, putative	0.68	-0.39
PF3D7_0804800	8	peptidyl-prolyl cis-trans isomerase (CYP24)	-	-0.08
PF3D7_0804700	8	conserved Plasmodium protein, unknown function	0.17	0.37
PF3D7_0804600	8	U2 snRNA/tRNA pseudouridine synthase, putative	-	-0.19
PF3D7_0804000	8	cactin homolog, putative	-	0.12
PF3D7_0804100	8	small nucleolar RNA snoR06	-	-
PF3D7_0803900	8	unspecified product	-	-
PF3D7_0804200	8	Plasmodium RNA of unkown function RUF3	-	-
PF3D7_0624600	6	SNF2 helicase, putative (ISWI)	0.12	0.01
PF3D7_0624700	6	N-acetylglucosaminylphosphatidylinositol deacetylase, putative	-	0.09
PF3D7_0624800	6	conserved Plasmodium protein, unknown function	0	-
PF3D7_0624900	6	conserved Plasmodium protein, unknown function	-	-
PF3D7_0625000.1	6	phosphatidic acid phosphatase (PAP)	-	-0.09
PF3D7_0625000.2	6	phosphatidic acid phosphatase	-	-0.09
PF3D7_0625100	6	sphingomyelin synthase, putative	0.83	-0.11
PF3D7_0625200	6	conserved Plasmodium protein, unknown function	0.86	0.1
PF3D7_0625300	6	DNA polymerase 1, putative	0.46	0.12
PF3D7_0625400	6	conserved Plasmodium protein, unknown function	1.61	0.39
PF3D7_0625500	6	conserved Plasmodium membrane protein, unknown function	-	0.47
PF3D7_0625600	6	poly(A) polymerase PAP, putative	0.53	-0.21

Table S3.3 (cont.)

Gene ID PlasmoDB 9.3	Chr	Description	HB3 × Dd2 CDS Score	Expression Correlation
PF3D7_0625700	6	conserved Plasmodium protein, unknown function	-	-
PF3D7_0625800	6	conserved Plasmodium protein, unknown function	-	-
PF3D7_0625900	6	conserved Plasmodium protein, unknown function	-	-0.38
PF3D7_0626000	6	conserved Plasmodium protein, unknown function	0.38	-0.08
PF3D7_0626100	6	oxidoreductase, short-chain dehydrogenase family, putative	0.87	0.24
PF3D7_0626200	6	conserved Plasmodium protein, unknown function	-	-0.52
PF3D7_0626300	6	3-oxoacyl-acyl-carrier protein synthase I/II (FabB/FabF)	-	0.33
PF3D7_0626400	6	Sec14 domain containing protein	2.59	0.12

Table S3. 4 Enriched molecular functions for LD_{50} Chr 6 locus.

Term	Description	p-value
All transferase terms	transferase	0.0024
GO:0016740	transferase activity	0.0049
GO:0003824	catalytic activity	0.0234
GO:0016772	transferase activity, transferring phosphorus-containing groups	0.0357
All zinc-finger terms	zinc-finger	0.0380
All nucleotidyltransferase terms	nucleotidyltransferase	0.1294

Table S3. 5 Enriched biological processes for LD_{50} Chr 6 locus.

Term	Description	p-value
GO:0016070	RNA metabolic process	0.0250
All zinc-finger terms	zinc-finger	0.0380
GO:0034641	cellular nitrogen compound metabolic process	0.0821
GO:0006807	nitrogen compound metabolic process	0.1114
GO:0055114	oxidation reduction	0.2201

Table S3. 6 Enriched molecular functions for LD_{50} Chr 6 × Chr 8 interaction locus.

Term	Description	p-value
All proteasome terms	proteasome	0.0233
GO:0070011	peptidase activity, acting on L-amino acid peptides	0.0586
pfa03050	Proteasome	0.0712
GO:0008233	peptidase activity	0.0817
All Protease terms	Protease	0.0870
All hydrolase terms	hydrolase	0.0902
GO:0003824	catalytic activity	0.1578
GO:0004175	endopeptidase activity	0.1623

Table S3. 7 Enriched biological processes for LD_{50} Chr 6 x Chr 8 interaction locus.

Term	Description	p-value
All proteasome terms	proteasome process	0.0233
pfa:03050	proteasome process	0.0712
All Protease terms	Protease process	0.0870
All hydrolase terms	hydrolase process	0.0902
GO:0006508	proteolysis	0.0930
GO:0019538	protein metabolic process	0.1329

3.6 Acknowledgements

The Roepe laboratory thanks Dr. Don Gardiner (Malaria Biology Laboratory Queensland Institute of Medical Research) for anti PfREX-1 antibody, Dr. Sean Prigge (Johns Hopkins University) for rat anti PfACP antibody, Ms. Chardai Gray and Lauren Jacobs for help with bioinformatics, and Dr. Paul Callaghan, Ds. Katy Sherlach and Dr. Nick Baro for helpful discussions. The following *Plasmodium falciparum* strains were obtained through the MR4 as part of the BEI Resources Repository, NIAID, NIH: HB3, Dd2, 7G8, and the progeny of the HB3×Dd2 cross, deposited by Drs. T. E. Wellems, D. Walliker, D. E. Kyle, and T. E. Wellems, respectively. Our group also thank Dr. David A. Fidock (Columbia University, New York, NY) for providing $C2^{GC03}$, $C4^{Dd2}$, and $C6^{7G8}$. This work was supported by National Institutes of Health (NIH) grants: NIH RO1 AI045957 (to PDR); NIH RO1 AI049367 (to APS); NIH RO1 AI071121 (to MTF); and Kentucky Science and Education Foundation grant: KSEF-2624-RDE015 (to APS).

CHAPTER IV

HIGH-THROUGHPUT MATRIX SCREENING IDENTIFIES SYNERGISTIC AND ANTAGONISTIC ANTIMALARIAL DRUG COMBINATIONS

Chapter IV previously published in part as; Mott, B. T.; Eastman, R. T.; Guha, R.; Sherlach, K. S.; **Siriwardana, A.**; Shinn, P.; McKnight, C.; Michael, S.; Lacerda-Queiroz, N.; Patel, P. R.; Khine, P.; Sun, H.; Kasbekar, M.; Aghdam, N.; Fontaine, S. D.; Liu, D.; Mierzwa, T.; Mathews-Griner, L. A.; Ferrer, M.; Renslo, A. R.; Inglese, J.; Yuan, J.; Roepe, P. D.; Su, X. Z.; Thomas, C. J., High-throughput matrix screening identifies synergistic and antagonistic antimalarial drug combinations. *Scientific reports* **2015,** *5*, 13891 © 2015 with permission extending to all reproduced content.

Contribution of authors:

A.S. conducted cell culture, single-cell photometry experiments to measure changes in DV and cytosolic [Ca^{2+}], immunofluorescence assays to visualize and quantify PfAtg8 puncta localization, and contributed to writing the manuscript.

4.1 Abstract

Drug resistance in *Plasmodium falciparum* parasites is a constant threat. Novel therapies must be discovered at a faster rate, especially drug combination therapies. A high-throughput screen was conducted at cytostatic levels to identify novel, potent antimalarial drug combinations. One interesting class of "partner drug" compounds identified was phosphatidylinositol 3´-kinase (PI3K) inhibitors. Results in chapter 3 suggest that an autophagy-like pathway is involved in stress-

induced cell-death as well as cytocidal chloroquine resistance. Thus, the discovery that PI3K inhibitors were both potent antimalarial drugs and excellent partner drugs for combination therapy was particularly intriguing and their action was further analyzed. Results indicate the ability of these PI3K inhibitors to significantly reduce the autophagy-related puncta response. Another interesting class of compounds revealed in the screen was ion channel modulators. The role of these compounds in calcium homeostasis and mitochondrial membrane polarization, both closely tied to parasite viability, were investigated further. Results suggest a relationship between the effects of ion channel modulators on calcium homeostasis and mitochondrial membrane polarization. Evaluation of drugs and drug combinations requires an appreciation of both IC_{50} (cytostatic) and LD_{50} (cytocidal) activities. Thus, particularly potent and intriguing drug combinations identified in the high-throughput screening were further analyzed using the Chou-Talalay method for assessing synergy.

4.2 Background

Emergence of resistance to antimalarial therapy has been an ongoing challenge for scientists for many decades. Resistance to quinolines such as chloroquine (CQ)[173] and drug combinations such as sulfadoxine-pyrimethamine (SP)[174], have led to the investigation and discovery of many novel antimalarial drugs and combinations. Current antimalarial treatments rely on drug combinations as recommended by the World Health Organization[175]. These combinations include pairing CQ, amodiaquine (AQ), or mefloquine (MQ) with SP, atovaquone (ATQ)/proguanil, quinine (QN) with either tetracycline or doxycycline[176] or artemisinin combination therapies (ACTs)[177-178]. WHO-recommended ACTs include artemether (ATM) + lumefantrine (LUM), artesunate (ATSU) + AQ, artesunate + MQ, dihydroartemisinin (DHA) + piperaquine (PPQ), and artesunate + SP[175]. The benefits of using combination therapies have been

known for decades[179-180] and they are the standard policy for diseases such as human immunodeficiency virus (HIV) infections and tuberculosis[181]. Some of these combinations therapies are administered due to necessity as sometimes monotherapies fail with certain patients. However, the purpose of administering drug combinations in malaria is different; it is mainly to prevent or delay the emergence of resistance[182].

This concept can be understood with a simple example: Assuming the mutation rate leading to resistance is 10^{-9} in a malaria parasite population, out of a parasite load of 10^{11} in a person, there will be $10^{11}\times10^{-9}=100$ parasites carrying a novel mutation to resistance. If this person is treated with a monotherapy, the likelihood of these 100 new parasites surviving is higher and will lead to recrudescence. However, if a drug combination is administered, assuming the drugs have different mechanisms of action, the parasites will have to gain mutations in two genes simultaneously to acquire resistance, thus dramatically reducing the likelihood of emergence of resistance ($10^{11}\times10^{-9}\times10^{-9}=10^{-7}$, which is one infection out of ten million)[182].

When designing an ACT, two factors should be considered: 1) the partner drug should have a longer half-life and 2) it should have a different mechanism of action (MOA). In the case of ATM + LUM, the pharmacokinetic properties of the two drugs complement each other. ATM is absorbed rapidly and metabolized to DHA. Both have a half-life of approximately 1 hour. LUM on the other hand, is absorbed more slowly and eliminated slowly as well; having a half life of 3-6 days[183]. There is also evidence of these drugs being synergistic in a preclinical setting, however, these claims remain unverified through independent methods[184]. The combination of a highly active drug with a slow-clearing drug ensures the rapid reduction in parasitemia as well as complete clearance of parasites over an extended period of time[183]. Although above mentioned factors should be considered when designing an ACT, most current ACTs were found empirically

without full validation of drug-drug interactions or mode of action (MOA) and therefore may not represent ideal combinations. For example, partner drugs such as mefloquine (MQ) or lumefantrine (LUM) appear to act on pathways similar to those of ART-derived drugs and mutations that modulate susceptibility to one drug may also alter effectiveness of the other, leading to increased tolerance to both compounds[115, 185-186].

The most intricate method to investigate synergy between potential partner drugs involves the generation of a plot named an isobologram[187]. To generate this plot, the activity of partner drugs must be assessed at multiple ratios between the drugs as well as by themselves (for example; ratios of 1:0, 1:1, 1:2, 1:3, 3:1, 2:1 0:1). Results from this analysis can be used to generate values named fractional inhibitory concentrations (FIC). These values are used to generate an isobologram that illustrates whether a drug combination is synergistic, antagonistic, or additive. However, this method is time consuming and requires performing a large number of individual assays. In order to investigate synergy in a simpler, yet mathematically sound method, David Chou and Paul Talalay, developed a technique, which is now known as the Chou-Talalay (C-T) method[96, 188]. This method is simple in nature and flexible. Results from this method are not dependent on the mechanism of action or the units used. It is efficient because of its simplicity and thus, economical as well. Most importantly, it gives a numerically indexed conclusion[188]. As in the case of generating isobolograms, an FIC needs to be calculated initially in this method. However, compared to an isobologram analysis, C-T analysis only requires one fixed ratio of the pair of drugs tested. The FIC values calculated for individual drugs are then added to generate an FIC_{Index}, and this is the term that gives the indication of the nature of interaction between drugs. Based on their derivations, Chou and Talalay assigned synergy when the FIC_{Index} is less than 1. An FIC_{Index} of 1 indicated additivity and greater than 1 indicated antagonism. However, cutoffs for

definition of drug pair behavior are sometimes altered from these values based on experimental variance and other factors - for example, in the literature, synergy has been defined as being less than 0.5 to antagonism being greater than 4 [98].

Similar to the study of potency of single drugs on malaria parasites, drug combination analysis has been traditionally done at cytostatic concentrations. Similar to the observation of the difference in drug target and mechanism of action at cytostatic versus cytocidal concentrations[17, 133-135], recent work by Gorka *et al*. indicates a difference in drug interaction at these varying levels of drug[103]. Therefore, it is also important to investigate the effect of drug combinations at cytocidal concentrations as these are the concentrations relevant for killing parasites. This analysis has to be expanded to also ensure that the partner drugs would have compatible pharmacokinetics and pharmacodynamics, MOAs that do not promote concurrent resistance, efficacy against existing drug-resistant parasites, and no toxicity. Another factor demanding the development of novel drug combinations is the disturbing emergence of parasites exhibiting reduced clearance following ACT treatment[62, 79, 189]. Developing effective, long lasting drug combinations requires evaluation of large numbers of known and candidate antimalarials. While large-scale single agent screens have identified novel antimalarials, there remains a need for an assessment of new antimalarial drug combinations[190-191]. Therefore, high-throughput combination screens were performed in collaboration with scientists at the National Center for Advancing Translational Science (NCATS) using compounds with diverse mechanisms of action (MOAs) to identify multiple classes of compounds that interact favorably against *P. falciparum*.

4.3 Results

Initially, 2317 single agents were evaluated, including known antimalarials, approved and investigational drugs and mechanistically annotated small molecules against three *P. falciparum* strains (3D7, HB3 and Dd2). The activities of many pharmacologically diverse agents were confirmed including alvespimycin (human HSP90 inhibitor), propafenone (ion channel modulator) and carfilzomib (human proteasome inhibitor) (Figure 4.1).

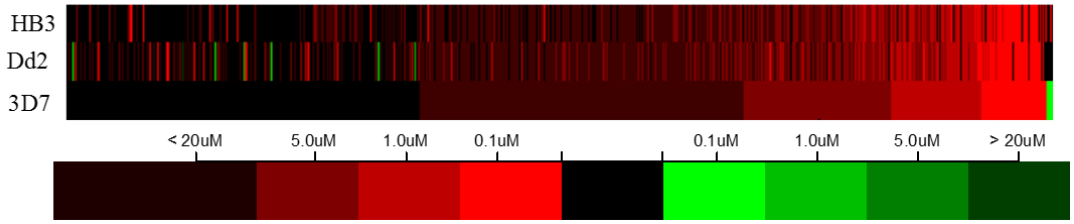

Figure 4. 1 Heat map representation of 2317 approved and investigational drugs. (Data available at *http://pubchem.ncbi.nlm.nih.gov/*)

Other notable findings were the potent activities associated with small molecules targeting human phosphatidylinositide 3-kinases (hPI3K) including GSK-2126458, NVP-BGT226, Torin 2, and PIK 93. The *Plasmodium falciparum* genome is known to contain only one PI3K[156], thus, these compounds were of particular interest. The involvement of autopaghy in the resistance mechanism to chloroquine as well as the potential of Vps34 being a regulatory step in the autophagy cascade in the absense of an mTOR homologue in the *Plasmodium* genome[17] aids in driving the interest in this class of compounds.

Next, eleven iterative combination screens were performed, with compounds selected from the single agent screen based on potency, mechanistic interest and clinical status. A comprehensive set of 240 combinations of interest was further assessed in duplicate against two individual cultures for each of the three parasite strains. The approved and investigational drugs included a collection of antimalarials including dihydroartemisinin (DHA), artemether (ATM), artesunate

(ATS), CQ, MQ, amodiaquine (AQ) and piperaquine (PPQ) as well as drugs designated for numerous and diverse indications. To better understand the standard-of-care for treating malaria infections, the currently approved ACTs (ATM-LUM, AS-MQ, ATS-pyronaridine, ATS-AQ, DHA-PPQ) were analyzed. Consistent with previous reports both ATM-LUM and ATS-MQ were noted to interact favorably[192-193].

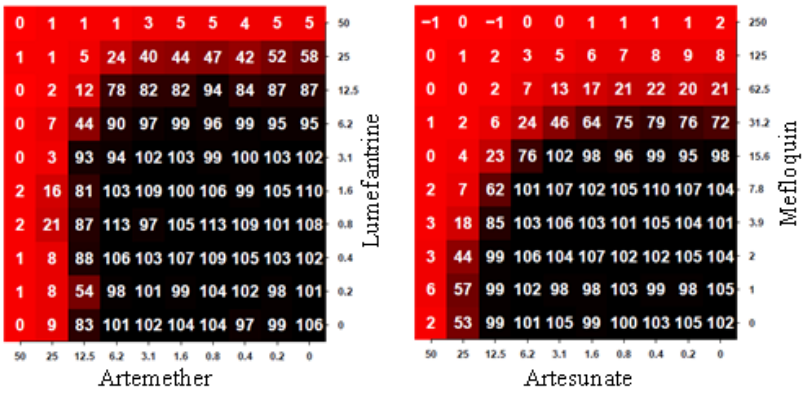

Figure 4. 2 Combination data (10×10 plots) for drug combinations representing the standard of care (ATM + LF, ATS + MQ).

Several combinations exceeded the synergy noted for ATM-LUM and ATS-MQ including 13 drug combinations listed in Table 1. Additionally, many hitherto unexplored drug combinations were identified as being synergistic or additive, including combinations of approved antimalarials (ARTs, LUM, MQ) with ion channel modulators (e.g. nicardipine), novel mitochondrial targeting agents (e.g. ML238), drugs targeting human enzymes and receptors (e.g. BIX-01294, alvespimycin and NVP-BGT226), and agents currently undergoing single agent clinical assessment in malaria trials (tafenoquine) (Table 1).

Table 4. 1 Noteworthy synergistic combination results from >4,000 discreet combinations tested. Data is against *P. falciparum* 3D7. Mechanistic class reflects general terms and is not intended to cover all putatively contributing pharmacologies of the drugs listed (may reflect hypothesized mechanism based on mammalian target).

Drug A	**Mechanistic Class**	**Drug B**	**Mechanistic Class**
ATM	Endoperoxide	Alvespimycin	HSP90 inhib.
ATM	Endoperoxide	M.B.	oxid. stress inducer
ATM	Endoperoxide	NVP-AUY992	HSP90 inhib.
ATM	Endoperoxide	NVP-BGT226	PI3K inhib.
ATM	Endoperoxide	Reserpine	Ca^{2+} channel inhib.
ATM	Endoperoxide	Quisinostat	HDAC inhib.
ATM	Endoperoxide	KN-62	CaM kinase II inhib.
ATM	Endoperoxide	LUM	Heme conversion inhib.
ATS	Endoperoxide	MFQ	Heme conversion inhib.
ATS	Endoperoxide	Propafenone	Na^{+} channel inhib.
DHA	Endoperoxide	LUM	Heme conversion inhib.
DHA	Endoperoxide	M.B.	oxid. stress inducer
LUM	Heme conversion inhib.	NVP-BGT226	PI3K inhib.
LUM	Heme conversion inhib.	Manidipine	Ca^{2+} channel inhib.
LUM	Heme conversion inhib.	Rifampin	Protein synthesis inhib.
LUM	Heme conversion inhib.	Midostaurin	multikinase inhib.
MFQ	Heme conversion inhib.	Nicardipine	Ca^{2+} channel inhib.
MFQ	Heme conversion inhib.	Midostaurin	multikinase inhib.
AQ	Heme conversion inhib.	BIX-01294	methylation inhib.
Atovaquone	e^{-} transport chain inhib.	ML238	e^{-} transport chain inhib.
Atovaquone	e^{-} transport chain inhib.	Decoquinate	e^{-} transport chain inhib.
Atovaquone	e^{-} transport chain inhib.	Genz-669178	PfDHODH inhib.
ML238	e^{-} transport chain inhib.	Genz-669178	PfDHODH inhib.
NITD-609	Protein synthesis/PfATPase4 inhib.	Trichostatin A	HDAC inhib.
Leptomycin B	Nuclear export inhib.	Nanchangmycin	Antibiotic

The calcium channel inhibitor verapamil is known to reverse CQ resistance in *P. falciparum*. Several reports demonstrate that this phenotype is the result of verapamil's interaction with the *P. falciparum* CQ resistance transporter (PfCRT) altering carrier-mediated drug efflux of CQ[194-196]. At least one study failed to associate the level of CQ efflux with sensitivity in the presence and absence of verapamil and a recent analysis confirmed that diverse PfCRT variants differ in their ability to modulate CQ transport[162, 197]. Results indicate that the level of synergy found for antimalarials and ion channel modulators is maintained across the CQ sensitive (CQS) 3D7 and HB3 strains and the CQR Dd2 strain (Figure 4.3A). This generalized and consistent level of synergy in both CQR and CQS lines is noteworthy given that the potential contribution of drug transporters might otherwise be theorized to result in differential synergy in these lines.

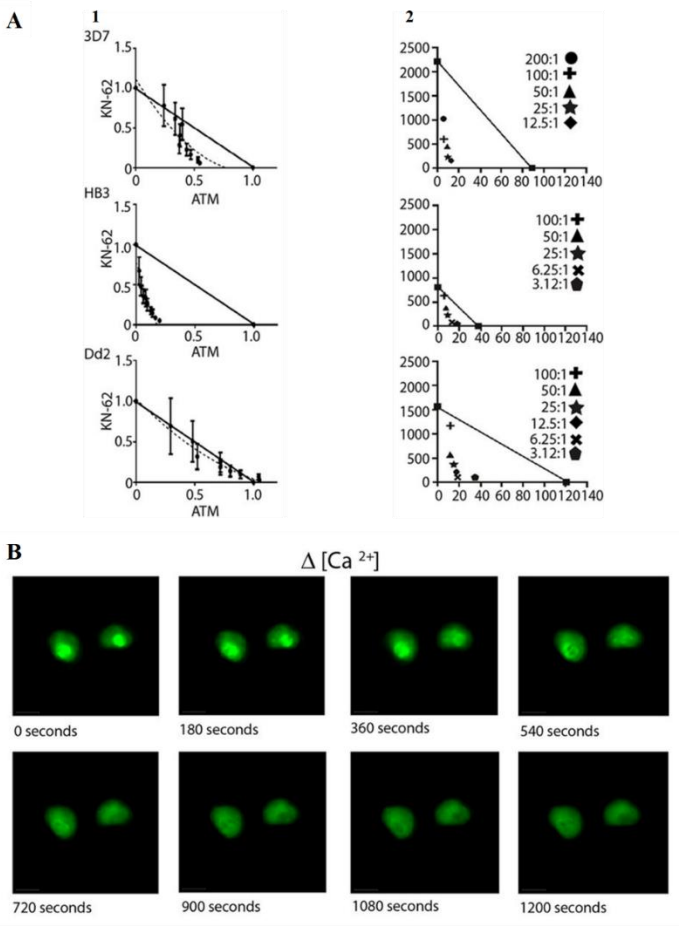

Figure 4. 3 Disruption of calcium homeostasis and alteration of mitochondrial potential for selected drugs and drug pairs. (A) Examination of the combination responses of KN-62 and ATM in three parasite lines via an isobologram analysis of the mitochondrial membrane potential as judged by a combination JC1 assay (panel 1) and isobolographic analysis of the viability combination response (panel 2). (B) Time lapsed capture of calcium dependent Fura −2 fluorescence for two live side-by-side intraerythrocytic strain Dd2 parasites showing rapid loss of digestive vacuole (DV) Ca^{2+}(bright green inner circle, top panels) upon perfusion with cytocidal ($2 \times LD_{50}$) dose of CQ (see methods).

An examination of calcium homeostasis and mitochondrial membrane polarization, both closely tied to parasite viability, was conducted for potential insight into the mechanism of these combination responses. Utilizing single cell photometry, I noted an acute release of Ca^{2+} from the parasite digestive vacuole (DV) with a concomitant increase in cytosolic Ca^{2+} upon treatment with CQ (Figure 4.3B, Table 4.2). A similar increase in cytosolic Ca^{2+} was noted for ATM, LUM, propafenone, nicardipine, reserpine and KN-62 (Table 4.2). Calcium homeostasis is regulated in all cells through several complementary mechanisms including the action of membrane transporters and the use of ER and lysosomal (DV) stores[198]. Mitochondrial Ca^{2+} uptake is also an important regulatory process and pronounced Ca^{2+} uptake can be accompanied by a transient loss of polarization which can be detected experimentally. By monitoring the mitochondrial potential in all three *P. falciparum* strains (3D7, HB3 and Dd2) in response to selected drugs applied singly or in combination, it could be determined which agents altered mitochondrial membrane potential and assess if these actions were synergistic (Figure S4.1-S4.4, Appendix B). Strikingly, each of the drugs shown to cause an increase in cytosolic Ca^{2+} was found to induce mitochondrial depolarization (Table 4.2, Figures S4.1-S4.4, Appendix B). Furthermore, several agents (PIK-93, cinacalcet, elesclomol, GSK-1059615) that did not modify cytosolic Ca^{2+} levels were found to have no effect on mitochondrial polarization (Table 4.2).

Table 4. 2 Change in cytosolic and DV [Ca^{2+}].

Strain	Location of Measurement	Drug	Change in [Ca^{2+}] (nM/min)
Dd2	DV	CQ ($2XIC_{50}$)	-0.08
		CQ ($2XLD_{50}$)	-3.82
	Cytosol	CQ ($2XIC_{50}$)	0.83
		CQ (2XLD50)	5.15
HB3	Cytosol	Artemether ($2XIC_{50}$)	1.11
		Artemether ($2XLD_{50}$)	3.91
		Lumefantrine ($2XIC_{50}$)	0.07
		Lumefantrine ($2XLD_{50}$)	2.82
		Propafenone ($2XIC_{50}$)	0.35
		Propafenone ($2XLD_{50}$)	6.50
		Nicardipine ($2XIC_{50}$)	0.04
		Nicardipine ($2XLD_{50}$)	4.84
		KN-62 ($2XIC_{50}$)	0.63
		KN-62 ($2XLD_{50}$)	2.20
		CQ ($2XIC_{50}$)	0.27
		CQ ($2XLD_{50}$)	1.30
		Reserpine (0.5 μM)	1.70
		Reserpine (1 μM)	1.85
		Reserpine (5 μM)	3.40
		PIK-93 ($2XIC_{50}$)	0.46
		PIK-93 ($2XLD_{50}$)	0.66
		Cinacalcet ($2XIC_{50}$)	0.76
		Cinacalcet ($2XLD_{50}$)	0.53
		Elesclomol ($2XIC_{50}$)	0.47
		Elesclomol ($2XLD_{50}$)	0.50
		GSK-1059615 ($2XIC_{50}$)	0.53
		GSK-1059615 ($2XLD_{50}$)	0.38

Examination of drug combination effects on mitochondrial depolarization mirrored the outcomes from the parasite viability screens. For instance, the effect on mitochondrial potential for the combination of ATM and KN-62 was synergistic or additive in each line (Figure 4.3A,

Panel 1) which mirrored the synergistic responses in this study (Figure 4.3A, Panel 2). Similar results were seen for many ARTs and ion channel modulator combinations including the combination of ATM and reserpine (Figure S4.4, Appendix B). These data suggest a relationship between Ca^{2+} release and mitochondrial depolarization, and further substantiate the connectivity of calcium homeostasis to the actions of multiple antimalarial agents. While these data represent a new element to the debate surrounding the contribution of calcium channel modulation to antimalarial action they do not eliminate the potential contribution of PfCRT or other drug transporters to the synergy noted between antimalarials and ion channel modulators.

Pharmacological induction of oxidative stress or alteration of the parasite response to elevated reactive oxygen species (ROS) is a postulated MOA for several antimalarial drug classes. ARTs are reportedly activated by hemoglobin degradation products, presumably heme or ferrous iron, thereby inducing oxidative stress within the DV[51]. The endoperoxide pharmacophore of ARTs is absolutely required for activity, and several studies have correlated excess ROS levels with activity[51, 199]. Recent reports suggest that a regulated autophagy cascade in response to oxidative stress may play a role in *P. falciparum* fitness and response to selected therapies (see previous chapter, this thesis). A quantitative trait loci (QTL) analysis of CQR versus CQS parasite strains correlates increased numbers of *Plasmodium* autophagy-related protein 8 (PfATG8) puncta with drug response and identified candidate drug resistance genes involved in modulating this cascade[17] (previous chapter, this thesis). Interestingly, in all eukaryotes, the autophagy cascade requires the coordinated function of multiple autophagy-related proteins and the regulatory activities of the PI3K Vps34[24, 35]. The single agent screens included numerous investigational drugs targeting human PI3Ks and mTOR (Figure 4.1), including the potent mTOR inhibitor torin 2 which was recently reported to have impressive

antimalarial activity against the asexual, liver and gametocyte stages of malaria[200-201]. Additional examples include advanced clinical candidates NVP-BGT226 (a structural congener of torin 2, Dd2 IC_{50} = 2.1 nM), GSK-2126458 (Dd2 IC_{50} = 124 nM), INK-128 (Dd2 IC_{50} = 69 nM) and ZSTK-474 (Dd2 IC_{50} = 67 nM) (Figure 4.1). The *Plasmodium* genome possesses only one PI3K (a class III Vps34 ortholog)[156], thus making it a possible target of these agents. There are, nevertheless, other potential targets for these drugs that could explain their strong activity.

An investigation of the parasite autophagy-related response to selected drug combinations proved insightful. In eukaryotes, PfAtg8 positive vesicle formation is downstream from Vps34. In *P. falciparum*, PfAtg8, in part, tracks to apicoplast-targeted vesicles[24, 27, 35]. In response to cytocidal CQ treatment, PfAtg8 has been shown to traffic in a more radially dispersed pattern along with an autophagosomal complex that includes PfRab7[17, 27, 35]. A similar radial distribution of puncta occurs upon treatment with ATM, LUM, and AQ (Figures 4.4-4.5). Similar to CQ, radial distribution of puncta in response to ATM was increased at LD_{50} dose (Figure 4.4B) relative to IC_{50} dose (Figure 4.4A), and application of Coartem (ATM+LUM) induced an even greater response (Figures 4.4C, 4.7). Interestingly, administration of NVP-BGT226 or GSK-2126458 at their LD_{50} concentrations in combination with ATM, LUM, AQ and CQ or applied to parasites cultured in starvation conditions did not elicit the same increase in autophagosomal trafficking (Figures 4.4D, 4,4E, 4.5-4.7). Similar reduction in autophagosomal trafficking was observed when starvation was administered with Torin 2, PIK-93 or INK-128 at LD_{50} (Figure 4.6). Autophagy is a prosurvival response; however, rapid overstimulation of the autophagy response can lead to cell death. Following administration of two autophagy-inducing agents (e.g. ATM and LUM), parasite fitness may be

compromised due to the rapid onset of the autophagy response. Administration of a stimulant and inhibitor (e.g. ATM and NVP-BGT226) may lead to parasite death through blockade of this key survival response. Inhibition of human class I PI3Ks (the targets of NVP-BGT226 and GSK-2126458) and mTOR can have contextually diverse effects on autophagy while inhibition of Vsp34 is generally regarded as a means to mitigate the autophagy response. If these drugs do inhibit PfVps34 it suggests a role for this key regulator protein and PI(3)P in the parasite autophagy response and that targeting this response is deleterious to parasite fitness.

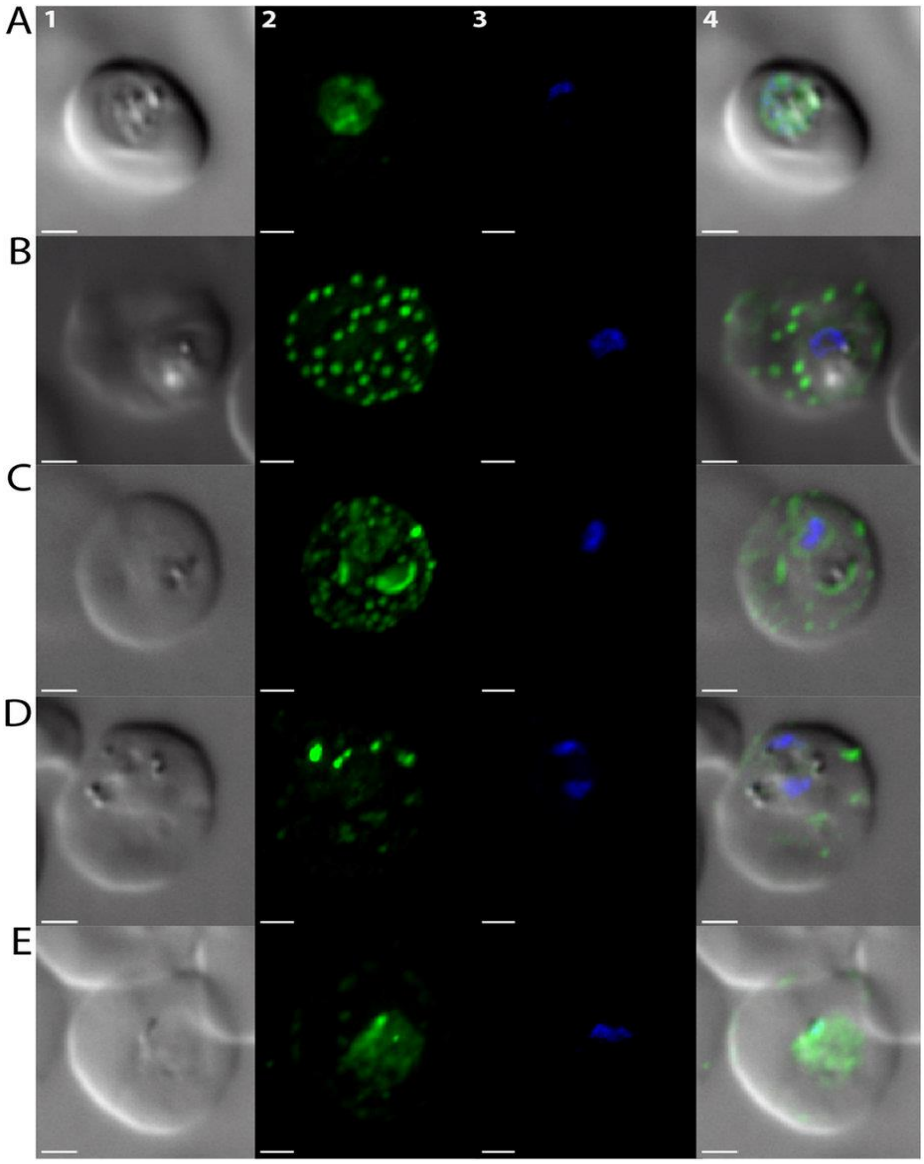

Figure 4. 4 Analysis of autophagosomal body puncta formation and trafficking in response to pharmacological stress. Imaging of PfAtg8 containing puncta within parasite (the *Plasmodium falciparum* HB3 strain) infected RBC after 6-hour bolus exposure to Artemether (ATM) or ATM combinations: (**A**) ATM at the defined IC_{50} value (7.2 nM). (**B**) ATM at the defined LD_{50} value (16.3 nM). (**C**) ATM and LUM at their respectively defined LD_{50} values (16.3 nM and 323 nM, respectively). (**D**) ATM at the defined LD_{50} value and GSK-2126458 at the defined LD_{50} value (101.7 μM). (**E**) ATM at the defined LD_{50} value and NVP-BGT226 at the defined LD_{50} value (17.5 nM). Panel 1: transmittance image. Panel 2: anti-PfAtg8 antibody imaging. Panel 3: DAPI nuclear staining. Panel 4: a merged image of all three channels. Bar = 2 μm.

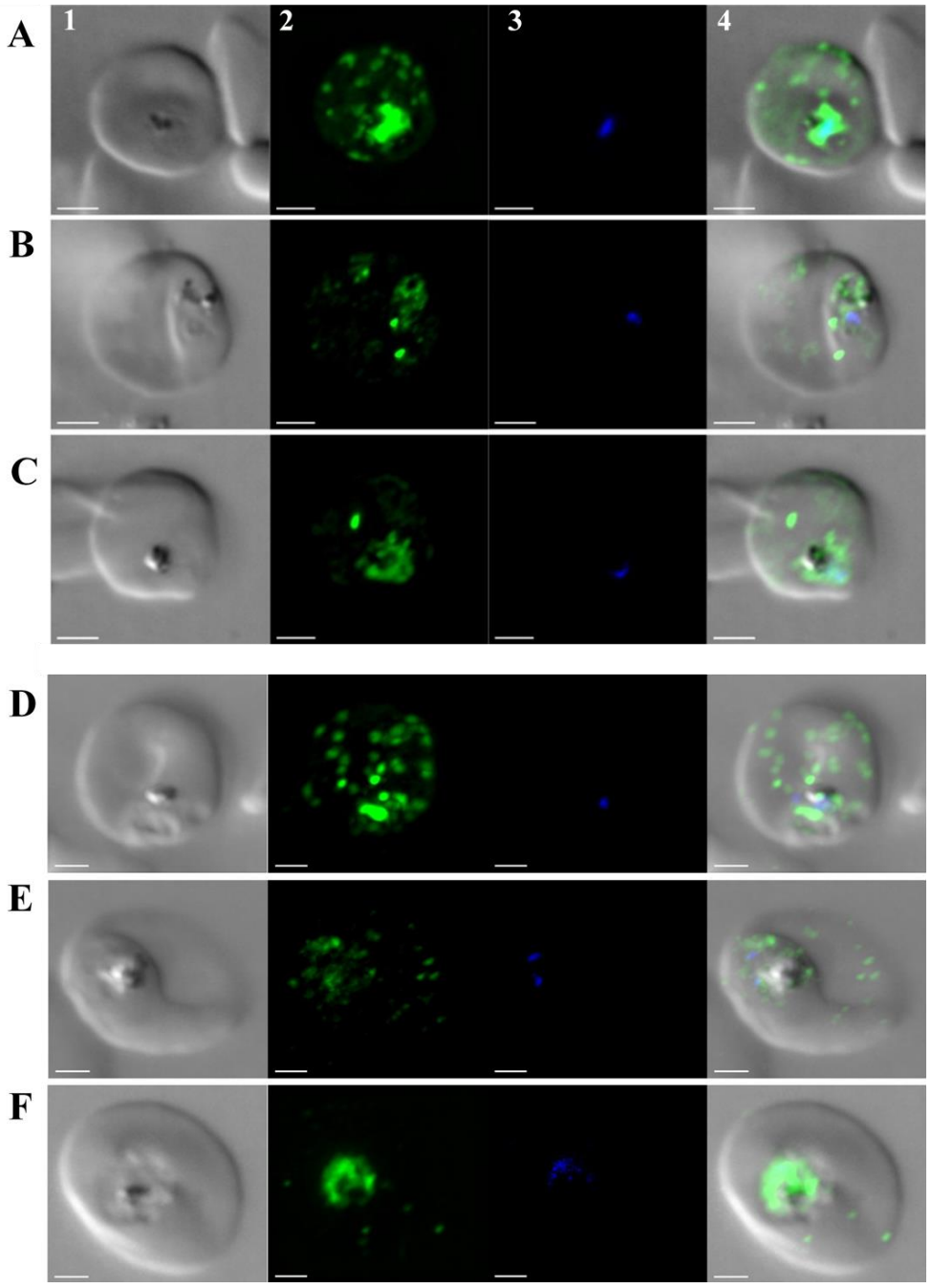

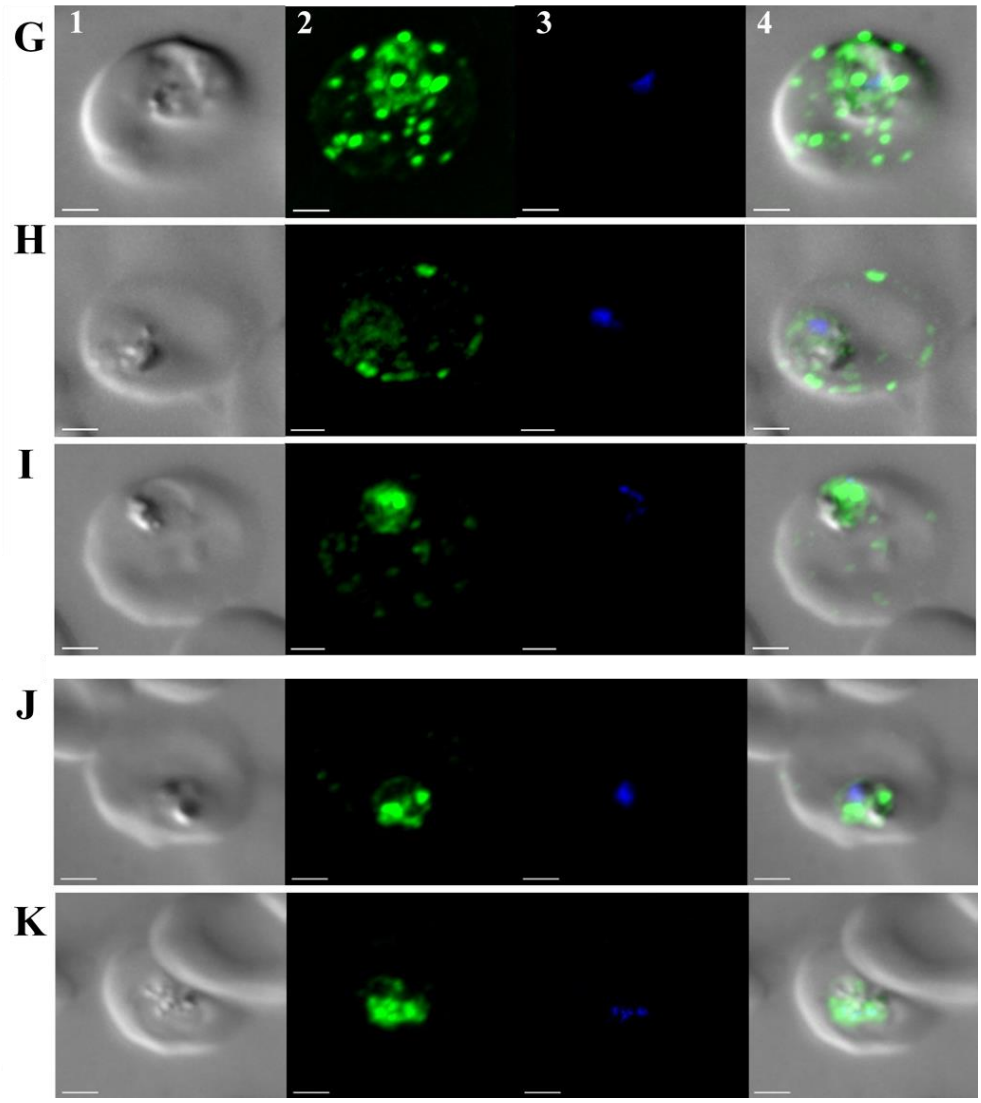

Figure 4.5 Analysis of autophagosomal body puncta formation and trafficking in response to pharmacological stress. Imaging of PfAtg8 containing puncta within parasite infected RBCs as judged by a static view of RBC and parasite (panel 1), anti-PfAtg8 peptide antibody imaging (panel 2), DAPI nuclei (panel 3), a merged image of all three views (panel 4) of (HB3) parasites following a 6-hour exposure to (**A**) CQ at the defined LD_{50} value. (**B**) CQ at the defined LD_{50} value and GSK-2126458 at 101.7 μM. (**C**) CQ at the defined LD_{50} value and NVP-BGT226 at 17.5 nM. (**D**) AQ at the defined LD_{50} value. (**E**) AQ at the defined LD_{50} value and GSK-2126458 at 101.7 μM. (**F**) AQ at the defined LD_{50} value and NVP- BGT226 at 17.5 nM. (**G**) LUM at the defined LD_{50} value. (**H**) LUM at the defined LD_{50} value and GSK-2126458 at 101.7 μM. (**I**) LUM at the defined LD_{50} value and NVP- BGT226 at 17.5 nM. (**J**) GSK-2126458 at the defined LD_{50} value. (**K**) NVP-BGT226 at the defined LD_{50} value. Bar = 2 μm.

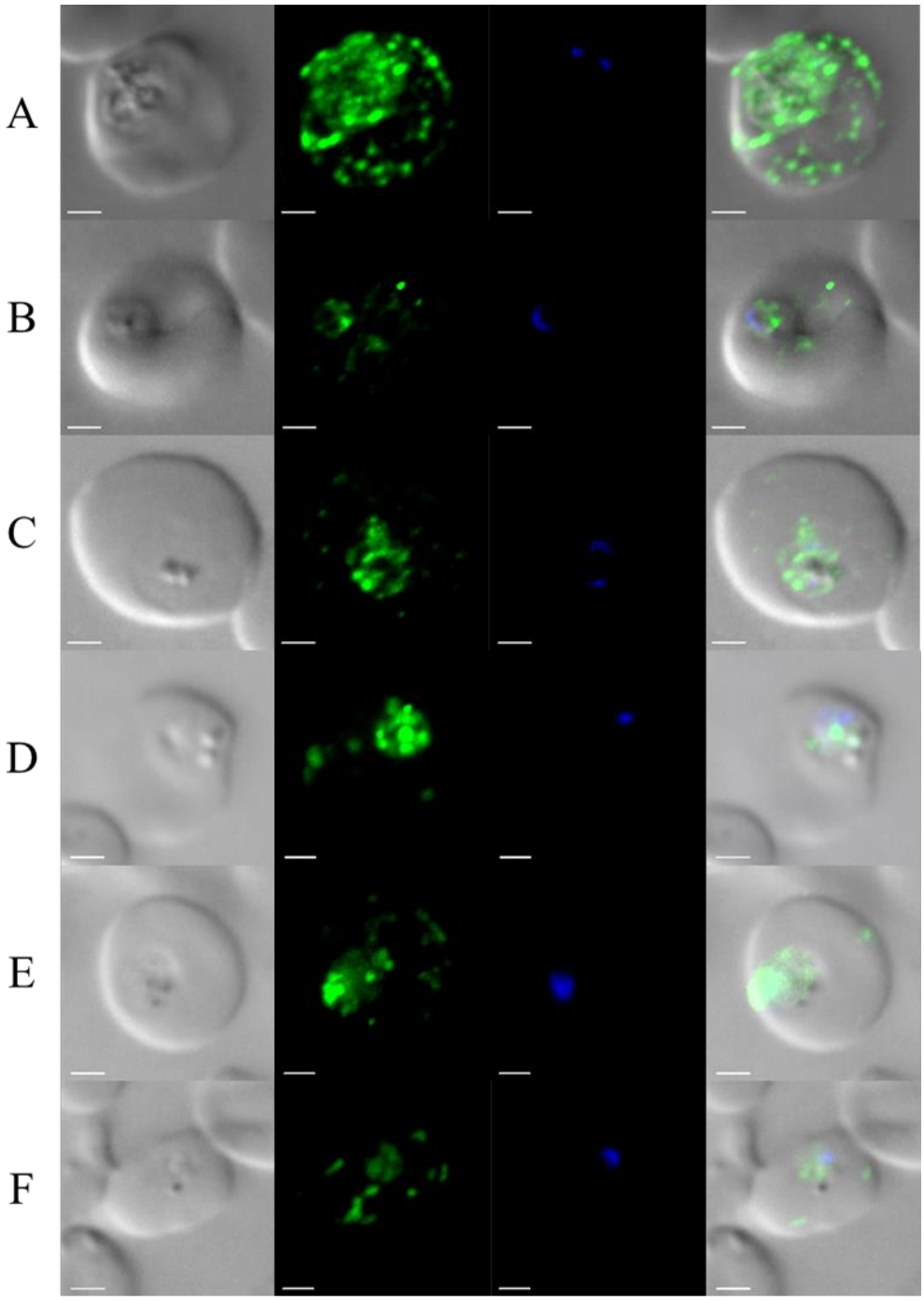

Figure 4. 6 Analysis of autophagosomal body puncta formation and trafficking in response to environmental and/or pharmacological stress. Imaging and quantitation of PfAtg8 containing puncta within parasite infected RBC as judged by a static view of RBC and parasite (panel 1), anti-PfAtg8 peptide antibody imaging (panel 2), DAPI nuclei staining (panel 3), a merged image of all three views (panel 4) of (HB3) parasites following a 6-hour exposure to starvation media (A) with no drug added. (B) GSK-2126458 at the defined LD_{50} value. (C) NVP-BGT226 at the defined LD_{50} value. (C) Torin 2 at the defined LD_{50} value. (D) PIK-93 at the defined LD_{50} value. (F) INK-218 at the defined LD_{50} value. Bar = 2 μm.

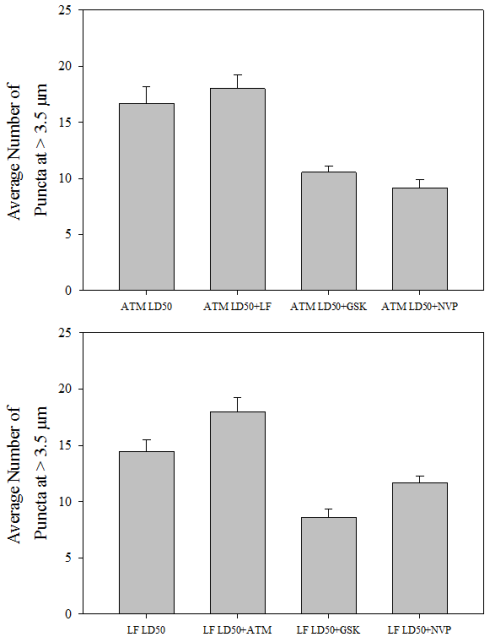

Figure 4. 7 Quantification of PfATG8 positive puncta. PfATG8 positive puncta, quantified as described previously[17], were measured upon treatment with LD_{50} – doses of ATM, LUM, ATM+LUM (CoArtem) as well as either ATM or LUM in the presence of two PI3K inhibitors (GSK-2126458 or NVP-BGT226). The first two bars (left) and the last two bars (right) in each plot are not statistically different (P value > 0.05), but either of the first two bars are statistically different from either of the second two bars in both plots (P value < 0.05).

Translation of drugs and drug combinations requires an appreciation of both IC_{50} and LD_{50} (cytocidal) activities. A recent study of quinoline-based combinations highlights that drug pairs found to be synergistic by a fixed-ratio isobologram methodology using IC_{50} derived values to quantify activity were not necessarily synergistic when LD_{50} values were tested[103]. Therefore, the LD_{50} values for several agents including ATM, LUM, NVP-BGT226, torin 2, and GSK-2126458 were examined (Table S4.1). Further, while LD_{50} doses for quinoline-based drugs are often higher relative to IC_{50} doses (for example CQ; LD_{50} = 250 nM, IC_{50} = 20 nM for the CQS strain HB3, LD_{50} = 16,000 nM, IC_{50} = 200 nM for the CQR strain Dd2), the LD_{50} and IC_{50} values for ARTs are more closely aligned. To appreciate how each alternate drug: drug

ratio will alter their combination profile, several combinations at ratios determined by their IC_{50} and LD_{50} were analyzed using the Chou-Talalay method (C-T).

There are multiple methods for assessing the efficacy of combination drug therapies[202-204]. Some of these methods can be extremely time consuming. The Chou-Talalay "one-point" method, in comparison, is simpler and it requires the evaluation of the drug pair at a singular ratio. In this method, the two drugs in question are utilized at a 1:1 effective dose (IC_{50}:IC_{50} or LD_{50}:LD_{50}; note absolute concentrations are not necessarily equal) over a range of multiple concentrations, generating C-T plots of parasite growth or survival as a function of each drug concentration. These plots are then used to calculate fractional inhibitory concentrations (FIC) for each drug in question using Equation 1-3.

$$FIC_A = \frac{IC_{50}\ of\ Drug\ A\ in\ Combination}{IC_{50}\ of\ Drug\ A\ alone} \qquad \text{(Equation 1)}$$

$$FIC_B = \frac{IC_{50}\ of\ Drug\ B\ in\ Combination}{IC_{50}\ of\ Drug\ B\ alone} \qquad \text{(Equation 2)}$$

$$FIC_{Index} = FIC_A + FIC_B \qquad \text{(Equation 3)}$$

The individual FICs are then added (Equation 3) to determine the FIC_{Index} of the drug combination therapy (or FLD_{Index} if examining cytocidal potency). This one point Chou-Talalay analysis provides a clear distinction between synergistic, additive and antagonistic drug pairs[96]. Based on their calculations, Chou and Talalay define additivity when the FIC_{Index} equals 1. When the FIC_{Index} is less than 1, the interaction is synergistic; when it is greater than 1, the interaction is antagonistic[96]. However, when warranted, these ranges can be altered based on experimental variance - from synergy being less than 0.5 to antagonism being greater than 4[98] or additivity being represented between 1 and 2[99]. For the purpose of this study, synergy was defined as having an $FIC_{Index}/FLD_{Index}<1$, additivity as FIC_{Index}/FLD_{Index} between 1-2 and antagonism as having an $FIC_{Index}/FLD_{Index}>2$.

Most of the studied combinations show additive interactions at the cytostatic level, including the combination of ATM and LUM (Coartem) (Table 4.3). Synergy is seen in both HB3 and Dd2 parasites for the LUM+GSK-2126458, ATM+GSK-2126458 in HB3 alone, and LUM+torin2 and LUM+PIK-93 in Dd2 alone. No antagonistic interactions were observed.

Table 4. 3 Average $FIC_{Indices}$

Combo	Average FIC_{Index}				IC Assignment	
A/B	**HB3**	**SEM**	**Dd2**	**SEM**	**HB3**	**Dd2**
ATM/LUM	1.1	0.2	1.1	0.2	**Add**	**Add**
LUM/ GSK212	1	0.2	0.67	0.2	**Syn**	**Syn**
ATM/GSK212	1	0.3	1.1	0.3	**Syn**	**Add**
LUM/NVP	1.6	0.1	1.5	0.3	**Add**	**Add**
ATM/NVP	1.6	0.2	2	0.4	**Add**	**Add**
LUM/Torin 2	1.4	0.4	0.9	0.1	**Add**	**Syn**
ATM/Torin 2	1.3	0.5	1.3	0.2	**Add**	**Add**
LUM/PIK93	1.2	0.3	0.81	0.2	**Add**	**Syn**
ATM/PIK93	1.8	0.6	1.1	0.2	**Add**	**Add**

Under cytocidal conditions, a greater number of combinations were determined to be synergistic (Table 4.4). Additive interactions were only observed for ATM+LUM, ATM+NVP-BGT226 for HB3 and LUM+NVP-BGT226, LUM+PIK-93 for Dd2. Contrary to cytostatic conditions, two combinations were observed to be antagonistic under cytocidal conditions; LUM+NVP-BGT226 in HB3 and ATM+PIK-93 in Dd2. GSK-2126458 was the most potent synergy partner, yielding the lowest $FLD_{Indices}$.

Table 4. 4 Average $FLD_{Indices}$

Combo	Average FLD_{Index}				LD Assignment	
A/B	**HB3**	**SEM**	**Dd2**	**SEM**	**HB3**	**Dd2**
ATM/LUM	1.3	0.4	1	0.3	**Add**	**Syn**
LUM/GSK212	0.18	0.04	0.35	0.1	**Syn**	**Syn**
ATM/GSK212	0.62	0.1	0.39	0.3	**Syn**	**Syn**
LUM/NVP	2.8	0.7	2	1	**Ant**	**Ant**
ATM/NVP	1.4	0.2	0.93	0.3	**Add**	**Syn**
LUM/Torin2	0.28	0.2	0.5	0.4	**Syn**	**Syn**
ATM/Torin2	0.46	0.2	0.94	0.4	**Syn**	**Syn**
LUM/PIK93	0.9	0.3	1.5	0.03	**Syn**	**Add**
ATM/PIK93	0.85	0.3	2.1	0.4	**Syn**	**Ant**

These results substantiate that synergy, additivity and antagonism are conditional and will depend on many variables including drug concentration and parasite strains.

4.4 Discussion

Most ACTs being used currently were discovered empirically and drug-drug interactions and compatibilities of modes of action were not fully investigated. Thus, there is a possibility that some drug combinations used today might not be ideal partners. Coartem, or the ATM/LUM combination is one such combination. Early work done on validating this combination are not available outside of China for the most part, and such available data is in Chinese. This makes it difficult to investigate the trajectory of this combination from China to one of the main ACTs supported by the WHO. Although there are claims on the activity of this combination in a preclinical setting, this is not verifiable[184]. Reports that can be found on this combination have declared a synergistic interaction based on discussions of pharmacokinetic properties of ATM and LUM and results from clearance of parasites in animal models[183, 205], but quantitative Chou-Talalay or classical isobologram data are lacking.

The emergence of parasites showing reduced clearance to ACTs[62, 79, 189] have amplified the significance of the discovery of new combination therapies. The high-throughput screening of single drugs and drug combinations led us to the identification of many pharmacologically diverse agents including alvespimycin (human HSP90 inhibitor), propafenone (ion channel modulator) and carfilzomib (human proteasome inhibitor) and a interestingly a few compounds that target human phosphatidylinositide 3-kinases (hPI3K) including GSK-2126458, NVP-BGT226, Torin 2, and PIK 93. This discovery was significant due to the presence of a single PI3K in the *Plasmodium* genome [156] and the absence of an mTOR homologue, thus making a potentially significant regulator of the autophagy pathway a drug target in *Plasmodium* parasites.

Work done by Gaviria *et al*. showed that an autophagy-like pathway is activated upon treatment of parasites with either nutrient-depleted medium or cytocidal concentrations of drug. This pathway was also shown to be dysregulated in parasites showing resistance to CQ. Taken together, these led us to further invertigate the mechanism of action of these PI3K inhibitor drugs. Immunofluorescence assays show that drugs such as ATM caused an increase in the autophagosomal-body puncta formation. This could cause parasite fitness to be compromised as a result of the rapid overstimulation of the autophagy response. PI3K inhibitor drugs (GSK-2126458 and NVP-BGT226) were capable of blocking, to a certain extent, the autophagosomal body puncta formation caused by these drugs or through starvation along with being synergistic with ATM in killing intraerythrocytic *P. falciparum*. In this case, administration of an inducer and an inhibitor to the survival mechanism could be deleterious and lead to death of parasites.

Another significant finding was the discovery of synergy between ion channel modulators and artemisinins. Studies with single cell photometry done using cytodical concentrations of CQ showed a rapid loss of Ca^{2+} from the parasite DV with a concomitant

increase in cytosolic Ca^{2+}. Similarly, an increase in cytosolic Ca^{2+} was observed for ATM, LUM, propafenone, nicardipine, reserpine and KN-62 at cytocidal concentrations. Many complementary mechanisms, including the action of membrane transporters and the use of ER and lysosomal (DV) Ca^{2+} stores, are involved in the regulation of calcium homeostasis in all cells[198]. Marked Ca^{2+} uptake by the mitochondria can lead to a transient loss of polarization. Interestingly, each drug that caused an increase in cytosolic Ca^{2+} was found to induce mitochondrial depolarization and drugs that did not modify cytosolic Ca^{2+} levels did not have an effect on mitochondrial polarization as well. These results often mirrored the outcomes of viability assays for these drug combinations.

It is important to note that drug combinations should be analyzed not only at cytostatic levels, as done traditionally, but also at cytocidal levels. These are the concentrations that parasites are exposed to in a clinical setting and thus, evaluating the efficacy of combination therapies at these levels of drug is vital. Results showed that most pairings under cytostatic conditions were additive, including the ATM+LUM combination (Coartem). However, under cytocidal conditions, most were synergistic, with LUM+NVP showing the greatest antagonism. ATM+LUM was additive under these conditions as well. Interestingly, immunofluorescence assays showed that the ATM+LUM combination led to an increase in the number of radially distributed autophagosomal-body puncta compared to single drug treatments. This could suggest an increased level of oxidative stress on parasites upon treatment with these two agents.

The response to a single drug or drug combination is a multi-step processes involving target engagement, drug transport, activation and degradation, with possible involvement of other unknown molecular interactions and genetic divergences. Variations in these steps as well as the natural parasite cycles which may alter target candidacy will have significant

consequences for drug efficacy. Strain-dependent differences further highlight the complexity of anti-malarial drug discovery efforts and many of the outcomes of this study will require detailed follow-up with these variabilities in mind.

4.5 Appendix B

Figure S4. 1 Compound effect on *P. falciparum* 3D7 mitochondrial transmembrane potential as assessed by JC1 staining**.**

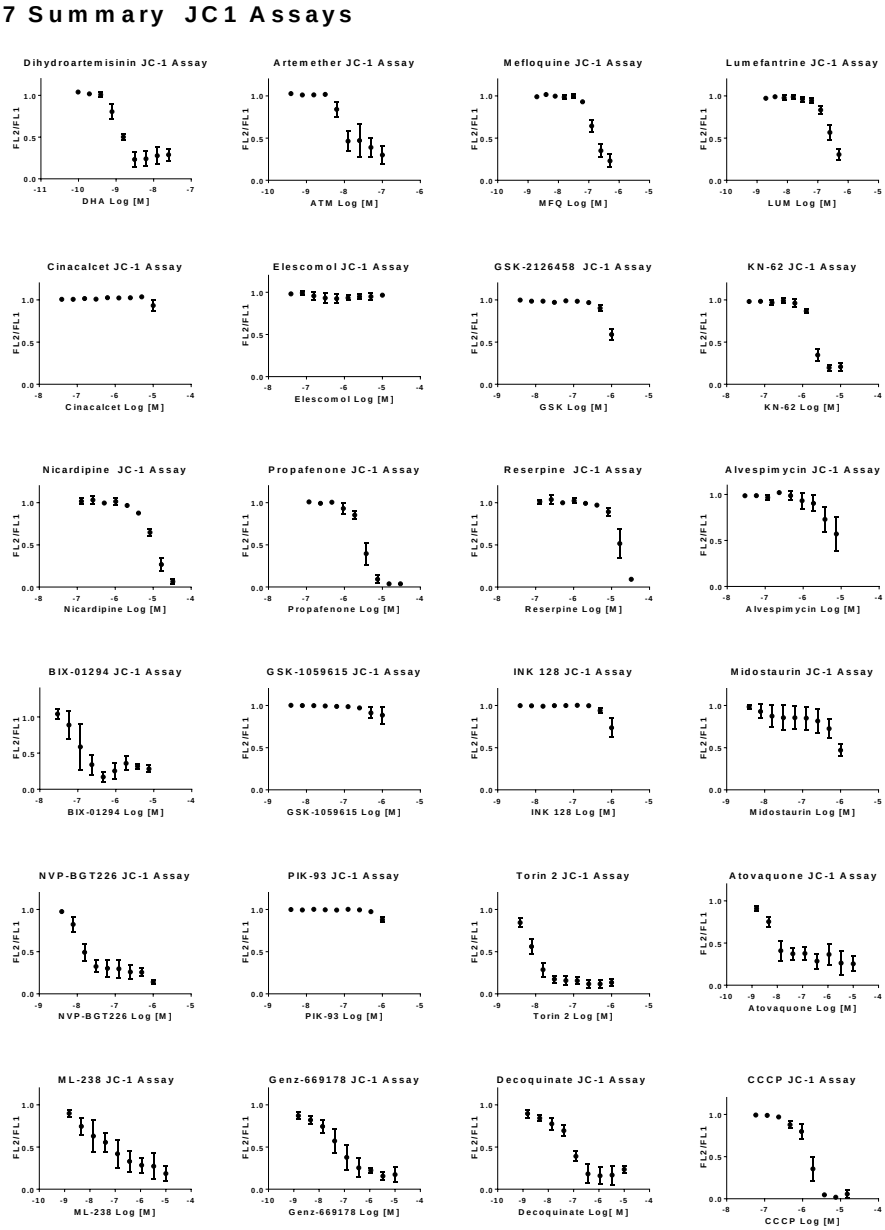

Evaluation of each compounds ability to perturb the mitochondrial membrane potential in a dose dependent manner. Graphs indicate the dose dependent ΔΨ dissipation expressed as FL2/FL1 (Red/green fluorescence ratio). Each value has been normalized versus the FL2/FL1 ratio of the vehicle treated control to which an arbitrary value of 1 has been assigned. Each point is the mean of three independent experiments performed in duplicate, error bars represent SEM.

Figure S4. 2 Compound effect on *P. falciparum* Dd2 mitochondrial transmembrane potential as assessed by JC1 staining**.**

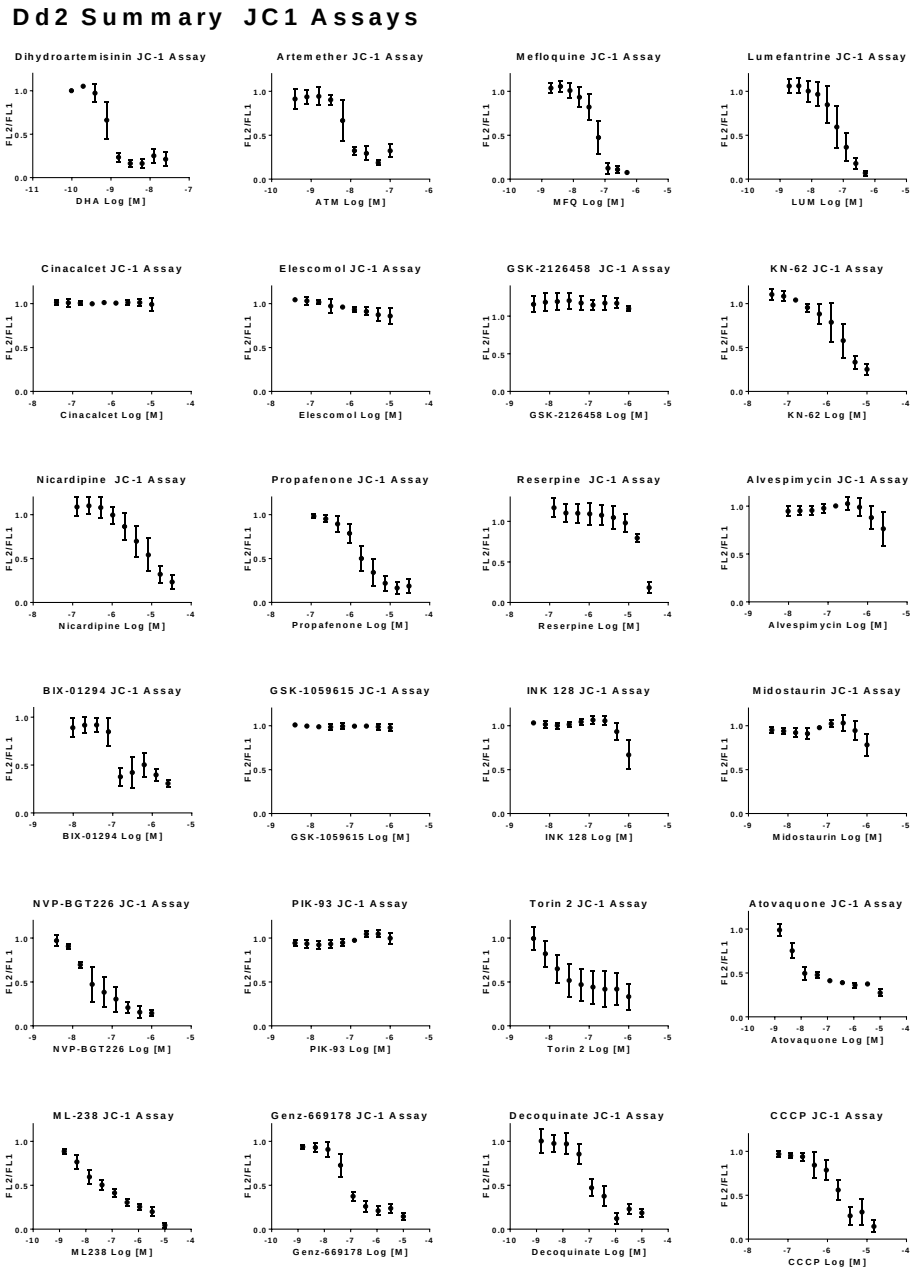

Evaluation of each compounds ability to perturb the mitochondrial membrane potential in a dose dependent manner. Graphs indicate the dose dependent ΔΨ dissipation expressed as FL2/FL1 (Red/green fluorescence ratio). Each value has been normalized versus the FL2/FL1 ratio of the vehicle treated control to which an arbitrary value of 1 has been assigned. Each point is the mean of three independent experiments performed in duplicate, error bars represent SEM.

Figure S4. 3 Compound effect on *P. falciparum* HB3 mitochondrial transmembrane potential as assessed by JC1 staining**.**

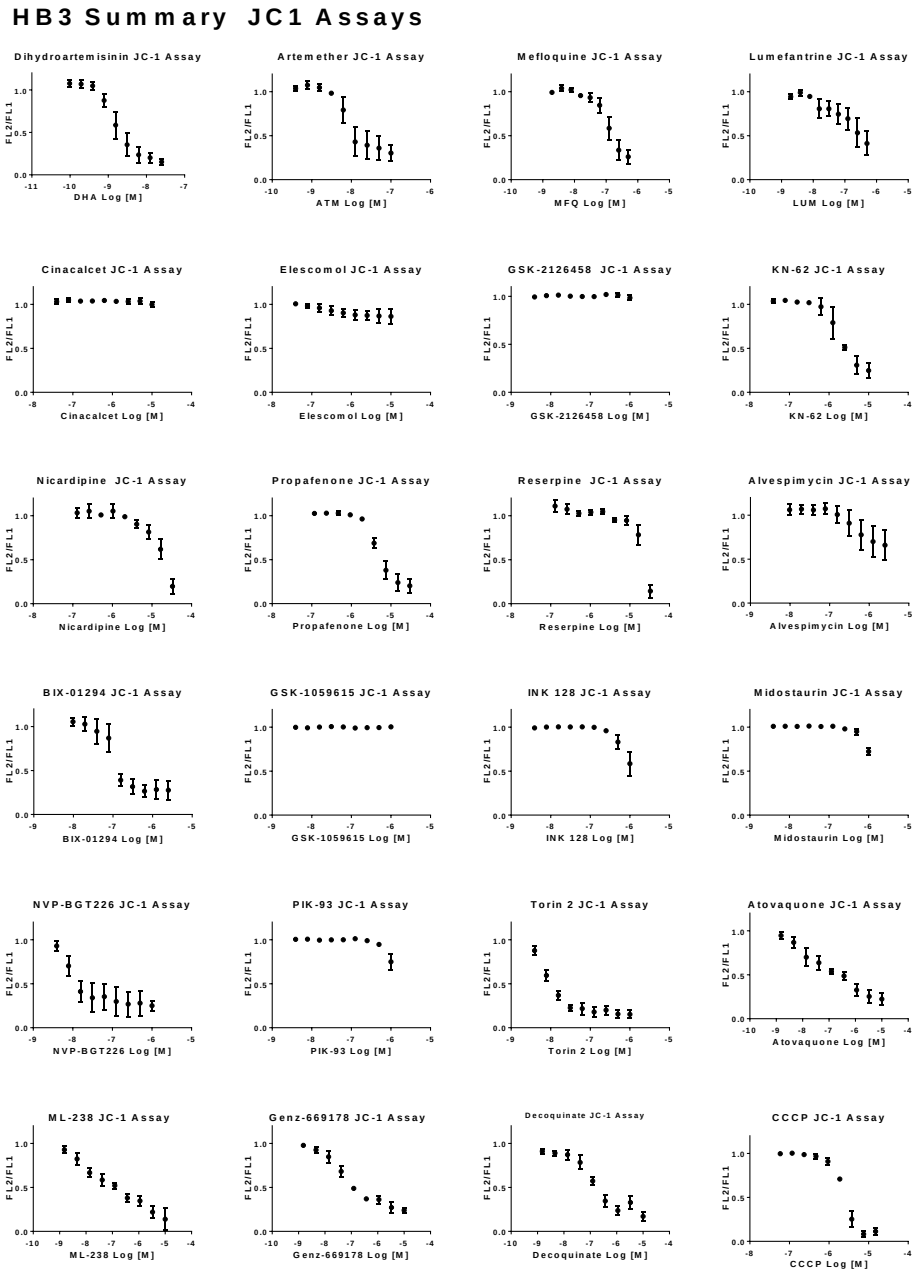

Evaluation of each compounds ability to perturb the mitochondrial membrane potential in a dose dependent manner. Graphs indicate the dose dependent ΔΨ dissipation expressed as FL2/FL1 (Red/green fluorescence ratio). Each value has been normalized versus the FL2/FL1 ratio of the vehicle treated control to which an arbitrary value of 1 has been assigned. Each point is the mean of three independent experiments performed in duplicate, error bars represent SEM.

Figure S4. 4 Compound interaction with artemether on *P. falciparum* mitochondrial transmembrane potential as assessed by JC1 staining**.**

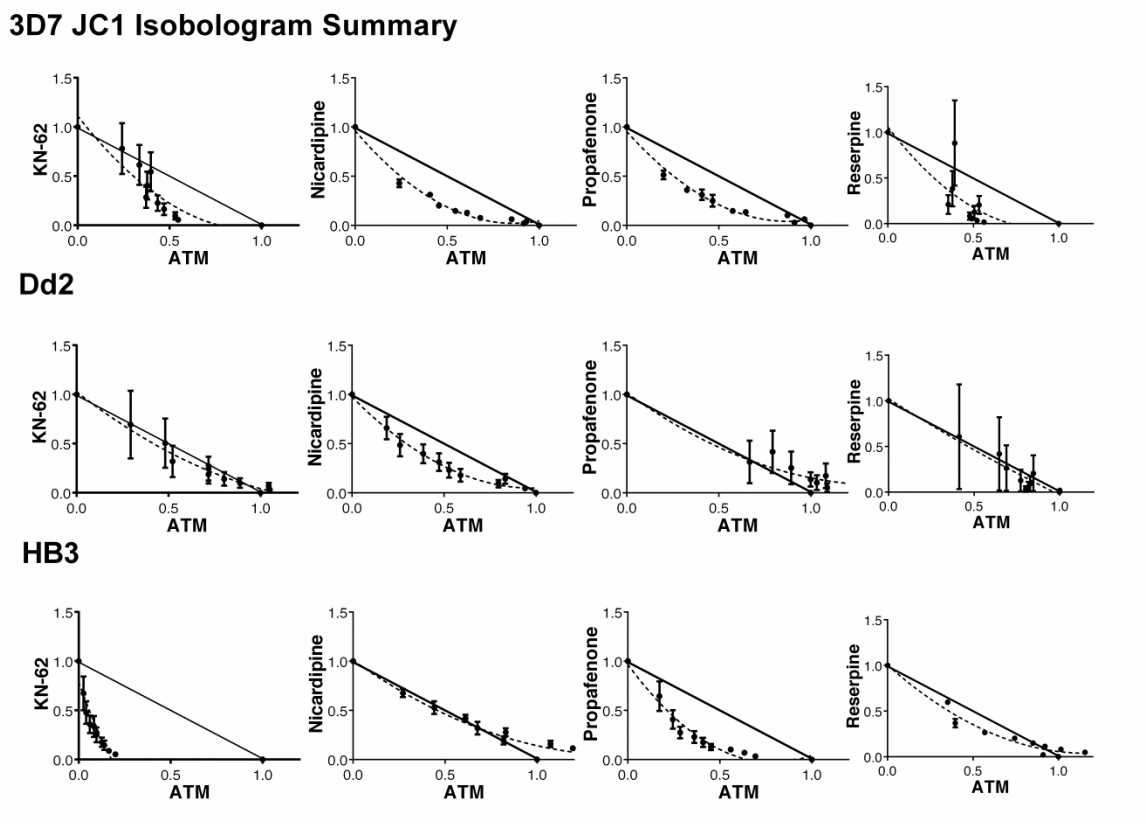

Evaluation of each compounds interaction with Artemether in modulating the mitochondrial membrane potential in a fixed ratio assay. Graphs indicate the fixed ratio dependent ΔΨ dissipation expressed as FL2/FL1 (Red/green fluorescence ratio). Each value has been normalized versus the FL2/FL1 ratio of the vehicle treated control to which an arbitrary value of 1 has been assigned. Each point is the mean of three independent experiments performed, error bars represent SEM.

Table S4. 1 IC_{50} and LD_{50} values for selected agents versus HB3 and Dd2 strains.

Compound	IC_{50} (nM)				LD_{50} (nM)				Reference
	HB3	SEM	Dd2	SEM	HB3	SEM	Dd2	SEM	
CQ	22.7	N/A	225.9	N/A	126.3	30	15669	2411	Paguio, M.F.; et al. *Mol Biochem Parasitol*. **2011,** *178*, 1-6.
AQ	10	N/A	27.7	N/A	37	7	51.4	4	Paguio, M.F.; et al. *Mol Biochem Parasitol*. **2011,** *178*, 1-6.
MQ	21	N/A	30.4	N/A	476.9	109	416.6	100	Paguio, M.F.; et al. *Mol Biochem Parasitol*. **2011,** *178*, 1-6.
QD	17.8	N/A	119.1	N/A	423.7	76	27238.2	3389	Paguio, M.F.; et al. *Mol Biochem Parasitol*. **2011,** *178*, 1-6.
QN	129.3	N/A	277.7	N/A	7121.4	1161	27308.1	3798	Paguio, M.F.; et al. *Mol Biochem Parasitol*. **2011,** *178*, 1-6.
eQN	6588.5	358.2	2237.6	76.4	16100	400	36300	900	Gorka, A.P.; et al. *Antimicrob. Agents Chemother*. **2013,** *57*, 365-374.
eQD	7893.6	46.8	3588.3	194.1	17600	1400	38900	900	Gorka, A.P.; et al. *Antimicrob. Agents Chemother*. **2013,** *57*, 365-374.
PQ	1990	16.6	4695	62.1	8640	50	2810	10	Gorka, A.P.; et al. *Malaria J.* **2013**, *12*, 332-?.
TQ	2189.9	18.7	2092.2	20	42700	2042.6	12100	706	Gorka, A.P.; et al. *Malaria J.* **2013**, *12*, 332-?.
MB	5.3	0.1	5.5	0.1	120.2	9.5	108	6.6	Gorka, A.P.; et al. *Malaria J.* **2013**, *12*, 332-?.
Art	22.6	0.7	21.2	2.3	80	N/A	80	N/A	NA
GSK-2126458	89	48.2	124	27	101700	20006	16100	3037	NA
Prop	1000	N/A	1000	N/A	116167	18606	24867	20067	NA
Artem	7.2	0.9	17.1	1.8	16.3	0.4	25.1	3.9	NA
Lumef	33.3	6.9	47.4	18.9	323	52	242.3	13.3	NA
NVP-BGT226	0.63	0.2	1.03	0.1	17.5	7.5	17.3	6.8	NA
Torin2	1	0.7	2.1	0.4	1875	384	2100	493	NA
PIK93	129	30.5	198	42	2250	250	2033	851	NA
INK128	23.9	N/A	69	N/A	N/A	N/A	N/A	N/A	NA
GSK615	7700	N/A	3800	N/A	N/A	N/A	N/A	N/A	NA
KN-62	2100	N/A	1300	N/A	N/A	N/A	N/A	N/A	NA

4.6 Acknowledgenemts

This work was supported by the Division of Preclinical Innovation, National Center for Advancing Translational Sciences, the Molecular Libraries Initiative of the National Institutes of Health Roadmap for Medical Research, the Division of Intramural Research at the National Institute of Allergy and Infectious Diseases (NIAID) and grants # U54CA143930 and RO1 AI111962.

CHAPTER V

ENDOPEROXIDE DRUG CROSS RESISTANCE PATTERNS FOR *PLASMODIUM FALCIPARUM* EXHIBITING A DELAYED CLEARANCE PHENOTYPE

Chapter V previously published in part as; **Siriwardana, A.**; Iyengar, K.; Roepe, P. D. Endoperoxide Drug Cross Resistance Patterns for *Plasmodium falciparum* Exhibiting a Delayed Clearance Phenotype. *Antimicrobial agents and chemotherapy*. **2016**, *60*, 6952-6956.

Contributions of authors:

A.S. conducted immunofluorescence experiments with Hsp60 and MitoTracker Deep Red, cell culture, RSA experiments, analysis of flow cytometry data and contributed to writing the manuscript.

5.1 Abstract

In the previous chapter, a high-throughput screening lead to the discovery of several novel, extremely potent antimalarial compounds. Specifically, it was found that PI3K inhibitors are synergistic with endoperoxide compounds. Endoperoxide compounds are used in artemisinin combination therapies (ACTs) as front-line antimalarial treatments. With the recent rise of artemisinin resistance and failure of ACTs, it is imperative to find novel therapies that can overcome this resistance. Thus, the ring-stage susceptibility assay (RSA) was modified to quantify susceptibility to seven endoperoxide antimalarial drugs, including two novel, synthetic

endoperoxide compounds. Multiple wild type versus K13-mutant *Plasmodium falciparum* strains were investigated using this method. Susceptibility of all DCP lines relative to controls was lower for six of the drugs tested. In contrast, DCP parasites did not show reduced susceptibility to the synthetic endoperoxide drug OZ439. These data show that it is possible to circumvent emerging artemisinin resistance with a modified endoperoxide drug. Combined with data from the previous chapter, the data also show that it may be possible to develop new ACTs with OZ439 and novel ACT partner drugs.

5.2 Background

Artemisinin (ART) Combination Therapies (ACT) are currently the front-line treatment against *Plasmodium falciparum* malaria. The WHO strongly recommends the use of combination antimalarial therapies instead of drug monotherapies as a method of reducing the risk of parasite development of drug resistance[1]. It is widely accepted that drug combination therapies are more effective at killing parasites than monotherapies and are vital in reducing the possibility of parasites developing resistance to either drug[182]. These recommended drug combinations typically include a fast-acting compound (such as artemisinin, which exerts its effects within 1-2 hours to quickly kill parasites and is eliminated from the body within hours) and a slow-acting partner drug (such as quinolines, which have a longer half-life on the order of days and exist in the human blood-stream for extended periods of time after treatment to prevent recurrence of the parasite infection). Commercial therapies include artemether-lumefantrine (Coartem) and dihydroartemisinin-piperaquine (duocotexin), two of the few ACTs still effective against multidrug-resistant *P. falciparum* in Southeast Asia[206]. Recent observations of an artemisinin - Delayed Clearance Phenotype (ART-DCP) in *P. falciparum* may portend the evolution of

resistance to artemisinin related endoperoxide compounds and commonly used ACTs[58-60]. The development of artemisinin resistance is of significant concern in Cambodia and Thailand, where the first reports of DCP originated between 2008-2009[61-63], especially since the Thai-Cambodia border is considered the world's hot-spot for the development of *P. falciparum* multidrug resistance[64].

Clinically, the artemisinin resistance phenotype is defined as either: 1) a patient having a parasite clearance half-life of greater than 5 hours or 2) a patient having detectable parasitemia on the third day of drug treatment[58]. Typically, infections with ACT sensitive *P. falciparum* are cleared by 50% within less than 5 hours and parasites are not detected after 3 days of treatment. Recently, resistance to the partner drug in Duo-Cotecxin – piperaquine (PPQ) – has also been reported[53, 65-67]. Previous reports showed a delayed parasite clearance, however, patients were still cured of malaria. Delayed clearance meant that ACT treatment may have been required for 4 days instead of the normal 3 day treatment[68]. However, recent reports have been published of complete ACT treatment failure, which implies parasites have become resistant to both the fast-acting and slow-acting drugs in the combination (e.g. both DHA and PPQ)[53, 65-67]. Additionally, the possibility of spread or emergence of artemisinin resistance within Africa, where the majority of malaria related deaths occur[69], is of enormous concern as well as the complete failure of other commonly used ACTs. Thus, it is crucial to investigate the mechanisms of ART resistance and examine compounds that may be able to circumvent these resistance mechanisms before ART resistance becomes a more widespread issue.

Traditionally, the quantification of drug resistance has been done by comparing IC_{50} values. These assays quantify the concentration of drug required to inhibit parasite growth by 50%. In other words, IC_{50} calculates the cytostatic potency of a drug. However, reports have shown that

the IC_{50} assay cannot distinguish the ART resistance phenotype[61-63]. In 2010, Witkowski *et al.* reported on a parasite strain that was established as a laboratory derived artemisinin resistant strain and was able to tolerate up to 9 µM ART[70]. Interestingly, this resistant strain was not distinguishable from the non-drug pressured control strain via IC_{50} (~9.9 nM ART IC_{50} for both strains). Thus, Witkowski *et al.* reported the first assay to successfully correlate in-vitro findings with ART sensitivity. An assay was developed in which parasites were treated with high micromolar concentrations of ART for 1-2 days and subsequently returned to control media and allowed to grow to 5% parasitemia. Although this assay was able to correlate a quicker recovery time with the drug-pressured strain, it required weeks to months to obtain results from one assay. Thus, other means of distinguishing ART resistant strains needed to be developed to allow quicker *in vitro* identification.

Recently, mutations in the propeller domains of a kelch domain-containing protein on chromosome 13 (K13) have been linked to ART-DCP[56, 87]. It has also been shown that the distinction between delayed-clearance parasites vs ART-sensitive parasites is pronounced during the early ring-stage of the parasite life-cycle[70-71]. Witkowski *et al.*[57] subsequently developed the ring-stage susceptibility assay (RSA) to quantify the ART resistance phenotype. In the RSA, early ring-stage parasites are bolus-dosed with 700 nM dihydroartemisinin (DHA) for six hours (a physiologically relevant dose and incubation time)[72-73]. The parasites are then washed, cultured in drug-free media, and relative survival then determined at 66 hours after removal of the drug. In the Witkowski method, parasite survival is measured microscopically by two microscopists from whom each other's data was masked. Each microscopist counted at least 10,000 erythrocytes from giemsa smears of each sample. If the disagreement between the two microscopists was greater than 20%, a third microscopist would assess the slides. Quantitatively, the RSA allows for the

calculation of percentage of parasite survival after a bolus dose of 700 nM DHA and survival rates have been directly correlated with observations of clinical clearance time. Typically, sensitive parasite strains have an RSA survival of ~0-1% and resistant strains have an RSA survival of >10%[57, 87].

In 2014, Straimer *et al.* genetically modified *P. falciparum* laboratory adapted isolates from Cambodia, as well as non-Cambodian parasite strains, to assess the contribution of these K13 mutations to the RSA phenotype of each strain[87]. Straimer *et al.* effectively show that, by introducing a novel, unique K13 mutation to non-Cambodian laboratory strains (that were previously K13-wild type), it is possible to induce ART resistance evidenced by a higher percentage survival in the RSA[87]. Importantly, these findings also suggest that, while K13 mutations are necessary to explain the RSA and clinical phenotype of ART resistance, these mutations are not sufficient to account for the observed phenotype. In other words, Cambodian isolates with differing genetic backgrounds and identical K13 mutations show varying RSA phenotypes. This implies that there are other factors in the parasite genetic background, separate from the K13 locus, which also determine ART sensitivity. Nevertheless, the RSA is an effective method for quantifying ART resistance and will be a useful tool in investigating potential novel antimalarials.

In 2014, Amaratunga *et al.* [74] introduced the use of two-color flow-cytometry to accelerate analysis of RSA data. This method utilized the DNA intercalating properties of SYBR Green I and MitoTracker Deep Red accumulation in response to membrane potential in the mitochondria to identify infected erythrocytes and subsequently categorize them as viable or non-viable. While MitoTracker Deep Red has been shown to selectively accumulate within in-tact mitochondrial

membranes in mammalian cells as an indicator of a large membrane potential[75], there has been little evidence to discern the mitochondrial membrane potential in *P. falciparum* parasites.

P. falciparum parasites have acristate mitochondria[76]. At 6 kb, their genomes are the smallest among eukaryotes[207]. Although they do not conduct oxidative phosphorylation, there is evidence that these parasites still require mitochondrial energy in the form of the electron transport chain[77]. In most eukaryotic cells, the mitochondrial electron transport chain (mETC) is necessary to generate a proton-motive force which is required for oxidative energy metabolism[208]. However, in organisms that favor glycolytic metabolism, including malaria parasites, the role of the mETC is greatly reduced. *Plasmodium* spp. lack the large, multisubunit Complex I of the mitochondrial inner membrane, however they do possess Complexes II-IV[209]. It has also been deduced through genome data that *Plasmodium* mETC complexes have a much simpler subunit composition than those found in mammalian cells or yeast[210]. MitoTracker dyes accumulate within membranes with high potential energy and, with a plasma membrane potential of ~-95mV[211], it is still unknown whether *P. falciparum* parasite mitochondria possess a membrane potential great enough to cause MitoTracker accumulation. Despite this uncertainty, results from the Amaratunga *et al.* RSA[74] were shown to correlate with results from the Witkowski *et al.* RSA[57], and thus, the Amaratunga *et al.* method is widely accepted as a more effective method of quantifying ART sensitivity.

Previous studies using the RSA to correlate DCP with K13 mutations have primarily focused on the effects of DHA and ART[50, 54, 68, 87]. Few studies have investigated the effects of other endoperoxide drugs based on the structure of ART[212-213]. These drugs include AMS, arterolane (OZ277) and artefenomel (OZ439), which have shown promise in clinical trials[91, 214-216]. No previous studies have precisely quantified relative degrees of resistance to these different endoperoxides for DCP parasites.

The dihydroartemisinin-piperaquine ACT has been used in Cambodia with 96-98% success rates since 2008. However, there are recent reports of piperaquine treatment failure in Cambodia[67]. Piperaquine is a long-acting partner drug and its main use is in preventing parasite recrudescence. The implications of piperaquine treatment failure are vast. The biggest concern is the spread of multidrug resistance, specifically widespread ACT resistance and treatment failure. Together, these points led our lab to investigate the activity of seven endoperoxide containing compounds.

5.3 Results

It was first observed that ART resistant *P. falciparum* parasites from Cambodia have a decreased susceptibility to artemisinin in the early-ring stage that manifests as a quiescence mechanism[70]. The ring-stage susceptibility assay (RSA), developed based on this observation, provide a major advance in the study of ART resistance. Results from the Amaratunga *et al.* RSA[74] were shown to correlate with results from the Witkowski *et al.* RSA[57], albeit with higher absolute percentage survival values. I was interested to further investigate MitoTracker Deep Red (MTDR) staining of *P. falciparum* parasites and test the ability of this dye to predict parasite viability, since it might provide an improvement for RSA design. The traditional RSA, according to the protocol by Amaratunga *et al*., utilizes 0.2X SYBR Green (SG) and 300 nM MTDR. I first utilized spinning-disk confocal microscopy to visualize intraerythrocytic *P. falciparum* parasites stained with this concentration of MTDR and observed a multi-faceted pattern of staining, resembling both the suggested branched structure of the mitochondria[209] and some diffuse cytosolic staining (Figure 5.1A). To test whether I could observe more specific organellar staining with MTDR, I examined the fluorescence at various concentrations between 3 nM – 300 nM. I found that at 20 nM, the fluorescence observed was bright enough to be used for flow cytometry, but also that the staining

was significantly more specific than at higher concentrations (Figure 5.1A). Thus, I used 20 nM MTDR moving forward.

Colocalization experiments were then conducted to determine whether MTDR, in fact, stains the mitochondria or other organelles. Mitochondrial heat-shock protein, Hsp60, has been shown to be specifically transported into the mitochondria[217-219]. Thus, an Hsp60 antibody was used in immunofluorescence experiments with MTDR. Results showed that MTDR indeed does colocalize with Hsp60. However, the two stains did not show complete colocalization, indicating that MTDR could be staining other cellular components as well, although to a small extent (Figure 5.1B).

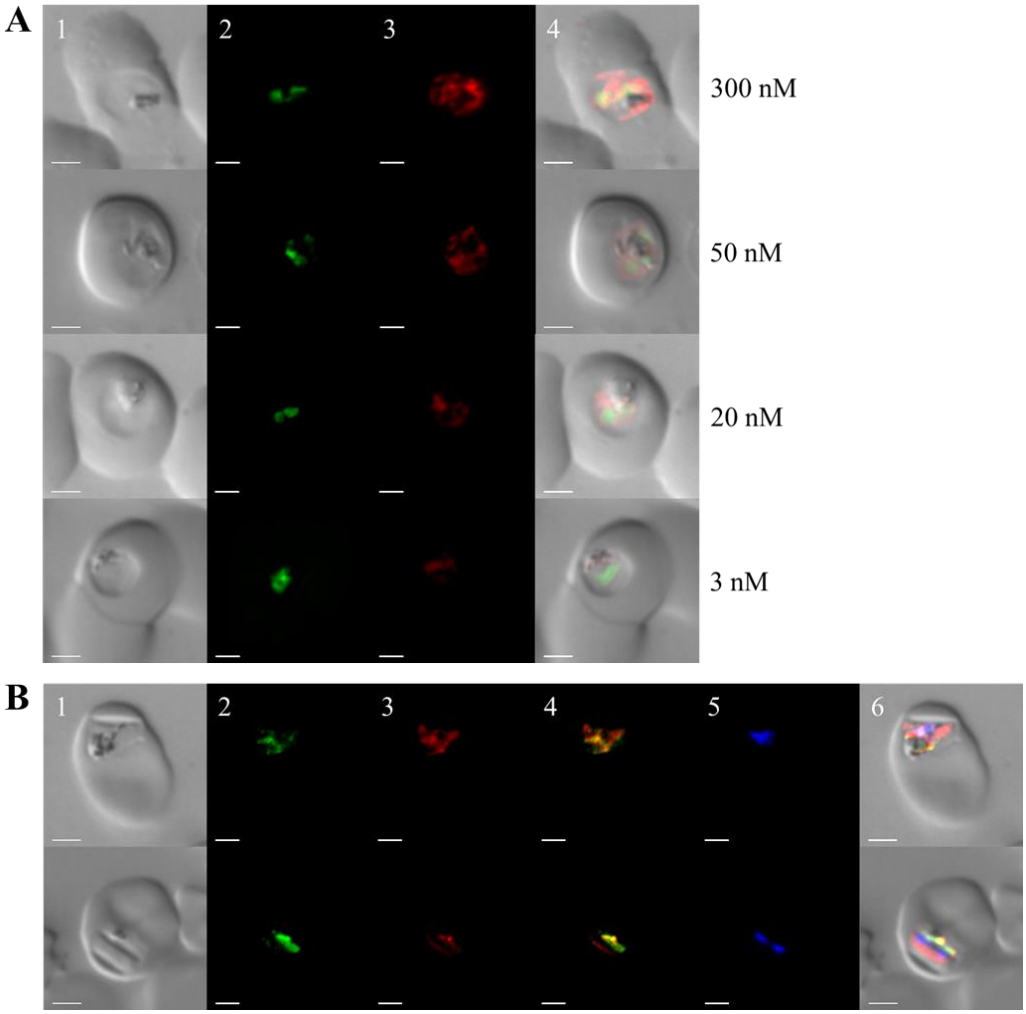

Figure 5. 1 Evaluating MTDR staining. (A) MTDR staining evaluated at varying concentrations (shown on right side of each row of images). Panel 1: transmittance image. Panel 2: SYBR Green

nuclear staining. Panel 3: MTDR staining. Panel 4: a merged image of all three channels. (B) Co-staining with MTDR and Rabbit anti-Hsp60 antibody. Panel 1: transmittance image. Panel 2: Rabbit anti-PfHsp60 antibody imaging. Panel 3: MTDR staining. Panel 4: A merged image of the MTDR and Rabbit anti-PfHsp60 channels. Panel 5: DAPI nuclear staining. Panel 6: a merged image of all four channels Bar = 2 μm.

The above data led us to conclude that even though SYBR Green I staining is not able to distinguish "live" vs "dead" parasites (SYBR Green I stains DNA regardless) in combination with lower MTDR it might be possible to improve quantification of DCP using RSA behavior.

Next, in consultation with others in our group I realized that while a 6 hour, 700 nM pulse is a pharmacologically relevant dose for DHA[72-73], this may not be the case for other endoperoxide antimalarial drugs derived from ART such as artesunate (ATS), artemether (ATM), or artemisone (AMS). Additionally, although ART, ATS and ATM all metabolize to DHA, the rate of metabolism differs and AMS does not metabolize to DHA at all[220-223] (see also Table 5.1). ART, ATS, and ATM show varying peak plasma concentrations dependent on the dose administered, the health of the patient and many other factors[224-230], suggesting that parasites infecting most patients receiving an ACT are likely exposed to various ratios of DHA: parent drug. Thus, it is important to take into account these differences in clinically relevant drug exposure when attempting to quantify ART resistance.

Table 5.1 Peak plasma concentration (C_{max}) and clearance half-time ($t_{1/2}$) for endoperoxide containing antimalarial compounds investigated in this study.

Compound	**$t_{1/2}$ (hr)**	**C_{max} (µg/mL)**
Artemether	3.1-4.2[231], 3.9[230], 2[227]	231[231], 593[230], 184[227]
Dihydroartemisinin	0.57[224], 3.9[232]	2500[224], 740[232]
Artemisone	2.79[226]	140.2[226]
Artemisinin	2.59[225], 1.1[233]	391[225], 244[233]
Artesunate	0.06[224], 0.41[229]	2000[87], 114[229]

Due to the variance in peak plasma concentration of several different endoperoxide containing antimalarials, in collaboration with my colleague Kalpana Iyengar, I modified the RSA to obtain dose-response curves in order to quantify the potency of these endoperoxide drugs for control vs DCP parasites. In this study, using the modified assay, I calculate 50% ring-stage lethal dose ($RSLD_{50}$) for ART, ATM, DHA, ATS, AMS, OZ277 and OZ439 (Figure 5.2). I analyzed laboratory-adapted isolates CamWT (wild-type K13 sequence) and Cam3.II (R539T K13 mutation) in addition to the transfectants $CamWT^{C580Y}$ (C580Y K13 mutation), $Cam3.II^{C580Y}$ (C580Y K13 mutation) and $Cam3.II^{Rev}$ (wild-type K13 sequence)[87] engineered using the zinc-finger nuclease (ZFN) method[234].

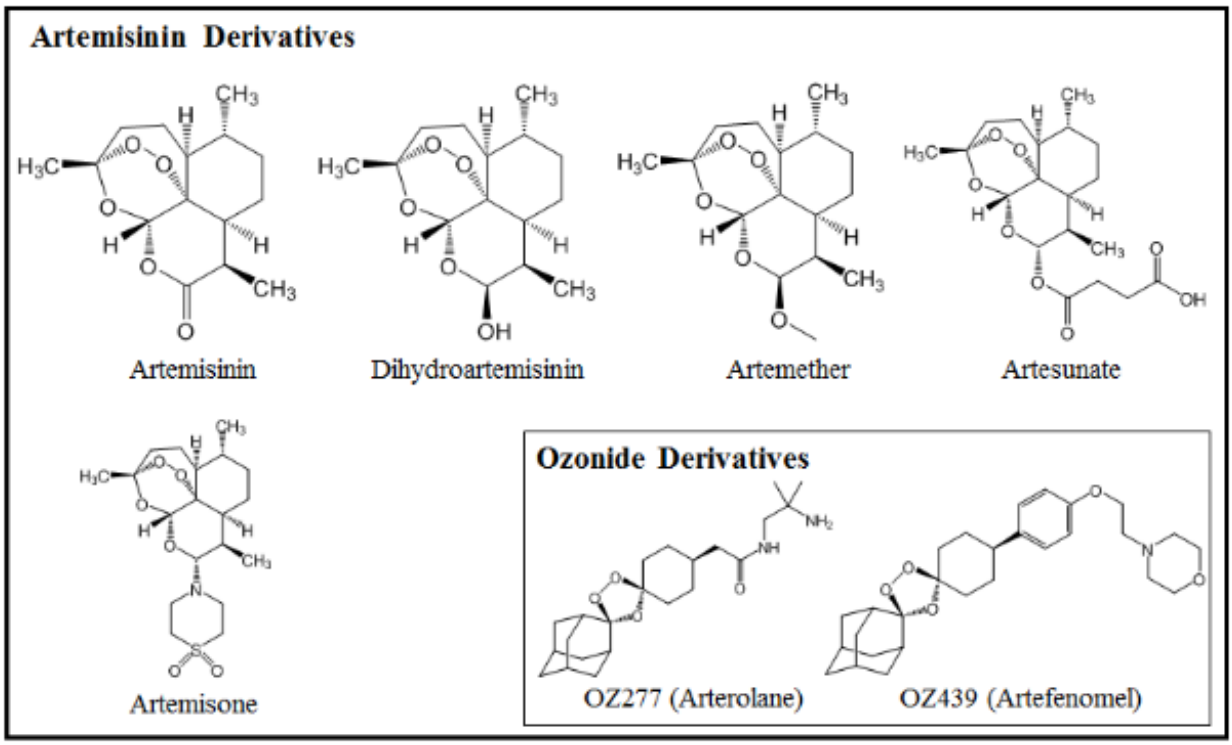

Figure 5. 2 Chemical structures of endoperoxide and synthetic ozonide compounds used.

All cultures were triple-synchronized using 5% D-sorbitol following established protocols[6] and 0-6 hour rings were used in all experiments. Each strain was incubated for 6 hours with various concentrations (typically 0.1 nM – 700 nM) of the seven compounds tested (Figure 5.2). After drug exposure, parasites were washed 3× with complete culture medium and plates were then incubated for an additional 66 hours. To determine percent outgrowth in each assay, the flow-cytometric method developed by Amaratunga *et al.*[74] was followed with a few modifications. Specifically, while Amaratunga *et al.* used 300 nM MitoTracker Deep Red (MTDR), in this study, I use 20 nM MTDR as I observed above that this is the ideal concentration to selectively stain parasite mitochondrion without producing diffuse, cytosolic staining that may not be indicative of parasite viability. Data were gated to exclude uninfected RBCs and to distinguish low (less viable) vs high (viable) MTDR staining (x-axis) using contour plots as described[57] (see also Figure 5.3).

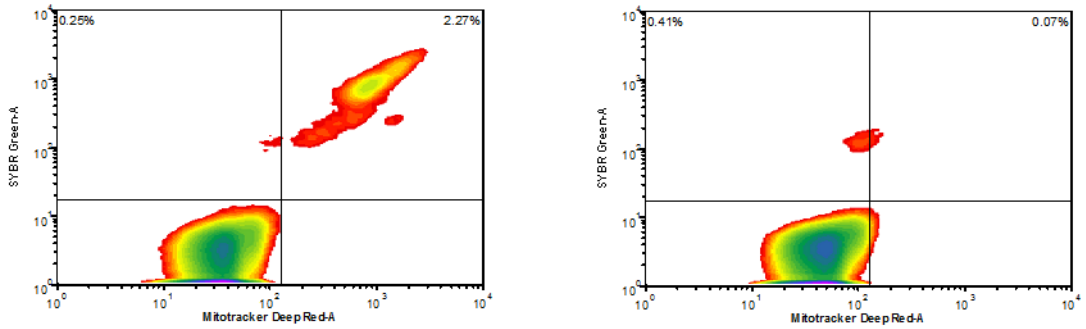

Figure 5. 3 Contour plot representation of flow cytometry scatter plots. The distinction between viable vs. non-viable parasites becomes more clear in this visualization as shown by Amaratunga *et al.*[74] and Witkowski *et al.*[57]

Sigmoidal curve fits of the raw data (Figure 5.4) were used to calculate $RSLD_{50}$ (e.g. Figure 5.5). All data represent the average of at least three independent experiments. Dose-response curves for the seven drugs were generated for each of the five strains tested (CamWT, $CamWT^{C580Y}$, Cam3.II, $Cam3.II^{C580Y}$, $Cam3.II^{Rev}$). By comparing these $RSLD_{50}$ values, I find that for each of six drugs (ART, ATM, DHA, ATS, AMS and OZ277), the K13 mutant strains display at least a 2-fold decreased susceptibility compared to the relevant parental strain expressing wild-type K13 (Table 5.2; $p < 0.05$ for each DCP vs wild-type comparison for each drug).

Table 5.2 $RSLD_{50}$ values (in nM) obtained via dose-response curves (see Figure 5.5) for 5 strains, tested against each of 7 compounds. "CamWT" and "$Cam3.II^{Rev}$" harbor wild type K13 and are drug sensitive, whereas the other strains have been engineered to express mutant forms of K13 and show a DCP as defined by the standard RSA (see Straimer *et al.*[87] for additional description of these strains). Data are the average of at least 3 independent trials. SEM = standard error of the mean.

Compound	CamWT	$CamWT^{C580Y}$	$Cam3.II^{Rev}$	$Cam3.II^{C580Y}$	Cam3.II
Artemether	15.0 ± 1.0	33.7 ± 4.1	15.1 ± 2.2	30.9 ± 3.4	34.0 ± 2.9
Dihydroartemisinin	6.4 ± 1.8	12.9 ± 1.8	5.1 ± 0.7	11.4 ± 0.8	14.1 ± 1.6
Artemisone	3.2 ± 0.3	6.5 ± 0.6	3.6 ± 0.8	9.4 ± 0.7	9.5 ± 1.6
Arterolane	5.9 ± 0.3	11.9 ± 0.7	9.2 ± 1.5	26.3 ± 7.0	27.3 ± 9.6
Artefenomel	10.2 ± 0.5	10.5 ± 1.0	11.8 ± 1.0	11.0 ± 0.7	11.0 ± 1.4
Artemisinin	19.4 ± 4.2	63.2 ± 14.8	54.4 ± 8.0	125.4 ± 13.6	112.6 ± 5.5
Artesunate	50.9 ± 13.9	130.0 ± 3.1	48.8 ± 17.6	122.6 ± 13.9	111.1 ± 13.0

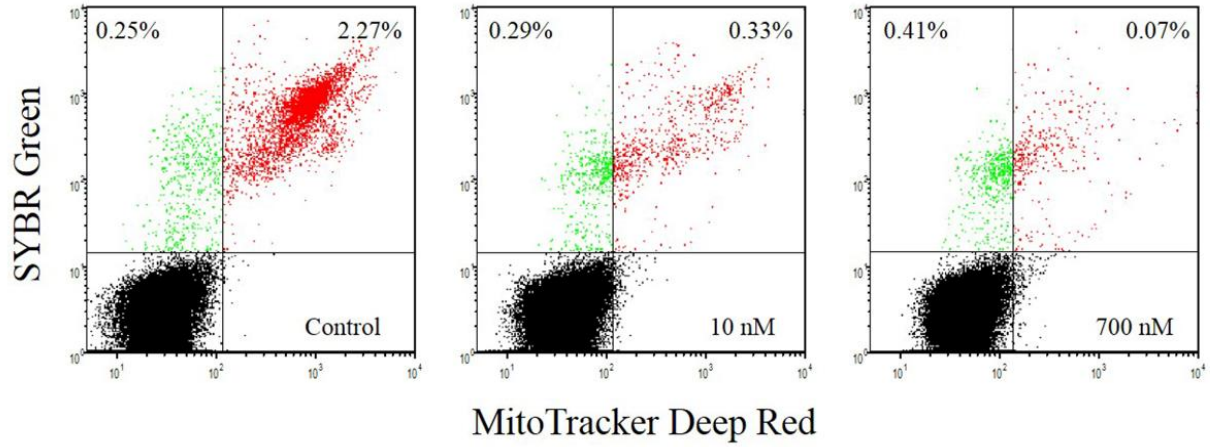

Figure 5. 4 Example of raw data obtained from two-color flow cytometry experiments for CamWT (wild type K13) treated with variable concentrations of AMS. A Becton Dickinson (BD) FACSAria IIu flow cytometer was used to collect data. Data was collected in the FSC (forward scatter), SSC (side scatter), FITC (488 ex. 530/30 em.) and APC (633 ex. 660/20 em.) channels. On the FSC x SSC plot, data were gated to exclude debris and cell aggregates. On the FITC x APC plot, data were gated to exclude uninfected RBCs as described in the text. From left to right, increasing concentrations of drug (0, 10 nM, 700 nM) cause decreased outgrowth as shown by the decrease in live parasite MitoTracker Deep Red staining (upper right quadrant)[57, 74, 235]. Percent survival was calculated via the ratio of viable parasitemias for drug treated vs control samples (e.g., 0.07%/2.27% Fig. 2A right vs left panels).

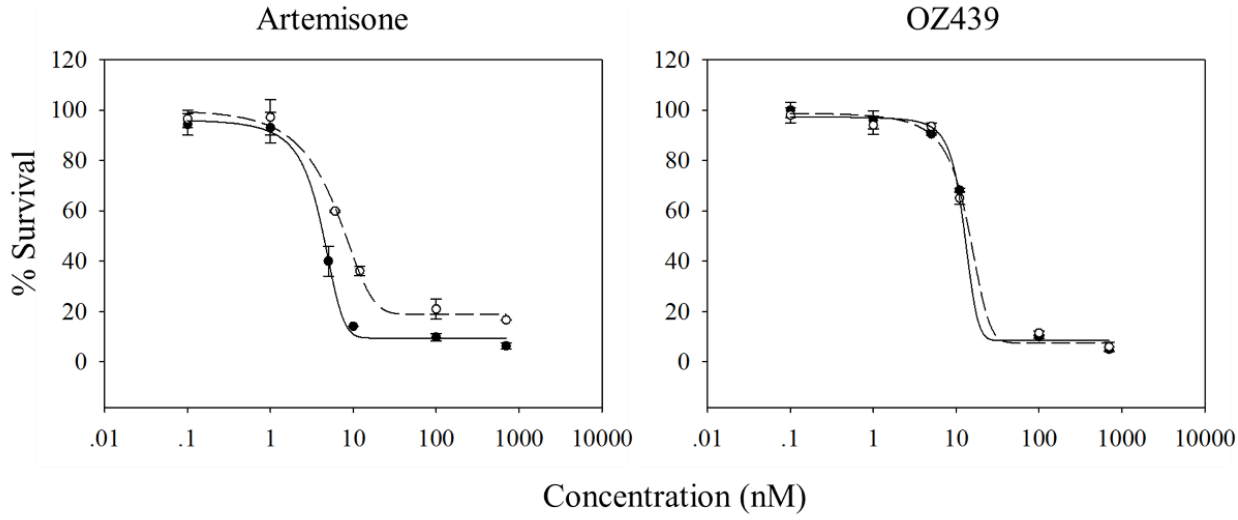

Figure 5. 5 Example of sigmoidal plots generated using raw flow cytometry data to compute $RSLD_{50}$. Filled circles represent CamWT (wild type K13) and open circles represent the K13 mutant $CamWT^{C580Y}$. Data are the average of 3 independent experiments +/- S.E.M.

A recent report suggests that different washing procedures might affect the response to some endoperoxide drugs used at concentrations above 500 nM[213], specifically OZ439 as it is more lipophilic and may be more stable in solution than other compounds tested. Thus, I removed all data points in the $RSLD_{50}$ curves obtained at > 500 nM drug and recalculated $RSLD_{50}$ (Figure 5.6 and Table 5.3). Although absolute magnitude of the $RSLD_{50}$ value changed slightly (<1%), computed $RSLD_{50}$ ratios for all possible WT vs DCP strain comparisons (Table 5.2) did not. At these $RSLD_{50}$ doses, I find no evidence for residual endoperoxide drug that may be present upon incubation at higher dose (>500 nM, see Yang *et al.*[213]), but note that some caution should perhaps be used in interpreting data obtained at high doses due to slightly different pharmacology of some endoperoxides[215].

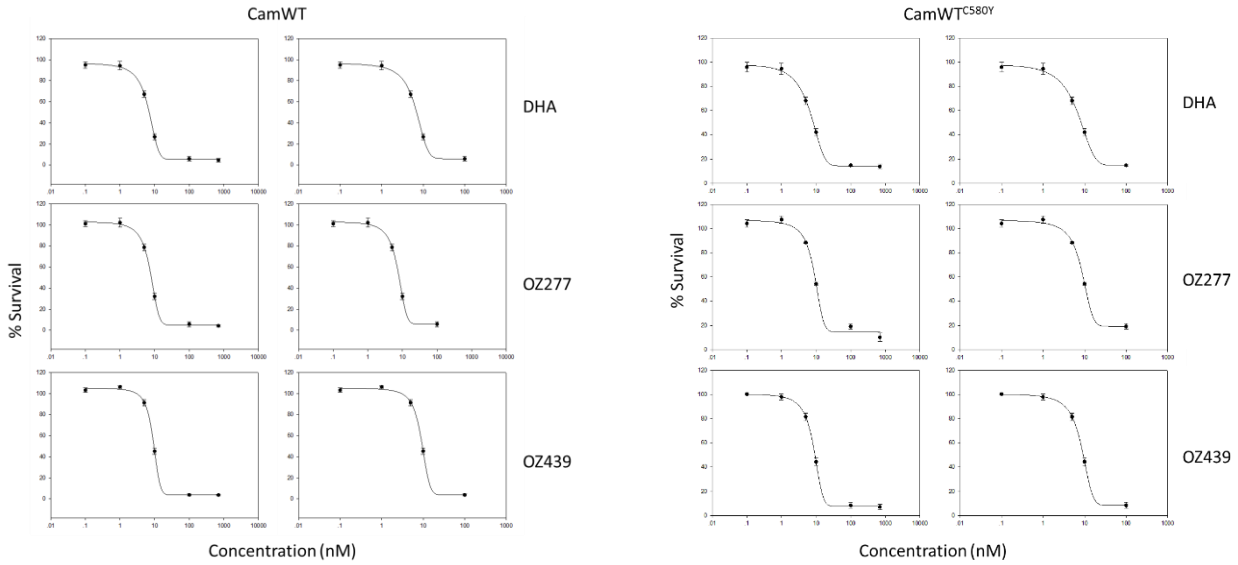

Figure 5. 6 $RSLD_{50}$ dose-response curves were modified to eliminate all drug concentrations used above 500 nM and $RSLD_{50}$ was recalculated for DHA, OZ277 and OZ439.

Table 5.3 $RSLD_{50}$ dose-response curves were modified to eliminate all drug concentrations used above 500 nM and $RSLD_{50}$ was recalculated for DHA, OZ277 and OZ439.

Strain	DHA		OZ277		OZ439	
	With all data	Without >500	With all data	Without >500	With all data	Without >500
CamWT	5.8587	5.8538	4.8296	4.8293	10.0239	10.0239
$CamWT^{C580Y}$	11.3449	11.3561	10.2589	10.2623	10.5969	10.6203

Yang *et al.* also reported that in order to completely remove all of the ozonide drug from the suspension during washing, the wells should be washed once, parasites subsequently transferred to a new 96-well plate and further washed an additional three times[213]. To further ensure that no residual drug remained after washing – which may cause artificially low results for $RSLD_{50}$ indicating a stronger potency –I performed experiments in which I incubated parasitized erythrocytes or empty well-plates with $RSLD_{50}$ doses of DHA, OZ277 or OZ439. Results showed no significant difference ($p > 0.05$) in parasite survival under any of the above tested conditions (Figure 5.7). Together, our data suggest that there is no residual drug present in the wells after the drugs are washed following the 6-hour incubation period. This further validates the significance of our lab's finding that OZ439 circumvents endoperoxide drug cross resistance patterns displayed by the laboratory-adapted Cambodian isolates used in this study.

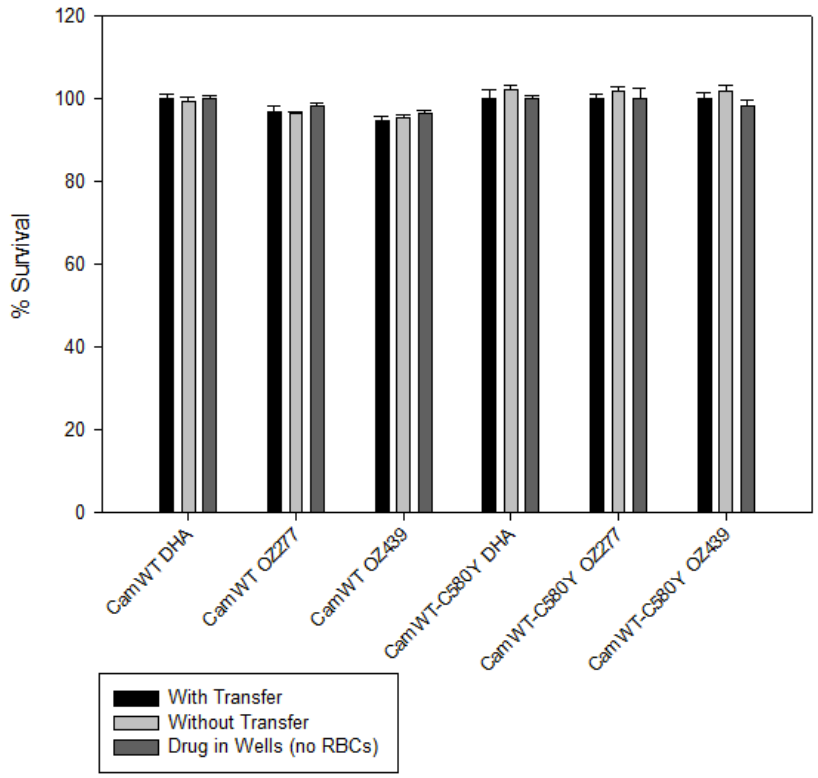

Figure 5. 7 Comparison of different washing methods used to ensure drugs are completely removed from 96-well plate. Parasitized erythrocytes or empty wells were incubated in a 96-well plate with DHA, OZ277 or OZ439 for 6 hours. The plates were then washed in one of two ways: 1) washed 3x in the same 96-well plate without transferring to a new plate (the method used in my study) or 2) washed 1x, contents transferred to a new, clean 96-well plate and washed 3x more. Finally, parasitized erythrocytes were added to the wells in which only drug containing media was originally added. After the standard RSA waiting period of 72 hours, the plates were read using SG and parasite survival compared to a control was determined.

I also tested each strain using the traditional RSA "percent growth after fixed 700 nM dose" assay[74]. For the same 6 drugs, I observed that K13 mutant strains show 2- to 6- fold increases in relative outgrowth compared to control (Table 5.4; $p < 0.05$ for each DCP vs wild-type comparison for the six drugs).

Table 5.4 RSA % survival for 5 strains tested against 7 compounds at 700 nM fixed dose via the standard RSA. Data are the average of at least 3 independent trials. SEM = standard error of the mean.

Compound	CamWT	CamWT^{C580Y}	Cam3.II^{Rev}	Cam3.II^{C580Y}	Cam3.II
Artemether	5.2 ± 1.3	17.8 ± 6.0	3.0 ± 0.5	12.2 ± 2.5	9.7 ± 2.1
Dihydroartemisinin	5.0 ± 1.0	21.4 ± 2.0	5.5 ± 1.2	17.0 ± 3.3	16.7 ± 3.0
Artemisone	3.0 ± 0.3	16.7 ± 0.1	3.5 ± 0.6	13.4 ± 2.8	12.3 ± 2.8
Arterolane	4.2 ± 1.0	13.0 ± 0.7	4.6 ± 0.3	10.1 ± 1.9	11.7 ± 2.5
Artefenomel	6.2 ± 0.5	7.2 ± 2.0	6.4 ± 1.5	7.4 ± 1.3	7.3 ± 0.8
Artemisinin	5.7 ± 1.0	26.3 ± 4.9	8.1 ± 1.4	24.7 ± 1.3	29.0 ± 4.8
Artesunate	5.7 ± 0.9	22.1 ± 3.3	4.5 ± 0.9	13.2 ± 0.9	24.9 ± 2.8

Interestingly, however, I did not observe similar results for OZ439 (artefenomel). OZ439 $RSLD_{50}$ for both CamWT and CamWT^{C580Y} were 10.2 ± 0.5 nM and 10.5 ± 1.0 nM respectively (Table 5.2) and average RSA survival at fixed 700 nM OZ439 were 6.2 ± 0.5% and 7.2 ± 2.0% for CamWT and CamWT^{C580Y} respectively (Table 5.4). OZ439 $RSLD_{50}$ for Cam3.II, Cam3.II^{C580Y} and Cam3.II^{Rev} were 11.8 ± 1.0 nM, 11.0 ± 0.7 nM and 11.0 ± 1.4 nM respectively (Table 5.2) and RSA survival at fixed 700 nM dose of OZ439 was 6.4 ± 1.5%, 7.4 ± 1.3% and 7.3 ± 0.8% for Cam3.II, Cam3.II^{C580Y} and Cam3.II^{Rev} respectively (Table 5.4). This indicated the ability of OZ439 to surpass the cross resistance shown by K13-mutant parasites to other endoperoxide drugs.

5.4 Discussion

Artemisinin (also known as Qinghaosu; Figure 5.2) is a sesquiterpene lactone derived from the Chinese medicinal herb *Artemisia annua*. Antimalarial activity of this drug is achieved through the activation of the endoperoxide bridge[236]. In order to improve bioavailability and efficacy, several derivatives of this compound, such as DHA, ATM, ATS, and AMS have been synthesized (Figure 5.2)[237]. DHA has also been found to be the active metabolite of ART and its semi-synthetic derivatives ATM and ATS but not for AMS[220-223]. The most significant property of ARTs is their ability to act rapidly and reduce the parasite burden up to about 10, 000-fold every 48 hours[238-239].

Although having significant advantages, one disadvantage of these compounds is their short *in vivo* half-lives. These can range from less than one hour to about 4 hours (Table 1). Due to this, ART drugs are administered as a combination therapy with a partner drug such as lumefantrine, mefloquine, amodiaquine, piperaquine, and pyronaridine, that have a significantly longer half-life. Half-life of the partner drug can range from a few days to few weeks[206]. This method of drug administration ensures the prevention of recrudescence and is predicted to lower the frequency of the development of resistance[182, 240-241]. Work done to address the issue of short half-lives have led to the development of the ozonide compounds, OZ277 and OZ439[215]. Of these two compounds, OZ439 has the much longer elimination half-life (ranging from 30-60 hours[214, 242]) and is fortuitously currently being evaluated as a single or a combination therapy in human trials[214, 243-244].

Recent reports indicate artemisinin DCP in *P. falciparum*[58-60]. This could be an early indication of the development of artemisinin resistance. The primary molecular marker that characterizes parasites displaying a DCP is mutations in the kelch domain of a protein on chromosome 13 (K13) in *P. falciparum* parasites[56-57]. This phenotype cannot, however, be identified *in vitro* through traditional drug susceptibility assays such as IC_{50} and LD_{50} assays. Thus, Witkowski *et al*. developed an assay named the RSA. Parasites having a DCP phenotype showed an increased survival in the RSA[57, 71]. The RSA was primarily developed to assess the potency of DHA on parasite strains. Thus, my goal was to modify this assay, incorporating improvements made by Amaratunga *et. al*.[74] to use flow cytometry, so I could assess the potency of other drugs containing an endoperoxide bridge.

Typically, resistance to one drug within a specific class implies some level of cross resistance to structurally related drugs since drugs within that class often share common

mechanisms of action. Examples include cross resistance to multiple ß-lactam antibiotics for some gram-negative bacteria, resistance to multiple vinca alkaloid antibiotics for multidrug resistant tumor cells, and pleiotropic quinoline drug resistance for *P. falciparum*. Thus, it is not surprising that DCP *P. falciparum* show shifted $RSLD_{50}$ for six of the seven endoperoxide antimalarial drugs tested. It is particularly striking then that a leading candidate synthetic endoperoxide drug (OZ439) does ***not*** overlap with this endoperoxide cross resistance pattern. Although the higher stability of OZ439 observed in solution [215] may lead to a comparatively higher concentration of residual drug after 6-hour drug pulse, this phenomenon does not interfere with observed cross-resistance patterns via $RSLD_{50}$ data obtained at low dose. My data suggest that OZ439 is able to overcome at least part of the mechanistic basis of DCP, and therefore would in theory provide the basis for an improved ACT.

Importantly, although ART, ATS and ATM all metabolize to DHA, such conversion does not occur in cell culture. Also, AMS does not convert to DHA at all, as obviously OZ277 and OZ439 do not either. I find it quite intriguing then that DCP parasites show reduced susceptibility to OZ277 but not to the related molecule OZ439. This suggests that groups added to the OZ439 structure negate association with DCP determinants. Although perhaps controversial, it has been suggested that a *P. falciparum* PI3´-kinase may represent the DCP determinant[54], therefore it may prove useful to compare any interactions between this kinase and these endoperoxide drugs.

5.5 Acknowledgements

The Roepe lab thanks Dr. David A. Fidock (Columbia University) for providing the laboratory-adapted isolates and ZFN engineered transfectants used in this study, and the Medicines for Malaria Venture (MMV) for providing AMS, OZ277, and OZ439. This work was supported by NIHI grant AI111962 to PDR.

CHAPTER VI

DYSREGULATION OF AUTOPHAGY IN ARTEMISININ RESISTANT *PLASMODIUM FALCIPARUM* AND USE OF OZ439 AND PI3K INHIBITORS AS PARTNERS TO OVERCOME RESISTANCE

Siriwardana, A., Iyengar, K., Roepe, P.D.

Contributions of authors:

A.S. designed and performed immunofluorescence assays, quantification of puncta, Chou-Talalay combination assays, and wrote the manuscript.

6.1 Abstract

Previous results have shown that *Plasmodium falciparum* parasites possess the machinery necessary for autophagy and that this pathway is triggered in response to cytocidal concentrations of drugs such as artemether. Additionally, PI3K inhibitors have been shown to be potent antimalarial compounds that inhibit the autophagy pathway and are synergistic with artemisinin compounds. OZ439 was found to be potent against both artemisinin resistant and sensitive *P. falciparum* strains. Taken together, these findings first lead to the investigation of the autophagy pathway in artemisinin resistant parasites. Results from experiments described in this chapter show that the autophagy pathway is further dysregulated in artemisinin resistant malaria. Due to the indication of dysregulation of autophagy in ART resistant parasites and the ability of PI3K inhibitors to target this pathway, the next step involved evaluating drug combinations with these

compounds in an attempt to discover novel antimalarial combination therapies to combat rising artemisinin resistance. Significant cytocidal synergy was found for drug combinations involving OZ439 and PI3K inhibitors, specifically during the ring stage of parasite development.

6.2 Background

Artemisinin (ART) Combination Therapies (ACT) are currently the front-line therapy for treating *Plasmodium falciparum* malaria. Typical combinations include a fast-acting compound (such as artemisinin, which exerts its effects within 1-2 hours to quickly kill parasites and is eliminated from the body within hours) and a slow-acting partner drug (such as quinolines, which have a longer half-life on the order of days and exist in the human blood-stream for extended periods of time after treatment to prevent recurrence of the parasite infection). Commercial ACTs include combinations of: artemether-lumefantrine (Coartem) and dihydroartemisinin-piperaquine (Duo-cotecxin), two of the few ACTs still effective against multidrug-resistant *P. falciparum* in Southeast Asia. Reports of artemisinin resistant *P. falciparum* are on the rise and could indicate the imminent failure of ACTs[58-60]. The development of artemisinin resistance is of significant concern in Cambodia and Thailand, where the first reports of delayed clearance originated[61-63], especially since the Thai-Cambodia border is considered the world's hot-spot for the development of *P. falciparum* multidrug resistance[64]. Thus, investigating mechanisms of ART resistance and understanding these mechanisms to inform the development of novel antimalarial therapies is of utmost importance.

Many of the ACTs currently in use were discovered empirically without validation of the drugs' mode of action (MOA). This led to combinations of drugs with similar MOAs which is not as beneficial for avoiding emergence of drug resistance phenomena[240-241]. That is, for an antimalarial therapy to truly be effective at both curing patients and reducing the risk of the

development of concurrent resistance, the drugs used must possess different MOAs. Mott *et al.* conducted a study investigating thousands of potential antimalarial compounds for potency, drug-drug interactions, MOAs and combination efficacy[49]. A particularly striking result from this study includes the discovery of phosphatidylinositol 3'-kinase (PI3K) inhibitors as extremely potent antimalarial compounds and partner drugs for new ACTs. Not only were these compounds potent at the cytostatic level, but they also showed significant cytocidal potency and were found to be cytocidal synergistic in combination with several other antimalarial compounds. This is extremely important in developing novel antimalarial therapies as clinically, malaria parasites are subjected to higher, cytocidal, concentrations of drugs and the goal is to kill parasites, not merely slow their growth. Additionally, Mott *et al.* also showed through *in vivo* experiments that, although several tested combinations resulted in a rebound of parasitemia, the combination of ATM and NVP-BGT226 (one of the PI3K inhibitors tested) was successful at curing mice, similarly to the standard ATM and LUM combination. Although the potency of ARTs and PI3K inhibitors has been validated in the canonical HB3 and Dd2 strains as well as *in vivo*, these drugs have not been tested against ART resistant strains of *P. falciparum.*

Further study of PI3K inhibitors could prove vital to understanding cytocidal drug resistance. As shown by Gaviria *et al.*, there is an autophagy-like process that exists in *P. falciparum* parasites as a survival mechanism[17]. The autophagy pathway is stimulated by cytocidal doses of chloroquine and other external stressors. Furthermore, this pathway becomes dysregulated in chloroquine resistant parasites strains such as Dd2, which indicates a role for this pathway in cytocidal antimalarial drug resistance. Therefore, investigating compounds which target this pathway can be extremely important in not only understanding the pathway better but also in assessing potential novel therapies to overcome cytocidal drug resistance.

P. falciparum parasites possess homologues of many key proteins involved in the autophagy pathway. Interestingly, the *Plasmodium* genome contains only one PI3'-kinase – the class III PI3K, Vps34[24]. Most of the PI3K inhibitors have been developed to target class I PI3'-kinases, however, class III PI3'-kinases are structurally very similar to class I PI3'-kinases and many compounds can target both classes[245]. Several class I PI3K inhibitors that have been shown to be potent antimalarial compounds (see Mott *et al.*[49]), recently have been validated through an *in vitro* assay directly examining the inhibition of the enzymatic activity of PfVps34 (unpublished data summarized in the recently completed Ph.D. thesis of my laboratory colleague Matthew Hassett and two recently submitted manuscripts from this thesis work). Since Vps34 is the only PI3K in *P. falciparum* parasites, it is possible that this protein is the target for PI3K inhibitors. This would suggest that PI3K inhibitors can target the autophagy pathway in malaria parasites and provide a novel class of compounds with a unique MOA that can be useful in combination with other compounds.

In addition being involved in cytocidal drug resistance to CQ[17], the autophagy pathway in *Plasmodium* parasites has been recently implicated as contributing to the ART resistance phenotype[53-54]. In 2015, Wang *et al.*[55] used a fluorescent ART probe to analyze the alkylated targets of ARTs and interestingly found Atg18 protein covalently bound to the probe. Additionally, in a genome-wide investigation of ART resistant parasite strains, T38N mutation in Atg18 was tentatively associated with decreased DHA and ATM susceptibility[53]. In the same year, Mbengue *et al.* reported the possible involvement of another component of the autophagy pathway in ART resistance; the increased activity of Vps34 was asociated with K13 mutations and ART resistance[54]. Together, these findings lead us to believe that the autophagy pathway is not only important in the context of cytocidal CQ resistance, but it is also important to ART resistance and

must be investigated further. Thus, I first investigated the cytocidal effects of DHA – the primary active metabolite of many ARTs – on Atg8 puncta formation in the canonical laboratory strains HB3 and Dd2, as well as in the laboratory-adapted Cambodian isolates CamWT, CamWT^{C580Y}, Cam3.II^{Rev} and Cam3.II^{R539T}.

Targeting the autophagy pathway is one method of introducing novel antimalarial therapies with unique MOAs that can be extremely useful in combination therapies. Recent reports have also provided evidence to support novel compounds with significant antimalarial potency[191, 246-249]. These include Torin 2 (which is an mTOR inhibitor), NITD609 (a spiroindolone), ELQ300 (part of the class of quinolone-3-diarylethers), DSM265 (a dihydroorotate dehydrogenase inhibitor), and DDD107498 (an elongation factor or protein synthesis inhibitor). Additionally, due to the excellent potency and quick action of endoperoxide compounds, attempts have been made to synthesize compounds containing endoperoxide bridge[250]. Of these synthetic endoperoxides, or ozonides, OZ277 and OZ439 have shown promise in clinical trials[91, 215, 242].

Endoperoxide drugs, like artemisinins, which possess a 1,2,4-trioxane heterocycle[251], are attractive antimalarial therapies. Due to their rapid action on parasites, this allows for less drug exposure time for parasites to develop resistance to the endoperoxide compound. These compounds are thought to exert their parasiticidal activity through reductive activation by heme, which is released as a result of hemoglobin digestion by malaria parasites[252-254]. This produces carbon-centered free radicals, which results in the alkylation of heme and various proteins, some of which may be critical to parasite survival[255]. However, as mentioned above, there has been a recent rise in the emergence of resistance to ACTs. Additionally, as a drug class, ARTs suffer from chemical (semi-synthetic availability, purity and cost)[256], biopharmaceutical (poor bioavailability and limiting pharmacokinetics)[257] and treatment (non-compliance with long treatment regimens

and recrudescence)[257-258] issues that limit their therapeutic potential. Therefore, it is imperative that this efficient class of drugs be improved upon to discover novel antimalarial treatments that are cheaper and more efficient at killing malaria parasites.

In 2004, Vennerstrom *et al.* described the synthesis of a large arrays of compounds in an attempt to create optimized, leading-candidate antimalarial compounds. One of the produced compounds included the ozonide compound, OZ277[250]. This compound also possesses the endoperoxide moiety necessary to cause oxidative damage to parasites in an efficient manner. This compound was optimized for half-life (1.4 hr) and bioavailability (35.0%). Typically, the general trend exhibited by ARTs is that increased lipophilicity leads to higher antimalarial activity but with compromised biopharmaceutical properties[259]. However, OZ277 was the exception to this trend and has an antimalarial potency of equal to or greater than artemether and artesunate.

Further development of the 1,2,4-trioxolane pharmacophore lead to the discovery of another ozonide compound, OZ439[215]. Similar to OZ277 and other endoperoxide antimalarials, OZ439 is fast-acting and has been shown to eliminate parasites within hours of treatment. Additionally, unlike other endoperoxide compounds, it has a significantly longer elimination half-life and increased blood concentration versus time profile. The outstanding efficacy and prolonged blood concentrations of OZ439 make it an excellent candidate for further investigation in antimalarial combination therapies. OZ439 has been shown to be tolerated up to doses of 1,600 mg, has completed Phase II clinical trials and is currently being marketed by Ranbaxy Pty Ltd in India[244, 260-261]. OZ439 has also been suggested to be a single-dose curative agent due to its extended elimination half-life of 23 hours, bioavailability of 76% and *in vitro* IC_{50} in the single-digit nanomolar range[215].

In 2016, Siriwardana *et al.* further validated the use of OZ439 in not only treating canonical laboratory strains of *P. falciparum,* but also in treating ACT resistant parasite strains[123]. A modified RSA capable of quantifying the DCP was conducted to study seven endoperoxide containing compounds against five laboratory-adapted Cambodian isolates, which were either K13 wild-type or contained a unique, ART resistance conferring, K13 mutation. As shown previously, K13 mutations are directly correlated with clinical findings of delayed parasite clearance or ART resistance[56-57, 87]. Siriwardana *et al.* showed that while six of the compounds tested were less potent against K13 mutant parasite strains, these mutant strains were not cross-resistant to OZ439. This finding was validated through determination of parasite survival through the standard RSA at a 700 nM dose of drug as well as through the calculation of an $RSLD_{50}$ derived from a modified dose-response version of the RSA. In 2017, Baumgartner *et al.* conducted a similar, dose-response RSA examining with several synthetic ozonide compounds[262] and this study also confirmed that OZ439 is significantly more potent than DHA or the previously discovered OZ277. These results suggest that OZ439 is an excellent candidate for further investigation and could provide an alternative therapy effective against ACT resistant malaria. In order to further validate the efficacy of OZ439, I sought to investigate its effect in combination with PI3K inhibitors.

6.3 Results

It has been established that antimalarial compounds can target different cellular pathways at cytostatic and cytocidal concentrations[15, 17, 263]. Additionally, it has been shown that the autophagy pathway is an important drug target at cytocidal concentrations of CQ and this pathway is dysregulated in CQ resistant parasite strains[17]. Recently, there has been evidence suggesting that the autophagy pathway also plays a role in the artemisinin resistance phenotype, with observations

of Atg18 mutations and increased enzymatic activity of Vps34[53-54]. We, therefore, were interested to further investigate the role of the autophagy pathway in the laboratory-adapted Cambodian isolates CamWT, CamWT^{C580Y}, Cam3.II^{Rev} and Cam3.II^{R539T}. A protocol similar to that used in Gaviria *et al.*[17] was utilized to assess the distribution of Atg8 containing puncta in the above mentioned strains, as well as the canonical laboratory strains HB3 and Dd2, under pressure with either control, drug-free media, starvation media or complete media containing an LD_{50} concentration of DHA.

As expected, under control, nutrient rich conditions, all strains tested displayed diffuse Atg8 staining, localized to the cytosol as reported previously[17] (data not shown). However, under both nutrient starved and DHA LD_{50} conditions, there were significant differences in the observed staining patterns and quantification of Atg8 containing puncta. For HB3 and Dd2 parasite strains, similar to previous observations (see Gaviria *et al.*[17]), a significant re-distribution of Atg8-labeled puncta was observed under both starved and DHA LD_{50} conditions (Figure 6.1). In CamWT and Cam3.II^{Rev}, both containing wild-type K13 sequences, I observed a reduced re-distribution of Atg8-labeled puncta in both starved and DHA LD_{50} treated parasites (Figure 6.1) which is distinct from the CQR (Dd2) phenotype. It should be noted that, to date, all observed cases of ART or ACT resistance have evolved in regions of the globe where CQR is prevalent and therefore on a CQR background. Thus, it could be assumed, according to results in Chapter 3, that the autophagy response to CQ would be muted. However, surprisingly, even the Cambodian strains harboring a wild-type K13 show a relatively muted autophagy response to nutrient starvation, as well as to stress caused by DHA, in comparison to the canonical HB3 and Dd2 strains. The most striking result was observed for the K13 mutant strains. CamWT^{C580Y} and Cam3.II^{R539T} strains, which

contain the mutations C580Y and R539T respectively in the K13 domain, did not display a re-distribution of Atg8-labeled puncta under either stress inducing condition (Figure 6.1).

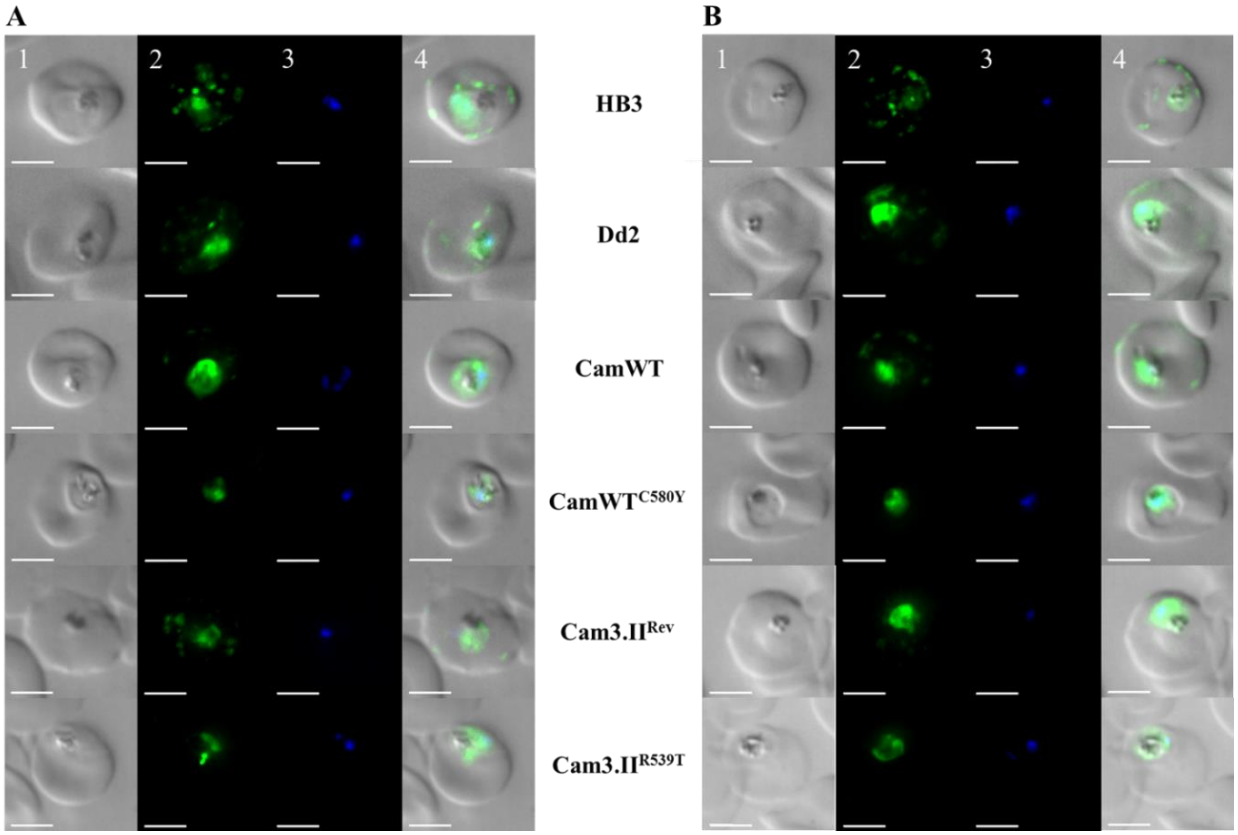

Figure 6. 1 Imaging of autophagosomal body puncta formation and trafficking in response to starvation and LD_{50} DHA. Imaging of PfAtg8 containing puncta within parasite (from top row to bottom - HB3, Dd2, CamWT, CamWT^{C580Y}, Cam3.II^{Rev}, and Cam3.II^{R539T}) infected RBCs after 6-hour exposure to either starvation (A) or a bolus dose of DHA at LD_{50} (B). Panel 1: transmittance image. Panel 2: anti-PfAtg8 antibody imaging. Panel 3: DAPI nuclear staining. Panel 4: a merged image of all three channels. Bar = 4 μm.

To better define this phenotype, I next quantified this puncta response as described previously[17]. Briefly, the number of puncta at a distance > 3.5 μm from the center of the parasite DV was quantified by combining confocal microscopy imaging with 3-dimentional image analysis software. In agreement with the visual observations, HB3 and Dd2 strains had the highest number of puncta in response to both starvation and DHA LD_{50}. A statistically significant difference was

not observed (p>0.05) in the autophagosomal body-puncta response for either HB3 or Dd2 under starvation conditions or DHA LD_{50} (Figure 6.2). Compared to these strains, there was a statistically significant reduction in the puncta-response (p<0.05) for both CamWT and Cam3.II^{Rev} strains, both harboring the wild-type K13 sequence (Figure 6.2). However, this pattern of Atg8 staining was distinct from that observed under control conditions (p<0.05). As seen in Figure 6.1, there was no significant re-distribution in the autophagosomal-body puncta for CamWT^{C580Y} and Cam3.II^{R539T} when stressed with either starvation or DHA LD_{50} (Figure 6.2). This response was not statistically different from Atg8 staining that is typically observed under control conditions (p>0.05).

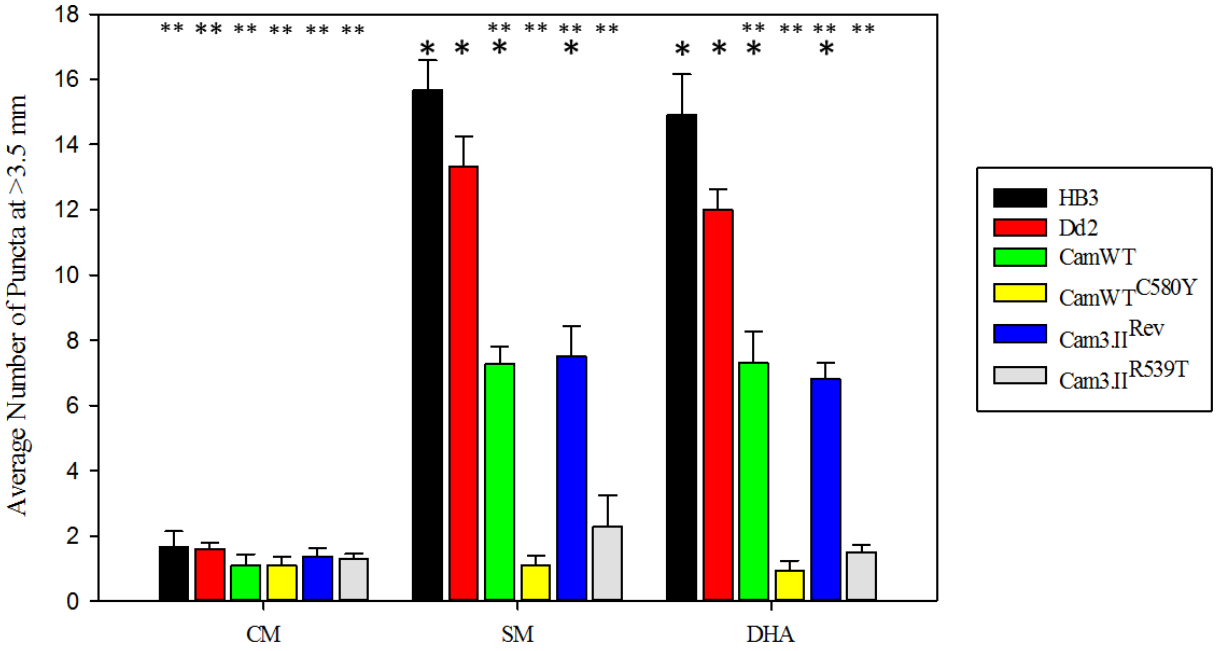

Figure 6. 2 Quantification of PfATG8 positive puncta**.** PfATG8 positive puncta, quantified as described previously[17], were measured upon treatment with control median (CM), starvation media (SM) or an LD_{50} dose of DHA. * indicates that the difference in puncta distribution is statistically significant compared to HB3 under control conditions (p value < 0.05). ** indicates that the difference in puncta distribution is statistically significant compared to HB3 under starvation conditions (p value < 0.05).

These results indicated that there was a difference in the autophagy response in K13 wild-type versus K13-mutant parasites. This is a significant observation given that dysregulation of the

autophagy process was also involved in acquiring choloroquine resistance at a cytocidal level[17]. It is also important to note here that Mbengue *et al.* recently reported the involvement of the increased activity of Vps34 in correlation with K13 mutations and ART resistance[54]. Another recent, and particularly intriguing, result was the discovery of PI3K inhibitors that were extremely potent against *Plasmodium* parasites[49]. Taken together, this could indicate the autophagy pathway as a vital drug target in overcoming ART resistance. As WHO currently recommends administering antimalarial drugs as combinations, it is important to identify a suitable partner drug for these PI3K inhibitors. Work done recently in our lab has shown that the compound OZ439 is capable of overcoming the cross-resistance shown by K13-mutant parasites to structurally related ART drugs[123]. ART resistance was initially defined as a delayed clearance phenotype[58]. However, patients were still cured of malaria. Delayed clearance meant that ACT treatment may have been required for 4 days instead of the normal 3 day treatment[68]. Disturbingly, resistance to the partner drug in Duo-Cotecxin – piperaquine (PPQ) – has also been reported recently[53, 65-67]. Therefore, it is important to discover partner drugs to existing ARTs to overcome resistance shown to the partner drug and it is also important to develop new combinations therapies with compounds such as OZ439, which have enhanced properties. This led our lab to look at combinations of PI3K inhibitors with two existing ART drugs – DHA and ATM – as well as combinations with OZ439, both at cytostatic and cytocidal levels using the Chou-Talalay (C-T) combination assay format (Figure 6.3)

There are multiple methods for assessing the efficacy of combination drug therapies[202-204]. Some of these methods can be extremely time consuming, requiring multiple assays to produce one output describing a unique drug pair. The Chou-Talalay method is simpler, in that it can be done at a singular drug pair ratio and it is, therefore, amenable to a high-throughput format,

allowing for the generation of large data sets and the evaluation of a vast array of drug pairs. In this method, the two drugs in question are utilized at a 1:1 ratio (IC_{50}:IC_{50} or LD_{50}:LD_{50}) over a range of multiple concentrations, generating C-T plots of parasite growth or survival (dependent on the nature of the assay, whether it is cytostatic or cytocidal, see Figure 6.3) as a function of each drug concentration. These plots are then used to calculate fractional inhibitory concentrations (FIC) for each drug in question using Equation 1-3.

$$FIC_A = \frac{IC_{50}\ of\ Drug\ A\ in\ Combination}{IC_{50}\ of\ Drug\ A\ alone} \qquad \text{(Equation 1)}$$

$$FIC_B = \frac{IC_{50}\ of\ Drug\ B\ in\ Combination}{IC_{50}\ of\ Drug\ B\ alone} \qquad \text{(Equation 2)}$$

$$FIC_{Index} = FIC_A + FIC_B \qquad \text{(Equation 3)}$$

These equations allow for the comparison of the activity of each drug within the combination versus the activity of each drug when it is used as a monotherapy. The individual FICs are then added (Equation 3) to determine the FIC_{Index} of the drug combination therapy (or FLD_{Index} if examining cytocidal potency). The Chou-Talalay analysis provides a clear distinction between synergistic, additive and antagonistic drug pairs[96]. For instance, if the presence of an inactive compound simply augments the activity of a drug, this is not synergy; it is potentiation. Synergy requires the presence of two active compounds. Additionally, the combined activity of drugs A and B being greater than the monotherapies does not mean the combination is necessarily synergistic; such a result could be caused by additive or slight antagonistic interactions[97]. Based on their calculations, Chou and Talalay define additivity when the FIC_{Index} equals 1. When the FIC_{Index} is less than 1, the interaction is synergistic; when it is greater than 1, the interaction is antagonistic[96]. However, these ranges can be altered based on experimental variance - from synergy being less than 0.5 to antagonism being greater than 4[98] or additivity being represented between 1 and 2[99]. This can be explained if analyzed from the perspective of isobologram analysis.

As previously described, isobolograms are constructed using the IC_{50}/LD_{50} of each compound on each of the x or y axis. The line of additivity connects each single-drug IC_{50}/LD_{50}. It is conceivable that for a particular drug combination, one could observe ratios of 1:1 and 1:2 below the line of additivity and ratios 2:3 and 3:1 above the line of additivity. In this case, it is unclear what interaction the drug pair presents. Thus, the cutoffs for synergy, additivity and antagonism using the Chou-Talalay assay are arbitrary and are not necessarily always accurate. For the purpose of this study and to utilize more stringent criteria, I defined synergy as having an $FIC_{Index}/FLD_{Index}<1$, additivity as FIC_{Index}/FLD_{Index} between 1-2 and antagonism as having an $FIC_{Index}/FLD_{Index}>2$. Synergy could potentially arise from inhibition of pathways that undergo downstream cross-talk, or through interacting with the same pathway in two different locations, or perhaps by inhibiting two different pathways completely. The isobologram or Chou-Talalay analysis only determines the nature of the interaction, not how it comes to be. Our hope is that by targeting two separate pathways, we may be able to discover synergistic drug pairs that could also prove useful in preventing the rise of antimalarial drug resistance.

A

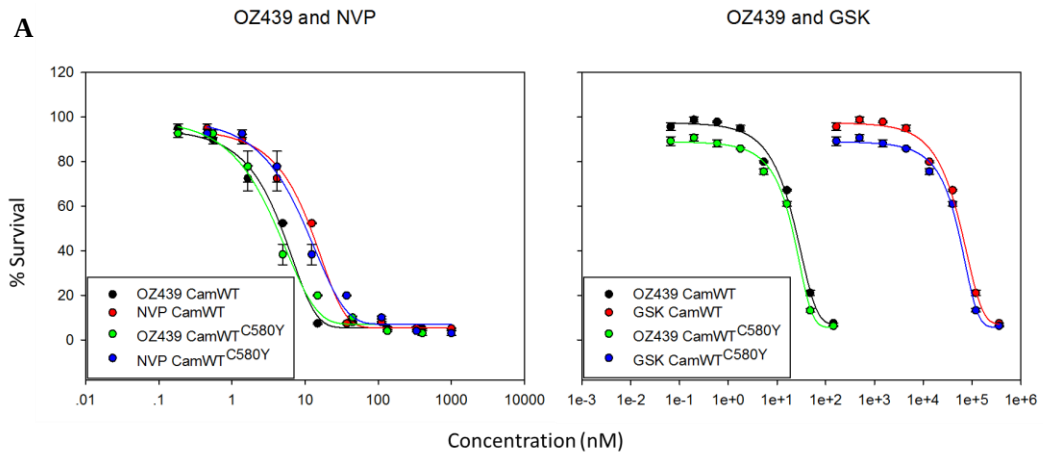

B

Strain	Drug	Psuedo LD_{50} (in combination)	LD_{50} (monotherapy)	FLD	FLD_{Index}	Assignment
CamWT	OZ439	3.69	10.24	0.36	0.80	**Synergistic**
	NVP	3.89	8.92	0.44		
	OZ439	18.17	10.24	1.77	3.01	**Antagonistic**
	GSK	45423	36772	1.24		
CamWT^{C580Y}	OZ439	6.56	17.74	0.37	0.75	**Synergistic**
	NVP	5.10	13.31	0.38		
	OZ439	15.00	17.74	0.85	2.13	**Antagonistic**
	GSK	37493	29302	1.28		

Figure 6. 3 Chou-Talalay combination analysis. **A)** Representative graphs of a Chou-Talalay cytocidal analysis performed on the combinations of OZ439 and NVP-BGT226/GSK2126458 for the laboratory-adapted Cambodian isolate, CamWT and the ZFN edited transfectant, CamWT^{C580Y}, which possesses a C580Y mutation in the K13 propeller domain. **B)** Sample calculation of FLD for each drug used and FLD_{Index} for the pair. Values < 1 considered synergistic, values above 2 antagonistic.

Initially, the combinations of endoperoxides with PI3K inhibitors were investigated at the cytostatic level, using the C-T method described above, to determine if any of these combinations have parasite growth inhibitory efficacy against CamWT, CamWT^{C580Y}, Cam3.II^{Rev}, Cam3.II^{C580Y} and Cam3.II^{R539T}. The activity of the combinations of ATM, DHA or OZ439 with PI3K inhibitors as well as the standard ACT parings of ATM+LUM and DHA+PPQ were employed. Many of the combinations tested were additive, however, there was significant synergy observed for the CamWT^{C580Y} strain (Table 6.1). This could indicate significant growth inhibitory potential of the

OZ439+PI3K combinations against ART resistant strains; however, similar synergy was not observed in the Cam3.II^{R539T} strain (which possesses a native K13 mutation) or the Cam3.II^{C580Y} strain (which was genetically engineered to contain a different K13 mutation). As mentioned previously, the cytostatic potency of drug monotherapy or combination therapy is not necessarily the most clinically relevant observation and with multiple indications of the role of autophagy in cytocidal drug resistance, it was extremely important to investigate the cytocidal potency of these combinations. Due to the different molecular targets at the cytostatic versus cytocidal levels, it is possible that results from these two different types of assays might not correlate with each other. In other words, it is possible to observe additivity or antagonism at the cytostatic level but also to observe synergy for the same drug combinations at the cytocidal level. Thus, my colleague, Kalpana Iyengar and I next investigated the previously tested drug combinations at the cytocidal level using the CamWT and CamWT^{C580Y} strains. The cytocidal (LD_{50}) combination assay involves a more sophisticated process, requiring multiple washing steps and thus, is not as amenable to a high-throughput format that we and our collaborators were able to use for the cytostatic (IC_{50}) assay[263]. As shown by Siriwardana *et al.*[123], two strains CamWT and CamWT^{C580Y} display a similar ART sensitive/resistance phenotype compared to the Cam3.II background strains and therefore, these two were used as representative strains to investigate possible synergy.

Table 6.1 Combination $FIC_{Indices}$ for endoperoxide + PI3K inhibitor treatments in comparison with standard ATM+LUM or DHA+PPQ, tested for all five DCP strains. Several combinations, including OZ439+PI3K inhibitors were synergistic for CamWT^{C580Y}.

Combination	FIC_{Index}									
	CamWT		$CamWT^{C580Y}$		$Cam3.II^{Rev}$		$Cam3.II^{C580Y}$		$Cam3.II^{R539T}$	
ATM/LF	0.89 ± 0.06	Syn	0.80 ± 0.10	Syn	0.88 ± 0.01	Syn	0.84 ± 0.07	Syn	0.82 ± 0.10	Syn
ATM/NVP	1.38 ± 0.19	Add	1.30 ± 0.29	Add	2.06 ± 0.18	Ant	2.07 ± 0.26	Ant	1.73 ± 0.03	Add
ATM/GSK	1.49 ± 0.21	Add	0.84 ± 0.09	Syn	1.88 ± 0.19	Add	1.81 ± 0.21	Add	1.45 ± 0.16	Add
ATM/Torin 1	1.37 ± 0.21	Add	0.96 ± 0.09	Syn	1.18 ± 0.21	Add	1.20 ± 0.16	Add	1.18 ± 0.04	Add
ATM/Torin 2	1.46 ± 0.10	Add	1.15 ± 0.08	Add	1.33 ± 0.36	Add	1.35 ± 0.35	Add	1.48 ± 0.26	Add
ATM/PIK93	1.74 ± 0.16	Add	1.10 ± 0.05	Add	1.74 ± 0.06	Add	1.66 ± 0.01	Add	1.58 ± 0.03	Add
DHA/PPQ	0.95 ± 0.02	Syn	0.78 ± 0.03	Syn	0.96 ± 0.03	Syn	0.75 ± 0.00	Syn	0.55 ± 0.02	Syn
DHA/NVP	0.97 ± 0.20	Syn	0.90 ± 0.03	Syn	1.61 ± 0.27	Add	1.18 ± 0.11	Add	1.37 ± 0.16	Add
DHA/GSK	0.83 ± 0.24	Syn	0.70 ± 0.06	Syn	1.26 ± 0.21	Add	0.82 ± 0.04	Syn	1.12 ± 0.42	Add
DHA/Torin 1	1.00 ± 029	Add	0.91 ± 0.20	Syn	2.04 ± 0.46	Ant	1.36 ± 0.34	Add	1.44 ± 0.25	Add
DHA/Torin 2	1.02 ± 0.26	Add	0.95 ± 0.21	Syn	1.59 ± 0.31	Add	1.31 ± 0.28	Add	1.44 ± 0.16	Add
DHA/PIK93	1.38 ± 0.22	Add	0.86 ± 0.18	Syn	1.34 ± 0.22	Add	1.14 ± 0.19	Add	1.19 ± 0.05	Add
OZ439/NVP	1.06 ± 0.32	Add	0.82 ± 0.19	Syn	1.62 ± 0.07	Add	1.32 ± 0.17	Add	1.32 ± 0.13	Add
OZ439/GSK	0.93 ± 0.03	Syn	0.80 ± 0.05	Syn	1.97 ± 0.09	Add	1.18 ± 0.19	Add	1.43 ± 0.10	Add
OZ439/Torin	1.19 ± 0.25	Add	0.88 ± 0.07	Syn	2.47 ± 0.09	Ant	2.12 ± 0.23	Ant	1.61 ± 0.51	Add
OZ439/Torin	1.14 ± 0.17	Add	0.93 ± 0.03	Syn	2.92 ± 0.40	Ant	2.21 ± 0.51	Ant	2.24 ± 0.49	Ant
OZ439/PIK93	1.10 ± 0.06	Add	1.01 ± 0.12	Add	1.90 ± 0.13	Add	1.88 ± 0.17	Add	1.85 ± 0.04	Add

The IC_{50} assay subjects parasites to a continuous, 72 hour exposure to the drug(s) and thus, parasites pass through multiple stages of their life-cycle during this time period. As previously mentioned, malaria parasites pass through the ring, trophozoite and schizont stages during the intraerythrocytic phase and this cycle repeats approximately every 45 hours. On the other hand, the LD_{50} assay subjects parasites to a 6 hour bolus dose of the drug(s). This is shorter than the amount of time that it required for the parasites to complete one stage of their life-cycle. Additionally, it has been shown that, in ART resistant parasite strains, early ring-stage parasites are less susceptible to ARTs compared to the trophozoite stage of the same parasite strains[50, 57, 71, 83, 123]. Thus, our lab wanted to investigate the cytocidal potency of endoperoxide+PI3K inhibitor combinations in both the ring and trophozoite stages of the parasite life cycle.

Similar to IC_{50} combinations, the standard ACT combinations as well as novel endoperoxide+PI3K inhibitor combinations were investigated in the LD_{50} format. Significant synergy or additivity was observed for most combinations tested at the trophozoite stage for both parasite strains (CamWT and CamWT^{C580Y}), with the exception of DHA+NVP (which was antagonistic vs one wild-type strain, see Table 6.2). However, due to the decreased sensitivity of ring stages to ARTs, my colleague, Kalpana Iyengar and I were particularly interested in examining combinations at the ring stage.

Of the drug combinations tested in the ring-stage cytocidal assay, OZ439+Torin 2 was found to be extremely synergistic (FLD_{Index}: 0.40 ± 0.14 for CamWT and 0.12 ± 0.02 for CamWT^{C580Y}, see Table 6.2). In the trophozoite stage assay, this same combination was also synergistic for both strains but with approximately equal activity (FLD_{Index}: 0.56 ± 0.04 for CamWT and 0.70 ± 0.12 for CamWT^{C580Y}). This was particularly interesting due to both partner drugs involved. As mentioned previously, OZ439 is an extremely potent antimalarial and ART

resistant strains do not display cross-resistance to this compound[123, 262]. Torin 2 acts on the autophagy pathway and thus, could be acting on a vital drug target in *Plasmodium* parasites. Further, both of these drugs are potent antimalarials as monotherapies as well. Also noteworthy is the fact that this combination was more synergistic in the K13-mutant strains compared to the K13 wild-type strain.

Additionally, several other combinations were found to have significant synergy against the ring-stage of parasites, with many of these combinations being more potent against the K13-mutant strain, $CamWT^{C580Y}$, than against the K13 wild-type strain, CamWT. Notably, DHA+Torin 1/Torin 2/PIK93, OZ439+NVP/Torin 1 and ATM+GSK/Torin 1 were all found to be synergistic against the ring stage of $CamWT^{C580Y}$. Of these, DHA+Torin 2, OZ439+NVP and ATM+GSK/Torin 1 were more potent against the $CamWT^{C580Y}$ strain. Although Torin 1 and Torin 2 are structural analogs of each other and both are thought to target mTOR, Torin 2 is a significantly more potent antimalarial than Torin 1 at both cytostatic and cytocidal levels[49]. Thus, it is encouraging to find that combinations involving Torin 2 are also more potent than combination involving Torin 1. OZ439+NVP was also significantly more potent in the ring stage than either ATM or DHA +NVP ($FLD_{Indices}$ for CamWT: 0.79 ± 0.01, 1.67 ± 0.20, 1.40 ± 0.48 respectively). This is another particularly promising result as it combines two compounds that are extremely potent as monotherapies and are also targeting different cellular pathways.

Table 6.2 Combination $FLD_{Indices}$ for endoperoxide + PI3K inhibitor treatments in comparison with standard ATM+LUM or DHA+PPQ, tested for CamWT and $CamWT^{C580Y}$. In particular, OZ439+Torin 1 or OZ439+Torin 2 were extremely synergistic (FLD for OZ439+Torin 2: 0.40 and 0.12 respectively for CamWT and $CamWT^{C580Y}$). OZ439 combinations were more synergistic in ring stage than in trophozoite stage. OZ439+NVP was also synergistic (FLD 0.79 and 0.77 for CamWT and $CamWT^{C580Y}$ respectively.

Combination	FLD_{Index} Rings				FLD_{Index} Trophs			
	CamWT		$CamWT^{C580Y}$		CamWT		$CamWT^{C580Y}$	
ATM/LF	0.49 ± 0.23	**Syn**	0.87 ± 0.20	**Syn**	0.83 ± 0.06	**Syn**	0.61 + 0.08	**Syn**
ATM/NVP	1.67 ± 0.20	**Add**	1.23 ± 0.13	**Add**	1.13 ± 0.08	**Add**	0.93 ± 0.22	**Syn**
ATM/GSK	0.87 ± 0.11	**Syn**	0.74 ± 0.07	**Syn**	0.44 ± 0.06	**Syn**	0.41 ± 0.11	**Syn**
ATM/Torin 1	1.16 ± 0.06	**Add**	0.50 ± 0.03	**Syn**	0.78 ± 0.10	**Syn**	0.69 ± 0.17	**Syn**
ATM/Torin 2	4.76 ± 0.51	**Ant**	3.38 ± 0.65	**Ant**	0.25 ± 0.04	**Syn**	0.44 ± 0.00	**Syn**
ATM/PIK93	1.55 ± 0.85	**Add**	11.32 ± 3.04	**Ant**	0.51 ± 0.01	**Syn**	0.50 ± 0.00	**Syn**
DHA/PPQ	1.15 ± 0.03	**Add**	1.92 ± 0.49	**Add**	0.81 ± 0.11	**Syn**	0.83 ± 0.09	**Syn**
DHA/NVP	1.40 ± 0.48	**Add**	1.07 ± 0.45	**Add**	2.18 ± 0.36	**Ant**	1.64 ± 0.09	**Add**
DHA/GSK	1.99 ± 1.10	**Add**	1.72 ± 0.80	**Add**	0.76 ± 0.23	**Syn**	0.97 ± 0.01	**Syn**
DHA/Torin 1	0.56 ± 0.12	**Syn**	0.76 ± 0.23	**Syn**	0.70 ± 0.07	**Syn**	0.54 ± 0.11	**Syn**
DHA/Torin 2	1.04 ± 0.54	**Add**	0.52 ± 0.24	**Syn**	1.51 ± 0.22	**Add**	1.33 ± 0.00	**Add**
DHA/PIK93	0.70 ± 0.13	**Syn**	0.85 ± 0.45	**Syn**	0.92 ± 0.00	**Syn**	0.72 ± 0.18	**Syn**
OZ439/NVP	0.79 ± 0.01	**Syn**	0.77 ± 0.08	**Syn**	1.43 ± 0.19	**Add**	1.70 ± 0.15	**Add**
OZ439/GSK	2.23 ± 0.64	**Ant**	2.51 ± 0.31	**Ant**	0.75 ± 0.33	**Syn**	1.03 ± 0.37	**Add**
OZ439/Torin 1	0.61 ± 0.05	**Syn**	0.77 ± 0.04	**Syn**	1.04 ± 0.06	**Add**	1.19 ± 0.04	**Add**
OZ439/Torin 2	0.40 ± 0.14	**Syn**	0.12 ± 0.02	**Syn**	0.56 ± 0.04	**Syn**	0.70 ± 0.12	**Syn**
OZ439/PIK93	5.32 ± 2.15	**Ant**	3.12 ± 0.80	**Ant**	0.65 ± 0.10	**Syn**	1.16 ± 0.04	**Add**

6.4 Discussion

Artemisinin (ART) Combination Therapies (ACT) are currently the front-line therapy for treating *Plasmodium falciparum* malaria. However, reports of artemisinin resistant *P. falciparum* are on the rise and could indicate the imminent failure of ACTs[58-60]. Thus, investigating mechanisms of ART resistance and understanding these mechanisms to inform the development of novel antimalarial therapies is of utmost importance. Many of the ACTs currently in use were discovered empirically without validation of the drugs' mode of action (MOA). This lead to combinations of drugs with similar MOAs. However, for an antimalarial therapy to have the best potential for both being effective at curing patients[206] and reducing the risk of the development of concurrent resistance[240-241], the drugs used should possess different MOAs.

It has been shown that phosphatidylinositol 3'-kinase (PI3K) inhibitors are extremely potent antimalarial compounds[49]. Not only are these compounds potent at the cytostatic level, but they also show significant cytocidal potency and are synergistic in combination with several other antimalarial compounds, including with ARTs[49]. Recent studies highlight the importance of studying cytocidal drug activity as traditional IC_{50} assays unable to distinguish ART sensitive versus ART resistant strains[57, 70-71]. At these cytocidal levels of drug, the activation of an autophagy-like pathway is responsible for drug-induced parasite death. This pathway is involved in acquiring cytocidal drug resistance as well[17, 49]. Of particular interest is the fact that *P. falciparum* parasites only possess one PI3'-kinase, namely, the class III Vps34. Thus, it is possible that this is the molecular target for PI3K inhibitors. Taken together, this suggests that by simultaneously inducing the cell-survival mechanism of autophagy and inhibiting it with drug, it

could be possible to induce parasite death through targeting the same pathway at multiple locations.

The use of PI3K inhibitors is attractive, not only because this class of drugs targets a cellular pathway that is integral to parasite survival under external stress, but also because the expected target pathway for these inhibitors has been implicated in the rise of ART resistance. In 2015, Wang *et al.*[55] used a fluorescent ART probe to analyze the alkylated targets of ARTs and interestingly found Atg18 covalently bound to the probe. Additionally, Mbengue *et al.* reported the involvement of another component of the autophagy pathway in ART resistance; the increased activity of Vps34 was associated with K13 mutations and ART resistance[54]. These findings show that the autophagy pathway is important to ART resistance and must be investigated further. Thus, I first investigated the cytocidal effects of DHA – the primary active metabolite of many ARTs – on Atg8 puncta formation in the canonical laboratory strains HB3 and Dd2, as well as in the laboratory-adapted Cambodian isolates CamWT, CamWT^{C580Y}, Cam3.II^{Rev} and Cam3.II^{R539T}.

My investigation of the autophagy response in both K13 wild-type and K13-mutant strains in comparison with canonical laboratory strains HB3 and Dd2 provided invaluable insight into an essential cell-survival and cell-death pathway. While a redistribution of Atg8 puncta was observed in K13 wild-type strains CamWT and Cam3.II^{Rev}, quantification of these puncta revealed a muted phenotype in comparison with HB3 and Dd2 parasite strains. This result was observed for both starvation treatment and LD_{50} treatment with DHA. Most surprisingly, I did not observe a redistribution of Atg8 puncta in CamWT^{C580Y} or Cam3.II^{R539T}, the K13-mutant strains. K13 mutations have been associated with clinical findings of ART resistance[57], thus, my results suggest that the autophagy response is dysregulated in ART resistant parasite strains. This could indicate

that targeting the autophagy pathway could lead to the development of novel antimalarial combination therapies to combat ART resistance.

Endoperoxide drugs, like artemisinins, which possess a 1,2,4-trioxane heterocycle[251], are attractive antimalarial drugs. Due to their rapid action on parasites, this allows for less drug exposure time for parasites to develop resistance to them. This, along with their excellent potency lead to multiple attempts to synthesize compounds containing an endoperoxide bridge[250]. Of these synthetic endoperoxides, the ozonides, OZ277 and OZ439 have shown promise in clinical trials[91, 215, 242]. In 2016, our group validated the use of OZ439 in treating ACT resistant parasite strains[123]. My colleague Kalpana Iyengar and I conducted an RSA analysis on both K13 wild-type and K13 mutant *P. falciparum* strains and found that most endoperoxide compounds tested were less effective against K13-mutant strains. OZ439 was the only compound to which the K13-mutant parasite strains were not cross-resistant. These results were further validated by a similar study done recently[262].

Together, our lab's findings that OZ439 is equipotent against both K13 wild-type and K13-mutant parasite strains as well as the observations of a dysregulation of the autophagy pathway in K13-mutant parasite strains led us to investigate the potency of drug combinations involving OZ439+PI3K inhibitors. While it is important to investigate the potency of these combinations at the cytostatic level, it has been shown that ART resistance cannot be distinguished through IC_{50} assays[57, 70-71]. Therefore, the potency of these antimalarial combinations was also investigated at the cytocidal level. Since ART resistance is associated with increased tolerance in the ring-stage[71], these cytocidal combination assays were done on synchronized parasites at either the ring or trophozoite stages for comparison. Comparison of the combinations indicate that while there is

synergy for multiple drug pairs, notably, the synergy is most pronounced in combinations with OZ439. The most potent combination found was OZ439+Torin 2. Additionally, OZ439+NVP/Torin 1 were synergistic but with decreased potency compared to OZ439+Torin 2. It is also interesting that for both combinations of OZ439+NVP/Torin 2, there is stronger synergy in CamWT^{C580Y}, the K13-mutant strain, than in CamWT, the K13 wild-type strain. This suggests that these two drug pairs may be able to circumvent emerging ART resistance and can serve as novel, leading-candidate replacement ACTs.

Ours results show that the autophagy pathway, which is essential to cytocidal CQ resistance, is also dysregulated in ART resistant parasite strains. Additionally, we show that it is possible to target this pathway to potentially overcome ART resistance by partnering PI3K inhibitors with OZ439, to which, we find, K13-mutant strains are not cross-resistant. This is extremely important, considering the rise of ART resistance and the possibility of spread to other countries, including Africa, where the majority of malaria related deaths occur. Thus, it is imperative that future work continues to investigate the targeting of the malaria autophagy pathway as a potential mechanism of overcoming drug resistance.

6.5 Acknowledgments

The Roepe lab thanks Dr. David A. Fidock (Columbia University) for providing the laboratory-adapted isolates and ZFN engineered transfectants used in this study, and the Medicines for Malaria Venture (MMV) for providing AMS, OZ277, and OZ439. This work was supported by NIH grant AI111962 to PDR.

CHAPTER VII

OVERALL CONCLUSIONS

Plasmodium falciparum malaria is a deadly parasite that continues to pose a global health burden. The advent of and continual development of drug resistance to front-line therapies necessitates research into drugs that target novel aspects of parasite biology. Since 2000, when investigators in this field identified the PfCRT gene[10], considerable progress has been made in understanding how mutations in PfCRT confer resistance to cytostatic (IC_{50}) dosages of drug[128, 143]. Although much progress has been made in recent decades understanding the genetic, cellular and molecular basis of antimalarial drug resistance phenomena at a growth inhibitory, or cytostatic, level, some questions still remain. One such central question is whether the resistance to cell kill effects (cytocidal activity) of drugs is via distinct pathways compared to resistance to growth inhibitory effects (cytostatic activity) of drugs; and, if so, how can these distinct mechanisms be better elucidated and targeted to overcome multidrug resistance?

To investigate resistance to death, one must first investigate programed cell death pathways. *P. falciparum* parasites lack caspases and other genes necessary to encode key apoptosis regulators and no molecular alterations in the apoptosis pathway have been found in correlation with chloroquine (CQ) resistance[16]. This thesis work sought to analyze cell death pathways in *P. falciparum* parasites and utilize this information to propose targeted and novel antimalarial combination therapies in the face of mounting drug resistance.

CQ is an antimalarial drug that can exert both cytostatic and cytocidal effects. In the clinical setting, resistance is developed via parasites that are not killed when exposed to typical plasma concentrations of CQ (which range from 1-10 μM)[263]. Thus, in order to understand mechanisms

of cytocidal CQ resistance, it is essential to study cell-death pathways in malaria parasites. Result from LD_{50} directed QTL mapping using the progeny of the HB3 (CQS) × Dd2 (CQR) cross, done in collaboration with Professor Michael Ferdig (Notre Dame), led our research group to inspect cytocidal activity and resistance from the perspective of one potential programmed cell-death (PCD) pathway, namely, autophagy. Recent literature suggests that autophagy plays a significant role in malarial parasites[24-28]. The *Plasmodium* genome possesses homologues of 15 of the 30 identified autophagy related (Atg) genes including all essential elements required for a functional autophagy pathway, although several homologues may be significantly different from other species; most notably mTOR as evidenced by the lack of a candidate homologue[24]. Interestingly, Vps34 is the only phosphatidylinositol 3'-kinase (PI3K) that has been identified in the *Plasmodium* genome and suggests a possible regulation step in the absence of an mTOR homologue.

Autophagy genes are found in all eukaryotes and a growing number of protozoa show evidence of functionality. The autophagy pathway has been well characterized in the related apicomplexan parasite, *Toxoplasma gondii*[29, 38]. In addition to being a cell-death pathway, autophagy serves housekeeping roles in the cell and it is necessary for processing misfolded or aged proteins as well as damaged organelles. It is also a survival pathway under conditions of nutrient starvation. Typically, it only operates as a death mechanism if conditions are too extreme to recover from or if the mitochondria become compromised[38]. These roles have been probed in malaria to a very small extent; to date, this thesis is one of the most comprehensive analyses of autophagy in malaria and methods of targeting this pathway to overcome resistance to front-line antimalarial therapies.

Chapter 3 suggests an alteration in the autophagy pathway in CQR parasites when probed at cytocidal concentrations of CQ. Thus, by targeting this pathway, it may be possible to overcome CQ resistance. Made possible through a collaboration with Dr. Craig Thomas at the National Center for Advancing Translational Sciences (NCATS), Chapter 4 identifies several novel compounds which were potent antimalarials and were synergistic partners with currently used drugs. An intriguing class of compounds that were identified included known human PI3K inhibitors. Chapter 4 further investigates the autophagy response in *P. falciparum* parasites under cytocidal doses of other antimalarial compounds, such as the endoperoxide artemether (ATM), which is currently used in artemisinin combination therapies (ACTs). Additionally, as the WHO recommends the use of drug combination therapies as a method of reducing the risk of the development of resistance, work in Chapter 4 also sought to discover novel synergistic drug combinations that combine potent monotherapies. One significant outcome of this analysis was the discovery of the effect of various drugs on the autophagy pathway. As mentioned before, drugs such as ATM which cause oxidative stress to parasites caused an induction of the autophagy pathway. A synergistic partner which is also a PI3K inhibitor, NVP-BGT226, was on the other hand able to reduce this response. Two drugs which act on the same pathway at different locations is a possible method of acquiring synergy. Therefore, this result was extremely significant. In addition, inhibition of the survival pathway simultaneously with induction of that pathway could have significantly deleterious effects on the parasite. Since Vps34 is the only PI3K that has been identified in *P. falciparum* parasites, it could be the molecular target for PI3K inhibitors such as NVP-BGT226 or GSK2126458. Additionally, many PI3K inhibitors have already been approved for use in the treatment of cancer, so these are attractive compounds to investigate in *P. falciparum.*

However, more information is still needed about PfVps34 as most PI3K inhibitors in use target class I PI3´-kinases but are still potent against *P. falciparum*. A crystal structure of this protein would give important details about its structure and its interaction with substrates and inhibitors. There are only two known Vps34 specific inhibitors that have been developed, namely SAR-405 and PIKIII[264-265]. Thus, it would prove useful if information was available about binding interactions of these compounds versus class I-targeted PI3K inhibitors with PfVps34.

The novel antimalarial compounds that were found via the high-throughput screen in Chapter 4 were further studied as both cytostatic and cytocidal drug combinations using the Chou-Talalay method[96]. As previously mentioned, it is important that any novel antimalarial therapy be evaluated at both levels since clinically parasites are exposed to cytocidal drug concentrations. The Chou-Talalay method studies drug pairs at a 1:1 effective ratio (IC_{50}:IC_{50} or LD_{50}:LD_{50}). The advantage to this method is that it is efficient and relatively easy to produce multiple data sets. However, the disadvantage to this method is that clinically, human plasma concentrations of these drugs are not necessarily at a 1:1 ratio. It may be logical, then, to attempt to conduct the Chou-Talalay analysis at physiologically relevant concentration ratios or at the ratio of concentrations each drug is found in plasma human when used as a monotherapy. This does not represent the most accurate method as well since it is possible that the presence of one drug can affect the metabolism or absorption of the other drug, thereby changing the plasma ratio of the two drugs. Thus, these physiologically relevant ratios must be further investigated in order to conduct physiologically accurate Chou-Talalay analyses.

Due to the rise of resistance to ACTs, which are the current front-line antimalarial therapies, it is imperative to discover novel antimalarial drug combination therapies that contain

potent compounds which have different modes of action (MOA) and work synergistically to kill malaria parasites. Original reports of ACT resistance in 2008 and 2009 suggested a delayed clearance phenotype (DCP), in which parasites persisted in the body for 1-2 additional days. However, all of these patients were still cured by the standard treatment[70-71, 79]. Commonly used ACTs include artemether (ATM) + lumefantrine (LUM) or dihydroartemisinin (DHA) + piperaquine (PPQ). Recently, there have been reports of complete treatment failure, suggesting that parasites have developed resistance to both of the drugs used in combination[53, 66]. It has been shown that mutations in the kelch propeller domains of a protein on chromosome 13 (K13) is associate with clinically observed phenotypes of artemisinin (ART) resistance[56, 87].

Work summarized in Chapter 5 focused on identifying novel endoperoxide containing compounds to target ART resistance and work summarized in Chapter 6 focused on identifying PI3K inhibitors that could be used as partner drugs to overcome complete ACT treatment failure. Chapter 5 identifies an ozonide compound, OZ439, as equally potent against both K13 wild-type and K13-mutant laboratory-adapted Cambodian isolates (parasites which come from a region riddled with multiple drug resistance). OZ439 was optimized from dozens of other ozonide compounds as having excellent antimalarial potency, low toxicity, high lipophilicity and increased bioavailability. Thus, this serves as a promising lead compound to battle rising ACT resistance. Although OZ439 is currently marketed in India by Ranbaxy Pty Ltd[244, 260-261], it has still not completed Phase III clinical trials and more work needs to be done to validate this compound as safe and effective for use as a standard antimalarial therapy.

Discovering the dysregulation of the autophagy pathway in CQR parasites[17] and recent studies identifying the involvement of components of the autophagy pathway in ART resistance[53-

[54] led me to investigate the autophagy pathway in ART resistant parasite strains. These reports find the association of a T38N mutation in Atg18 is with ART resistance and the association of increased enzymatic activity of Vps34 (leading to increased production of its product, phosphatidylinositol 3-phosphate) with ART resistance. Results from my work suggest a muted autophagy phenotype in K13-mutant parasites, which is distinct from the CQR phenotype. It should be noted that, to date, all observed cases of ART or ACT resistance have evolved on a CQR background (or in regions of the globe where CQR is already present and thus alternative therapies had to be introduced). Thus, it could be assumed, according to results in Chapter 3, that the autophagy response to CQ would be muted. However, surprisingly, all tested strains with a Cambodian genetic background show a relatively muted autophagy response to nutrient starvation, as well as to stress caused by DHA, in comparison to the canonical HB3 and Dd2 strains. Parasite strains harboring wild-type K13 do show a redistribution of autophagosomal puncta in response to starvation and DHA treatment, although to a relatively smaller extent. Most significantly, K13-mutant strains (or parasites with a Cambodian background that have been genetically modified to possess K13 mutations) show no significant re-distribution of autophagosomal puncta under both nutrient starvation or LD_{50} dose of DHA. These results suggest further modification of the autophagy pathway in K13-mutant strains compared to CQR parasite strains.

Work needs to be done to elucidate the extent of the modification of the autophagy pathway in K13-mutant strains in order to better understand its role in ACT resistance and to inform the development of novel antimalarial therapies. With the advent of CRISPR[266-268], which makes genetic modifications of *P. falciparum* parasites significantly more efficient and easily accessible than before, it is conceivable that significant progress could be made in this domain. Since all

observed cases of ACT resistance have been developed on a CQR background, it would be useful to genetically modify various CQS strains to possess K13 mutations and investigate the autophagy response in these parasite lines. Since these parasite strains would be CQS, it would be expected that the autophagy response to nutrient starvation or an LD_{50} dose of DHA would be in between that of HB3 and CamWT (a K13 wild-type strain with a Cambodian genetic background and is CQR). This information would be invaluable in determining the extent of the Cambodian genetic background influencing the autophagy response in ART resistant parasites. Additionally, it would be interesting to revert the T38N mutation to the wild-type sequence in Atg18, which is a phosphatidylinositol 3-phosphate (PI3P) binding protein, and determine if any changes are observed in ART susceptibility as well as the autophagy response.

The autophagy-related puncta response was not only reduced in the Cambodian parasite lines when treated with LD_{50} DHA, but this response was also reduced under nutrient starvation conditions. This has not been observed before in comparing CQS versus CQR malaria and thus it is unclear why these particular parasite strains do not respond to nutrient starvation in the same way or to the same extent as other parasite strains. Further, K13-mutant strains do not show an autophagy-related puncta redistribution at all under nutrient starvation conditions. Further work must be done to understand this observation. It is possible that this observation arises from the ability of these parasites to enter a quiescent state, as previously observed in correlation with ART resistance[70]. Or it is also possible that these parasites have an altered, more efficient/resistant autophagy process that needs extensive stress to trigger a re-distributed puncta response and thus not visible in a 6 hour experiment. An experiment could be designed to test the time-dependence of the autophagy response (similar to that in Gaviria *et al.*[17]), including additional, longer time

points. These results could inform whether a 6 hour pulse is sufficient to induce autophagy at all in these parasite strains or if a longer duration of the incubation in nutrient deprived conditions in necessary. One obstacle to this investigation would be the transition of parasites to later stages of the life cycle. This would alter the Atg8 response as seen in the observations of chapter 3. Thus, incubations could be started at the rings stage and carried out to the trophozoite stage where the autophagy response is quantified. Another approach would be to measure the resistance of parasites to nutrient starvation in a plate format as done for LD_{50} assays. Cells could be incubated for varying time periods in starvation media and survival could be measured as in LD50 determination using SYBR Green 1 after letting them out-grow in control media for an additional amount of time.

Chapter 6 also identifies several drug combinations which are synergistic against both K13 wild-type and K13 mutant strains of *P. falciparum.* Only a few tested combinations were found to be antagonistic, with the majority of combinations being additive or synergistic. Most interestingly, a greater level of synergy was observed in some OZ439+PI3K inhibitor combinations in comparison with standard ATM+LUM or DHA+PPQ combinations as well as ATM or DHA +PI3K inhibitor combinations. These results show that by simultaneously inducing and inhibiting the autophagy pathway, it is possible to devise an antimalarial combination therapy that is extremely potent and could provide a unique way of combating ACT resistance. Most of the currently available therapies were discovered empirically, without validation of MOA of the drug pairs. Thus, further work needs to be done in this field to identify compounds with differing MOA that either target unique processes in *P. falciparum* parasites or that target the same pathway in multiple locations. The combination found in Chapter 6 of OZ439+Torin 2 could be a start in

the right direction towards this goal. Endoperoxide compounds, such as OZ439, are thought to cause oxidative damage to parasites and are activated by iron released from hemoglobin digestion in the parasite DV. These compounds cause stress to the parasite and thus induce the autophagy response. Torin 2 is a PI3K inhibitor that is extremely potent against malaria parasites. By using these two compounds in combination, the autophagy process is simultaneously induced and inhibited, which could provide a novel method of killing malaria parasites and significantly reducing the risk of the development of resistance.

As shown by Straimer *et al.*, K13 mutations are necessary but not sufficient to describe the ART resistance phenotype[87]. Several genome-wide analyses have been conducted to compare ART sensitive versus resistant strains and to determine which genetic factors associate with ART resistance[53, 56, 66, 78-82]. This information can be utilized to inform further experiments to systematically perform genetic modifications to Cambodian parasite strains in an effort to identify other genetic loci associated with ART resistance. This is an area which has not been studied extensively and most researchers are basing experimentation on K13 mutations, which does not provide a complete picture of ART resistance. It is imperative that further studies be done to fully understand the mechanism and genetic basis of ART resistance in order to be able to properly devise treatments to overcome this basis of resistance.

APPENDIX C RIGHTS AND PERMISSIONS

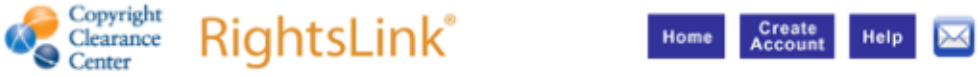

Title: Spinning Disk Confocal Microscopy of Live, Intraerythrocytic Malarial Parasites. 1. Quantification of Hemozoin Development for Drug Sensitive versus Resistant Malaria

Author: Bojana Gligorijevic, Ryan McAllister, Jeffrey S. Urbach, et al

Publication: Biochemistry

Publisher: American Chemical Society

Date: Oct 1, 2006

LOGIN

If you're a copyright.com user, you can login to RightsLink using your copyright.com credentials. Already a RightsLink user or want to learn more?

PERMISSION/LICENSE IS GRANTED FOR YOUR ORDER AT NO CHARGE

This type of permission/license, instead of the standard Terms & Conditions, is sent to you because no fee is being charged for your order. Please note the following:

- Permission is granted for your request in both print and electronic formats, and translations.
- If figures and/or tables were requested, they may be adapted or used in part.
- Please print this page for your records and send a copy of it to your publisher/graduate school.
- Appropriate credit for the requested material should be given as follows: "Reprinted (adapted) with permission from (COMPLETE REFERENCE CITATION). Copyright (YEAR) American Chemical Society." Insert appropriate information in place of the capitalized words.
- One-time permission is granted only for the use specified in your request. No additional uses are granted (such as derivative works or other editions). For any other uses, please submit a new request.

If credit is given to another source for the material you requested, permission must be obtained from that source.

BACK CLOSE WINDOW

Creative Commons Attribution License (CC BY)

AMERICAN SOCIETY FOR MICROBIOLOGY

Title: Increased Tolerance to Artemisinin in Plasmodium falciparum Is Mediated by a Quiescence Mechanism

Author: Benoit Witkowski, Joel Lelièvre, María José López Barragán et al.

Publication: Antimicrobial Agents and Chemotherapy

Publisher: American Society for Microbiology

Date: May 1, 2010

Permissions Request

ASM authorizes an advanced degree candidate to republish the requested material in his/her doctoral thesis or dissertation. If your thesis, or dissertation, is to be published commercially, then you must reapply for permission.

BACK CLOSE WINDOW

Title: K13-propeller mutations confer artemisinin resistance in *Plasmodium falciparum* clinical isolates

Author: Judith Straimer,Nina F. Gnädig,Benoit Witkowski,Chanaki Amaratunga,Valentine Duru,Arba Pramundita Ramadani,Mélanie Dacheux,Nimol Khim,Lei Zhang,Stephen Lam,Philip D. Gregory,Fyodor D. Urnov,Odile Mercereau-Puijalon,Françoise Benoit-Vical,Rick M. Fairhurst,Didier Ménard,David A. Fidock

Publication: Science

Publisher: The American Association for the Advancement of Science

Date: Jan 23, 2015

Order Completed

Thank you for your order.

This Agreement between Amila Siriwardana ("You") and The American Association for the Advancement of Science ("The American Association for the Advancement of Science") consists of your license details and the terms and conditions provided by The American Association for the Advancement of Science and Copyright Clearance Center.

Your confirmation email will contain your order number for future reference.

Printable details.

License Number	4081951176310
License date	Apr 04, 2017
Licensed Content Publisher	The American Association for the Advancement of Science
Licensed Content Publication	Science
Licensed Content Title	K13-propeller mutations confer artemisinin resistance in *Plasmodium falciparum* clinical isolates
Licensed Content Author	Judith Straimer,Nina F. Gnädig,Benoit Witkowski,Chanaki Amaratunga,Valentine Duru,Arba Pramundita Ramadani,Mélanie Dacheux,Nimol Khim,Lei Zhang,Stephen Lam,Philip D. Gregory,Fyodor D. Urnov,Odile Mercereau-Puijalon,Françoise Benoit-Vical,Rick M. Fairhurst,Didier Ménard,David A. Fidock
Licensed Content Date	Jan 23, 2015
Licensed Content Volume	347
Licensed Content Issue	6220
Volume number	347
Issue number	6220
Type of Use	Thesis / Dissertation
Requestor type	Scientist/individual at a research institution
Format	Print and electronic
Portion	Figure
Number of figures/tables	1
Order reference number	
Title of your thesis / dissertation	Physiology directed drug discovery in multidrug resistant plasmodium falciparum

Title:	Flow Cytometry-Based Analysis of Artemisinin-Resistant Plasmodium falciparum in the Ring-Stage Survival Assay
Author:	Chanaki Amaratunga, Aaron T. Neal, Rick M. Fairhurst et al.
Publication:	Antimicrobial Agents and Chemotherapy
Publisher:	American Society for Microbiology
Date:	Aug 1, 2014

Permissions Request

ASM authorizes an advanced degree candidate to republish the requested material in his/her doctoral thesis or dissertation. If your thesis, or dissertation, is to be published commercially, then you must reapply for permission.

BACK CLOSE WINDOW

BIBLIOGRAPHY

1. World Malaria Report 2016. *World Health Organization, Geneva, Switzerland.* (http://www.who.int/malaria/publications/atoz/9789241564106/en/).

2. Gething, P. W.; Patil, A. P.; Hay, S. I., Quantifying aggregated uncertainty in Plasmodium falciparum malaria prevalence and populations at risk via efficient space-time geostatistical joint simulation. *PLoS computational biology* **2010,** *6* (4), e1000724.

3. Roepe, P. D., Molecular and physiologic basis of quinoline drug resistance in Plasmodium falciparum malaria. *Future microbiology* **2009,** *4* (4), 441-55.

4. Ta, T. H.; Hisam, S.; Lanza, M.; Jiram, A. I.; Ismail, N.; Rubio, J. M., First case of a naturally acquired human infection with Plasmodium cynomolgi. *Malaria journal* **2014,** *13*, 68.

5. Centers for Disease Control and Prevention. Malaria Biology. Centers for Disease Control and Prevention, Atlanta, GA. (http://www.cdc.gov/malaria/about/biology/.), Updated 8 February 2010.

6. Gligorijevic, B.; McAllister, R.; Urbach, J. S.; Roepe, P. D., Spinning disk confocal microscopy of live, intraerythrocytic malarial parasites. 1. Quantification of hemozoin development for drug sensitive versus resistant malaria. *Biochemistry* **2006,** *45* (41), 12400-10.

7. Sherman, I. W., Transport of amino acids and nucleic acid precursors in malarial parasites. *Bulletin of the World Health Organization* **1977,** *55* (2-3), 211-25.

8. Babbitt, S. E.; Altenhofen, L.; Cobbold, S. A.; Istvan, E. S.; Fennell, C.; Doerig, C.; Llinas, M.; Goldberg, D. E., Plasmodium falciparum responds to amino acid starvation by entering into a hibernatory state. *Proceedings of the National Academy of Sciences of the United States of America* **2012,** *109* (47), E3278-87.

9. Bennett, T. N.; Paguio, M.; Gligorijevic, B.; Seudieu, C.; Kosar, A. D.; Davidson, E.; Roepe, P. D., Novel, rapid, and inexpensive cell-based quantification of antimalarial drug efficacy. *Antimicrobial agents and chemotherapy* **2004,** *48* (5), 1807-10.

10. Fidock, D. A.; Nomura, T.; Talley, A. K.; Cooper, R. A.; Dzekunov, S. M.; Ferdig, M. T.; Ursos, L. M.; Sidhu, A. B.; Naude, B.; Deitsch, K. W.; Su, X. Z.; Wootton, J. C.; Roepe, P. D.; Wellems, T. E., Mutations in the P. falciparum digestive vacuole transmembrane protein PfCRT and evidence for their role in chloroquine resistance. *Molecular cell* **2000,** *6* (4), 861-71.

11. Patel, J. J.; Thacker, D.; Tan, J. C.; Pleeter, P.; Checkley, L.; Gonzales, J. M.; Deng, B.; Roepe, P. D.; Cooper, R. A.; Ferdig, M. T., Chloroquine susceptibility and reversibility in a Plasmodium falciparum genetic cross. *Molecular microbiology* **2010,** *78* (3), 770-87.

12. Gabryszewski, S. J.; Modchang, C.; Musset, L.; Chookajorn, T.; Fidock, D. A., Combinatorial Genetic Modeling of pfcrt-Mediated Drug Resistance Evolution in Plasmodium falciparum. *Molecular biology and evolution* **2016,** *33* (6), 1554-70.

13. Callaghan, P. S.; Hassett, M. R.; Roepe, P. D., Functional Comparison of 45 Naturally Occurring Isoforms of the Plasmodium falciparum Chloroquine Resistance Transporter (PfCRT). *Biochemistry* **2015,** *54* (32), 5083-94.

14. Sedlak, D.; Paguio, A.; Bartunek, P., Two panels of steroid receptor luciferase reporter cell lines for compound profiling. *Combinatorial chemistry & high throughput screening* **2011,** *14* (4), 248-66.

15. Cabrera, M.; Paguio, M. F.; Xie, C.; Roepe, P. D., Reduced digestive vacuolar accumulation of chloroquine is not linked to resistance to chloroquine toxicity. *Biochemistry* **2009,** *48* (47), 11152-4.

16. Sinai, A. P.; Roepe, P. D., Autophagy in Apicomplexa: a life sustaining death mechanism? *Trends in parasitology* **2012,** *28* (9), 358-64.

17. Gaviria, D.; Paguio, M. F.; Turnbull, L. B.; Tan, A.; Siriwardana, A.; Ghosh, D.; Ferdig, M. T.; Sinai, A. P.; Roepe, P. D., A process similar to autophagy is associated with cytocidal chloroquine resistance in Plasmodium falciparum. *PloS one* **2013,** *8* (11), e79059.

18. Reilly Ayala, H. B.; Wacker, M. A.; Siwo, G.; Ferdig, M. T., Quantitative trait loci mapping reveals candidate pathways regulating cell cycle duration in Plasmodium falciparum. *BMC genomics* **2010,** *11*, 577.

19. Tooze, S. A.; Yoshimori, T., The origin of the autophagosomal membrane. *Nature cell biology* **2010,** *12* (9), 831-5.

20. Mizushima, N.; Yoshimori, T.; Ohsumi, Y., The role of Atg proteins in autophagosome formation. *Annual review of cell and developmental biology* **2011,** *27*, 107-32.

21. Nakatogawa, H.; Suzuki, K.; Kamada, Y.; Ohsumi, Y., Dynamics and diversity in autophagy mechanisms: lessons from yeast. *Nature reviews. Molecular cell biology* **2009,** *10* (7), 458-67.

22. Suzuki, K.; Kubota, Y.; Sekito, T.; Ohsumi, Y., Hierarchy of Atg proteins in pre-autophagosomal structure organization. *Genes to cells : devoted to molecular & cellular mechanisms* **2007,** *12* (2), 209-18.

23. Meijer, W. H.; van der Klei, I. J.; Veenhuis, M.; Kiel, J. A., ATG genes involved in non-selective autophagy are conserved from yeast to man, but the selective Cvt and pexophagy pathways also require organism-specific genes. *Autophagy* **2007,** *3* (2), 106-16.

24. Hain, A. U.; Bosch, J., Autophagy in Plasmodium, a multifunctional pathway? *Computational and structural biotechnology journal* **2013,** *8*, e201308002.

25. Duszenko, M.; Ginger, M. L.; Brennand, A.; Gualdron-Lopez, M.; Colombo, M. I.; Coombs, G. H.; Coppens, I.; Jayabalasingham, B.; Langsley, G.; de Castro, S. L.; Menna-Barreto, R.; Mottram, J. C.; Navarro, M.; Rigden, D. J.; Romano, P. S.; Stoka, V.; Turk, B.; Michels, P. A., Autophagy in protists. *Autophagy* **2011,** *7* (2), 127-58.

26. Mizushima, N.; Sahani, M. H., ATG8 localization in apicomplexan parasites: apicoplast and more? *Autophagy* **2014,** *10* (9), 1487-94.

27. Kitamura, K.; Kishi-Itakura, C.; Tsuboi, T.; Sato, S.; Kita, K.; Ohta, N.; Mizushima, N., Autophagy-related Atg8 localizes to the apicoplast of the human malaria parasite Plasmodium falciparum. *PloS one* **2012,** *7* (8), e42977.

28. Cervantes, S.; Bunnik, E. M.; Saraf, A.; Conner, C. M.; Escalante, A.; Sardiu, M. E.; Ponts, N.; Prudhomme, J.; Florens, L.; Le Roch, K. G., The multifunctional autophagy pathway in the human malaria parasite, Plasmodium falciparum. *Autophagy* **2014,** *10* (1), 80-92.

29. Besteiro, S.; Brooks, C. F.; Striepen, B.; Dubremetz, J. F., Autophagy protein Atg3 is essential for maintaining mitochondrial integrity and for normal intracellular development of Toxoplasma gondii tachyzoites. *PLoS pathogens* **2011,** *7* (12), e1002416.

30. Wang, T.; Ming, Z.; Xiaochun, W.; Hong, W., Rab7: role of its protein interaction cascades in endo-lysosomal traffic. *Cellular signalling* **2011,** *23* (3), 516-21.

31. Gutierrez, M. G.; Munafo, D. B.; Beron, W.; Colombo, M. I., Rab7 is required for the normal progression of the autophagic pathway in mammalian cells. *Journal of cell science* **2004,** *117* (Pt 13), 2687-97.

32. Jager, S.; Bucci, C.; Tanida, I.; Ueno, T.; Kominami, E.; Saftig, P.; Eskelinen, E. L., Role for Rab7 in maturation of late autophagic vacuoles. *Journal of cell science* **2004,** *117* (Pt 20), 4837-48.

33. Langsley, G.; van Noort, V.; Carret, C.; Meissner, M.; de Villiers, E. P.; Bishop, R.; Pain, A., Comparative genomics of the Rab protein family in Apicomplexan parasites. *Microbes and infection* **2008,** *10* (5), 462-70.

34. Quevillon, E.; Spielmann, T.; Brahimi, K.; Chattopadhyay, D.; Yeramian, E.; Langsley, G., The Plasmodium falciparum family of Rab GTPases. *Gene* **2003,** *306*, 13-25.

35. Tomlins, A. M.; Ben-Rached, F.; Williams, R. A.; Proto, W. R.; Coppens, I.; Ruch, U.; Gilberger, T. W.; Coombs, G. H.; Mottram, J. C.; Muller, S.; Langsley, G., Plasmodium falciparum ATG8 implicated in both autophagy and apicoplast formation. *Autophagy* **2013,** *9* (10), 1540-52.

36. Brennand, A.; Gualdron-Lopez, M.; Coppens, I.; Rigden, D. J.; Ginger, M. L.; Michels, P. A., Autophagy in parasitic protists: unique features and drug targets. *Molecular and biochemical parasitology* **2011,** *177* (2), 83-99.

37. Dittmar, A. J.; Drozda, A. A.; Blader, I. J., Drug Repurposing Screening Identifies Novel Compounds That Effectively Inhibit Toxoplasma gondii Growth. *mSphere* **2016,** *1* (2).

38. Ghosh, D.; Walton, J. L.; Roepe, P. D.; Sinai, A. P., Autophagy is a cell death mechanism in Toxoplasma gondii. *Cellular microbiology* **2012,** *14* (4), 589-607.

39. Lavine, M. D.; Arrizabalaga, G., Analysis of monensin sensitivity in Toxoplasma gondii reveals autophagy as a mechanism for drug induced death. *PloS one* **2012,** *7* (7), e42107.

40. Kirisako, T.; Ichimura, Y.; Okada, H.; Kabeya, Y.; Mizushima, N.; Yoshimori, T.; Ohsumi, M.; Takao, T.; Noda, T.; Ohsumi, Y., The reversible modification regulates the membrane-binding state of Apg8/Aut7 essential for autophagy and the cytoplasm to vacuole targeting pathway. *The Journal of cell biology* **2000,** *151* (2), 263-76.

41. Kim, K.; Weiss, L. M., Toxoplasma gondii: the model apicomplexan. *International journal for parasitology* **2004,** *34* (3), 423-32.

42. Yu, Z. Q.; Ni, T.; Hong, B.; Wang, H. Y.; Jiang, F. J.; Zou, S.; Chen, Y.; Zheng, X. L.; Klionsky, D. J.; Liang, Y.; Xie, Z., Dual roles of Atg8-PE deconjugation by Atg4 in autophagy. *Autophagy* **2012,** *8* (6), 883-92.

43. Hain, A. U.; Weltzer, R. R.; Hammond, H.; Jayabalasingham, B.; Dinglasan, R. R.; Graham, D. R.; Colquhoun, D. R.; Coppens, I.; Bosch, J., Structural characterization and inhibition of the Plasmodium Atg8-Atg3 interaction. *Journal of structural biology* **2012,** *180* (3), 551-62.

44. Hanaoka, H.; Noda, T.; Shirano, Y.; Kato, T.; Hayashi, H.; Shibata, D.; Tabata, S.; Ohsumi, Y., Leaf senescence and starvation-induced chlorosis are accelerated by the disruption of an Arabidopsis autophagy gene. *Plant physiology* **2002,** *129* (3), 1181-93.

45. Chen, P. M.; Gombart, Z. J.; Chen, J. W., Chloroquine treatment of ARPE-19 cells leads to lysosome dilation and intracellular lipid accumulation: possible implications of lysosomal dysfunction in macular degeneration. *Cell & bioscience* **2011,** *1* (1), 10.

46. Mizushima, N.; Yoshimori, T.; Levine, B., Methods in mammalian autophagy research. *Cell* **2010,** *140* (3), 313-26.

47. Ronning, O. W.; Pettersen, E. O.; Seglen, P. O., Protein synthesis and protein degradation through the cell cycle of human NHIK 3025 cells in vitro. *Experimental cell research* **1979,** *123* (1), 63-72.

48. Lavine, M. D.; Arrizabalaga, G., The antibiotic monensin causes cell cycle disruption of Toxoplasma gondii mediated through the DNA repair enzyme TgMSH-1. *Antimicrobial agents and chemotherapy* **2011,** *55* (2), 745-55.

49. Mott, B. T.; Eastman, R. T.; Guha, R.; Sherlach, K. S.; Siriwardana, A.; Shinn, P.; McKnight, C.; Michael, S.; Lacerda-Queiroz, N.; Patel, P. R.; Khine, P.; Sun, H.; Kasbekar, M.; Aghdam, N.; Fontaine, S. D.; Liu, D.; Mierzwa, T.; Mathews-Griner, L. A.; Ferrer, M.; Renslo, A. R.; Inglese, J.; Yuan, J.; Roepe, P. D.; Su, X. Z.; Thomas, C. J., High-throughput matrix screening identifies synergistic and antagonistic antimalarial drug combinations. *Scientific reports* **2015,** *5*, 13891.

50. Klonis, N.; Xie, S. C.; McCaw, J. M.; Crespo-Ortiz, M. P.; Zaloumis, S. G.; Simpson, J. A.; Tilley, L., Altered temporal response of malaria parasites determines differential sensitivity to artemisinin. *Proceedings of the National Academy of Sciences of the United States of America* **2013,** *110* (13), 5157-62.

51. Klonis, N.; Crespo-Ortiz, M. P.; Bottova, I.; Abu-Bakar, N.; Kenny, S.; Rosenthal, P. J.; Tilley, L., Artemisinin activity against Plasmodium falciparum requires hemoglobin uptake and digestion. *Proceedings of the National Academy of Sciences of the United States of America* **2011,** *108* (28), 11405-10.

52. Choi, K. S., Autophagy and cancer. *Experimental & molecular medicine* **2012,** *44* (2), 109-20.

53. Wang, Z.; Cabrera, M.; Yang, J.; Yuan, L.; Gupta, B.; Liang, X.; Kemirembe, K.; Shrestha, S.; Brashear, A.; Li, X.; Porcella, S. F.; Miao, J.; Yang, Z.; Su, X. Z.; Cui, L., Genome-wide association analysis identifies genetic loci associated with resistance to multiple antimalarials in Plasmodium falciparum from China-Myanmar border. *Scientific reports* **2016,** *6*, 33891.

54. Mbengue, A.; Bhattacharjee, S.; Pandharkar, T.; Liu, H.; Estiu, G.; Stahelin, R. V.; Rizk, S. S.; Njimoh, D. L.; Ryan, Y.; Chotivanich, K.; Nguon, C.; Ghorbal, M.; Lopez-Rubio, J. J.; Pfrender, M.; Emrich, S.; Mohandas, N.; Dondorp, A. M.; Wiest, O.; Haldar, K., A molecular mechanism of artemisinin resistance in Plasmodium falciparum malaria. *Nature* **2015,** *520* (7549), 683-7.

55. Wang, J.; Zhang, C. J.; Chia, W. N.; Loh, C. C.; Li, Z.; Lee, Y. M.; He, Y.; Yuan, L. X.; Lim, T. K.; Liu, M.; Liew, C. X.; Lee, Y. Q.; Zhang, J.; Lu, N.; Lim, C. T.; Hua, Z. C.; Liu, B.; Shen, H. M.; Tan, K. S.; Lin, Q., Haem-activated promiscuous targeting of artemisinin in Plasmodium falciparum. *Nature communications* **2015,** *6*, 10111.

56. Ariey, F.; Witkowski, B.; Amaratunga, C.; Beghain, J.; Langlois, A. C.; Khim, N.; Kim, S.; Duru, V.; Bouchier, C.; Ma, L.; Lim, P.; Leang, R.; Duong, S.; Sreng, S.; Suon, S.; Chuor, C. M.; Bout, D. M.; Menard, S.; Rogers, W. O.; Genton, B.; Fandeur, T.; Miotto, O.; Ringwald, P.; Le Bras, J.; Berry, A.; Barale, J. C.; Fairhurst, R. M.; Benoit-Vical, F.; Mercereau-Puijalon, O.; Menard, D., A molecular marker of artemisinin-resistant Plasmodium falciparum malaria. *Nature* **2014,** *505* (7481), 50-5.

57. Witkowski, B.; Amaratunga, C.; Khim, N.; Sreng, S.; Chim, P.; Kim, S.; Lim, P.; Mao, S.; Sopha, C.; Sam, B.; Anderson, J. M.; Duong, S.; Chuor, C. M.; Taylor, W. R.; Suon, S.; Mercereau-Puijalon, O.; Fairhurst, R. M.; Menard, D., Novel phenotypic assays for the detection of artemisinin-resistant Plasmodium falciparum malaria in Cambodia: in-vitro and ex-vivo drug-response studies. *The Lancet. Infectious diseases* **2013,** *13* (12), 1043-9.

58. Ashley, E. A.; Dhorda, M.; Fairhurst, R. M.; Amaratunga, C.; Lim, P.; Suon, S.; Sreng, S.; Anderson, J. M.; Mao, S.; Sam, B.; Sopha, C.; Chuor, C. M.; Nguon, C.; Sovannaroth, S.; Pukrittayakamee, S.; Jittamala, P.; Chotivanich, K.; Chutasmit, K.; Suchatsoonthorn, C.; Runcharoen, R.; Hien, T. T.; Thuy-Nhien, N. T.; Thanh, N. V.; Phu, N. H.; Htut, Y.; Han, K. T.; Aye, K. H.; Mokuolu, O. A.; Olaosebikan, R. R.; Folaranmi, O. O.; Mayxay, M.; Khanthavong, M.; Hongvanthong, B.; Newton, P. N.; Onyamboko, M. A.; Fanello, C. I.; Tshefu, A. K.; Mishra, N.; Valecha, N.; Phyo, A. P.; Nosten, F.; Yi, P.; Tripura, R.; Borrmann, S.; Bashraheil, M.; Peshu, J.; Faiz, M. A.; Ghose, A.; Hossain, M. A.; Samad, R.; Rahman, M. R.; Hasan, M. M.; Islam, A.; Miotto, O.; Amato, R.; MacInnis, B.; Stalker, J.; Kwiatkowski, D. P.; Bozdech, Z.; Jeeyapant, A.; Cheah, P. Y.; Sakulthaew, T.; Chalk, J.; Intharabut, B.; Silamut, K.; Lee, S. J.; Vihokhern, B.; Kunasol, C.; Imwong, M.; Tarning, J.; Taylor, W. J.; Yeung, S.; Woodrow, C. J.; Flegg, J. A.; Das, D.; Smith, J.; Venkatesan, M.; Plowe, C. V.; Stepniewska, K.; Guerin, P. J.; Dondorp, A. M.; Day, N. P.; White, N. J.; Tracking Resistance to Artemisinin, C., Spread of artemisinin resistance in Plasmodium falciparum malaria. *The New England journal of medicine* **2014,** *371* (5), 411-23.

59. Dondorp, A. M.; Ringwald, P., Artemisinin resistance is a clear and present danger. *Trends in parasitology* **2013,** *29* (8), 359-60.

60. Siriwardana, A.; Iyengar, K.; Roepe, P. D., Endoperoxide Drug Cross Resistance Patterns for Plasmodium falciparum Exhibiting an Artemisinin Delayed Clearance Phenotype. *Antimicrobial agents and chemotherapy* **2016**.

61. Amaratunga, C.; Sreng, S.; Suon, S.; Phelps, E. S.; Stepniewska, K.; Lim, P.; Zhou, C.; Mao, S.; Anderson, J. M.; Lindegardh, N.; Jiang, H.; Song, J.; Su, X. Z.; White, N. J.; Dondorp, A. M.; Anderson, T. J.; Fay, M. P.; Mu, J.; Duong, S.; Fairhurst, R. M., Artemisinin-resistant Plasmodium falciparum in Pursat province, western Cambodia: a parasite clearance rate study. *The Lancet. Infectious diseases* **2012,** *12* (11), 851-8.

62. Dondorp, A. M.; Nosten, F.; Yi, P.; Das, D.; Phyo, A. P.; Tarning, J.; Lwin, K. M.; Ariey, F.; Hanpithakpong, W.; Lee, S. J.; Ringwald, P.; Silamut, K.; Imwong, M.; Chotivanich, K.; Lim, P.; Herdman, T.; An, S. S.; Yeung, S.; Singhasivanon, P.; Day, N. P.; Lindegardh, N.; Socheat, D.; White, N. J., Artemisinin resistance in Plasmodium falciparum malaria. *The New England journal of medicine* **2009,** *361* (5), 455-67.

63. Noedl, H.; Se, Y.; Schaecher, K.; Smith, B. L.; Socheat, D.; Fukuda, M. M.; Artemisinin Resistance in Cambodia 1 Study, C., Evidence of artemisinin-resistant malaria in western Cambodia. *The New England journal of medicine* **2008,** *359* (24), 2619-20.

64. Enserink, M., Malaria's drug miracle in danger. *Science* **2010,** *328* (5980), 844-6.

65. Witkowski, B.; Duru, V.; Khim, N.; Ross, L. S.; Saintpierre, B.; Beghain, J.; Chy, S.; Kim, S.; Ke, S.; Kloeung, N.; Eam, R.; Khean, C.; Ken, M.; Loch, K.; Bouillon, A.; Domergue, A.; Ma, L.; Bouchier, C.; Leang, R.; Huy, R.; Nuel, G.; Barale, J. C.; Legrand, E.; Ringwald, P.; Fidock, D. A.; Mercereau-Puijalon, O.; Ariey, F.; Menard, D., A surrogate marker of piperaquine-resistant Plasmodium falciparum malaria: a phenotype-genotype association study. *The Lancet. Infectious diseases* **2017,** *17* (2), 174-183.

66. Amato, R.; Lim, P.; Miotto, O.; Amaratunga, C.; Dek, D.; Pearson, R. D.; Almagro-Garcia, J.; Neal, A. T.; Sreng, S.; Suon, S.; Drury, E.; Jyothi, D.; Stalker, J.; Kwiatkowski, D. P.; Fairhurst, R. M., Genetic markers associated with dihydroartemisinin-piperaquine failure in Plasmodium falciparum malaria in Cambodia: a genotype-phenotype association study. *The Lancet. Infectious diseases* **2017,** *17* (2), 164-173.

67. Amaratunga, C.; Lim, P.; Suon, S.; Sreng, S.; Mao, S.; Sopha, C.; Sam, B.; Dek, D.; Try, V.; Amato, R.; Blessborn, D.; Song, L.; Tullo, G. S.; Fay, M. P.; Anderson, J. M.; Tarning, J.; Fairhurst, R. M., Dihydroartemisinin-piperaquine resistance in Plasmodium falciparum malaria in Cambodia: a multisite prospective cohort study. *The Lancet. Infectious diseases* **2016,** *16* (3), 357-65.

68. Dogovski, C.; Xie, S. C.; Burgio, G.; Bridgford, J.; Mok, S.; McCaw, J. M.; Chotivanich, K.; Kenny, S.; Gnadig, N.; Straimer, J.; Bozdech, Z.; Fidock, D. A.; Simpson, J. A.; Dondorp, A. M.; Foote, S.; Klonis, N.; Tilley, L., Targeting the cell stress response of Plasmodium falciparum to overcome artemisinin resistance. *PLoS biology* **2015,** *13* (4), e1002132.

69. WHO, Emergency response to artemisinin resistance in the Greater Mekong subregion: regional framework for action, 2013-2015. *Geneva: World Health Organization.* **2013.**

70. Witkowski, B.; Lelievre, J.; Barragan, M. J.; Laurent, V.; Su, X. Z.; Berry, A.; Benoit-Vical, F., Increased tolerance to artemisinin in Plasmodium falciparum is mediated by a quiescence mechanism. *Antimicrobial agents and chemotherapy* **2010,** *54* (5), 1872-7.

71. Witkowski, B.; Khim, N.; Chim, P.; Kim, S.; Ke, S.; Kloeung, N.; Chy, S.; Duong, S.; Leang, R.; Ringwald, P.; Dondorp, A. M.; Tripura, R.; Benoit-Vical, F.; Berry, A.; Gorgette, O.; Ariey, F.; Barale, J. C.; Mercereau-Puijalon, O.; Menard, D., Reduced artemisinin susceptibility of Plasmodium falciparum ring stages in western Cambodia. *Antimicrobial agents and chemotherapy* **2013,** *57* (2), 914-23.

72. van Agtmael, M. A.; Cheng-Qi, S.; Qing, J. X.; Mull, R.; van Boxtel, C. J., Multiple dose pharmacokinetics of artemether in Chinese patients with uncomplicated falciparum malaria. *International journal of antimicrobial agents* **1999,** *12* (2), 151-8.

73. Halpaap, B.; Ndjave, M.; Paris, M.; Benakis, A.; Kremsner, P. G., Plasma levels of artesunate and dihydroartemisinin in children with Plasmodium falciparum malaria in Gabon after administration of 50-milligram artesunate suppositories. *The American journal of tropical medicine and hygiene* **1998,** *58* (3), 365-8.

74. Amaratunga, C.; Neal, A. T.; Fairhurst, R. M., Flow cytometry-based analysis of artemisinin-resistant Plasmodium falciparum in the ring-stage survival assay. *Antimicrobial agents and chemotherapy* **2014,** *58* (8), 4938-40.

75. Macho, A.; Decaudin, D.; Castedo, M.; Hirsch, T.; Susin, S. A.; Zamzami, N.; Kroemer, G., Chloromethyl-X-Rosamine is an aldehyde-fixable potential-sensitive fluorochrome for the detection of early apoptosis. *Cytometry* **1996,** *25* (4), 333-40.

76. Fry, M.; Beesley, J. E., Mitochondria of mammalian Plasmodium spp. *Parasitology* **1991,** *102 Pt 1*, 17-26.

77. Ginsburg, H.; Divo, A. A.; Geary, T. G.; Boland, M. T.; Jensen, J. B., Effects of mitochondrial inhibitors on intraerythrocytic Plasmodium falciparum in in vitro cultures. *The Journal of protozoology* **1986,** *33* (1), 121-5.

78. Cheeseman, I. H.; Miller, B. A.; Nair, S.; Nkhoma, S.; Tan, A.; Tan, J. C.; Al Saai, S.; Phyo, A. P.; Moo, C. L.; Lwin, K. M.; McGready, R.; Ashley, E.; Imwong, M.; Stepniewska, K.; Yi, P.; Dondorp, A. M.; Mayxay, M.; Newton, P. N.; White, N. J.; Nosten, F.; Ferdig, M. T.; Anderson, T. J., A major genome region underlying artemisinin resistance in malaria. *Science* **2012,** *336* (6077), 79-82.

79. Miotto, O.; Almagro-Garcia, J.; Manske, M.; Macinnis, B.; Campino, S.; Rockett, K. A.; Amaratunga, C.; Lim, P.; Suon, S.; Sreng, S.; Anderson, J. M.; Duong, S.; Nguon, C.; Chuor, C. M.; Saunders, D.; Se, Y.; Lon, C.; Fukuda, M. M.; Amenga-Etego, L.; Hodgson, A. V.; Asoala, V.; Imwong, M.; Takala-Harrison, S.; Nosten, F.; Su, X. Z.; Ringwald, P.; Ariey, F.; Dolecek, C.; Hien, T. T.; Boni, M. F.; Thai, C. Q.; Amambua-Ngwa, A.; Conway, D. J.; Djimde, A. A.; Doumbo, O. K.; Zongo, I.; Ouedraogo, J. B.; Alcock, D.; Drury, E.; Auburn, S.; Koch, O.; Sanders, M.; Hubbart, C.; Maslen, G.; Ruano-Rubio, V.; Jyothi, D.; Miles, A.; O'Brien, J.; Gamble, C.; Oyola, S. O.; Rayner, J. C.; Newbold, C. I.; Berriman, M.; Spencer, C. C.; McVean, G.; Day, N. P.; White, N. J.; Bethell, D.; Dondorp, A. M.; Plowe, C. V.; Fairhurst, R. M.; Kwiatkowski, D. P., Multiple populations of artemisinin-resistant Plasmodium falciparum in Cambodia. *Nature genetics* **2013,** *45* (6), 648-55.

80. Takala-Harrison, S.; Clark, T. G.; Jacob, C. G.; Cummings, M. P.; Miotto, O.; Dondorp, A. M.; Fukuda, M. M.; Nosten, F.; Noedl, H.; Imwong, M.; Bethell, D.; Se, Y.; Lon, C.; Tyner, S. D.; Saunders, D. L.; Socheat, D.; Ariey, F.; Phyo, A. P.; Starzengruber, P.; Fuehrer, H. P.; Swoboda, P.; Stepniewska, K.; Flegg, J.; Arze, C.; Cerqueira, G. C.; Silva, J. C.; Ricklefs, S. M.; Porcella, S. F.; Stephens, R. M.; Adams, M.; Kenefic, L. J.; Campino, S.; Auburn, S.; MacInnis, B.; Kwiatkowski, D. P.; Su, X. Z.; White, N. J.; Ringwald, P.; Plowe, C. V., Genetic loci associated with delayed clearance of Plasmodium falciparum following artemisinin treatment in Southeast Asia. *Proceedings of the National Academy of Sciences of the United States of America* **2013,** *110* (1), 240-5.

81. Miotto, O.; Amato, R.; Ashley, E. A.; MacInnis, B.; Almagro-Garcia, J.; Amaratunga, C.; Lim, P.; Mead, D.; Oyola, S. O.; Dhorda, M.; Imwong, M.; Woodrow, C.; Manske, M.; Stalker,

J.; Drury, E.; Campino, S.; Amenga-Etego, L.; Thanh, T. N.; Tran, H. T.; Ringwald, P.; Bethell, D.; Nosten, F.; Phyo, A. P.; Pukrittayakamee, S.; Chotivanich, K.; Chuor, C. M.; Nguon, C.; Suon, S.; Sreng, S.; Newton, P. N.; Mayxay, M.; Khanthavong, M.; Hongvanthong, B.; Htut, Y.; Han, K. T.; Kyaw, M. P.; Faiz, M. A.; Fanello, C. I.; Onyamboko, M.; Mokuolu, O. A.; Jacob, C. G.; Takala-Harrison, S.; Plowe, C. V.; Day, N. P.; Dondorp, A. M.; Spencer, C. C.; McVean, G.; Fairhurst, R. M.; White, N. J.; Kwiatkowski, D. P., Genetic architecture of artemisinin-resistant Plasmodium falciparum. *Nature genetics* **2015,** *47* (3), 226-34.

82. Mok, S.; Ashley, E. A.; Ferreira, P. E.; Zhu, L.; Lin, Z.; Yeo, T.; Chotivanich, K.; Imwong, M.; Pukrittayakamee, S.; Dhorda, M.; Nguon, C.; Lim, P.; Amaratunga, C.; Suon, S.; Hien, T. T.; Htut, Y.; Faiz, M. A.; Onyamboko, M. A.; Mayxay, M.; Newton, P. N.; Tripura, R.; Woodrow, C. J.; Miotto, O.; Kwiatkowski, D. P.; Nosten, F.; Day, N. P.; Preiser, P. R.; White, N. J.; Dondorp, A. M.; Fairhurst, R. M.; Bozdech, Z., Drug resistance. Population transcriptomics of human malaria parasites reveals the mechanism of artemisinin resistance. *Science* **2015,** *347* (6220), 431-5.

83. Hott, A.; Casandra, D.; Sparks, K. N.; Morton, L. C.; Castanares, G. G.; Rutter, A.; Kyle, D. E., Artemisinin-resistant Plasmodium falciparum parasites exhibit altered patterns of development in infected erythrocytes. *Antimicrobial agents and chemotherapy* **2015,** *59* (6), 3156-67.

84. Paloque, L.; Ramadani, A. P.; Mercereau-Puijalon, O.; Augereau, J. M.; Benoit-Vical, F., Plasmodium falciparum: multifaceted resistance to artemisinins. *Malaria journal* **2016,** *15*, 149.

85. Peatey, C. L.; Chavchich, M.; Chen, N.; Gresty, K. J.; Gray, K. A.; Gatton, M. L.; Waters, N. C.; Cheng, Q., Mitochondrial Membrane Potential in a Small Subset of Artemisinin-Induced Dormant Plasmodium falciparum Parasites In Vitro. *The Journal of infectious diseases* **2015,** *212* (3), 426-34.

86. Grobler, L.; Chavchich, M.; Haynes, R. K.; Edstein, M. D.; Grobler, A. F., Assessment of the induction of dormant ring stages in Plasmodium falciparum parasites by artemisone and artemisone entrapped in Pheroid vesicles in vitro. *Antimicrobial agents and chemotherapy* **2014,** *58* (12), 7579-82.

87. Straimer, J.; Gnadig, N. F.; Witkowski, B.; Amaratunga, C.; Duru, V.; Ramadani, A. P.; Dacheux, M.; Khim, N.; Zhang, L.; Lam, S.; Gregory, P. D.; Urnov, F. D.; Mercereau-Puijalon, O.; Benoit-Vical, F.; Fairhurst, R. M.; Menard, D.; Fidock, D. A., Drug resistance. K13-propeller mutations confer artemisinin resistance in Plasmodium falciparum clinical isolates. *Science* **2015,** *347* (6220), 428-31.

88. Hsu, E., The history of qing hao in the Chinese materia medica. *Transactions of the Royal Society of Tropical Medicine and Hygiene* **2006,** *100* (6), 505-8.

89. Wright, C. W.; Linley, P. A.; Brun, R.; Wittlin, S.; Hsu, E., Ancient Chinese methods are remarkably effective for the preparation of artemisinin-rich extracts of Qing Hao with potent antimalarial activity. *Molecules* **2010,** *15* (2), 804-12.

90. O'Neill, P. M.; Barton, V. E.; Ward, S. A., The molecular mechanism of action of artemisinin--the debate continues. *Molecules* **2010,** *15* (3), 1705-21.

91. Wang, X.; Dong, Y.; Wittlin, S.; Charman, S. A.; Chiu, F. C.; Chollet, J.; Katneni, K.; Mannila, J.; Morizzi, J.; Ryan, E.; Scheurer, C.; Steuten, J.; Santo Tomas, J.; Snyder, C.; Vennerstrom, J. L., Comparative antimalarial activities and ADME profiles of ozonides (1,2,4-trioxolanes) OZ277, OZ439, and their 1,2-dioxolane, 1,2,4-trioxane, and 1,2,4,5-tetraoxane isosteres. *Journal of medicinal chemistry* **2013,** *56* (6), 2547-55.

92. Kaiser, M.; Wittlin, S.; Nehrbass-Stuedli, A.; Dong, Y.; Wang, X.; Hemphill, A.; Matile, H.; Brun, R.; Vennerstrom, J. L., Peroxide bond-dependent antiplasmodial specificity of artemisinin and OZ277 (RBx11160). *Antimicrobial agents and chemotherapy* **2007,** *51* (8), 2991-3.

93. Alin, K., [Synergism and antagonism of antibiotics]. *Svenska lakartidningen* **1952,** *49* (21), 1379-86.

94. Haque, R.; Thriemer, K.; Wang, Z.; Sato, K.; Wagatsuma, Y.; Salam, M. A.; Akther, S.; Akter, J.; Fukuda, M.; Miller, R. S.; Noedl, H., Therapeutic efficacy of artemether-lumefantrine for the treatment of uncomplicated Plasmodium falciparum malaria in Bangladesh. *The American journal of tropical medicine and hygiene* **2007,** *76* (1), 39-41.

95. Wong, R. P.; Salman, S.; Ilett, K. F.; Siba, P. M.; Mueller, I.; Davis, T. M., Desbutyl-lumefantrine is a metabolite of lumefantrine with potent in vitro antimalarial activity that may influence artemether-lumefantrine treatment outcome. *Antimicrobial agents and chemotherapy* **2011,** *55* (3), 1194-8.

96. Chou, T. C.; Talalay, P., Quantitative analysis of dose-effect relationships: the combined effects of multiple drugs or enzyme inhibitors. *Advances in enzyme regulation* **1984,** *22*, 27-55.

97. Chou, T. C., Theoretical basis, experimental design, and computerized simulation of synergism and antagonism in drug combination studies. *Pharmacological reviews* **2006,** *58* (3), 621-81.

98. Bell, A., Antimalarial drug synergism and antagonism: mechanistic and clinical significance. *FEMS microbiology letters* **2005,** *253* (2), 171-84.

99. Matthews, H.; Usman-Idris, M.; Khan, F.; Read, M.; Nirmalan, N., Drug repositioning as a route to anti-malarial drug discovery: preliminary investigation of the in vitro anti-malarial efficacy of emetine dihydrochloride hydrate. *Malaria journal* **2013,** *12*, 359.

100. Suberu, J. O.; Gorka, A. P.; Jacobs, L.; Roepe, P. D.; Sullivan, N.; Barker, G. C.; Lapkin, A. A., Anti-plasmodial polyvalent interactions in Artemisia annua L. aqueous extract--possible synergistic and resistance mechanisms. *PloS one* **2013,** *8* (11), e80790.

101. Abiodun, O. O.; Brun, R.; Wittlin, S., In vitro interaction of artemisinin derivatives or the fully synthetic peroxidic anti-malarial OZ277 with thapsigargin in Plasmodium falciparum strains. *Malaria journal* **2013,** *12,* 43.

102. Bhattacharya, A.; Mishra, L. C.; Sharma, M.; Awasthi, S. K.; Bhasin, V. K., Antimalarial pharmacodynamics of chalcone derivatives in combination with artemisinin against Plasmodium falciparum in vitro. *European journal of medicinal chemistry* **2009,** *44* (9), 3388-93.

103. Gorka, A. P.; Jacobs, L. M.; Roepe, P. D., Cytostatic versus cytocidal profiling of quinoline drug combinations via modified fixed-ratio isobologram analysis. *Malaria journal* **2013,** *12,* 332.

104. Trager, W.; Jensen, J. B., Human Malaria Parasites in Continuous Culture. *Science* **1976,** *193* (4254), 673-675.

105. Olazabal Eizaguirre, N.; Chavez, R.; Gonzalez-Torres, M. A.; Gaviria, M., [Panic disorder and atrial fibrillation]. *Semergen* **2013,** *39* (7), 370-5.

106. Gligorijevic, B.; Bennett, T.; McAllister, R.; Urbach, J. S.; Roepe, P. D., Spinning disk confocal microscopy of live, intraerythrocytic malarial parasites. 2. Altered vacuolar volume regulation in drug resistant malaria. *Biochemistry* **2006,** *45* (41), 12411-23.

107. Inoue, S., Progress in video microscopy. *Cell motility and the cytoskeleton* **1988,** *10* (1-2), 13-7.

108. Biggs, D. S.; Andrews, M., Acceleration of iterative image restoration algorithms. *Applied optics* **1997,** *36* (8), 1766-75.

109. Wolf, D. E., Quantitative digital and video microscopy. *Methods in cell biology* **2003,** *72,* 319-36.

110. de Monvel, J. B.; Scarfone, E.; Le Calvez, S.; Ulfendahl, M., Image-adaptive deconvolution for three-dimensional deep biological imaging. *Biophysical journal* **2003,** *85* (6), 3991-4001.

111. Boutet de Monvel, J.; Le Calvez, S.; Ulfendahl, M., Image restoration for confocal microscopy: improving the limits of deconvolution, with application to the visualization of the mammalian hearing organ. *Biophysical journal* **2001,** *80* (5), 2455-70.

112. Suberu, J. O.; Gorka, A. P.; Jacobs, L.; Roepe, P. D.; Sullivan, N.; Barker, G. C.; Lapkin, A. A., Anti-Plasmodial Polyvalent Interactions in Artemisia annua L. Aqueous Extract - Possible Synergistic and Resistance Mechanisms. *Plos One* **2013,** *8* (11).

113. Bell, A., Antimalarial drug synergism and antagonism: mechanistic and clinical significance. *FEMS Microbiol. Lett.* **2005,** *253* (2), 171-184.

114. Griner, L. A. M.; Guha, R.; Shinn, P.; Young, R. M.; Keller, J. M.; Liu, D.; Goldlust, I. S.; Yasgar, A.; McKnight, C.; Boxer, M. B., High-throughput combinatorial screening identifies drugs that cooperate with ibrutinib to kill activated B-cell–like diffuse large B-cell lymphoma cells. *Proc. Nat. Acad. Sci.* **2014,** *111* (6), 2349-2354.

115. Yuan, J.; Cheng, K. C.; Johnson, R. L.; Huang, R.; Pattaradilokrat, S.; Liu, A.; Guha, R.; Fidock, D. A.; Inglese, J.; Wellems, T. E.; Austin, C. P.; Su, X. Z., Chemical genomic profiling for antimalarial therapies, response signatures, and molecular targets. *Science* **2011,** *333* (6043), 724-9.

116. Inglese, J.; Auld, D. S.; Jadhav, A.; Johnson, R. L.; Simeonov, A.; Yasgar, A.; Zheng, W.; Austin, C. P., Quantitative high-throughput screening: a titration-based approach that efficiently identifies biological activities in large chemical libraries. *Proceedings of the National Academy of Sciences of the United States of America* **2006,** *103* (31), 11473-8.

117. Dobson, A., 1. The Oxford Dictionary of Statistical Terms. Yadolah Dodge (ed.), Oxford University Press, Oxford, 2003,Hardcover. No. of pages: 506. Price: GBP 25.00. ISBN 0-19-850994-4. *Statistics in Medicine* **2004,** *23* (11), 1824-1825.

118. Mathews Griner, L. A.; Guha, R.; Shinn, P.; Young, R. M.; Keller, J. M.; Liu, D.; Goldlust, I. S.; Yasgar, A.; McKnight, C.; Boxer, M. B.; Duveau, D. Y.; Jiang, J. K.; Michael, S.; Mierzwa, T.; Huang, W.; Walsh, M. J.; Mott, B. T.; Patel, P.; Leister, W.; Maloney, D. J.; Leclair, C. A.; Rai, G.; Jadhav, A.; Peyser, B. D.; Austin, C. P.; Martin, S. E.; Simeonov, A.; Ferrer, M.; Staudt, L. M.; Thomas, C. J., High-throughput combinatorial screening identifies drugs that cooperate with ibrutinib to kill activated B-cell-like diffuse large B-cell lymphoma cells. *Proceedings of the National Academy of Sciences of the United States of America* **2014,** *111* (6), 2349-54.

119. Moran, P. A., Notes on continuous stochastic phenomena. *Biometrika* **1950,** *37* (1-2), 17-23.

120. Petraitis, V.; Petraitiene, R.; Hope, W. W.; Meletiadis, J.; Mickiene, D.; Hughes, J. E.; Cotton, M. P.; Stergiopoulou, T.; Kasai, M.; Francesconi, A.; Schaufele, R. L.; Sein, T.; Avila, N. A.; Bacher, J.; Walsh, T. J., Combination Therapy in Treatment of Experimental Pulmonary Aspergillosis: In Vitro and In Vivo Correlations of the Concentration- and Dose-Dependent Interactions between Anidulafungin and Voriconazole by Bliss Independence Drug Interaction Analysis. *Antimicrobial agents and chemotherapy* **2009,** *53* (6), 2382-2391.

121. Ayala, H. B. R.; Wacker, M. A.; Siwo, G.; Ferdig, M. T., Quantitative trait loci mapping reveals candidate pathways regulating cell cycle duration in Plasmodium falciparum. *Bmc Genomics* **2010,** *11*, 577.

122. Gonzales, J. M.; Patel, J. J.; Ponmee, N.; Jiang, L.; Tan, A.; Maher, S. P.; Wuchty, S.; Rathod, P. K.; Ferdig, M. T., Regulatory hotspots in the malaria parasite genome dictate transcriptional variation. *Plos Biol* **2008,** *6* (9), 2016-2027.

123. Siriwardana, A.; Iyengar, K.; Roepe, P. D., Endoperoxide Drug Cross-Resistance Patterns for Plasmodium falciparum Exhibiting an Artemisinin Delayed-Clearance Phenotype. *Antimicrobial agents and chemotherapy* **2016,** *60* (11), 6952-6956.

124. Young, R. D.; Rathod, P. K., Clonal viability measurements on Plasmodium falciparum to assess in vitro schizonticidal activity of leupeptin, chloroquine, and 5-fluoroorotate. *Antimicrobial agents and chemotherapy* **1993,** *37* (5), 1102-7.

125. Gligorijevic, B.; Purdy, K.; Elliott, D. A.; Cooper, R. A.; Roepe, P. D., Stage independent chloroquine resistance and chloroquine toxicity revealed via spinning disk confocal microscopy. *Molecular and biochemical parasitology* **2008,** *159* (1), 7-23.

126. Ferdig, M. T.; Cooper, R. A.; Mu, J.; Deng, B.; Joy, D. A.; Su, X. Z.; Wellems, T. E., Dissecting the loci of low-level quinine resistance in malaria parasites. *Molecular microbiology* **2004,** *52* (4), 985-97.

127. Sa, J. M.; Twu, O.; Hayton, K.; Reyes, S.; Fay, M. P.; Ringwald, P.; Wellems, T. E., Geographic patterns of Plasmodium falciparum drug resistance distinguished by differential responses to amodiaquine and chloroquine. *Proceedings of the National Academy of Sciences of the United States of America* **2009,** *106* (45), 18883-9.

128. Roepe, P. D., PfCRT-mediated drug transport in malarial parasites. *Biochemistry* **2011,** *50* (2), 163-71.

129. Maser, P.; Wittlin, S.; Rottmann, M.; Wenzler, T.; Kaiser, M.; Brun, R., Antiparasitic agents: new drugs on the horizon. *Current opinion in pharmacology* **2012,** *12* (5), 562-6.

130. Salako, L. A.; Aderounmu, A. F.; Walker, O., Influence of route of administration on the pharmaco-kinetics of chloroquine and desethylchloroquine. *Bulletin of the World Health Organization* **1987,** *65* (1), 47-50.

131. Hodel, E. M.; Zanolari, B.; Mercier, T.; Biollaz, J.; Keiser, J.; Olliaro, P.; Genton, B.; Decosterd, L. A., A single LC-tandem mass spectrometry method for the simultaneous determination of 14 antimalarial drugs and their metabolites in human plasma. *Journal of chromatography. B, Analytical technologies in the biomedical and life sciences* **2009,** *877* (10), 867-86.

132. Khalil, I. F.; Alifrangis, M.; Recke, C.; Hoegberg, L. C.; Ronn, A.; Bygbjerg, I. C.; Koch, C., Development of ELISA-based methods to measure the anti-malarial drug chloroquine in plasma and in pharmaceutical formulations. *Malaria journal* **2011,** *10*, 249.

133. Gorka, A. P.; Alumasa, J. N.; Sherlach, K. S.; Jacobs, L. M.; Nickley, K. B.; Brower, J. P.; de Dios, A. C.; Roepe, P. D., Cytostatic versus cytocidal activities of chloroquine analogues and inhibition of hemozoin crystal growth. *Antimicrobial agents and chemotherapy* **2013,** *57* (1), 356-64.

134. Gorka, A. P.; Sherlach, K. S.; de Dios, A. C.; Roepe, P. D., Relative to quinine and quinidine, their 9-epimers exhibit decreased cytostatic activity and altered heme binding but similar cytocidal activity versus Plasmodium falciparum. *Antimicrobial agents and chemotherapy* **2013,** *57* (1), 365-74.

135. Gorka, A. P.; de Dios, A.; Roepe, P. D., Quinoline drug-heme interactions and implications for antimalarial cytostatic versus cytocidal activities. *Journal of medicinal chemistry* **2013,** *56* (13), 5231-46.

136. Totino, P. R.; Daniel-Ribeiro, C. T.; Corte-Real, S.; de Fatima Ferreira-da-Cruz, M., Plasmodium falciparum: erythrocytic stages die by autophagic-like cell death under drug pressure. *Experimental parasitology* **2008,** *118* (4), 478-86.

137. Meslin, B.; Beavogui, A. H.; Fasel, N.; Picot, S., Plasmodium falciparum metacaspase PfMCA-1 triggers a z-VAD-fmk inhibitable protease to promote cell death. *PloS one* **2011,** *6* (8), e23867.

138. Suradji, E. W.; Hatabu, T.; Kobayashi, K.; Yamazaki, C.; Abdulah, R.; Nakazawa, M.; Nakajima-Shimada, J.; Koyama, H., Selenium-induced apoptosis-like cell death in Plasmodium falciparum. *Parasitology* **2011,** *138* (14), 1852-62.

139. Ch'ng, J. H.; Kotturi, S. R.; Chong, A. G.; Lear, M. J.; Tan, K. S., A programmed cell death pathway in the malaria parasite Plasmodium falciparum has general features of mammalian apoptosis but is mediated by clan CA cysteine proteases. *Cell death & disease* **2010,** *1*, e26.

140. Nyakeriga, A. M.; Perlmann, H.; Hagstedt, M.; Berzins, K.; Troye-Blomberg, M.; Zhivotovsky, B.; Perlmann, P.; Grandien, A., Drug-induced death of the asexual blood stages of Plasmodium falciparum occurs without typical signs of apoptosis. *Microbes and infection* **2006,** *8* (6), 1560-8.

141. Sanchez, C. P.; Mayer, S.; Nurhasanah, A.; Stein, W. D.; Lanzer, M., Genetic linkage analyses redefine the roles of PfCRT and PfMDR1 in drug accumulation and susceptibility in Plasmodium falciparum. *Molecular microbiology* **2011,** *82* (4), 865-78.

142. Cooper, R. A.; Ferdig, M. T.; Su, X. Z.; Ursos, L. M.; Mu, J.; Nomura, T.; Fujioka, H.; Fidock, D. A.; Roepe, P. D.; Wellems, T. E., Alternative mutations at position 76 of the vacuolar transmembrane protein PfCRT are associated with chloroquine resistance and unique stereospecific quinine and quinidine responses in Plasmodium falciparum. *Molecular pharmacology* **2002,** *61* (1), 35-42.

143. Ecker, A.; Lehane, A. M.; Clain, J.; Fidock, D. A., PfCRT and its role in antimalarial drug resistance. *Trends in parasitology* **2012,** *28* (11), 504-14.

144. Sidhu, A. B.; Verdier-Pinard, D.; Fidock, D. A., Chloroquine resistance in Plasmodium falciparum malaria parasites conferred by pfcrt mutations. *Science* **2002,** *298* (5591), 210-3.

145. Waller, K. L.; Muhle, R. A.; Ursos, L. M.; Horrocks, P.; Verdier-Pinard, D.; Sidhu, A. B.; Fujioka, H.; Roepe, P. D.; Fidock, D. A., Chloroquine resistance modulated in vitro by expression levels of the Plasmodium falciparum chloroquine resistance transporter. *The Journal of biological chemistry* **2003,** *278* (35), 33593-601.

146. Wilson, C. M.; Serrano, A. E.; Wasley, A.; Bogenschutz, M. P.; Shankar, A. H.; Wirth, D. F., Amplification of a gene related to mammalian mdr genes in drug-resistant Plasmodium falciparum. *Science* **1989,** *244* (4909), 1184-6.

147. Reed, M. B.; Saliba, K. J.; Caruana, S. R.; Kirk, K.; Cowman, A. F., Pgh1 modulates sensitivity and resistance to multiple antimalarials in Plasmodium falciparum. *Nature* **2000,** *403* (6772), 906-9.

148. Amoah, L. E.; Lekostaj, J. K.; Roepe, P. D., Heterologous expression and ATPase activity of mutant versus wild type PfMDR1 protein. *Biochemistry* **2007,** *46* (20), 6060-73.

149. Pleeter, P.; Lekostaj, J. K.; Roepe, P. D., Purified Plasmodium falciparum multi-drug resistance protein (PfMDR 1) binds a high affinity chloroquine analogue. *Molecular and biochemical parasitology* **2010,** *173* (2), 158-61.

150. Notte, A.; Leclere, L.; Michiels, C., Autophagy as a mediator of chemotherapy-induced cell death in cancer. *Biochemical pharmacology* **2011,** *82* (5), 427-34.

151. Platini, F.; Perez-Tomas, R.; Ambrosio, S.; Tessitore, L., Understanding autophagy in cell death control. *Current pharmaceutical design* **2010,** *16* (1), 101-13.

152. Gozuacik, D.; Kimchi, A., Autophagy and cell death. *Current topics in developmental biology* **2007,** *78*, 217-45.

153. Shpilka, T.; Weidberg, H.; Pietrokovski, S.; Elazar, Z., Atg8: an autophagy-related ubiquitin-like protein family. *Genome biology* **2011,** *12* (7), 226.

154. Matsui, A.; Kamada, Y.; Matsuura, A., The role of autophagy in genome stability through suppression of abnormal mitosis under starvation. *PLoS genetics* **2013,** *9* (1), e1003245.

155. Dotiwala, F.; Eapen, V. V.; Harrison, J. C.; Arbel-Eden, A.; Ranade, V.; Yoshida, S.; Haber, J. E., DNA damage checkpoint triggers autophagy to regulate the initiation of anaphase. *Proceedings of the National Academy of Sciences of the United States of America* **2013,** *110* (1), E41-9.

156. Vaid, A.; Ranjan, R.; Smythe, W. A.; Hoppe, H. C.; Sharma, P., PfPI3K, a phosphatidylinositol-3 kinase from Plasmodium falciparum, is exported to the host erythrocyte and is involved in hemoglobin trafficking. *Blood* **2010,** *115* (12), 2500-7.

157. Taguchi, K.; Fujikawa, N.; Komatsu, M.; Ishii, T.; Unno, M.; Akaike, T.; Motohashi, H.; Yamamoto, M., Keap1 degradation by autophagy for the maintenance of redox homeostasis.

Proceedings of the National Academy of Sciences of the United States of America **2012,** *109* (34), 13561-6.

158. Lin, M.; Chandramani-Shivalingappa, P.; Jin, H.; Ghosh, A.; Anantharam, V.; Ali, S.; Kanthasamy, A. G.; Kanthasamy, A., Methamphetamine-induced neurotoxicity linked to ubiquitin-proteasome system dysfunction and autophagy-related changes that can be modulated by protein kinase C delta in dopaminergic neuronal cells. *Neuroscience* **2012,** *210*, 308-32.

159. Lanzer, M.; Wickert, H.; Krohne, G.; Vincensini, L.; Braun Breton, C., Maurer's clefts: a novel multi-functional organelle in the cytoplasm of Plasmodium falciparum-infected erythrocytes. *International journal for parasitology* **2006,** *36* (1), 23-36.

160. Richards, W. H.; Maples, B. K., Studies on Plasmodium falciparum in continuous cultivation. I. The effect of chloroquine and pyrimethamine on parasite growth and viability. *Annals of tropical medicine and parasitology* **1979,** *73* (2), 99-108.

161. Bakshi, R. P.; Nenortas, E.; Tripathi, A. K.; Sullivan, D. J.; Shapiro, T. A., Model system to define pharmacokinetic requirements for antimalarial drug efficacy. *Science translational medicine* **2013,** *5* (205), 205ra135.

162. Baro, N. K.; Callaghan, P. S.; Roepe, P. D., Function of resistance conferring Plasmodium falciparum chloroquine resistance transporter isoforms. *Biochemistry* **2013,** *52* (24), 4242-9.

163. Roberts, L.; Egan, T. J.; Joiner, K. A.; Hoppe, H. C., Differential effects of quinoline antimalarials on endocytosis in Plasmodium falciparum. *Antimicrobial agents and chemotherapy* **2008,** *52* (5), 1840-2.

164. Federici, E.; Palazzino, G.; Nicoletti, M.; Galeffi, C., Antiplasmodial activity of the alkaloids of Peschiera fuchsiaefolia. *Planta medica* **2000,** *66* (1), 93-5.

165. Ramanitrahasimbola, D.; Rasoanaivo, P.; Ratsimamanga-Urverg, S.; Federici, E.; Palazzino, G.; Galeffi, C.; Nicoletti, M., Biological activities of the plant-derived bisindole voacamine with reference to malaria. *Phytotherapy research : PTR* **2001,** *15* (1), 30-3.

166. Meschini, S.; Condello, M.; Marra, M.; Formisano, G.; Federici, E.; Arancia, G., Autophagy-mediated chemosensitizing effect of the plant alkaloid voacamine on multidrug resistant cells. *Toxicology in vitro : an international journal published in association with BIBRA* **2007,** *21* (2), 197-203.

167. Liu, J.; Istvan, E. S.; Gluzman, I. Y.; Gross, J.; Goldberg, D. E., Plasmodium falciparum ensures its amino acid supply with multiple acquisition pathways and redundant proteolytic enzyme systems. *Proceedings of the National Academy of Sciences of the United States of America* **2006,** *103* (23), 8840-5.

168. Istvan, E. S.; Dharia, N. V.; Bopp, S. E.; Gluzman, I.; Winzeler, E. A.; Goldberg, D. E., Validation of isoleucine utilization targets in Plasmodium falciparum. *Proceedings of the National Academy of Sciences of the United States of America* **2011,** *108* (4), 1627-32.

169. Gonzales, J. M.; Patel, J. J.; Ponmee, N.; Jiang, L.; Tan, A.; Maher, S. P.; Wuchty, S.; Rathod, P. K.; Ferdig, M. T., Regulatory hotspots in the malaria parasite genome dictate transcriptional variation. *PLoS biology* **2008,** *6* (9), e238.

170. Tawk, L.; Chicanne, G.; Dubremetz, J. F.; Richard, V.; Payrastre, B.; Vial, H. J.; Roy, C.; Wengelnik, K., Phosphatidylinositol 3-phosphate, an essential lipid in Plasmodium, localizes to the food vacuole membrane and the apicoplast. *Eukaryotic cell* **2010,** *9* (10), 1519-30.

171. Baguley, B. C., Multiple drug resistance mechanisms in cancer. *Molecular biotechnology* **2010,** *46* (3), 308-16.

172. de Duve, C.; de Barsy, T.; Poole, B.; Trouet, A.; Tulkens, P.; Van Hoof, F., Commentary. Lysosomotropic agents. *Biochemical pharmacology* **1974,** *23* (18), 2495-531.

173. Ursos, L. M.; Roepe, P. D., Chloroquine resistance in the malarial parasite, Plasmodium falciparum. *Medicinal research reviews* **2002,** *22* (5), 465-91.

174. Gatton, M. L.; Martin, L. B.; Cheng, Q., Evolution of resistance to sulfadoxine-pyrimethamine in Plasmodium falciparum. *Antimicrobial agents and chemotherapy* **2004,** *48* (6), 2116-23.

175. WHO, Guidelines for the treatment of malaria. *World Health Organization: Geneva, Switzerland* **2010**.

176. Greyer, M., Antimalarial Drug Combination Therapy. *WHO Technical Consulation* **2001**, Geneva, Switzerland.

177. Nzila, A. M.; Mberu, E. K.; Sulo, J.; Dayo, H.; Winstanley, P. A.; Sibley, C. H.; Watkins, W. M., Towards an understanding of the mechanism of pyrimethamine-sulfadoxine resistance in Plasmodium falciparum: genotyping of dihydrofolate reductase and dihydropteroate synthase of Kenyan parasites. *Antimicrobial agents and chemotherapy* **2000,** *44* (4), 991-6.

178. Kuhn, S.; Gill, M. J.; Kain, K. C., Emergence of atovaquone-proguanil resistance during treatment of Plasmodium falciparum malaria acquired by a non-immune north American traveller to west Africa. *The American journal of tropical medicine and hygiene* **2005,** *72* (4), 407-9.

179. Laveran, A., Le trypanroth dans le traitement de quelques Trypanosomiases. *Comptes rendus hebdomadaires des séances de l'Académie des sciences* **1904,** *139*, 19-22.

180. Ehrlich, P., Chemotherapeutische Trypanosomen-Studien. *Berliner klinische Wochenschrift* **1907,** *44*, 233-236. 280-283, 310-314 and 341-344.

181. Hastings, I. M.; Hodel, E. M., Pharmacological considerations in the design of anti-malarial drug combination therapies - is matching half-lives enough? *Malaria journal* **2014,** *13*, 62.

182. Hastings, I., How artemisinin-containing combination therapies slow the spread of antimalarial drug resistance. *Trends in parasitology* **2011,** *27* (2), 67-72.

183. White, N. J.; van Vugt, M.; Ezzet, F., Clinical pharmacokinetics and pharmacodynamics and pharmacodynamics of artemether-lumefantrine. *Clinical pharmacokinetics* **1999,** *37* (2), 105-25.

184. Olliaro, P. L.; Trigg, P. I., Status of antimalarial drugs under development. *Bulletin of the World Health Organization* **1995,** *73* (5), 565-71.

185. Sidhu, A. B.; Uhlemann, A. C.; Valderramos, S. G.; Valderramos, J. C.; Krishna, S.; Fidock, D. A., Decreasing pfmdr1 copy number in plasmodium falciparum malaria heightens susceptibility to mefloquine, lumefantrine, halofantrine, quinine, and artemisinin. *The Journal of infectious diseases* **2006,** *194* (4), 528-35.

186. Sidhu, A. B.; Valderramos, S. G.; Fidock, D. A., pfmdr1 mutations contribute to quinine resistance and enhance mefloquine and artemisinin sensitivity in Plasmodium falciparum. *Molecular microbiology* **2005,** *57* (4), 913-26.

187. Berenbaum, M. C., A method for testing for synergy with any number of agents. *The Journal of infectious diseases* **1978,** *137* (2), 122-30.

188. Chou, T. C., Drug combination studies and their synergy quantification using the Chou-Talalay method. *Cancer research* **2010,** *70* (2), 440-6.

189. Wongsrichanalai, C., Artemisinin resistance or artemisinin-based combination therapy resistance? *The Lancet. Infectious diseases* **2013,** *13* (2), 114-5.

190. Guiguemde, W. A.; Shelat, A. A.; Bouck, D.; Duffy, S.; Crowther, G. J.; Davis, P. H.; Smithson, D. C.; Connelly, M.; Clark, J.; Zhu, F.; Jimenez-Diaz, M. B.; Martinez, M. S.; Wilson, E. B.; Tripathi, A. K.; Gut, J.; Sharlow, E. R.; Bathurst, I.; El Mazouni, F.; Fowble, J. W.; Forquer, I.; McGinley, P. L.; Castro, S.; Angulo-Barturen, I.; Ferrer, S.; Rosenthal, P. J.; Derisi, J. L.; Sullivan, D. J.; Lazo, J. S.; Roos, D. S.; Riscoe, M. K.; Phillips, M. A.; Rathod, P. K.; Van Voorhis, W. C.; Avery, V. M.; Guy, R. K., Chemical genetics of Plasmodium falciparum. *Nature* **2010,** *465* (7296), 311-5.

191. Rottmann, M.; McNamara, C.; Yeung, B. K.; Lee, M. C.; Zou, B.; Russell, B.; Seitz, P.; Plouffe, D. M.; Dharia, N. V.; Tan, J.; Cohen, S. B.; Spencer, K. R.; Gonzalez-Paez, G. E.; Lakshminarayana, S. B.; Goh, A.; Suwanarusk, R.; Jegla, T.; Schmitt, E. K.; Beck, H. P.; Brun, R.; Nosten, F.; Renia, L.; Dartois, V.; Keller, T. H.; Fidock, D. A.; Winzeler, E. A.; Diagana, T. T., Spiroindolones, a potent compound class for the treatment of malaria. *Science* **2010,** *329* (5996), 1175-80.

192. Hassan Alin, M.; Bjorkman, A.; Wernsdorfer, W. H., Synergism of benflumetol and artemether in Plasmodium falciparum. *The American journal of tropical medicine and hygiene* **1999,** *61* (3), 439-45.

193. Cokol, M.; Chua, H. N.; Tasan, M.; Mutlu, B.; Weinstein, Z. B.; Suzuki, Y.; Nergiz, M. E.; Costanzo, M.; Baryshnikova, A.; Giaever, G.; Nislow, C.; Myers, C. L.; Andrews, B. J.; Boone, C.; Roth, F. P., Systematic exploration of synergistic drug pairs. *Molecular systems biology* **2011,** *7*, 544.

194. Krogstad, D. J.; Gluzman, I. Y.; Kyle, D. E.; Oduola, A. M.; Martin, S. K.; Milhous, W. K.; Schlesinger, P. H., Efflux of chloroquine from Plasmodium falciparum: mechanism of chloroquine resistance. *Science* **1987,** *238* (4831), 1283-5.

195. Martin, R. E.; Marchetti, R. V.; Cowan, A. I.; Howitt, S. M.; Broer, S.; Kirk, K., Chloroquine transport via the malaria parasite's chloroquine resistance transporter. *Science* **2009,** *325* (5948), 1680-2.

196. Lakshmanan, V.; Bray, P. G.; Verdier-Pinard, D.; Johnson, D. J.; Horrocks, P.; Muhle, R. A.; Alakpa, G. E.; Hughes, R. H.; Ward, S. A.; Krogstad, D. J.; Sidhu, A. B.; Fidock, D. A., A critical role for PfCRT K76T in Plasmodium falciparum verapamil-reversible chloroquine resistance. *The EMBO journal* **2005,** *24* (13), 2294-305.

197. Summers, R. L.; Dave, A.; Dolstra, T. J.; Bellanca, S.; Marchetti, R. V.; Nash, M. N.; Richards, S. N.; Goh, V.; Schenk, R. L.; Stein, W. D.; Kirk, K.; Sanchez, C. P.; Lanzer, M.; Martin, R. E., Diverse mutational pathways converge on saturable chloroquine transport via the malaria parasite's chloroquine resistance transporter. *Proceedings of the National Academy of Sciences of the United States of America* **2014,** *111* (17), E1759-67.

198. Cavanaugh, A.; Huang, Y.; Breitwieser, G. E., Behind the curtain: cellular mechanisms for allosteric modulation of calcium-sensing receptors. *British journal of pharmacology* **2012,** *165* (6), 1670-7.

199. Becker, K.; Tilley, L.; Vennerstrom, J. L.; Roberts, D.; Rogerson, S.; Ginsburg, H., Oxidative stress in malaria parasite-infected erythrocytes: host-parasite interactions. *International journal for parasitology* **2004,** *34* (2), 163-89.

200. Sun, W.; Tanaka, T. Q.; Magle, C. T.; Huang, W.; Southall, N.; Huang, R.; Dehdashti, S. J.; McKew, J. C.; Williamson, K. C.; Zheng, W., Chemical signatures and new drug targets for gametocytocidal drug development. *Scientific reports* **2014,** *4*, 3743.

201. Hanson, K. K.; Ressurreicao, A. S.; Buchholz, K.; Prudencio, M.; Herman-Ornelas, J. D.; Rebelo, M.; Beatty, W. L.; Wirth, D. F.; Hanscheid, T.; Moreira, R.; Marti, M.; Mota, M. M., Torins are potent antimalarials that block replenishment of Plasmodium liver stage parasitophorous vacuole membrane proteins. *Proceedings of the National Academy of Sciences of the United States of America* **2013,** *110* (30), E2838-47.

202. Zhao, W.; Sachsenmeier, K.; Zhang, L.; Sult, E.; Hollingsworth, R. E.; Yang, H., A New Bliss Independence Model to Analyze Drug Combination Data. *Journal of biomolecular screening* **2014,** *19* (5), 817-21.

203. Berenbaum, M. C., The expected effect of a combination of agents: the general solution. *Journal of theoretical biology* **1985,** *114* (3), 413-31.

204. Zhao, L.; Au, J. L.; Wientjes, M. G., Comparison of methods for evaluating drug-drug interaction. *Front Biosci (Elite Ed)* **2010,** *2*, 241-9.

205. Makanga, M.; Krudsood, S., The clinical efficacy of artemether/lumefantrine (Coartem). *Malaria journal* **2009,** *8 Suppl 1*, S5.

206. Eastman, R. T.; Fidock, D. A., Artemisinin-based combination therapies: a vital tool in efforts to eliminate malaria. *Nature reviews. Microbiology* **2009,** *7* (12), 864-74.

207. Vaidya, A. B.; Mather, M. W., A post-genomic view of the mitochondrion in malaria parasites. *Current topics in microbiology and immunology* **2005,** *295*, 233-50.

208. Saraste, M., Oxidative phosphorylation at the fin de siecle. *Science* **1999,** *283* (5407), 1488-93.

209. Vaidya, A. B.; Mather, M. W., Mitochondrial evolution and functions in malaria parasites. *Annual review of microbiology* **2009,** *63*, 249-67.

210. Mather, M. W.; Henry, K. W.; Vaidya, A. B., Mitochondrial drug targets in apicomplexan parasites. *Current drug targets* **2007,** *8* (1), 49-60.

211. Allen, R. J.; Kirk, K., The membrane potential of the intraerythrocytic malaria parasite Plasmodium falciparum. *The Journal of biological chemistry* **2004,** *279* (12), 11264-72.

212. Menard, S.; Ben Haddou, T.; Ramadani, A. P.; Ariey, F.; Iriart, X.; Beghain, J.; Bouchier, C.; Witkowski, B.; Berry, A.; Mercereau-Puijalon, O.; Benoit-Vical, F., Induction of Multidrug Tolerance in Plasmodium falciparum by Extended Artemisinin Pressure. *Emerging infectious diseases* **2015,** *21* (10), 1733-41.

213. Yang, T.; Xie, S. C.; Cao, P.; Giannangelo, C.; McCaw, J.; Creek, D. J.; Charman, S. A.; Klonis, N.; Tilley, L., Comparison of the Exposure Time Dependence of the Activities of Synthetic Ozonide Antimalarials and Dihydroartemisinin against K13 Wild-Type and Mutant Plasmodium falciparum Strains. *Antimicrobial agents and chemotherapy* **2016,** *60* (8), 4501-10.

214. Phyo, A. P.; Jittamala, P.; Nosten, F. H.; Pukrittayakamee, S.; Imwong, M.; White, N. J.; Duparc, S.; Macintyre, F.; Baker, M.; Mohrle, J. J., Antimalarial activity of artefenomel (OZ439), a novel synthetic antimalarial endoperoxide, in patients with Plasmodium falciparum and Plasmodium vivax malaria: an open-label phase 2 trial. *The Lancet. Infectious diseases* **2016,** *16* (1), 61-9.

215. Charman, S. A.; Arbe-Barnes, S.; Bathurst, I. C.; Brun, R.; Campbell, M.; Charman, W. N.; Chiu, F. C.; Chollet, J.; Craft, J. C.; Creek, D. J.; Dong, Y.; Matile, H.; Maurer, M.; Morizzi, J.; Nguyen, T.; Papastogiannidis, P.; Scheurer, C.; Shackleford, D. M.; Sriraghavan, K.; Stingelin, L.; Tang, Y.; Urwyler, H.; Wang, X.; White, K. L.; Wittlin, S.; Zhou, L.; Vennerstrom, J. L., Synthetic ozonide drug candidate OZ439 offers new hope for a single-dose cure of uncomplicated malaria. *Proceedings of the National Academy of Sciences of the United States of America* **2011,** *108* (11), 4400-5.

216. Lanteri, C. A.; Chaorattanakawee, S.; Lon, C.; Saunders, D. L.; Rutvisuttinunt, W.; Yingyuen, K.; Bathurst, I.; Ding, X. C.; Tyner, S. D., Ex vivo activity of endoperoxide antimalarials, including artemisone and arterolane, against multidrug-resistant Plasmodium falciparum isolates from Cambodia. *Antimicrobial agents and chemotherapy* **2014,** *58* (10), 5831-40.

217. Cheng, M. Y.; Hartl, F. U.; Martin, J.; Pollock, R. A.; Kalousek, F.; Neupert, W.; Hallberg, E. M.; Hallberg, R. L.; Horwich, A. L., Mitochondrial heat-shock protein hsp60 is essential for assembly of proteins imported into yeast mitochondria. *Nature* **1989,** *337* (6208), 620-5.

218. Reading, D. S.; Hallberg, R. L.; Myers, A. M., Characterization of the yeast HSP60 gene coding for a mitochondrial assembly factor. *Nature* **1989,** *337* (6208), 655-9.

219. Singh, B.; Patel, H. V.; Ridley, R. G.; Freeman, K. B.; Gupta, R. S., Mitochondrial import of the human chaperonin (HSP60) protein. *Biochemical and biophysical research communications* **1990,** *169* (2), 391-6.

220. Haynes, R. K.; Fugmann, B.; Stetter, J.; Rieckmann, K.; Heilmann, H. D.; Chan, H. W.; Cheung, M. K.; Lam, W. L.; Wong, H. N.; Croft, S. L.; Vivas, L.; Rattray, L.; Stewart, L.; Peters, W.; Robinson, B. L.; Edstein, M. D.; Kotecka, B.; Kyle, D. E.; Beckermann, B.; Gerisch, M.; Radtke, M.; Schmuck, G.; Steinke, W.; Wollborn, U.; Schmeer, K.; Romer, A., Artemisone--a highly active antimalarial drug of the artemisinin class. *Angewandte Chemie* **2006,** *45* (13), 2082-8.

221. Haynes, R. K., Artemisinin and derivatives: the future for malaria treatment? *Current opinion in infectious diseases* **2001,** *14* (6), 719-26.

222. Woodrow, C. J.; Haynes, R. K.; Krishna, S., Artemisinins. *Postgraduate medical journal* **2005,** *81* (952), 71-8.

223. Li, Q. G.; Peggins, J. O.; Fleckenstein, L. L.; Masonic, K.; Heiffer, M. H.; Brewer, T. G., The pharmacokinetics and bioavailability of dihydroartemisinin, arteether, artemether, artesunic acid and artelinic acid in rats. *The Journal of pharmacy and pharmacology* **1998,** *50* (2), 173-82.

224. Batty, K. T.; Ilett, K. F.; Davis, T.; Davis, M. E., Chemical stability of artesunate injection and proposal for its administration by intravenous infusion. *The Journal of pharmacy and pharmacology* **1996,** *48* (1), 22-6.

225. Duc, D. D.; de Vries, P. J.; Nguyen, X. K.; Le Nguyen, B.; Kager, P. A.; van Boxtel, C. J., The pharmacokinetics of a single dose of artemisinin in healthy Vietnamese subjects. *The American journal of tropical medicine and hygiene* **1994,** *51* (6), 785-90.

226. Nagelschmitz, J.; Voith, B.; Wensing, G.; Roemer, A.; Fugmann, B.; Haynes, R. K.; Kotecka, B. M.; Rieckmann, K. H.; Edstein, M. D., First assessment in humans of the safety, tolerability, pharmacokinetics, and ex vivo pharmacodynamic antimalarial activity of the new artemisinin derivative artemisone. *Antimicrobial agents and chemotherapy* **2008,** *52* (9), 3085-91.

227. Ali, S.; Najmi, M. H.; Tarning, J.; Lindegardh, N., Pharmacokinetics of artemether and dihydroartemisinin in healthy Pakistani male volunteers treated with artemether-lumefantrine. *Malaria journal* **2010,** *9*, 275.

228. Zhao, S. S., High-performance liquid chromatographic determination of artemisinine (qinghaosu) in human plasma and saliva. *The Analyst* **1987,** *112* (5), 661-4.

229. Teja-Isavadharm, P.; Watt, G.; Eamsila, C.; Jongsakul, K.; Li, Q.; Keeratithakul, G.; Sirisopana, N.; Luesutthiviboon, L.; Brewer, T. G.; Kyle, D. E., Comparative pharmacokinetics and effect kinetics of orally administered artesunate in healthy volunteers and patients with uncomplicated falciparum malaria. *The American journal of tropical medicine and hygiene* **2001,** *65* (6), 717-21.

230. Mwesigwa, J.; Parikh, S.; McGee, B.; German, P.; Drysdale, T.; Kalyango, J. N.; Clark, T. D.; Dorsey, G.; Lindegardh, N.; Annerberg, A.; Rosenthal, P. J.; Kamya, M. R.; Aweeka, F., Pharmacokinetics of artemether-lumefantrine and artesunate-amodiaquine in children in Kampala, Uganda. *Antimicrobial agents and chemotherapy* **2010,** *54* (1), 52-9.

231. Bangchang, K. N.; Songsaeng, W.; Thanavibul, A.; Choroenlarp, P.; Karbwang, J., Pharmacokinetics of primaquine in G6PD deficient and G6PD normal patients with vivax malaria. *Transactions of the Royal Society of Tropical Medicine and Hygiene* **1994,** *88* (2), 220-2.

232. Batty, K. T.; Ilett, K. F.; Edwards, G.; Powell, S. M.; Maggs, J. L.; Park, B. K.; Davis, T. M., Assessment of the effect of malaria infection on hepatic clearance of dihydroartemisinin using rat liver perfusions and microsomes. *British journal of pharmacology* **1998,** *125* (1), 159-67.

233. Gordi, T.; Huong, D. X.; Hai, T. N.; Nieu, N. T.; Ashton, M., Artemisinin pharmacokinetics and efficacy in uncomplicated-malaria patients treated with two different dosage regimens. *Antimicrobial agents and chemotherapy* **2002,** *46* (4), 1026-31.

234. Straimer, J.; Lee, M. C.; Lee, A. H.; Zeitler, B.; Williams, A. E.; Pearl, J. R.; Zhang, L.; Rebar, E. J.; Gregory, P. D.; Llinas, M.; Urnov, F. D.; Fidock, D. A., Site-specific genome editing in Plasmodium falciparum using engineered zinc-finger nucleases. *Nature methods* **2012,** *9* (10), 993-8.

235. Pasini, E. M.; van den Ierssel, D.; Vial, H. J.; Kocken, C. H., A novel live-dead staining methodology to study malaria parasite viability. *Malaria journal* **2013,** *12*, 190.

236. Meunier, B.; Robert, A., Heme as trigger and target for trioxane-containing antimalarial drugs. *Accounts of chemical research* **2010,** *43* (11), 1444-51.

237. O'Neill, P. M.; Posner, G. H., A medicinal chemistry perspective on artemisinin and related endoperoxides. *Journal of medicinal chemistry* **2004,** *47* (12), 2945-64.

238. White, N. J., Qinghaosu (artemisinin): the price of success. *Science* **2008,** *320* (5874), 330-4.

239. White, N. J.; Pukrittayakamee, S.; Hien, T. T.; Faiz, M. A.; Mokuolu, O. A.; Dondorp, A. M., Malaria. *Lancet* **2014,** *383* (9918), 723-35.

240. Cui, L.; Su, X. Z., Discovery, mechanisms of action and combination therapy of artemisinin. *Expert review of anti-infective therapy* **2009,** *7* (8), 999-1013.

241. Greene, S. E., Reid, A. In *Moving targets: Fighting the evolution of resistance in infections, pests, and cancer*, Proceedings of the American Academy of Microbiology Colloquim, Philadelphia, Pennsylvania, American Academy of Microbiology: Philadelphia, Pennsylvania, 2012.

242. Moehrle, J. J.; Duparc, S.; Siethoff, C.; van Giersbergen, P. L.; Craft, J. C.; Arbe-Barnes, S.; Charman, S. A.; Gutierrez, M.; Wittlin, S.; Vennerstrom, J. L., First-in-man safety and pharmacokinetics of synthetic ozonide OZ439 demonstrates an improved exposure profile relative to other peroxide antimalarials. *British journal of clinical pharmacology* **2013,** *75* (2), 524-37.

243. Rosenthal, P. J., Artefenomel: a promising new antimalarial drug. *The Lancet. Infectious diseases* **2016,** *16* (1), 6-8.

244. Wells, T. N.; Hooft van Huijsduijnen, R.; Van Voorhis, W. C., Malaria medicines: a glass half full? *Nature reviews. Drug discovery* **2015,** *14* (6), 424-42.

245. Miller, S.; Tavshanjian, B.; Oleksy, A.; Perisic, O.; Houseman, B. T.; Shokat, K. M.; Williams, R. L., Shaping development of autophagy inhibitors with the structure of the lipid kinase Vps34. *Science* **2010,** *327* (5973), 1638-42.

246. Liu, Q.; Wang, J.; Kang, S. A.; Thoreen, C. C.; Hur, W.; Ahmed, T.; Sabatini, D. M.; Gray, N. S., Discovery of 9-(6-aminopyridin-3-yl)-1-(3-(trifluoromethyl)phenyl)benzo[h][1,6]naphthyridin-2(1H)-one (Torin2) as a potent, selective, and orally available mammalian target of rapamycin (mTOR) inhibitor for treatment of cancer. *Journal of medicinal chemistry* **2011,** *54* (5), 1473-80.

247. Nilsen, A.; LaCrue, A. N.; White, K. L.; Forquer, I. P.; Cross, R. M.; Marfurt, J.; Mather, M. W.; Delves, M. J.; Shackleford, D. M.; Saenz, F. E.; Morrisey, J. M.; Steuten, J.; Mutka, T.; Li, Y.; Wirjanata, G.; Ryan, E.; Duffy, S.; Kelly, J. X.; Sebayang, B. F.; Zeeman, A. M.; Noviyanti, R.; Sinden, R. E.; Kocken, C. H.; Price, R. N.; Avery, V. M.; Angulo-Barturen, I.; Jimenez-Diaz, M. B.; Ferrer, S.; Herreros, E.; Sanz, L. M.; Gamo, F. J.; Bathurst, I.; Burrows, J. N.; Siegl, P.;

Guy, R. K.; Winter, R. W.; Vaidya, A. B.; Charman, S. A.; Kyle, D. E.; Manetsch, R.; Riscoe, M. K., Quinolone-3-diarylethers: a new class of antimalarial drug. *Science translational medicine* **2013,** *5* (177), 177ra37.

248. Phillips, M. A.; Lotharius, J.; Marsh, K.; White, J.; Dayan, A.; White, K. L.; Njoroge, J. W.; El Mazouni, F.; Lao, Y.; Kokkonda, S.; Tomchick, D. R.; Deng, X.; Laird, T.; Bhatia, S. N.; March, S.; Ng, C. L.; Fidock, D. A.; Wittlin, S.; Lafuente-Monasterio, M.; Benito, F. J.; Alonso, L. M.; Martinez, M. S.; Jimenez-Diaz, M. B.; Bazaga, S. F.; Angulo-Barturen, I.; Haselden, J. N.; Louttit, J.; Cui, Y.; Sridhar, A.; Zeeman, A. M.; Kocken, C.; Sauerwein, R.; Dechering, K.; Avery, V. M.; Duffy, S.; Delves, M.; Sinden, R.; Ruecker, A.; Wickham, K. S.; Rochford, R.; Gahagen, J.; Iyer, L.; Riccio, E.; Mirsalis, J.; Bathhurst, I.; Rueckle, T.; Ding, X.; Campo, B.; Leroy, D.; Rogers, M. J.; Rathod, P. K.; Burrows, J. N.; Charman, S. A., A long-duration dihydroorotate dehydrogenase inhibitor (DSM265) for prevention and treatment of malaria. *Science translational medicine* **2015,** *7* (296), 296ra111.

249. Baragana, B.; Hallyburton, I.; Lee, M. C.; Norcross, N. R.; Grimaldi, R.; Otto, T. D.; Proto, W. R.; Blagborough, A. M.; Meister, S.; Wirjanata, G.; Ruecker, A.; Upton, L. M.; Abraham, T. S.; Almeida, M. J.; Pradhan, A.; Porzelle, A.; Luksch, T.; Martinez, M. S.; Luksch, T.; Bolscher, J. M.; Woodland, A.; Norval, S.; Zuccotto, F.; Thomas, J.; Simeons, F.; Stojanovski, L.; Osuna-Cabello, M.; Brock, P. M.; Churcher, T. S.; Sala, K. A.; Zakutansky, S. E.; Jimenez-Diaz, M. B.; Sanz, L. M.; Riley, J.; Basak, R.; Campbell, M.; Avery, V. M.; Sauerwein, R. W.; Dechering, K. J.; Noviyanti, R.; Campo, B.; Frearson, J. A.; Angulo-Barturen, I.; Ferrer-Bazaga, S.; Gamo, F. J.; Wyatt, P. G.; Leroy, D.; Siegl, P.; Delves, M. J.; Kyle, D. E.; Wittlin, S.; Marfurt, J.; Price, R. N.; Sinden, R. E.; Winzeler, E. A.; Charman, S. A.; Bebrevska, L.; Gray, D. W.; Campbell, S.; Fairlamb, A. H.; Willis, P. A.; Rayner, J. C.; Fidock, D. A.; Read, K. D.; Gilbert, I. H., A novel multiple-stage antimalarial agent that inhibits protein synthesis. *Nature* **2015,** *522* (7556), 315-20.

250. Vennerstrom, J. L.; Arbe-Barnes, S.; Brun, R.; Charman, S. A.; Chiu, F. C.; Chollet, J.; Dong, Y.; Dorn, A.; Hunziker, D.; Matile, H.; McIntosh, K.; Padmanilayam, M.; Santo Tomas, J.; Scheurer, C.; Scorneaux, B.; Tang, Y.; Urwyler, H.; Wittlin, S.; Charman, W. N., Identification of an antimalarial synthetic trioxolane drug development candidate. *Nature* **2004,** *430* (7002), 900-4.

251. Klayman, D. L., Qinghaosu (artemisinin): an antimalarial drug from China. *Science* **1985,** *228* (4703), 1049-55.

252. Jefford, C. W., Why artemisinin and certain synthetic peroxides are potent antimalarials. Implications for the mode of action. *Current medicinal chemistry* **2001,** *8* (15), 1803-26.

253. Wu, Y., How might qinghaosu (artemisinin) and related compounds kill the intraerythrocytic malaria parasite? A chemist's view. *Accounts of chemical research* **2002,** *35* (5), 255-9.

254. Cumming, J. N.; Ploypradith, P.; Posner, G. H., Antimalarial activity of artemisinin (qinghaosu) and related trioxanes: mechanism(s) of action. *Advances in pharmacology* **1997,** *37*, 253-97.

255. Meshnick, S. R., Artemisinin: mechanisms of action, resistance and toxicity. *International journal for parasitology* **2002,** *32* (13), 1655-60.

256. Avery, M. A.; Fan, P.; Karle, J. M.; Bonk, J. D.; Miller, R.; Goins, D. K., Structure-activity relationships of the antimalarial agent artemisinin. 3. Total synthesis of (+)-13-carbaartemisinin and related tetra- and tricyclic structures. *Journal of medicinal chemistry* **1996,** *39* (9), 1885-97.

257. Ridley, R. G., Medical need, scientific opportunity and the drive for antimalarial drugs. *Nature* **2002,** *415* (6872), 686-93.

258. White, N., Antimalarial drug resistance and combination chemotherapy. *Philosophical transactions of the Royal Society of London. Series B, Biological sciences* **1999,** *354* (1384), 739-49.

259. Tang, Y.; Dong, Y.; Vennerstrom, J. L., Synthetic peroxides as antimalarials. *Medicinal research reviews* **2004,** *24* (4), 425-48.

260. Valecha, N.; Krudsood, S.; Tangpukdee, N.; Mohanty, S.; Sharma, S. K.; Tyagi, P. K.; Anvikar, A.; Mohanty, R.; Rao, B. S.; Jha, A. C.; Shahi, B.; Singh, J. P.; Roy, A.; Kaur, P.; Kothari, M.; Mehta, S.; Gautam, A.; Paliwal, J. K.; Arora, S.; Saha, N., Arterolane maleate plus piperaquine phosphate for treatment of uncomplicated Plasmodium falciparum malaria: a comparative, multicenter, randomized clinical trial. *Clinical infectious diseases : an official publication of the Infectious Diseases Society of America* **2012,** *55* (5), 663-71.

261. Valecha, N.; Looareesuwan, S.; Martensson, A.; Abdulla, S. M.; Krudsood, S.; Tangpukdee, N.; Mohanty, S.; Mishra, S. K.; Tyagi, P. K.; Sharma, S. K.; Moehrle, J.; Gautam, A.; Roy, A.; Paliwal, J. K.; Kothari, M.; Saha, N.; Dash, A. P.; Bjorkman, A., Arterolane, a new synthetic trioxolane for treatment of uncomplicated Plasmodium falciparum malaria: a phase II, multicenter, randomized, dose-finding clinical trial. *Clinical infectious diseases : an official publication of the Infectious Diseases Society of America* **2010,** *51* (6), 684-91.

262. Baumgartner, F.; Jourdan, J.; Scheurer, C.; Blasco, B.; Campo, B.; Maser, P.; Wittlin, S., In vitro activity of anti-malarial ozonides against an artemisinin-resistant isolate. *Malaria journal* **2017,** *16* (1), 45.

263. Paguio, M. F.; Bogle, K. L.; Roepe, P. D., Plasmodium falciparum resistance to cytocidal versus cytostatic effects of chloroquine. *Molecular and biochemical parasitology* **2011,** *178* (1-2), 1-6.

264. Dowdle, W. E.; Nyfeler, B.; Nagel, J.; Elling, R. A.; Liu, S.; Triantafellow, E.; Menon, S.; Wang, Z.; Honda, A.; Pardee, G.; Cantwell, J.; Luu, C.; Cornella-Taracido, I.; Harrington, E.; Fekkes, P.; Lei, H.; Fang, Q.; Digan, M. E.; Burdick, D.; Powers, A. F.; Helliwell, S. B.; D'Aquin, S.; Bastien, J.; Wang, H.; Wiederschain, D.; Kuerth, J.; Bergman, P.; Schwalb, D.; Thomas, J.; Ugwonali, S.; Harbinski, F.; Tallarico, J.; Wilson, C. J.; Myer, V. E.; Porter, J. A.; Bussiere, D. E.; Finan, P. M.; Labow, M. A.; Mao, X.; Hamann, L. G.; Manning, B. D.; Valdez, R. A.; Nicholson, T.; Schirle, M.; Knapp, M. S.; Keaney, E. P.; Murphy, L. O., Selective VPS34 inhibitor blocks

autophagy and uncovers a role for NCOA4 in ferritin degradation and iron homeostasis in vivo. *Nature cell biology* **2014,** *16* (11), 1069-79.

265. Ronan, B.; Flamand, O.; Vescovi, L.; Dureuil, C.; Durand, L.; Fassy, F.; Bachelot, M. F.; Lamberton, A.; Mathieu, M.; Bertrand, T.; Marquette, J. P.; El-Ahmad, Y.; Filoche-Romme, B.; Schio, L.; Garcia-Echeverria, C.; Goulaouic, H.; Pasquier, B., A highly potent and selective Vps34 inhibitor alters vesicle trafficking and autophagy. *Nature chemical biology* **2014,** *10* (12), 1013-9.

266. Ghorbal, M.; Gorman, M.; Macpherson, C. R.; Martins, R. M.; Scherf, A.; Lopez-Rubio, J. J., Genome editing in the human malaria parasite Plasmodium falciparum using the CRISPR-Cas9 system. *Nature biotechnology* **2014,** *32* (8), 819-21.

267. Wagner, J. C.; Platt, R. J.; Goldfless, S. J.; Zhang, F.; Niles, J. C., Efficient CRISPR-Cas9-mediated genome editing in Plasmodium falciparum. *Nature methods* **2014,** *11* (9), 915-8.

268. Zhang, C.; Xiao, B.; Jiang, Y.; Zhao, Y.; Li, Z.; Gao, H.; Ling, Y.; Wei, J.; Li, S.; Lu, M.; Su, X. Z.; Cui, H.; Yuan, J., Efficient editing of malaria parasite genome using the CRISPR/Cas9 system. *mBio* **2014,** *5* (4), e01414-14.